

**STUDY OF ALBUMIN AND ANTI-SNAP25 MIXTURES ON  
LIPID MONOLAYERS USING THE LANGMUIR-BLODGETT  
TECHNIQUE**

**GEW LAI TI**

**FACULTY OF SCIENCE  
UNIVERSITY OF MALAYA  
KUALA LUMPUR**

**2017**

**STUDY OF ALBUMIN AND ANTI-SNAP25  
MIXTURES ON LIPID MONOLAYERS USING THE  
LANGMUIR-BLODGETT TECHNIQUE**

**GEW LAI TI**

**THESIS SUBMITTED IN FULFILMENT OF THE  
REQUIREMENTS FOR THE DEGREE OF DOCTOR OF  
PHILOSOPHY**

**DEPARTMENT OF CHEMISTRY  
FACULTY OF SCIENCE  
UNIVERSITY OF MALAYA  
KUALA LUMPUR**

**2017**



## ABSTRACT

Lipid-protein interactions are essential for biological membrane functions. Lipid composition and its molecular packing are the key determinants for distinct functions of the biological membrane. A better knowledge of lipid-protein interactions may be useful for preparing mixed lipid systems, for example, targeted drug-delivery systems. To elucidate the interactions between proteins and the surrounding lipids, C18 fatty acids with different degrees of saturation in their hydrocarbon chain, namely stearic acid (SA), oleic acid (L1), linoleic acid (L2), and linolenic acid (L3), and phospholipids with saturated hydrocarbon chain but different headgroup, such as sucrose stearate (SS), 1,2-distearoyl-*sn*-glycero-3-phosphoglycerol (DSPG), 1,2-distearoyl-*sn*-glycero-3-phosphocholine (DSPC), and dipalmitoylphosphatidylcholine (DPPC) were used to create a monolayer mimicking a half bilayer membrane to be incorporated with various concentrations of an integral protein, bovine serum albumin (BSA) and a polyclonal antibody, Anti-SNAP25 (AS25) onto the respective monolayer using the Langmuir-Blodgett technique accompanied by atomic force microscopy (AFM) imaging. Lipid-protein interactions that occur in the mixed system can be studied from data on miscibility, compressibility and thermodynamic stability from the isotherms obtained. The analyzed data would give an insight into intermolecular interactions between the lipid and protein, thereby providing useful information on the different ways proteins associate with lipid membranes. The *cis*-double bonds in unsaturated lipids (L1, L2 and L3) have kinks in their molecular conformation and thus could not pack as tightly and uniformly as SA. The bends and kinks in the molecular structure may interfere with the packing of the lipid monolayer which will promote fluidity as shown in the analyzed compressibility modulus ( $C_s^{-1}$ ) data. The headgroup of phospholipids with different functional groups has distinctive intermolecular interaction with both proteins. Gibbs

free energy of mixing ( $G_{mix}$ ) values of lipids/BSA were found to be more negative than lipids/AS25 that explained how the integral and membrane-bound protein are embedded in membranes. The amount of protein incorporated into the monolayer strongly affected the thermodynamic properties of the membrane. AFM surface roughness analyses also indicated that BSA homogeneously penetrated in between the lipid membrane and AS25 molecules are strongly bounded on the surface membrane as predicted by the energetic data. Subsequently, Langmuir energetic findings were compared to fatty acid DPPC liposomes preparation. The stability of liposomes was characterized by their mean particle size and zeta potential for 28 days. The formation of liposomes was confirmed by transmission electron microscopy (TEM) images. DPPC/DP/AS25 liposome system was found more stable than L1/DP/AS25. The particle size and zeta potential measurements of DPPC/DP/AS25 liposomes remained nearly constant for 28 days and 14 days respectively. This stability showed agreement with the LB findings as large negative values of  $G_{mix}$  were obtained for DPPC/DP/AS25 mixed monolayer.

## ABSTRAK

Interaksi antara lipid dan protein penting untuk mengekalkan fungsi membran biologi. Komposisi lipid dan pepadatan susunan molekul menjadi penentu utama bagi fungsi membran biologi yang tertentu. Pengetahuan terkini berkaitan dengan interaksi lipid dan protein sangat berguna untuk menyediakan sistem yang melibatkan campuran lipid, sebagai contohnya, sistem penghantar ubat bersasaran. Untuk menjelaskan interaksi antara protein dengan kejiranan lipid, asid lemak C18 dengan darjah ketepuan yang berbeza dalam rantaian hidrokarbonnya, iaitu asid stearik (SA), asid oleik (L1), asid linoleik (L2), dan asid linolenik (L3), dan fosfolipid dengan rantai hidrokarbon sama ketepuan tetapi kumpulan kepala yang berbeza, seperti stearat sukrosa (SS), 1,2-distearoil-*sn*-glisero-3-fosfoglisero (DSPG), 1,2-distearoil-*sn*-glisero-3-fosfokolina (DSPC), dan dipalmitoilfosfatidilkolina (DPPC) digunakan untuk mewujudkan ekalapisan yang meniru sebahagian kecil dari lapisan ganda membran semula jadi untuk dimasukkan dengan pelbagai kepekatan protein integral, albumin bovine serum (BSA) dan antibodi poliklonal, anti-SNAP25 (AS25) kepada ekalapisan lipid masing-masing dengan menggunakan teknik Langmuir-Blodgett berserta dengan mikroskop kuasa atom (AFM) pengimejan. Interaksi antara lipid dan protein yang berlaku dalam sistem campuran boleh dikaji daripada maklumat tentang keterlarutcampuran, ketertampatan dan kestabilan termodinamik dari isoterma. Data analisis akan memberi ilustrasi tentang interaksi antara molekul lipid dan protein, oleh yang demikian maklumat yang berguna mengenai cara-cara yang berbeza protein kaitkan dengan lapisan membran lipid akan dipersembahkan. Geometri molekul *cis*-ikatan kembar lipid tak tepu (L1, L2 dan L3) memberi kesan punding dan menyebabkannya tidak boleh diatur dengan ketat dan seragam seperti SA. Struktur molekul yang bengkok dan punding akan mengganggu kepadatan susunan ekalapisan lipid yang akan menggalakkan sifat kebendaliran seperti

yang ditunjukkan dalam data modulus mampatan ( $C_s^{-1}$ ). Fosfolipid dengan kumpulan kepala yang berbeza kumpulan berfungsi mempunyai interaksi antara molekul tersendiri dengan kedua-dua protein. Nilai-nilai Gibbs tenaga bebas campuran ( $G_{mix}$ ) lipid/BSA didapati lebih negatif daripada lipid/AS25 yang mengusulkan bagaimana integral dan perifer protein berinteraksi dalam membran. Kandungan protein yang dimasukkan ke dalam ekalapisan lipid amat mempengaruhi sifat-sifat termodinamik lapisan. AFM permukaan ketidakrataan analisis juga menunjukkan bahawa BSA menembusi secara seragam di antara membran lipid dan molekul AS25 melekat pada atas permukaan lapisan seperti yang diramalkan oleh data bertenaga yang diperolehi. Kemudian, penemuan Langmuir bertenaga yang didapati telah digunakan sebagai rujukan untuk menyediakan nanoliposom asid lemak dan DPPC liposom. Kestabilan liposom dicirikan oleh min saiz zarah dan potensi zeta selama 28 hari dan 14 hari masing masing. Kehadiran liposom dalam larutan disahkan oleh micrograf yang digambar oleh transmisi electron mikroskop (TEM). sistem liposom DPPC/DP/AS25 adalah lebih stabil daripada L1/DP/AS25. Min saiz zarah dan potensi zeta masing-masing kekal malar selama 28 dan 14 hari. Kestabilan system liposome DPPC/DP/AS25 bersetuju dengan data Langmuir bertenaganya.

## ACKNOWLEDGEMENTS

First, and most of all, I would like to thank my supervisor, Prof. Dr. Misni Misran, for his expertise, knowledge, guidance, and patience throughout my studies. The good advice, support, and friendship with Prof. Misni has been invaluable on both at an academic and personal level, for which I am extremely thankful. Without him, this Phd would not have been achievable.

I would like to thank my colloid laboratory team members, for their countless help, supports, and kept me accompanied in this long walks. They have each made my time at the Colloid Chemistry laboratory in University of Malaya more positive and enjoyable.

I am deeply grateful to my employer, Sunway University for giving me time that was required for me to complete all experimental work in a laboratory at the University of Malaya as I am currently serving as a full-time Chemistry Lecturer in Sunway University, Malaysia. This Phd would not have been possible without the support and kind understanding from my bosses and colleagues.

I gratefully acknowledge the funding received from Sunway University Research Grant (INT-ADTP-02-01) and Postgraduate Research Fund (PS348/2010A) by University of Malaya.

I would like to say a heartfelt thank you to my family and friends for making it possible for me to complete what I started. They consistently remind me that "Great works are performed not by strength, but perseverance".

Last of all, I would like to express my special thanks to Phra Phrom for his countless blessings. With his godly blessings, I survive with this journey with peaceful mind and happiness.

## TABLE OF CONTENTS

ABSTRACT	iii
ABSTRAK	v
ACKNOWLEDGEMENTS	vii
TABLE OF CONTENTS	viii
LIST OF FIGURES	xiv
LIST OF TABLES	xxiii
LIST OF SYMBOLS	xxiv
LIST OF ABBREVIATIONS	xxv
LIST OF APPENDICES	xxvii
<b>CHAPTER 1: INTRODUCTION</b>	<b>1</b>
1.1 Biological membrane	1
1.2 Lipid-protein interactions	2
1.2.1 Lipids	4
1.2.2 Proteins	7
1.2.2.1 Albumin	7
1.2.2.2 Anti-SNAP25 (AS25)	10
1.2.2.3 SNARE protein and membrane fusion	10
1.3 Application of lipid-protein interactions	13
1.3.1 Liposomal drug delivery systems	13
1.4 Objectives of research	14
<b>CHAPTER 2: LITERATURE REVIEW</b>	<b>15</b>
2.1 Introduction	15
	viii

2.2 Liposomes in protein delivery	20
2.2.1 Immunoliposomes (Antibody-targeted liposomes)	21
2.2.2 Gene delivery	22
2.2.3 Virus antigen delivery	23
2.2.4 Therapeutic enzyme delivery	24
2.3 Conclusions	25
<b>CHAPTER 3: MATERIALS AND METHODS</b>	<b>26</b>
3.1 Introduction	26
3.2 Materials	26
3.2.1 Lipids	26
3.2.2 Proteins	28
3.2.3 Chemicals and solvents	28
3.3 Instrumentations	29
3.3.1 Langmuir-Blodgett (LB) technique	29
3.3.1.1 Surface pressure–mean molecular area ( $\Pi$ – $A$ ) isotherms	30
3.3.1.2 Deposition of monolayer on a substrate	31
3.3.1.3 Precaution steps when handling LB	33
3.3.1.4 LB data analysis	33
3.3.2 Atomic force microscopy	35
3.3.2.1 The operation of tapping-mode atomic force microscopy (TM-AFM)	35
3.3.2.2 Cantilever and spring constants	37
3.3.2.3 AFM topography: Surface roughness	37
3.3.3 Zetasizer Nano system	38
3.4 Methods	39

3.4.1	Preparation of Langmuir monolayers/mixed monolayers for Langmuir-Blodgett measurement	39
3.4.1.1	Mixed monolayers of C18 fatty acids	40
3.4.1.2	Mixed monolayers of C18 fatty acids–BSA and phospholipids–BSA	41
3.4.1.3	Mixed monolayers of C18 fatty acids–AS25 and phospholipids–AS25	41
3.4.1.4	Mixed monolayers of C18 fatty acids–DOPE PEG2000 and DPPC–DOPE PEG2000	41
3.4.1.5	C18 fatty acids/DOPE PEG2000–AS25 and DPPC/DOPE PEG2000–AS25 mixed monolayers	42
3.4.2	Deposition of bilayer of lipid-lipid and lipid-protein on the oxidized silicon wafer for AFM imaging	42
3.4.3	Atomic force microscopy (AFM) imaging	43
3.4.4	Determination of $K_{ow}$ of proteins by reverse phase-high performance liquid chromatography (RP-HPLC)	43
3.4.5	Preparation of liposomes	45
3.4.5.1	Unsaturated C18 fatty acids/AS25, C18 fatty acids/DP and C18 fatty acids/DP/AS25 liposomes	45
3.4.5.2	DPPC, DPPC/AS25, DPPC/DP and DPPC/DP/AS25 Liposomes	46
3.4.6	Transmission electron microscopy (TEM) imaging	47
	<b>CHAPTER 4: RESULTS AND DISCUSSION</b>	<b>48</b>
4.1	Introduction	48

4.2 Lipid-protein interactions: Effect of degree of saturation C18 fatty acids	49
4.2.1 $\Pi$ - <i>A</i> Isotherms	49
4.2.1.1 Pure monolayers of SA, L1, L2, and L3	49
4.2.1.2 Mixed monolayers of C18 fatty acids: Effect of degree of saturation	51
4.2.1.3 Mixed monolayers of C18 fatty acids and DP	54
4.2.1.4 Mixed monolayers of C18 fatty acids and BSA	58
4.2.1.5 Mixed monolayers of C18 fatty acids and AS25	62
4.2.1.6 C18 fatty acids, DP and AS25 mixed monolayers	65
4.2.2 Compressibility analysis	67
4.2.2.1 Pure monolayers of SA, L1, L2, and L3	67
4.2.2.2 Mixed monolayers of C18 fatty acids: Effect of degree of saturation	68
4.2.2.3 Mixed monolayers of C18 fatty acids and DP	72
4.2.2.4 Mixed monolayers of C18 fatty acids and BSA	74
4.2.2.5 Mixed monolayers of C18 fatty acids and AS25	76
4.2.2.6 C18 fatty acids, DP and AS25 mixed monolayers	79
4.2.3 Energetic stability of mixed monolayers	81
4.2.3.1 Mixed monolayers of C18 fatty acids: Effect of degree of saturation	81
4.2.3.2 Mixed monolayers of C18 fatty acids and DP	88
4.2.3.3 Mixed monolayers of C18 fatty acids and BSA	91
4.2.3.4 Mixed monolayers of C18 fatty acids and AS25	95
4.2.3.5 C18 fatty acids, DP and AS25 mixed monolayers	99
4.3 Lipid-protein interactions: Effect of headgroups	101
4.3.1 $\Pi$ - <i>A</i> Isotherms	101

4.3.1.1	Pure monolayers SS, DSPC and DSPG	101
4.3.1.2	Mixed monolayers of SS, DSPC and DSPG and BSA	103
4.3.1.3	Mixed monolayers of SS, DSPC and DSPG and AS25	105
4.3.2	Compressibility analysis	107
4.3.2.1	Pure monolayers SS, DSPC and DSPG	107
4.3.2.2	Mixed monolayers of SS, DSPC and DSPG and BSA	109
4.3.2.3	Mixed monolayers of SS, DSPC and DSPG and AS25	111
4.3.3	Energetic stability of mixed monolayers	113
4.3.3.1	Mixed monolayers of SS, DSPC and DSPG and BSA	113
4.3.3.2	Mixed monolayers of SS, DSPC and DSPG and AS25	117
4.4	Lipid-protein interactions: DPPC	120
4.4.1	$\Pi$ - <i>A</i> Isotherms	120
4.4.1.1	Mixed monolayers of DPPC and BSA	121
4.4.1.2	Mixed monolayers of DPPC/AS25, DPPC/ DP and DPPC/DP/AS25	122
4.4.2	Compressibility analysis	125
4.4.2.1	Mixed monolayers of DPPC and BSA	125
4.4.2.2	Mixed monolayers of DPPC/AS25, DPPC/ DP and DPPC/DP/AS25	125
4.4.3	Energetic stability of mixed monolayers	127
4.4.3.1	Mixed monolayers of DPPC and BSA	127
4.4.3.2	Mixed monolayers of DPPC/AS25, DPPC/DP and DPPC/DP/AS25	131
4.5	AFM observations	135
4.5.1	Lipid-protein interactions: Effect of degree of saturation C18 fatty acids	135

4.2.1.1	Pure monolayers of SA, L1, L2, and L3	135
4.2.1.2	Mixed monolayers of C18 fatty acids and DP	137
4.2.1.3	Mixed monolayers of C18 fatty acids and BSA	140
4.2.1.4	Mixed monolayers of C18 fatty acids and AS25	142
4.2.1.5	C18 fatty acids, DP and AS25 mixed monolayers	145
4.5.2	Lipid-protein interactions: Effect of headgroup	148
4.5.2.1	Mixed monolayers of SS, DSPC and DSPG and proteins (BSA and AS25)	148
4.5.3	Lipid-protein interactions: DPPC	154
4.5.3.1	Mixed monolayers of DPPC and proteins (BSA and AS25)	154
4.6	Liposomes	157
4.6.1	Particle size and zeta potential	157
4.6.1.1	C18 fatty acid liposomes	157
4.6.1.2	L1/DP, L2/DP, L3/DP liposomes	158
4.6.1.3	L1/AS25, L2/AS25, L3/AS25 liposomes	162
4.6.1.4	L1/DP/AS25, L2/DP/AS25 and L3/DP/AS25 liposomes	163
4.6.1.5	DPPC/DP, DPPC/AS25 and DPPC/DP/AS25 liposomes	165
4.6.2	Transmission electron microscopy (TEM) micrographs	173
	<b>CHAPTER 5: CONCLUSION</b>	<b>177</b>
5.0	Conclusions	177
5.1	Future works	180
	<b>REFERENCES</b>	<b>181</b>
	LIST OF PUBLICATIONS	197

## LIST OF FIGURES

Figure 1.1:	The “fluid mosaic model” proposed by Singer and Nicolson in 1972. (Reprinted permission granted by AAAS – Appendix A).....	1
Figure 1.2:	A schematic illustration of types of membrane proteins that associated with lipid bilayer membrane: (i) integral (intrinsic) protein, (ii) peripheral (extrinsic) protein span on the membrane surface, (iii) and (iv) lipid-linked proteins, where proteins are anchored to the surface containing sugar such as glycoproteins.....	3
Figure 1.3:	A schematic illustration of various interactions and forces that influence and stabilize proteins structures.....	8
Figure 2.1:	An illustration of the role of liposomes in various therapeutic proteins delivery such as antibody, nuclei acid, virus antigen and therapeutic enzymes for an effective delivery.....	21
Figure 3.1:	A schematic representation of surface pressure–mean molecular area ( $\Pi$ – $A$ ) isotherm of Langmuir film and molecular in different phase.....	30
Figure 3.2:	(a) Langmuir monolayer, (b) deposition of LB film onto solid substrate, (c) various LB deposition onto solid substrate, X-type is obtained when the sample’s tails are deposited hydrophobic surface of substrate, Y- and Z-type is obtained when sample’s headgroups are deposited on hydrophilic surface of substrate, in contrast Y is bilayer, and Z is monolayer.....	32
Figure 3.3:	The AFM tip-cantilever assembly oscillates at the sample surface while the tip is scanned, thus, the tip taps lightly on the surface of the sample while imaging and only touches the sample at the bottom each oscillation. By using constant oscillation amplitude, a constant tip-sample distance is maintained until the scan is completed.....	36
Figure 4.1:	The surface pressure–area ( $\Pi$ – $A$ ) isotherms of C18 fatty acids (SA, L1, L2 and L3), spread on water subphase at 25°C.....	50
Figure 4.2:	The surface pressure–area ( $\Pi$ – $A$ ) isotherms of mixed monolayers (plotted in mole fraction of SA): a) SA/L1, (b) SA/L2, and (c) SA/L3 spread on a nanopure water subphase at 25°C.....	52
Figure 4.3:	The surface pressure–area ( $\Pi$ – $A$ ) isotherms of mixed monolayers (plotted in mole fraction of L1 or L2): (a) L1/L2, (b) L1/L3, and (c) L2/L3 spread on a nanopure water subphase at 25°.....	53
Figure 4.4:	(a) Molecular structure of DP; (b) Three types of intermolecular interactions that occur between DP and DP: (1) Head-to-head; (2) tail-to-tail; (3) head-to-tail.....	54

Figure 4.5:	The surface pressure–area ( $\Pi$ – $A$ ) isotherm of DOPE PEG2000 monolayer, and its compressibility modulus ( $C_s^{-1}$ ), spread on water subphase at 25°C.....	55
Figure 4.6:	The surface pressure–area ( $\Pi$ – $A$ ) isotherms of mixed monolayers (plotted in mole ratio of C18 fatty acids to DOPE PEG2000): (a) SA/DOPE PEG2000, (b) L1/DOPE PEG2000, (c) L2/DOPE PEG2000, and (d) L3/DOPE PEG2000, spread on a nanopure water subphase at 25°C.....	57
Figure 4.7:	The surface pressure–area ( $\Pi$ – $A$ ) isotherm of BSA monolayer, and its compressibility modulus ( $C_s^{-1}$ ), spread on water subphase at 25°C.....	58
Figure 4.8:	The surface pressure–area ( $\Pi$ – $A$ ) isotherms of mixed monolayers (plotted in mole fraction of BSA): (a) SA/BSA, (b) L1/BSA, (c) L2/BSA, and (d) L3/BSA spread on a nanopure water subphase at 25°C.....	61
Figure 4.9:	The surface pressure–area ( $\Pi$ – $A$ ) isotherm of Anti-SNAP25 monolayer and, its compressibility modulus ( $C_s^{-1}$ ), spread on water subphase at 25°C.....	63
Figure 4.10:	The surface pressure–area ( $\Pi$ – $A$ ) isotherms of mixed monolayers (plotted in mole ratio of C18 fatty acids to Anti-SNAP25): (a) SA/Anti-SNAP25, (b) L1/Anti-SNAP25, (c) L2/Anti-SNAP25 and (d) L3/Anti-SNAP25, spread on water subphase at 25°C.....	64
Figure 4.11:	The surface pressure–area ( $\Pi$ – $A$ ) isotherms of mixed monolayers (plotted in nmole of AS25): (a) SA/DP/AS25, (b) L1/DP/AS25, (c) L2/DP/AS25, and (d) L3/DP/AS25, spread on water subphase at 25°C.....	66
Figure 4.12:	The compression modulus ( $C_s^{-1}$ ) of C18 fatty acids (stearic acid, oleic acid, linoleic acid and linolenic acid), spread on water subphase at 25°C.....	68
Figure 4.13:	A schematic illustration of the molecular packing of SA/L1, and (b) L1/L2 mixed monolayers.....	69
Figure 4.14:	The compressibility modulus ( $C_s^{-1}$ ) vs surface pressure ( $\Pi$ ) of mixtures saturated and unsaturated C18 fatty acids: (a) SA/L1, (b) SA/L2, (c) SA/L3 mixed monolayers (plotted in mole fraction of SA), spread on a nanopure water subphase at 25°C.....	70
Figure 4.15:	The compressibility modulus ( $C_s^{-1}$ ) vs surface pressure ( $\Pi$ ) of mixtures unsaturated C18 fatty acids: (a) L1/L2, (b) L1/L3, (c) L2/L3 mixed monolayers (plotted in mole fraction of L1 or L2), spread on a nanopure water subphase at 25°C.....	71

Figure 4.16:	The compressibility modulus ( $C_s^{-1}$ ) vs surface pressure ( $\Pi$ ) of mixed monolayers (plotted in mole ratio of C18 fatty acids to DOPE PEG2000): (a) SA/DOPE PEG2000, (b) L1/DOPE PEG2000, (c) L2/DOPE PEG2000, and (d) L3/DOPE PEG2000, spread on a nanopure water subphase at 25°C.....	73
Figure 4.17:	The compressibility modulus ( $C_s^{-1}$ ) vs surface pressure ( $\Pi$ ) of mixed monolayers (plotted in mole fraction of BSA): (a) SA/BSA, (b) L1/BSA (c) L2/BSA, (d) L3/BSA, spread on a nanopure water subphase at 25°C.....	75
Figure 4.18:	The compressibility modulus ( $C_s^{-1}$ ) vs surface pressure ( $\Pi$ ) of mixed monolayers (plotted in mole ratio of C18 fatty acids to Anti-SNAP25): (a) SA/Anti-SNAP25, (b) L1/Anti-SNAP25, (c) L2/Anti-SNAP25 and (d) L3/Anti-SNAP25, spread on water subphase at 25°C.....	78
Figure 4.19:	The possibilities of AS25 molecules interacting with SA/DP monolayer.....	79
Figure 4.20:	The compressibility modulus ( $C_s^{-1}$ ) vs surface pressure ( $\Pi$ ) of mixed monolayers (plotted in nmole of AS25): (a) SA/DP/AS25, (b) L1/DP/AS25, (c) L2/DP/AS25, and (d) L3/DP/AS25, spread on water subphase at 25°C.....	80
Figure 4.21:	Mean molecular area of C18 fatty acids mixed monolayers vs $X_{SA}$ of (a) SA/L1, (b) SA/L2, and (c) SA/L3 on pure water subphase at 25°C. For discrete surface pressure of $\blacksquare = 5 \text{ mN m}^{-1}$ , $\bullet = 10 \text{ mN m}^{-1}$ , $\blacktriangle = 15 \text{ mN m}^{-1}$ , $\blacktriangledown = 20 \text{ mN m}^{-1}$ and $\blacklozenge = 25 \text{ mN m}^{-1}$ .....	84
Figure 4.22:	Gibbs free excess energy $G_{mix}$ of C18 fatty acids mixed monolayers vs $X_{SA}$ of (a) SA/L1, (b) SA/L2, and (c) SA/L3 on pure water subphase at 25°C. For discrete surface pressure of $\blacksquare = 5 \text{ mN m}^{-1}$ , $\bullet = 10 \text{ mN m}^{-1}$ , $\blacktriangle = 15 \text{ mN m}^{-1}$ , $\blacktriangledown = 20 \text{ mN m}^{-1}$ and $\blacklozenge = 25 \text{ mN m}^{-1}$ .....	85
Figure 4.23:	Mean molecular area of C18 fatty acids monolayers vs mole fraction of L1 or L2: (a) L1/L2, (b) L1/L3, and (c) L2/L3 on pure water subphase at 25°C. For discrete surface pressure of $\blacksquare = 5 \text{ mN m}^{-1}$ , $\bullet = 10 \text{ mN m}^{-1}$ , $\blacktriangle = 15 \text{ mN m}^{-1}$ , $\blacktriangledown = 20 \text{ mN m}^{-1}$ and $\blacklozenge = 25 \text{ mN m}^{-1}$ .....	86
Figure 4.24:	Gibbs free excess energy $G_{mix}$ of C18 fatty acids monolayers vs mole fraction of L1 or L2: (a) L1/L2, (b) L1/L3 and (c) L2/L3 on pure water subphase at 25°C. For discrete surface pressure of $\blacksquare = 5 \text{ mN m}^{-1}$ , $\bullet = 10 \text{ mN m}^{-1}$ , $\blacktriangle = 15 \text{ mN m}^{-1}$ , $\blacktriangledown = 20 \text{ mN m}^{-1}$ and $\blacklozenge = 25 \text{ mN m}^{-1}$ .....	87

Figure 4.25:	(a) Excess mean molecular area ( $A_{ex}$ ), (b) Gibbs free energy of mixing ( $G_{mix}$ ) vs mole ratio of C18 fatty acids to DOPE PEG2000 mixed monolayers: $\nabla$ = SA/DOPE PEG2000, $\bullet$ = L1/DOPE PEG2000, $\blacktriangle$ = L2/DOPE PEG2000, and $\square$ = L3/DOPE PEG2000, spread on a nanopure water subphase at 25°C.....	90
Figure 4.26:	Mean molecular area of C18 fatty acids/BSA monolayers vs $X_{BSA}$ : (a) SA/BSA, (b) L1/BSA, (c) L2/BSA, and (d) L3/BSA on pure water subphase at 25°C. For discrete surface pressure of $\blacksquare$ = 5 mN m <sup>-1</sup> , $\bullet$ = 10 mN m <sup>-1</sup> , $\blacktriangle$ = 15 mN m <sup>-1</sup> , $\nabla$ = 20 mN m <sup>-1</sup> and $\blacklozenge$ = 25 mN m <sup>-1</sup> .....	92
Figure 4.27:	Gibbs free excess energy $G_{mix}$ of C18 fatty acids/BSA monolayers vs $X_{BSA}$ : (a) SA/BSA, (b) L1/BSA, (c) L2/BSA, and (d) L3/BSA on pure water subphase at 25°C. For discrete surface pressure of $\blacksquare$ = 5 mN m <sup>-1</sup> , $\bullet$ = 10 mN m <sup>-1</sup> , $\blacktriangle$ = 15 mN m <sup>-1</sup> , $\nabla$ = 20 mN m <sup>-1</sup> and $\blacklozenge$ = 25 mN m <sup>-1</sup> .....	93
Figure 4.28:	A cartoon illustration to describe the interactions between C18 fatty acids and BSA.....	94
Figure 4.29:	(a) Excess mean molecular area ( $A_{ex}$ ), (b) Gibbs free energy of mixing ( $G_{mix}$ ) vs mole ratio of C18 fatty acids to Anti-SNAP25 for mixed systems: $\blacksquare$ = SA/Anti-SNAP25, $\bullet$ = L1/Anti-SNAP25, $\blacktriangle$ = L2/Anti-SNAP25, and $\nabla$ = L3/Anti-SNAP25, spread on water subphase at 25°C.....	97
Figure 4.30:	The possibilities of AS25 molecules interacting with the fatty acid monolayer: (i) like an integral protein, (ii) AS25 is partially embedded into the monolayer, (iii) presence on the monolayer surface, interacting with the head-group of fatty acids, or (iv) excess antibody remaining in the water subphase.....	98
Figure 4.31:	(a) Excess mean molecular area ( $A_{ex}$ ), (b) Gibbs free energy of mixing ( $G_{mix}$ ) vs mole of Anti-SNAP25 for mixed systems: $\nabla$ = SA/DP/AS25, $\bullet$ = L1/DP/AS25, $\blacktriangle$ = L2/DP/AS25, and $\square$ = L3/DP/AS25, spread on water subphase at 25°C.....	100
Figure 4.32:	The surface pressure–area ( $\Pi$ – $A$ ) isotherms of pure monolayer of SA, SS, DSPC, and DSPG, spread on a nanopure water subphase at 25°C.....	102
Figure 4.33:	The surface pressure–area ( $\Pi$ – $A$ ) isotherms of mixed monolayers (plotted in $X_{BSA}$ ): (a) SA/BSA, (b) SS/BSA, (c) DSPC/BSA, and (d) DSPG/BSA spread on a nanopure water subphase at 25°C.....	104
Figure 4.34:	The surface pressure–area ( $\Pi$ – $A$ ) isotherms of mixed monolayers (plotted in mole ratio of phospholipids to AS25): (a) SA/AS25, (b) SS/AS25, (c) DSPC/AS25, and (d) DSPG/AS25, spread on a nanopure water subphase at 25°C.....	106

Figure 4.35:	The compression modulus ( $C_s^{-1}$ ) vs surface pressure ( $\Pi$ ) of mixed monolayers of SA, SS, DSPC, and DSPG, spread on a nanopure water subphase at 25°C.....	108
Figure 4.36:	The compression modulus ( $C_s^{-1}$ ) vs surface pressure ( $\Pi$ ) of mixed monolayers (plotted in $X_{BSA}$ ): (a) SA/BSA, (b) SS/BSA, (c) DSPC/BSA, and (d) DSPG/BSA, spread on a nanopure water subphase at 25°C.....	110
Figure 4.37:	The compression modulus ( $C_s^{-1}$ ) vs surface pressure ( $\Pi$ ) of mixed monolayers (plotted in mole ratio of phospholipids to AS25): (a) SA/AS25, (b) SS/AS25, (c) DSPC/AS25, and (d) DSPG/AS25, spread on a nanopure water subphase at 25°C.....	112
Figure 4.38:	Excess mean molecular area of phospholipids/BSA mixed monolayers vs $X_{BSA}$ on pure water subphase at 25°C. For discrete surface pressure of $\blacksquare = 5 \text{ mN m}^{-1}$ , $\bullet = 10 \text{ mN m}^{-1}$ , $\circ = 15 \text{ mN m}^{-1}$ , $\nabla = 20 \text{ mN m}^{-1}$ and $\blacklozenge = 25 \text{ mN m}^{-1}$ . $\blacktriangleleft = 30 \text{ mN m}^{-1}$ and $\blacktriangleright = 35 \text{ mN m}^{-1}$ .....	114
Figure 4.39:	Gibbs free excess energy $G_{mix}$ of phospholipids/BSA monolayers vs $X_{BSA}$ on pure water subphase at 25°C. For discrete surface pressure of $\blacksquare = 5 \text{ mN m}^{-1}$ , $\bullet = 10 \text{ mN m}^{-1}$ , $\circ = 15 \text{ mN m}^{-1}$ , $\nabla = 20 \text{ mN m}^{-1}$ and $\blacklozenge = 25 \text{ mN m}^{-1}$ . $\blacktriangleleft = 30 \text{ mN m}^{-1}$ and $\blacktriangleright = 35 \text{ mN m}^{-1}$ .....	115
Figure 4.40:	A cartoon illustration to describe the interactions of BSA and phospholipids.....	116
Figure 4.41:	Excess mean molecular area of phospholipids/AS25 mixed monolayers vs $X_{BSA}$ on pure water subphase at 25°C. For discrete surface pressure of $\blacksquare = 5 \text{ mN m}^{-1}$ , $\bullet = 10 \text{ mN m}^{-1}$ , $\blacktriangle = 15 \text{ mN m}^{-1}$ , $\blacktriangledown = 20 \text{ mN m}^{-1}$ , $\blacklozenge = 25 \text{ mN m}^{-1}$ (diamond), $\blacktriangleleft = 30 \text{ mN m}^{-1}$ , $\blacktriangleright = 35 \text{ mN m}^{-1}$ and $\ast = 40 \text{ mN m}^{-1}$ .....	118
Figure 4.42:	Gibbs free energy of mixing $G_{mix}$ of phospholipids/AS25 monolayers vs $X_{BSA}$ on pure water subphase at 25°C. For discrete surface pressure of $\blacksquare = 5 \text{ mN m}^{-1}$ , $\bullet = 10 \text{ mN m}^{-1}$ , $\blacktriangle = 15 \text{ mN m}^{-1}$ , $\blacktriangledown = 20 \text{ mN m}^{-1}$ , $\blacklozenge = 25 \text{ mN m}^{-1}$ (diamond), $\blacktriangleleft = 30 \text{ mN m}^{-1}$ , $\blacktriangleright = 35 \text{ mN m}^{-1}$ and $\ast = 40 \text{ mN m}^{-1}$ .....	119
Figure 4.43:	A cartoon illustration to describe interactions of AS25 on the surface of phospholipid membrane.....	120
Figure 4.44:	The surface pressure–area ( $\Pi$ – $A$ ) isotherm of pure DPPC monolayer, and its compressibility modulus ( $C_s^{-1}$ ), spread on water subphase at 25°C.....	121
Figure 4.45:	The surface pressure–area ( $\Pi$ – $A$ ) isotherms of DPPC/BSA mixed monolayers (plotted in mole fraction of BSA), spread on a nanopure water subphase at 25°C.....	122

- Figure 4.46: The surface pressure–area ( $\Pi$ – $A$ ) isotherms of mixed monolayers of: (a) DPPC/DP (plotted in mole fraction of DPPC to DP), (b) DPPC/AS25 (nmole of AS25), and (c) DPPC/DP/AS25 (plotted in nmole of AS25), spread on a nanopure water subphase at 25°C..... 124
- Figure 4.47: The compression modulus ( $C_s^{-1}$ ) vs surface pressure ( $\Pi$ ) of mixed monolayers of DPPC/BSA (plotted in mole fraction of BSA), spread on a nanopure water subphase at 25°C..... 126
- Figure 4.48: The compressibility modulus ( $C_s^{-1}$ ) vs surface pressure ( $\Pi$ ) of mixed monolayers of: (a) DPPC/DP (plotted in mole fraction of DPPC to DP), (b) DPPC/AS25 (mole of AS25), and (c) DPPC/DP/AS25 (plotted in nmole of AS25), spread on a nanopure water subphase at 25°C..... 128
- Figure 4.49: (a) Excess mean molecular area, and (b) Gibbs free energy of mixing of DPPC/BSA mixed monolayers vs  $X_{BSA}$  on pure water subphase at 25°C. For discrete surface pressure of  $\blacksquare = 5 \text{ mN m}^{-1}$ ,  $\bullet = 10 \text{ mN m}^{-1}$ ,  $\blacktriangle = 15 \text{ mN m}^{-1}$ ,  $\blacktriangledown = 20 \text{ mN m}^{-1}$ ,  $\blacklozenge = 25 \text{ mN m}^{-1}$ ,  $\blacktriangleleft = 30 \text{ mN m}^{-1}$  and  $\blacktriangleright = 35 \text{ mN m}^{-1}$ ..... 130
- Figure 4.50: Excess mean molecular area ( $A_{ex}$ ) of (a)  $\blacksquare =$  DPPC/DP (b)  $\square =$  DPPC/AS25 (plotted in nmole of AS25), and (c)  $\bullet =$  DPPC/DP/AS25 (plotted in nmole of AS25), spread on a nanopure water subphase at 25°C..... 133
- Figure 4.51: Gibbs free energy of mixing ( $G_{mix}$ ) of (a)  $\blacksquare =$  DPPC/DOPE PEG2000 (plotted in mole ratio of DPPC to DP), (b)  $\square =$  DPPC/AS25 (plotted in nmole of AS25), and  $\bullet =$  DPPC/DP/AS25 (plotted in nmole of AS25), spread on a nanopure water subphase at 25°C..... 134
- Figure 4.52: AFM images of pure C18 fatty-acids bilayer deposited on oxidized silicon wafer at scan size of  $1 \mu\text{m} \times 1 \mu\text{m}$  with a data scale of 25 nm for: (a) stearic acid, (b) oleic acid, (c) linoleic acid, and (d) linolenic acid..... 136
- Figure 4.53: AFM images of pure DOPE PEG2000 bilayer deposited on oxidized silicon wafer obtained in scan size of (a)  $5 \mu\text{m} \times 5 \mu\text{m}$  with a data scale of 25 nm. A cross section was drawn on a selected DP molecule incorporated on the membrane depicted in (a) to obtain more information of the height and width of AS25 molecule. The height and width of this PEG were found to be approximately  $500 \text{ nm} \times 286 \text{ nm}$ , respectively as shown in (b) and (c)..... 137
- Figure 4.54: AFM images of mixed monolayers of C18 fatty acids/DP (mole ratio of 50:1) bilayer deposited on oxidized silicon wafer obtained in a  $5.0 \mu\text{m} \times 5.0 \mu\text{m}$  scan area with a data scale of 25 nm for: (a) SA/DP, (b) L1/DP, (c) L2/DP, and (d) L3/DP..... 138

Figure 4.55:	A cartoon illustration of surface topography to describe the surface roughness values, $R_a$ and $R_q$ in Table 1. (a) A flat surface of pure C18 fatty acids, owing to the identical of carboxyl head-groups of fatty acid. (b) pure DP, that PEG head-groups tend to fold on itself; (c) saturated C18 fatty acid - SA/DP, the present of PEG head-group on SA bilayer membrane creating the <i>globular</i> -like structure on the membrane surface; and (d) unsaturated C18 fatty acid - L3/DP, the polar PEG head-groups cloak around L3 polar carboxyl head-group in the membrane.....	139
Figure 4.56:	AFM images of pure BSA bilayer deposited on oxidized silicon wafer obtained in a $1.0 \mu\text{m} \times 1.0 \mu\text{m}$ scan area with a data scale of 25 nm.....	140
Figure 4.57:	AFM images of C18 fatty acids/BSA bilayer deposited on oxidized silicon wafer obtained in a $1 \mu\text{m} \times 1 \mu\text{m}$ scan area with a data scale of 25 nm for: (a) SA/BSA, (b) L1/BSA, (c) L2/BSA, and (d) L3/BSA.....	141
Figure 4.58:	AFM images of pure Anti-SNAP25 bilayer deposited on oxidized silicon wafer obtained in scan size of (a) $5 \mu\text{m} \times 5 \mu\text{m}$ with a data scale of 25 nm. A cross section was drawn on a selected AS25 molecule incorporated on the membrane depicted in (a) to obtain more information of the height and width of AS25 molecule. The height (b) and width (c) of this membrane bound protein were found to be $453 \text{ nm} \times 166 \text{ nm}$ , respectively. Protein structure predictions of AS25 from its protein sequences that it is a coiled-coil structure as illustrated in Figure 4.30, and scanned images as above showed the shape of AS25 is true as predicted.....	142
Figure 4.59:	AFM images of binary mixture of C18 fatty acids/AS25 bilayer deposited on oxidized silicon wafer obtained in a $5.0 \mu\text{m} \times 5.0 \mu\text{m}$ scan area with a data scale of 25 nm for: (a) SA/AS25, (b) L1/AS25, (c) L2/AS25, and (d) L3/AS25.....	144
Figure 4.60:	AFM images of binary mixture of C18 fatty acids/DP/AS25 bilayer deposited on oxidized silicon wafer obtained in a $5.0 \mu\text{m} \times 5.0 \mu\text{m}$ scan area with a data scale of 25 nm for: (a) SA/DP/AS25, (b) L1/DP/AS25, (c) L2/DP/AS25, and (d) L3/DP/AS25.....	146
Figure 4.61:	AFM images of binary mixture of (a) SS, (b) DSPC, and (c) DSPG bilayer deposited on oxidized silicon wafer obtained in a $5.0 \mu\text{m} \times 5.0 \mu\text{m}$ scan area with a data scale of 25 nm.....	149
Figure 4.62:	AFM images of binary mixture of (a) SS/BSA, (b) DSPC/BSA, and (c) DSPG/BSA bilayer deposited on oxidized silicon wafer obtained in a $5.0 \mu\text{m} \times 5.0 \mu\text{m}$ scan area with a data scale of 25 nm.....	151

Figure 4.63:	AFM images of binary mixture of (a) SS/AS25, (b) DSPC/AS25, and (c) DSPG/AS25 bilayer deposited on oxidized silicon wafer obtained in a $5.0 \mu\text{m} \times 5.0 \mu\text{m}$ scan area with a data scale of 25 nm.....	152
Figure 4.64:	AFM images of (a) DPPC, and (b) DPPC/DOPE PEG2000 bilayer deposited on oxidized silicon wafer obtained in a $5.0 \mu\text{m} \times 5.0 \mu\text{m}$ scan area with a data scale of 25 nm.....	154
Figure 4.65:	AFM images of binary mixture of DPPC/BSA bilayer deposited on oxidized silicon wafer obtained in a $1.0 \mu\text{m} \times 1.0 \mu\text{m}$ scan area with a data scale of 25 nm.....	155
Figure 4.66:	AFM images of (a) DPPC/AS25, and (b) DPPC/DP/AS25 bilayer deposited on oxidized silicon wafer obtained in a $5.0 \mu\text{m} \times 5.0 \mu\text{m}$ scan area with a data scale of 25 nm.....	156
Figure 4.67:	A schematic diagram illustrates the surface of (a) liposomes, (b) antibody-targeted liposomes, (c) stealth liposomes, and (d) stealth antibody-targeted liposomes.....	158
Figure 4.68:	Mean particle size of C18 fatty acids/DP liposomes: (a) L1/DP, (b) L2/DP, and (c) L3/DP for 28 days at $30^\circ\text{C}$ . For $\blacksquare$ = C18 fatty acids liposomes; the mole ratio of C18 fatty acids to DP: $\bullet$ = 0.01, $\blacktriangle$ = 0.02, $\blacktriangledown$ = 0.03, $\blacktriangleleft$ = 0.04, and $\blacktriangleright$ = 0.05 in the liposomes.....	160
Figure 4.69:	Mean zeta potential of C18 fatty acids/DP liposomes, (a) L1/DP, (b) L2/DP, and (c) L3/DP for 14 days at $30^\circ\text{C}$ . For $\blacksquare$ = C18 fatty acids liposomes; the mole ratio of C18 fatty acids to DP: $\bullet$ = 0.01, $\blacktriangle$ = 0.02, $\blacktriangledown$ = 0.03, $\blacktriangleleft$ = 0.04, and $\blacktriangleright$ = 0.05 in the liposomes.....	161
Figure 4.70:	Mean particle size of C18 fatty acids/AS25 liposomes: (a) L1/AS25, (b) L2/AS25, and (c) L3/AS25 for 28 days at $30^\circ\text{C}$ . For $\blacksquare$ = C18 fatty acids/DP liposomes; the amount of AS25: $\bullet$ = 3.36 nmole, $\blacktriangle$ = 7.40 nmole, $\blacktriangledown$ = 16.8 nmole, $\blacktriangleleft$ = 25.2 nmole incorporated into liposomes.....	166
Figure 4.71:	Mean zeta potential of C18 fatty acids/AS25 liposomes, (a) L1/AS25, (b) L2/AS25, and (c) L3/AS25 for 14 days at $30^\circ\text{C}$ . For $\blacksquare$ = C18 fatty acids liposomes; the amount of AS25: $\bullet$ = 3.36 nmole, $\blacktriangle$ = 7.40 nmole, $\blacktriangledown$ = 16.8 nmole, $\blacktriangleleft$ = 25.2 nmole incorporated into liposomes.....	167
Figure 4.72:	Mean particle size of C18 FA/DP/AS25 liposomes: (a) L1/DP/AS25, (b) L2/DP/AS25, and (c) L3/DP/AS25 for 28 days at $30^\circ\text{C}$ . For $\blacksquare$ = C18 fatty acids/DP liposomes; the amount of AS25: $\bullet$ = 3.36 nmole, $\blacktriangle$ = 7.40 nmole, $\blacktriangledown$ = 16.8 nmole, $\blacktriangleleft$ = 25.2 nmole incorporated into liposomes.....	168

Figure 4.73:	Mean zeta potential of C18 FA/DP/AS25 liposomes, (a) L1/DP/AS25, (b) L2/DP/AS25, and (c) L3/DP/AS25 for 14 days at 30°C. For ■ = C18 fatty acids/DP liposomes; the amount of AS25: ● = 3.36 nmole, ▲ = 7.40 nmole, ▼ = 16.8 nmole, ◀ = 25.2 nmole incorporated into liposomes.....	169
Figure 4.74:	Mean particle size of DPPC/DP, DPPC/AS25, DPPC/DP/AS25 liposomes for 28 days at 30°C. For ■ = DPPC liposomes; (a) the mole ratio of DPPC to DP are ○ = 20:1, ◐ = 35:1, ▽ = 50:1, ◑ = 75:1, ◒ = 100:1. (b) and (c) the amount of AS25: ● = 3.36 nmole, ▲ = 7.40 nmole, ▼ = 16.8 nmole, ◀ = 25.2 nmole incorporated into DPPC and DPPC/DP liposomes.....	171
Figure 4.75:	Mean zeta potential of DPPC/DP, DPPC/AS25, DPPC/DP/AS25 liposomes for 28 days at 30°C. For ■ = DPPC liposomes; (a) the mole ratio of DPPC to DP are ○ = 20:1, ◐ = 35:1, ▽ = 50:1, ◑ = 75:1, ◒ = 100:1. (b) and (c) the amount of AS25: ● = 3.36 nmole, ▲ = 7.40 nmole, ▼ = 16.8 nmole, ◀ = 25.2 nmole incorporated into DPPC and DPPC/DP liposomes.....	172
Figure 4.76:	Transmission electron micrographs of: (a) 1 mM L1, (b) L1/DP at mole of 50:1, (c) 1 mM L2, (d) L2/DP at mole of 50:1, (e) 1 mM L3, (f) L3/DP at mole of 50:1 liposomes at pH 7.4.....	174
Figure 4.77:	Transmission electron micrographs of: (a) 1mM L1/AS25, (b) L1/DP/AS25, (c) 1 mM L2/AS25, (d) L2/DP/AS25, (e) 1 mM L3/AS25, (f) L3/DP/AS25 liposomes at pH 7.4.....	175
Figure 4.78:	Transmission electron micrographs of: (a) 1 mM DPPC, (b) DPPC/DP at mole ratio of 50:1, (c) DP/AS25, and (d) DPPC/DP/AS25 liposomes at pH 7.4.....	176

## LIST OF TABLES

Table 1.1:	(a) Protein sequences, and (b) X-ray crystallography structure of BSA (obtained from PDB).....	9
Table 1.2:	Amino acid composition of BSA (grouped in three- and one-letter-notations).....	9
Table 1.3:	(a) Protein sequences, and (b) X-ray crystallography structure of SNAP25 (obtained from PDB).....	12
Table 1.4:	Amino acid composition of SNAP25 (grouped in three- and one-letter-notations).....	12
Table 2.1:	Liposomal drugs and vaccines available in the market. (Source obtained from <a href="https://www.quora.com/How-many-liposome-based-drugs-are-in-the-market">https://www.quora.com/How-many-liposome-based-drugs-are-in-the-market</a> was accessed on 1 October 2016).....	17
Table 3.1:	Chemical structures of C18 fatty acids, and some of their physical properties.....	27
Table 3.2:	Chemical structures of phospholipids with same chain length but different head group, and some of their physical properties.....	27
Table 3.3:	Trough area used for each lipid-lipid and lipid-protein mixtures.....	40
Table 4.1:	Surface roughness, $R_a$ of pure C18 fatty acids, DP, BSA, AS25, binary systems of C18 fatty acids/BSA, C18 fatty acids/DP, C18 fatty acids/AS25 and ternary systems of C18 fatty acids/DP/AS25 (obtained using NanoScope Analysis 1.5).....	147
Table 4.2:	Surface roughness, $R_a$ of pure phospholipids, AS25, BSA, mixed systems of phospholipids/AS25 and phospholipids/BSA (obtained using NanoScope Analysis 1.5).....	153
Table 4.3:	Surface roughness, $R_a$ of pure DPPC, AS25, and BSA, mixed systems of DPPC/DP, DPPC/BSA, DPPC/AS25, and DPPC/DP/AS25 (obtained using NanoScope Analysis 1.5).....	156
Table 5.1:	Gibbs free energy of mixing ( $G_{mix}$ ) values of C18 fatty acids/BSA and phospholipids/BSA at surface pressure of $15 \text{ mN m}^{-1}$ .....	178

## LIST OF SYMBOLS

$A_1$	mean molecular area of component 1
$A_2$	mean molecular area of component 2
$A_{12}$	ideality of mixing
$A_{ex}$	excess mean molecular area
$C_s^{-1}$	compression modulus
$F$	net downward force
$F$	force used to extend the spring
$g$	gravitation constant
$G_{ex}$	excess Gibbs free energy of mixing
$G_{mix}$	Gibbs free energy of mixing
$h_l$	depth of subphase in the trough
$k$	cantilever spring constant
$K_{ow}$	octanol-water partition coefficient
$L$	evaluation length of AFM surface profile
$l_p$	length of Wilhelmy plate
$\rho_p$	density of Wilhelmy plate material
$\rho_l$	density of subphase
$s$	extended distance of spring
$R_a$	Mean value of the surface relative to the center plane
$R_q$	rms of surface measurements of peaks and valleys
$t_p$	thickness of Wilhelmy plate
$w_p$	width of Wilhelmy plate
$x$	position of AFM surface profile
$X_1$	mole fraction of component 1
$X_2$	mole fraction of component 2
$Z$	height of AFM surface profile
$\Pi$	surface pressure
$\gamma$	liquid surface tension
$\theta$	contact angle

## LIST OF ABBREVIATIONS

AFM	atomic force microscopy
AS25	Anti-SNAP25
BSA	bovine serum albumin
BPD-MA	benzoporphyrin derivative monoacid
chol	cholesterol
CHCl <sub>3</sub>	chloroform
DDS	drug delivery system
DLS	dynamic light scattering
EPC	egg phosphatidylcholine
G	gaseous state
HPLC	high-performance liquid chromatography
HSA	human serum albumin
HSPC	hydrogenated soy phosphatidylcholine
DMPC	1,2-Dimyristoyl- <i>sn</i> -glycero-3-phosphocholine
DOPC	1,2-dioleoyl- <i>sn</i> -glycero-3-phosphocholine
DOPE	1,2-Dioleoyl- <i>sn</i> -glycero-3-phosphoethanolamine
DOPE PEG2000	1,2-dioleoyl- <i>sn</i> -glycero-3-phosphoethanolamide-N-[methoxy(polyethyleneglycol)-2000]
DP	DOPE PEG2000
DPPC	1,2-dipalmitoyl- <i>sn</i> -glycero-3-phosphorylcholine
DPPE PEG2000	1,2 dipalmitoyl- <i>sn</i> -glycero-3-phosphoethanolamine-N-[methoxy(polyethylene glycol)-2000]
DPPG	1,2-dipalmitoyl- <i>sn</i> -glycero-3-phosphoglycerol
DSPC	1,2-distearoyl- <i>sn</i> -glycero-3-phosphocholine
DSPE	1,2-Distearoyl- <i>sn</i> -glycero-3-phosphoethanolamine
DSPE PEG 2000	1,2-distearoyl- <i>sn</i> -glycero-3-phosphoethanolamine-N-[amino(polyethylene glycol)-2000]
DSPG	1,2-dioctadecanoyl- <i>sn</i> -glycero-3-phospho- <i>rac</i> -(1-glycerol)
LB	Langmuir-Blodgett
LSD	lysosomal storage diseases
L1	oleic acid
L2	linoleic acid

L3	linolenic acid
LC	liquid-condensed state
LE	liquid-expanded state
MSPC	mono steroyl phosphatidylcholine
<i>mRNA</i>	<i>microRNA</i>
PBS	phosphate buffered saline
PC	phosphatidylcholine
PDB	protein data bank
PE	phosphatidylethanolamines
PG	phosphatidylglycerol
PTA	phosphotungstic acid
<i>RNAi</i>	RNA interference
rms	root mean square
S	solid state
SA	stearic acid
<i>siRNA</i>	small interfering RNA
SNAP-25	synaptosome-associated protein of 25 kDa
SNARE	soluble <i>N</i> -ethylmaleimide-sensitive factor protein receptor
Soy PC	soy phosphatidylcholine
STM	scanning tunneling microscopy
TEM	transmission electron microscopy
TM-AFM	tapping-mode atomic force microscopy

## LIST OF APPENDICES

APPENDIX A: The American Association for the Advancement of Science License Terms and Conditions (An agreement license to reprint Figure 1.1)

University of Malaya

## CHAPTER 1: INTRODUCTION

### 1.1 Biological Membrane

In 1972, Singer and Nicolson made the important distinction between integral and peripheral membrane proteins in the fluid mosaic model of biological membranes (Singer & Nicolson, 1972). The “fluid mosaic model” was described as a fluid bilayer of phospholipids into which movable globular integral membrane proteins and glycoproteins were embedded in the biological membranes, in contrast, peripheral proteins were loosely attached or spanned on the membrane surface (Figure 1.1). They also mentioned that membrane protein were not distributed homogenously in the membrane, and their specific function may be influenced by the surrounding lipids (Singer & Nicolson, 1972).

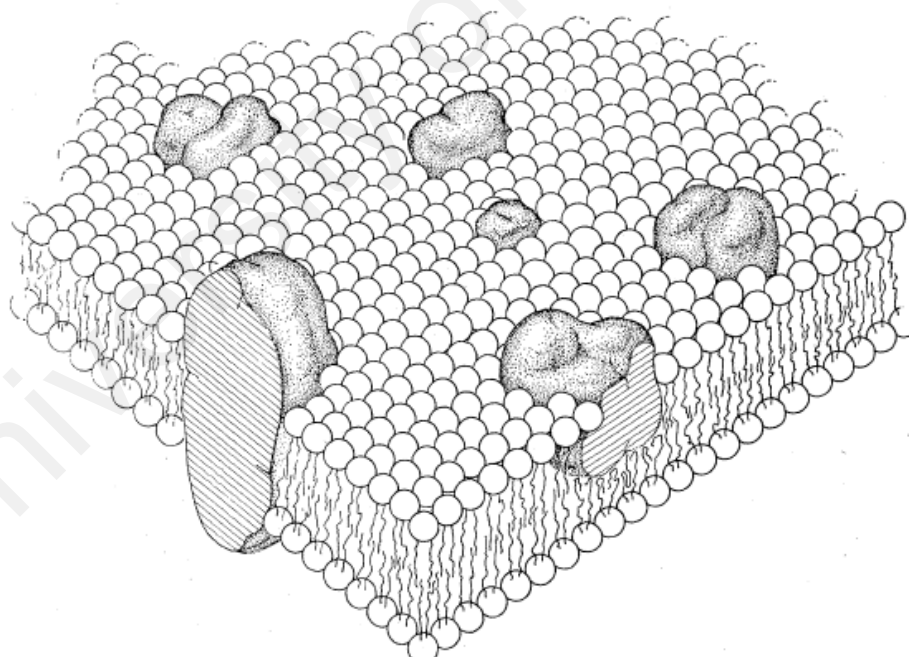


**Figure 1.1:** The “fluid mosaic model” proposed by Singer and Nicolson in 1972. (Reprinted permission granted by AAAS – Appendix A)

Biological membranes consist of two major classes of molecules: Lipid membrane and membrane proteins. Membrane lipids are mainly phospholipids forming bilayers with their hydrophobic tails by the van der Waals forces and hydrophobic

effects. Membrane proteins (such as integral or intrinsic proteins) were proposed to be globular in structure, and their interactions with membrane lipids were mainly due to hydrophobic forces, and the hydrophilic interactions between the lipid headgroups and hydrophilic side chains on proteins.

Lipid is an amphipathic structure, the hydrophobic effect from hydrocarbon tail and van der Waals interactions between the tails, and hydrogen bonding from the head group will drive the spontaneous organization into an ordered or disordered lipid bilayer membrane. In general, they consist of one or two C10-C20 hydrocarbon chains and one or more functional groups like, phosphate, hydroxyl, ester or amino in their head group. The combination of multiple head groups and hydrophobic tails gives rise to thousands of species. Lipids are soluble in organic solvents (such as chloroform) and insoluble or slightly soluble in water. When lipids are dispersed in water, it will self-assemble into lamellar and non-lamellar phases. Lamellar, or also known as bilayer, is commonly found in biological systems. In a membrane model system, lipids exhibit multiple phase transitions such as gas, liquid or solid phase, which greatly depend on their chemical compositions and temperature.

## **1.2 Lipid-protein interactions**

Lipid-protein interactions are essential for biological membrane functions (Hunte & Richers, 2008; Laganowsky et al., 2014; Lee, 2003; Lee, 2011; Singer & Nicolson, 1972). Lipid may cause a protein conformational change to bury the hydrophobic surfaces of the membrane protein within the limited thickness of the hydrophobic interior of the membrane lipid bilayer. If the protein is in a bilayer that is thinner than the hydrophobic surface of the protein, the protein may alter its conformation to accommodate the hydrophobic portion surface on the transmembrane protein better. The binding of lipid also can induce changes in membrane protein conformation and

subsequently change the membrane protein function (Camejo, Colacicco, & Rapport, 1968; Escribá et al., 2008; Hunte & Richers, 2008; Laganowsky et al., 2014; Mita, 1989; Palsdottir & Hunte, 2004). Two major type of protein's associate with lipid bilayer membrane; they are integral (intrinsic) protein and peripheral (extrinsic) protein (Figure 1.2).

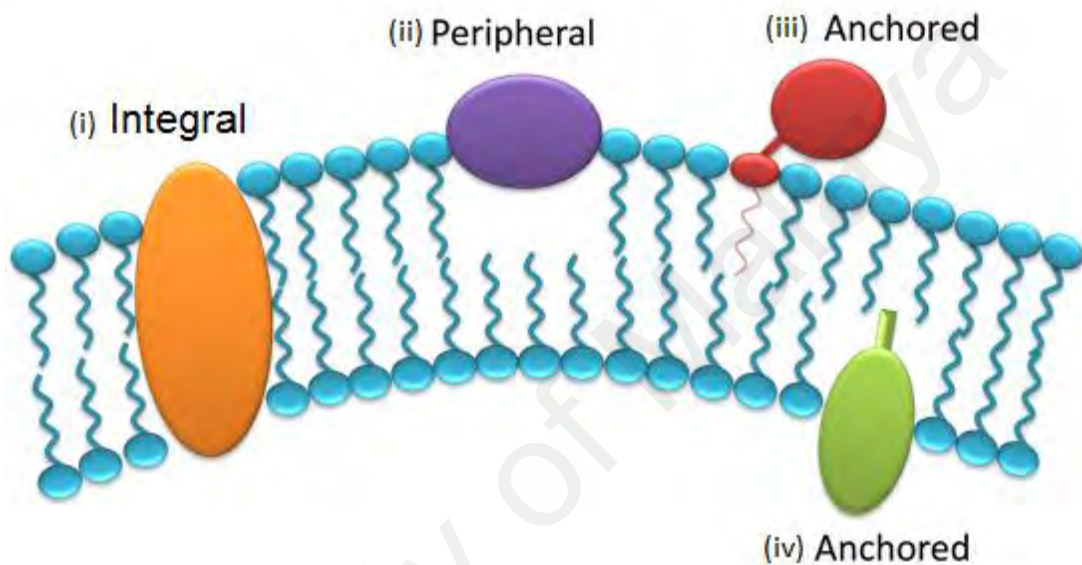


**Figure 1.2:** A schematic illustration of types of membrane proteins that associated with lipid bilayer membrane: (i) integral (intrinsic) protein, (ii) peripheral (extrinsic) protein span on the membrane surface, (iii) and (iv) lipid-linked proteins, where proteins are anchored to the surface containing sugar such as glycoproteins.

An integral membrane protein is the membrane protein that associated to the biological membrane permanently. The roles of integral membrane proteins in the biological membrane are usually as transporters, receptors, enzymes, structural membrane-anchoring domains, and also cell-adhesion proteins. Peripheral membrane proteins are the membrane proteins that are temporarily attached to the biological membrane with which they are associated. These proteins will attach to integral membrane proteins, or penetrate the peripheral regions of the lipid bilayer. They are the transmembrane receptors and regulatory protein subunits of many ion channels in the

cell membrane. Peripheral proteins are attached to the membrane surface by electrostatic interactions with lipid polar head groups. Integral proteins interact directly with the hydrophobic hydrocarbon chain of the lipid bilayer. The cohesive attraction of integral proteins on the membrane is influenced by the degree of saturation of the hydrocarbon chain. In general, membrane fluidity is affected by the length and degree of saturation in the fatty acid chains. The most common fatty acids contain 12 to 22 carbon atoms.

The key determinants for distinct functions of the biological membrane are the lipid composition and their molecular packing. Membrane protein functions are greatly influenced by membrane fluidity of lipid bilayer (Bos & Nylander, 1996; Hąc-Wydro & Dynarowicz-Lątka, 2006; Kamilya, Pal, & Talapatra, 2007; Yeagle, 2014). The binding of proteins to the membrane depends on membrane fluidity which refers to the molecular motions in the membrane. The main focus of this thesis is lipid-protein interactions, however, lipid-protein interactions will be affected by lipid-lipid interactions and protein-protein interactions in the lipid bilayer membrane. For this reason, three linked interactions must be considered in such two component systems, namely, lipid-lipid interactions, protein-protein interactions, and lipid-protein interactions.

### **1.2.1 Lipids**

Phospholipids are one of the major building blocks of biological membranes (Lingwood & Simons, 2010). They have a phosphate polar head-group bonded to two nonpolar hydrocarbon chains, which are usually fatty acids between 14-24 carbon atoms. The length and degree of saturation of fatty acid tails will influence the ability of phospholipid molecules packing, subsequently will affect the fluidity of the membrane. Some commonly found phospholipids in the membrane are

phosphatidylethanolamines (PE), phosphatidylcholine (PC), and phosphatidylglycerol (PG). PC is the last phospholipid for which there are multiple examples of binding to membrane proteins from X-ray crystallography. The headgroup of PE is a zwitterion, with a positive charged amine and a negatively charged phosphate group. It stabilizes the bilayer structure by forming a strong hydrogen bond between its two charges headgroup and the neighboring phospholipids. PC is a strong bilayer-forming lipid and the most common phospholipid in mammalian membranes. The headgroup consists of a quaternary amine (positive charge) and a phosphate (negative charge). PG is one of the typical phospholipids that contain two acyl chains esterified to glycerol, which in turn is bonded to a headgroup structure that contains net charges. It contains a negative charge phosphate in its headgroup and no other groups with compensating positive charges (the remaining structure is a glycerol); thus it contributes net negative charge to the membrane surface and lipid–protein interface. In this studies, the focus was emphasized on PC and PG headgroup, thus DSPC and DSPG were used to mimic the biological membrane to illustrate the interaction between the phospholipids' headgroup interactions with proteins.

The molecular structure of phospholipid generally consists of two hydrophobic fatty acid hydrocarbon chain. Fatty acids have a hydrophobic tail and hydrophilic headgroup, that will also form the same type of bilayer membranes. The most common fatty acids contain 12 to 22 carbon atoms. Saturated and unsaturated fatty acids with 18 carbon atoms, namely stearic acid (18:0), oleic acid (18:1), linoleic acid (18:2), and linolenic acid (18:3) (Table 1) were chosen to study their intermolecular interactions between with an integral protein and peripheral protein, respectively. The *cis*-double bonds in oleic acid (L1), linoleic acid (L2), and linolenic acid (L3) have a kink in their molecular conformation and could therefore not pack as tightly and uniformly as (Hac-Wydro, Jędrzejek, & Dynarowicz-Łątka, 2009; Hac-Wydro, Kapusta, Jagoda, Wydro, &

Dynarowicz-Latka, 2007; Kanicky & Shah, 2002; Vollhardt, 2007). They are thermodynamically unstable compared to *trans* configuration. The bends and kinks in the molecular structure may interfere with the packing of the lipid monolayer which will promote fluidity.

A number of published work have demonstrated the lipid-lipid interactions in the biomembrane by performing experiment on the interaction of fatty acids or phospholipids with cholesterol (Chou & Chang, 2000; Hąc-Wydro & Wydro, 2007; Jurak, 2013; Kim, Kim, & Byun, 2001; Korchowiec, Paluch, Corvis, & Rogalska, 2006; Makyla & Paluch, 2009; Makyla & Paluch, 2009; Yong-Hoon, Ryugo, Morio, & Tsuneo, 2004), fatty acids with different chain length (Bayrak, 2006; Kanicky & Shah, 2002; Loste, Díaz-Martí, Zarbakhsh, & Meldrum, 2003), and between fatty acids and phospholipids (Hąc-Wydro et al., 2009; Hąc-Wydro & Wydro, 2007; Hao, Sun, & Zhang, 2013; Kanicky & Shah, 2002; Makyla & Paluch, 2009). Although the understanding of biological interaction between fatty acid (and phospholipids) molecules and proteins exists to some extent (Bos & Nylander, 1996; Charbonneau & Tajmir-Riahi, 2009; Girard-Egrot, Godoy, & Blum, 2005; Kamilya et al., 2007), however the knowledge on the in-depth lipid-protein mechanisms of such system is scarce. Therefore, it would be an interest to all to understand further (i) the interactions of C18 fatty acids with the integral and membrane-bound protein on the model membranes which directly demonstrate the effect caused by the degree of saturation of the C18 fatty acids, and (ii) the effect of head group of phospholipids influence the binding of integral and membrane-bound protein on the lipid membrane.

## **1.2.2 Proteins**

### **1.2.2.1 Albumin**

Albumin is the most abundant plasma protein. Albumin is commonly found as ovalbumin (egg white), bovine serum albumin (BSA) and human serum albumin (HSA). BSA is a globular protein that is highly water soluble, biodegradable, nontoxic, and readily available at low cost. Its structural similarity to the human homologue makes it a widely studied protein, as it is often used as a protein concentration standard. BSA has 607 amino acids (Peters, 1995), which are two amino acids shorter than HSA (609) (Fanali et al., 2012). BSA sequences and its amino acid composition are presented in Table 1.1(a) and 1.2, respectively.

The tertiary protein structure of BSA (Table 1.1(b)) is formed by the interactions between the side chains of amino acids, such as hydrophobic interactions, van der Waals, electrostatics, ionic bonding, hydrogen bonding and disulfide linkages (Figure 1.3). When protein folding takes place in the aqueous solution, the hydrophobic side chains of nonpolar amino acids mostly lie in the interior of the proteins, while the hydrophilic side chains lie mostly on the surface of the proteins that interact with the aqueous environment. Cysteine, an amino acid containing a thiol group, participates in disulfide bonding to hold a tertiary structure together. Disulfide bonds in proteins are formed between the thiol-group of cysteine residues. Protein-protein interactions play a major role in studying protein folding, structure, and stability. BSA was proposed to be amphipathic with their hydrophobic domains embedded in the hydrophobic region of the lipid bilayer and some part of hydrophilic domains extended from the hydrophobic portion of the lipid bilayer into the aqueous surrounding.

Albumin is a versatile protein carrier for drug targeting and it improves the pharmacokinetic profile of peptide or protein-based drugs (Elsadek & Kratz, 2012; Kratz, 2008, 2014; Sułkowska, 2002).

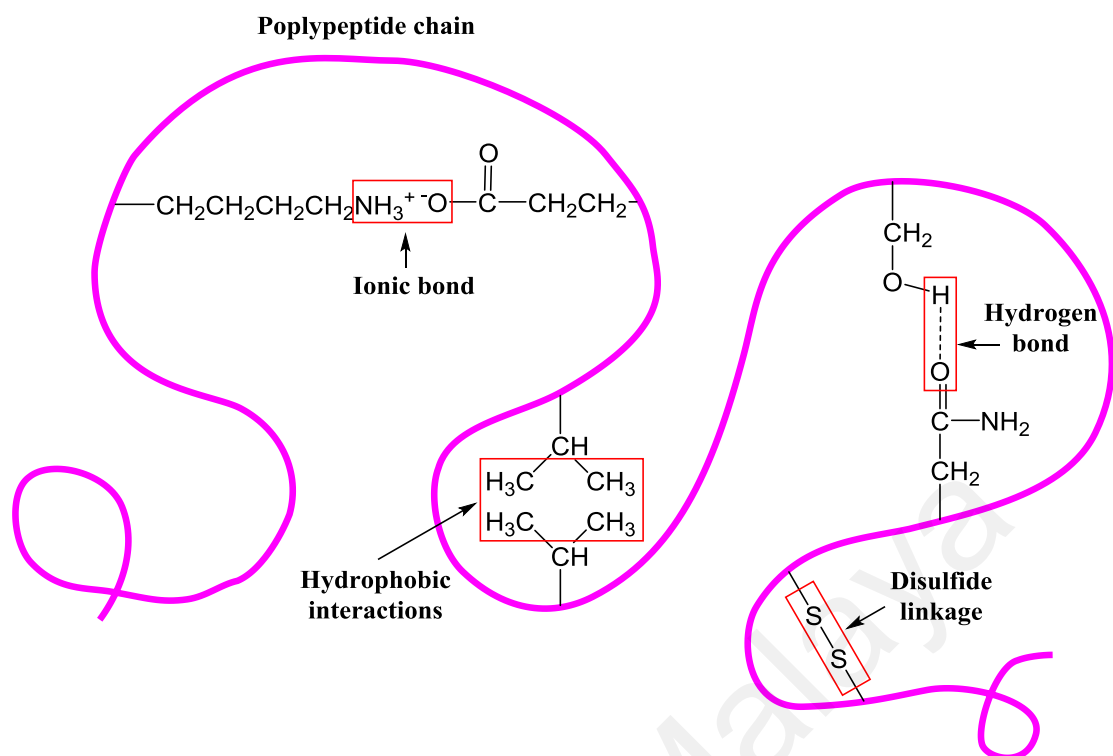


**Figure 1.3:** A schematic illustration of various interactions and forces that influence and stabilize its structures.

The charged amino acids such as lysine, arginine, aspartate and glutamate that present in the albumin molecules give rise to multiple drug binding sites for high binding capacity for various drugs that make it an excellent candidate as drug delivery system. The presence of functional groups such as carboxylic and amino groups on the albumin surface enables surface modification with various ligands such as an antibody for successive specific sites drug targeting, or polymer to prolong the release rate of the drug in the blood circulation. Albumin-binding prodrug, such as Abraxane (albumin-bound paclitaxel) delivers high concentration of paclitaxel into the cancer cells with minimized drug side effects as compared to the pure drug, it demonstrates a better approach to cancer therapy by delaying cancer cells growth and better tolerance from patients, subsequently, lengthen the patients' survival rate effectively (Desai, 2016; Gradishar et al., 2005; Miele, Spinelli, Miele, Tomao, & Tomao, 2009).

**Table 1.1:** (a) Protein sequences, and (b) X-ray crystallography structure of BSA (obtained from PDB).

(a)	10	20	30	40	50	(b)
	MKWVTFISLL	LLFSSAYSRG	VFRRDTHKSE	IAHRFKDLGE	EHFKGLVLIA	
	60	70	80	90	100	
	FSQYLQQCPF	DEHVKLVNEL	TEFAKTCVAD	ESHAGCEKSL	HTLFGDELCK	
	110	120	130	140	150	
	VASLRETYGD	MADCCEKQEP	ERNECFLSHK	DDSPDLPKLK	PDPNTLCDEF	
	160	170	180	190	200	
	KADEKKFWGK	YLYEIARRHP	YFYAPELLYY	ANKYNGVFQE	CCQAEDKGAC	
	210	220	230	240	250	
	LLPKIETMRE	KVLASSARQR	LRCASIQKFG	ERALKAWSVA	RLSQKFPKAE	
	260	270	280	290	300	
	FVEVTKLVTD	LTKVHKECCH	GDLLECADDR	ADLAKYICDN	QDTISSKLKE	
	310	320	330	340	350	
	CCDKPLLEKS	HCIAEVEKDA	IPENLPPLTA	DFAEDKDVCCK	NYQEAKDAFL	
	360	370	380	390	400	
	GSFLYEYSRR	HPEYAVSVLL	RLAKEYEATL	EECCAADDPH	ACYSTVFDKL	
	410	420	430	440	450	
	KHLVDEPQNL	IKQNCDFEK	LGEYGFQNAL	IVRYTRKVPQ	VSTPTLVEVS	
	460	470	480	490	500	
	RSLGKVGTRC	CTKPESERMP	CTEDYLSLIL	NRLCVLHEKT	PVSEKVTKCC	
	510	520	530	540	550	
	TESLVNRRPC	FSALTPDETY	VPKAFDEKLF	TFHADICTLP	DTEKQIKKQT	
	560	570	580	590	600	
	ALVELLKHKP	KATEEQLKTV	MENFVAFVDK	CCAADDKEAC	FAVEGPKLVV	
	STQTALA					

**Table 1.2:** Amino acid composition of BSA (grouped in three- and one-letter-notations).

Ala	A	48	Pro	P	28	Thr	T	34	Asn	N	14	Arg	R	26
Gly	G	17	Phe	F	30	Tyr	Y	21	Gln	Q	21	Glu	E	58
Ile	L	15	Val	V	38	Cys	C	35	Trp	W	3	His	H	16
Leu	I	65	Ser	S	32	Met	M	5	Asp	D	41	Lys	K	60

### **1.2.2.2 Anti-SNAP25 (AS25)**

AS25 is a polyclonal antibody produced in rabbits. Polyclonal antibodies are extensively used for research purposes. They are relatively inexpensive and large quantities can be produced compared to monoclonal antibodies. It is useful when the nature of the antigen is unknown, and they are nonspecific which enables them to recognize multiple epitopes on antigens. The synaptosome-associated protein of 25 kDa (SNAP-25) antibody shows expression in the neuroblastoma cell line SH-SY5Y (Glassa, Aabeb, Garcia, & Kokea, 2002), this cell line is widely used as an in vitro study model for Parkinson's disease (Cheung et al., 2009; Constantinescu, Constantinescu, Reichmann, & Janetzky, 2007; Hasegawa et al., 2003). In our future studies, we will use the findings from this work to further investigate the incorporation of such protein into liposomes for specific targeting and the delivery of encapsulated drugs.

SNAP-25 is a soluble protein with a molecular weight of 25 kDa, containing 206 amino acids (Hodel, 1998). SNAP-25 sequences and its amino acid composition are presented in Table 1.3(a) and 1.4, respectively. It is a membrane bound, presynaptic nerve terminal protein, which plays an essential role in vesicle membrane fusion events with the plasma membrane (Table 1.3(b)). In regulating neuronal exocytosis, SNAP-25 is a soluble *N*-ethylmaleimide-sensitive factor protein receptor (SNARE) protein complexes that are intrinsically water soluble, but anchored to the presynaptic plasma membrane via four cysteine-linked likely fatty acylation site, and behaves as an integral protein (James E. Rothman, 1994).

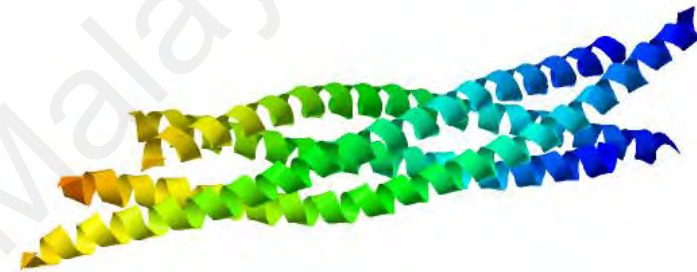
### **1.2.2.3 SNARE protein and membrane fusion**

Membrane fusion is a key process in all living cells as it facilitates the transport of molecules between and within the cells. It is essential for the entry of encapsulated

drugs into the targeted site. Membrane fusion during intracellular transport is thought to be mediated by a large family of protein known as soluble *N*-ethylmaleimide-sensitive factor protein receptors (SNARE) proteins. During exocytosis, SNARE proteins mediate vesicle fusion, where the docking and merging of neurotransmitter release into the synaptic cleft. The bulk of experiments on membrane fusion is based on SNARE proteins. Neurotoxins, such as botulinum and tetanus toxins greatly affect the performance of SNARE complexes. These toxins prevent proper vesicle fusion functions and result in poor muscle control, paralysis or even death. SNAREs are small, abundant, tail-anchored proteins which are often inserted into membrane via C-terminal transmembrane domain.

In developing a drug delivery system (DDS), it is also important to consider how to enhance the systems to be merged to cancer (or tumor) cells in order for entrance the encapsulated drug into cancer or tumor cell successfully. Membrane fusion plays a significant role in DDS in delivering the drug to the body (Joshua & Chernomordik, 1999; Marsden, Tomatsu, & Kros, 2011; James Edward Rothman, 2014; Zimmerberg, Vogel, & Chernomordik, 1993). Many fusion processes are mediated and regulated by SNARE proteins, such as, SNAP-25. It is one of the SNARE protein that has been widely studied because they induce the extremely fast release of synaptic vesicles (Cevc & Richardsen, 1999; Hodel, 1998; Ma & Bong, 2013; Marsden et al., 2011; James E. Rothman, 1994). The event of anti-SNAP25 partially embedded onto the bilayer (and subsequently liposomes) will promote fusion of liposomes on the targeted site, where protein-protein interactions between SNAP-25 and anti-SNAP25 will be taken place first on the cell membrane, which will then draw two lipid bilayers together, driving hemifusion and finally full fusion for the entry of the drugs (Cevc & Richardsen, 1999; Ma & Bong, 2013; Marsden et al., 2011; Nakamura et al., 2004).

**Table 1.3:** (a) Protein sequences, and (b) X-ray crystallography structure of SNAP25 (obtained from PDB).

(a)	10	20	30	40	50	(b)
	MAEDADMRNE	LEEMQRRADQ	LADESLESTR	RMLQLVEESK	DAGIRTLVML	
	60	70	80	90	100	
	DEQGEQLERI	EEGMDQINKD	MKEAEKNLTD	LGKFCGLCVC	PCNKLKSSDA	
	110	120	130	140	150	
	YKKAWGNNQD	GVVASQPARV	VDEREQMAIS	GGFIRRV TND	ARENEMDENL	
	160	170	180	190	200	
	EQVSGIIGNL	RHMALDMGNE	IDTQNRQIDR	IMEKADSNKT	RIDEANQRAT	
	KMLGSG					

**Table 1.4:** Amino acid composition of SNAP25 (grouped in three- and one-letter-notations).

Ala	A	16	Phe	F	2	Cys	C	4	Asp	D	19
Gly	G	14	Val	V	8	Met	M	13	Arg	R	18
Ile	L	16	Ser	S	9	Asn	N	14	Glu	E	24
Leu	I	11	Thr	T	6	Gln	Q	14	His	H	1
Pro	P	2	Tyr	Y	1	Trp	W	1	Lys	K	12

### **1.3 Application of lipid-protein interactions**

#### **1.3.1 Liposomal drug delivery systems**

Lipid systems offer good alternative to liposomes, emulsions, or microemulsions for pharmaceutical applications due to their stability and in the range of nanometer size (Laouini, Charcosset, Fessi, Holdich, & Vladisavljević, 2013; Liao, Hook, Prestidge, & Barnes, 2015; Samad, Sultana, & Aqil, 2007; Torchilin & Weissig, 2003; Torchilin, 2005). The structure and stability of colloidal dispersions depend highly on the interaction forces between colloidal particles and the confining geometries. In preparing lipid-based formulations, the lipid molecular structures and properties, such as their hydrocarbon chain lengths and degrees of saturation, their head-group sizes and charges should be considered (Samad et al., 2007). The molecular structures of lipids greatly affect the intermolecular interactions that occur between lipids and lipids, lipids and proteins, as well as lipids and the encapsulated drug in the lipid-protein-mixed system. Molecular packing and membrane fluidity are significantly influenced by the degree of saturation on the hydrocarbon chains of the lipids, the sizes of their head groups, and their charges. Lipid-lipid and lipid-protein interactions play an essential role in designing lipid-based drug delivery systems (Pisal, Kosloski, & Balu-Iyer, 2010; Weiss, Neuberg, Philippot, Erbacher, & Weill, 2011). To obtain a stable lipid-based system, such as a liposomal drug carrier, lipid selection is rather important to ensure that the lipid-drug pairing is compatible in mixed systems.

#### **1.4 Objectives of research**

- a) To compare the behaviour of albumin and anti-SNAP25 in saturated and unsaturated C18 fatty acids monolayer and their behaviour in different degrees of saturation; as well as in monolayer of phospholipids with different headgroup of phospholipids using LB technique accompanied by atomic force microscopy (AFM) imaging.
- b) To determine the intermolecular interaction of DOPE PEG2000 in C18 fatty acids and DPPC monolayer, and their liposomes.
- c) To prepare and characterize liposomes of unsaturated C18 fatty acids (and DPPC) with the incorporation of DOPE PEG2000 and AS25.

University of Malaysia

## CHAPTER 2: LITERATURE REVIEW

### 2.1 Introduction

The delivery of anticancer drugs from the blood stream to the targeted sites remains challenging in cancer therapy even with the rapid development of various drug delivery nanocarriers (Allen & Cullis, 2013; Pattni, Chupin, & Torchilin, 2015; Samad, Sultana, & Aqil, 2007). Most of the anticancer drugs are highly toxic and nonspecific delivery in the body, consequently, resulting in undesirable side-effects, organ damage, and some are likely to cause the death of patients after several times of drug administrations. In response to these challenges, numerous drug delivery systems (DDS) have been developed, including lipid-based liposomal DDS, antibody-targeted DDS and polymeric antibody-targeted DDS, and prodrugs. An efficient DDS should be able to overcome problems such as low-water solubility or lipid-solubility hydrophobic drug, poor drug stability, high toxicity of drug, harmful adverse effects, nonspecific targeting and fast clearance of drug during the delivery. Some of the marketed liposomal drugs that are currently widely used in cancer patients are listed in Table 2.1.

Phospholipids tend to form a spherical and self-closed structured bilayer membrane which is known as liposomes. Liposomes have been employed as carriers for an extensive range of therapeutic compounds and diagnostic agents, such as drug molecules (Manjappa et al., 2011; Mastrobattista, Koning, & Storm, 1999; Ng, Zhao, Liu, & Mahapatro, 2000; Park et al., 2001; Yanga et al., 2007), gene therapy (Jing, Shishkov, & Ponnappa, 2008; Qiu et al., 2015; Sakurai et al., 2013), and bioactive agents. As a DDS, liposomes offer several advantages including biocompatibility, capability for self-assembly, ability to encapsulate drugs with bigger molecule size or higher payloads of the drug, protect the encapsulated therapeutic compounds from early

clearance or degradation of during the circulation, and ease lipid surface modification to control their functions and behaviour in our biological systems.

Lipid-based liposomal DDS have been widely employed as drug carrier in cancer research studies in recent years, it offers several advantages including (Allen & Cullis, 2013; Anselmo & Mitragotri, 2014; Mishra, Patel, & Tiwari, 2010; Simone, Dziubla, & Muzykantov, 2008): (i) similar constituent as our biological membrane are made up of bilayers of phospholipid, (ii) liposomal lipid bilayer are commonly used as model the biological membrane; (iii) their dual characters enable to encapsulate both hydrophobic and hydrophilic drugs respectively in order to improve the stability of encapsulated drugs and minimize drug toxicity; (iv) surface modifications can be performed by incorporating proteins into (onto) to the lipid bilayer for specific targeting of drugs to tumor/cancer cell and promote accumulation of drugs in tumor tissues via improved permeability and retention effect; (v) the presence of polyethylene glycol (PEG) liposomal drug will prolong the drug circulation in the blood stream, offer sustainable drug release, and subsequently minimize the drug toxicity.

Liposomal DDS formulations are characterized by properties such as lipid composition, particle size, surface charge, the number of bilayers, surface modification by incorporating polymers and ligands (such as an antibody) to improve the *in vitro* and *in vivo* stability. Lipid DDS is rather versatile, it can be formed by phospholipids with different molecular structures (varying in their chain length, headgroup and degree of saturation) at various molar compositions. The surface charge of each liposome depends on the molecular composition of phospholipids in the liposome, they can be either negatively or positively charged. The presence of polymers or ligands conjugated will also contribute to the surface charge.

**Table 2.1:** Liposomal drugs and vaccines available in the market. (Source obtained from <https://www.quora.com/How-many-liposome-based-drugs-are-in-the-market> was accessed on 1 Oct 2016)

Drug/ vaccine	Brand name	Type of lipid-based DDS	Formulations	Applications	References
Doxorubicin	Myocet	non PEGylated liposomal	EPC:chol in 55:45 molar ratio	Treatment of reoccurrence of breast cancer.	(Batist, Barton, Chaikin, Swenson, & Welles, 2002; Mrozek, Rhoades, Allen, Hade, & Shapiro, 2005)
	Doxil, Caelyx	PEGylated liposomal	HSPC:chol:PEG 2000-DSPE in 56:39:5 molar ratio	Treatment of refractory Kaposi's sarcoma, reoccurrence breast cancer and ovarian cancer.	(Barenholz, 2012; Frenkel et al., 2006; Wibroe, Ahmadvand, Oghabian, Yaghmur, & Moghimi, 2016)
	LipoDox	PEGylated liposomal	DSPC:chol:PEG 2000-DSPE in 56:39:5 molar ratio		(Chou, Lin, & Liu, 2015; Hsu et al., 2014; O'Shaughnessy, 2003)
	Thermodox (Phase III of clinical trial)	PEGylated liposomal	DPPC, MSPC and PEG2000-DSPE	Treatment of primary liver cancer (Hepatocellular carcinoma) and reoccurrence chest wall breast cancer.	(K. J. Chen et al., 2012; Reddy & Couvreur, 2011)
Daunorubicin	DaunoXome	nonPEGylated liposomal	DSP:chol in 2:1 molar ratio	Treatment of Kaposi's sarcoma.	(Ermacora et al., 2000; Fassas & Anagnostopoulos, 2005; Piccaluga et al., 2002)
Amphotericin B	Ambisome	nonPEGylated liposomal	HSPC, DSPG, chol and amphotericin B in 2:0.8:1:0.4 molar ratio	Treatment of fungal infection.	(Adler-Moore & Proffitt, 2002; Fleming et al., 2001; Hay, 1994)
Vincristine	Marqibo (Phase III of clinical trial)	nonPEGylated liposomal	Egg sphingomyelin and chol	Treatment of metastatic malignant uveal melanoma.	(Cullis et al., 2007; O'Brien et al., 2010; Silverman & Deitcher, 2013)
Verteporfin	Visudyne	nonPEGylated liposomal	BPD-MA:EPG:DMPC in 1:05:3:5 molar ratio	Treatment of age-related macular degeneration, pathologic myopia and ocular histoplasmosis.	(Bressler & Bressler, 2000; Funk et al., 2006; Khurana et al., 2007)
Cytarabine	DepoCyt	nonPEGylated liposomal	Chol:Triolein:DOPC:D PPG in 11:1:7:1 molar ratio. (Also known as Depo-Foam)	Treatment of neoplastic meningitis and lymphomatous meningitis.	(Hamada, Kawaguchi, & Nakano, 2002; Phuphanich, Maria, Braeckman, & Chamberlain, 2007; Thomas, Jabbour, Kantarjian, & O'Brien, 2007)

**Table 2.1 continued**

<b>Drug/ vaccine</b>	<b>Brand name</b>	<b>Type of lipid-based DDS</b>	<b>Formulations</b>	<b>Applications</b>	<b>References</b>
Morphine sulfate	DepoDur	nonPEGylated liposomal	Depo-Foam	Epidural administration for treatment of postoperative pain following major surgery.	(Carvalho, Roland, Chu, Campitelli Iii, & Riley, 2007; Gambling et al., 2005; Nagle & Gerancher, 2007)
Amikacin	Arikace (Phase III of clinical trial)	nonPEGylated liposomal	DPPC and chol	Treatment of lung infections due to susceptible pathogens. (Arikace is to be inhaled by the patients in form of nebulizer)	(Ehsan, Wetzel, & Clancy, 2014; Singh, Prateeksha, Rawat, Upreti, & Singh, 2015; Stockmann, Roberts, Yellepeddi, & Sherwin, 2015)
Cisplatin	Lipoplatin	PEGylated liposomal	DPPG, Soy PC, chol and PEG2000-DSPE	Treatment of epithelial malignancies such as lung, head and neck, ovarian, bladder and testicular cancers.	(Andrews & Howell, 1990; Markman et al., 2001; Zamble & Lippard, 1995)
Paclitaxel	LEP-ETU	nonPEGylated liposomal	DOPE, chol and cardiolipin	Treatment of lung, breast and ovarian cancer.	(Miele, Spinelli, Miele, Tomao, & Tomao, 2009; Yan et al., 2013; Yoshizawa, Kono, Ogawara, Kimura, & Higaki, 2011)
Hepatitis A vaccine	Epaxal	nonPEGylated liposomal	Inactivated HAV (strain RG-SB) is conjugated on liposomal DOPC/DOPE in 75:25 molar ratio	Vaccination to prevent Hepatitis A infections.	(Ambrosch et al., 1997; Patrick A Bovier, 2008; Ott, Irving, & Wiersma, 2012)
Influenza vaccine	Inflexal V	nonPEGylated liposomal	Conjugation of inactivated influenza virosomes to liposomal DOPC/DOPE in 75:25 molar ratio	Vaccination to prevent influenza infections.	(Herzog et al., 2009; Kürsteiner, Moser, Lazar, & Durrer, 2006; Mischler & Metcalfe, 2002)

There are several ways to prepare liposomes such as thin lipid film hydration method (J. Chen et al., 2014; Isailović et al., 2013; Liau, Hook, Prestidge, & Barnes, 2015; Patil & Jadhav, 2014; Wang et al., 2014), reverse phase evaporation technique (Akbarzadeh et al., 2013; Cortesi et al., 1999; Pattni et al., 2015), and ethanolic injection (Gentine, Bourel-Bonnet, & Frisch, 2013; Jaafar-Maalej, Diab, Andrieu, Elaissari, & Fessi, 2010; Laouini, Charcosset, Fessi, Holdich, & Vladislavljević, 2013; Maitani, Soeda, Junping, & Takayama, 2001; Pons, Foradada, & Estelrich, 1993). Thin lipid film hydration is the most widely in preparing liposomes. It can be performed by drying a lipid solution from an organic solvent (such as chloroform) in a round bottom flask using rotary vacuum evaporator, and then hydrate the lipid layers in buffer aqueous solutions. Sonicate to detach the lipid layers from the surface of the flask and multilamellar vesicles will form. The suspension will be then top up with buffer solution to obtain desired concentration. Reverse phase evaporation method will produce inverted micelles. Firstly, a water-to-oil emulsion is formed by sonication of lipid in a mixture organic solvent and aqueous buffer solution. The removal of organic solvent by rotary evaporation under reduced pressure resulting in gel formation. Large unilamellar vesicles will form by this method, consequently may result in a higher drug encapsulation efficiency and capable of encapsulating macromolecules such as therapeutic proteins. Ethanolic injection is carried out by rapidly injecting a lipid solution into an aqueous buffer solution. Multilamellar vesicles will be first formed, and then sonicated to obtain the uniform size of liposomes.

In the recent years, lipid-based drug formulation systems are actively developed to help overcome the limitations of therapeutic proteins. The conventional liposomes have evolved to highly responsive delivery vehicles with active/passive targeting, increased stealth, and controlled drug-release ability (Chatin et al., 2015; Jain et al., 2013; Pisal, Kosloski, & Balu-Iyer, 2010). In this review, the focus on lipid-based DDS

for various therapeutic proteins delivery in the blood stream will be discussed. Lipid-based DDS seems to be promising to overcome the current limitations of protein therapeutics. Therapeutic proteins of interest can be either encapsulated in the liposome or chemically conjugated to the surface group, thus help to protect them from degradation, rapid excreted or metabolized, fast elimination in the blood stream, protein-protein aggregation, slow release, and offer target delivery to the desired location as well.

## **2.2 Liposomes in protein delivery**

Proteins and peptides are important bioactive macromolecules that offer numerous advantages of highly specific and effective therapeutic mechanisms of action. Peptides are small high-specific biomolecules acting as substrates, inhibitors or regulators that play important roles in monitoring biological functions (Weiss, Neuberg, Philippot, Erbacher, & Weill, 2011). Insulin, a peptide hormone is among the most widely used drugs. Due to the physiochemical properties, peptides have limited ability to cross the cell membrane to reach their intracellular target site; hence, most peptides need to be entrapped into nanoscale delivery systems to efficiently aid their intracellular delivery efficiently. Protein therapeutics are limited by several pharmaceutical issues, such as high molecular weight, *in vitro* and *in vivo* short half-lives which cause side effects such as immunogenicity resulted from repeatable injections of rapidly degradable protein drugs over a long diagnostic period, and lack of an effective way to deliver functional proteins across plasma membrane to apply their therapeutic action due to their large molecular size and biochemical properties (Martins, Sarmiento, Ferreira, & Souto, 2007; Pisal et al., 2010; Rawat, Singh, Saraf, & Saraf, 2008). Therapeutic proteins such as antibody can be conjugated onto the surface of liposome; nuclei acids (such as DNA or

siRNA), virus antigen, therapeutic enzyme can be encapsulated into liposomes as illustrated in Figure 2.1.

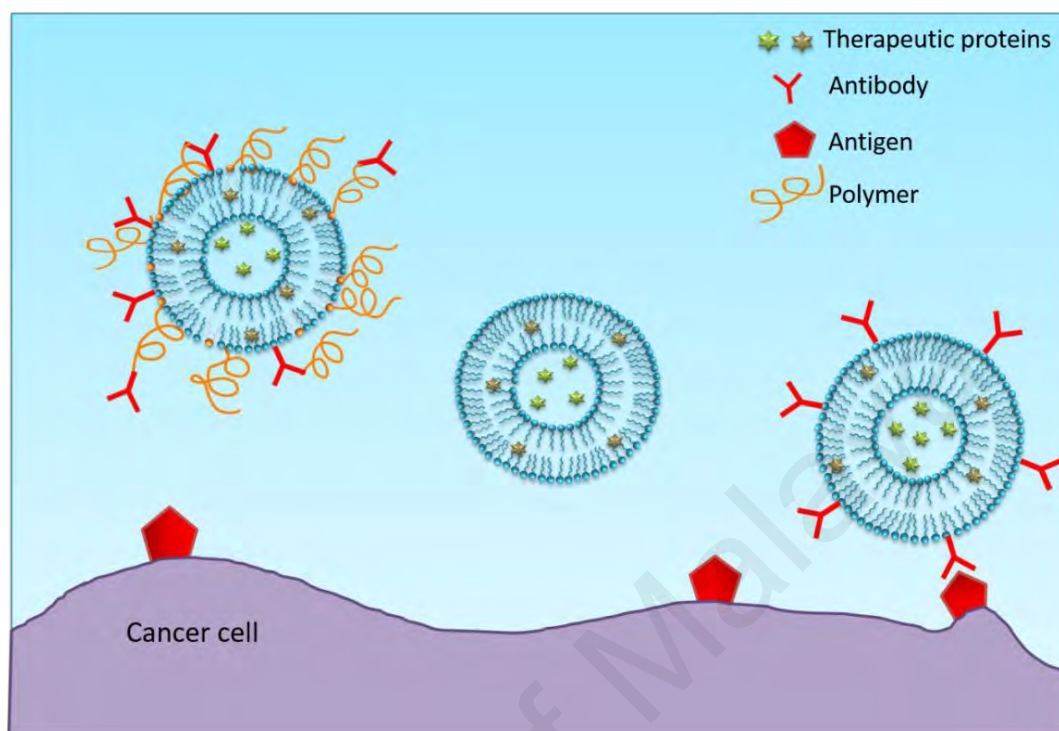


**Figure 2.1:** An illustration of the role of liposomes in various therapeutic proteins delivery such as antibody, nucleic acid, virus antigen and therapeutic enzyme for an effective delivery.

### 2.2.1 Immunoliposomes (Antibody-targeted liposomes)

Antibody-targeted liposomes are made by conjugating antibodies to the lipid bilayer of a liposome surface which promotes a specific interaction with the cancer cells (Chang & Yeh, 2012; Chonn & Cullis, 1998; Mastrobattista et al., 1999; Torchilin, 2005). Pharmacokinetic analysis and therapeutic studies revealed that antibody-targeted liposomes have considerable potential to be used as a DDS for cancer therapy. It optimizes efficiently the delivery of the drug to the tumor cells, reduces the exposure of highly toxic anticancer drug to healthy cells, and minimizes side effects (Debottona, Parnesa, Kadoucheb, & Benita, 2005; Laginha, Mumbengegwi, & Allen, 2005; Lundberga, Griffithsb, & Hansen, 2004; Park et al., 2001). Some methods have been

reported for coupling or conjugating antibodies or their fragments to the surface of liposomes.

### **2.2.2 Gene delivery**

Gene therapy is a therapeutic method using nucleic acid as agents to the delivery genetic material into cells to alter the functions in the living organism. Genetic materials such as small interfering RNA (siRNA) is one of the widely used RNA interference (RNAi) tool to temporarily silence multiple (or specific) genes of interests simultaneously. It can be artificially designed and synthesized according to the sequence of the target microRNA (mRNA), and its ability to regulate gene expression in cell proliferation and metastasis. These features certainly favourable to treat numerous genetic diseases and cancers (Aliabadi & Uludağ, 2016; Burnett, Rossi, & Tiemann, 2011; Kim, Kim, Miyata, & Kataoka, 2016; Komano, Yagi, & Nanki, 2015; Tokatlian & Segura, 2010; Uludağ, Landry, Valencia-Serna, Remant-Bahadur, & Meneksedağ-Erol, 2016). However, siRNA is not stable, easily degraded by protein in blood serum and poor cell membrane permeability due to its large molecular size and highly polar negative charged properties (Sakurai et al., 2013; Xia, Tian, & Chen, 2016; Xu & Wang, 2015). Hence, an effective carrier for siRNA for therapeutic purposes is essential to prolong its lifespan in the blood circulation, better cell membrane penetration to reach the cancerous cells. In order to overcome the obstacles in siRNA delivery, many researchers employed delivery carriers such as liposomes, cationic polymers, and gold nanoparticle. Among all the carriers, biocompatibility and nontoxic liposome are the most extensively used in siRNA delivery (Pattni et al., 2015; Sarisozen, Salzano, & P Torchilin, 2016; Sarisozen, Salzano, & Torchilin, 2015), in particular those composed of cationic lipids. Cationic liposomes have been proven to be an efficient vehicle for delivery of anionic siRNA to the negatively charged cell membrane (Xia et al., 2016). siRNA delivery by liposomes

has proven to overcome some drawbacks of gene therapy, such as stability in blood serum, longer circulation time, and effective cell membrane penetration (Komano et al., 2015; Pattni et al., 2015; Sakurai et al., 2013; Sarisozen et al., 2016; Uludağ et al., 2016; Xia et al., 2016).

### **2.2.3 Virus antigen delivery**

Liposomal DDS has also received attention as potential delivery vehicles for vaccine antigens which can both stabilize vaccine antigens and act as adjuvants to prolong the life span of vaccine thus minimize the foreign disturbance materials during the delivery in the blood stream (Gregory, Williamson, & Titball, 2013). The biocompatible lipids mimicking biological bilayer membrane enable it to enter antigen-presenting cells (such as macrophages and B-lymphocytes) by various pathways and also modulate their immune response. Their biodegradable and biocompatibility properties also make them suitable for the delivery of antigens at mucosal surfaces and intradermal administration.

Virosomes are liposome with incorporated virus-derived proteins that serve as vaccine or adjuvants, and delivery carriers for bioactive materials such as drugs, or gene for therapeutic purposes. Virosomes are biocompatible, biodegradable, nontoxic, and non-autoimmunogenic. Inflexal V is the first virosomal adjuvant influenza vaccines made available in the market in 1997 for a human at all age (Herzog et al., 2009). Another marketed virosome vaccine is Epaxal® for hepatitis A virus (HAV) (P. A. Bovier, 2008). Both vaccines show excellent tolerability and highly immunogenic in healthy and affected patients. Epaxal® protects up to 9-10 year in the vaccinated individual.

#### **2.2.4 Therapeutic enzyme delivery**

Enzymes are biological catalysts that speed up various biological reactions. They involve in all processes such as metabolisms, protein synthesis, DNA replication and transcription. A little change in their structure conformation may lead to the loss of their specific activity and mechanism.

Lysosomal storage diseases (LSD) are genetically inherited diseases caused by specific enzyme deficiencies that caused by the accumulation of non-hydrolyse substances in lysosomes. Lysosomes are membrane-bound vesicles that contain of digestive enzymes such as glycosidases, proteases, and sulfatases. They are responsible for breaking down the biomolecules such as carbohydrates, proteins (or peptides), nuclei acid and lipids into small molecules that can be used by the cell. Gaucher's disease is one of the most common LSD, it occurs due to deficiencies of enzyme glucocerebrosidase that lead to the build-up of glycolipid glucocerebroside in the liver, spleen, bone marrow, and some exceptional case, the brain. Consequently, it causes bone lesions, enlargement of liver and spleen, and some will suffer from severe neurological problems.

The most recent and promising therapy for Gaucher's disease is enzyme replacement therapy, but enzymes are generally unstable in the blood stream; therefore frequent administration is required which subsequently lead to immunogenicity issues (Martín-Banderas et al., 2016). To overcome these limitations, many investigators carried out liposome-based enzyme delivery by using liposomes specifically targeted to lysosomes. The use of liposome encapsulated therapeutic enzymes has been considered as a promising way to improve enzyme replacement therapy for more than 30 years (Gregoriadis, 1978). The applications of modified liposomes in therapeutic delivery enzymes significantly increased the delivery of encapsulated enzymes into lysosomes

for the treatment of LSD (Korablyov, Zimran, & Barenholz, 1999; Martín-Banderas et al., 2016; Suzuki, 2013; Thekkedath, Koshkaryev, & Torchilin, 2013).

### **2.3 Conclusions**

The rapid development of lipid-based carrier systems seems to be promising to overcome the challenges of therapeutic proteins delivery. Liposomes exhibit numerous advantages in term of amphiphilic characters, biocompatibility, reduced toxicity of the encapsulated drug, and the ease of surface modifications for targeted delivery and prolong circulations in the blood stream. Liposomal DDS with encapsulated proteins and peptides may improve the pharmacokinetic performance and therapeutic efficacy of these therapeutics molecules in the biological systems.

University of Malaya

## CHAPTER 3: MATERIALS AND METHODS

### 3.1 Introduction

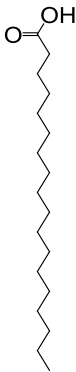
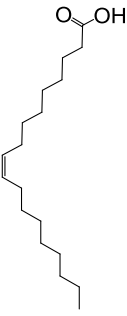
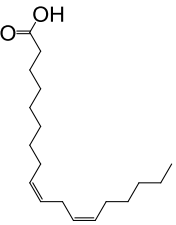
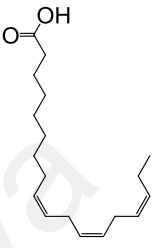
The lipids, proteins and solvents used in this study are listed in this chapter. The purities and sources of these substances will be stated as references. All of them were used as received without further purification. Solvents were double-distilled at the respective boiling point before used. Instrumentations, important calculations for data analysis, and methods performed in this work will be explained in detail.

### 3.2 Materials

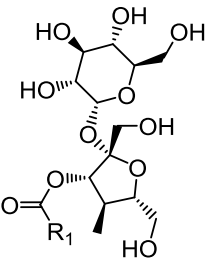
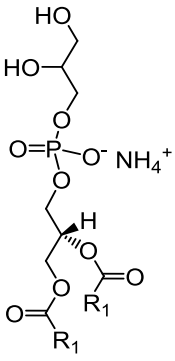
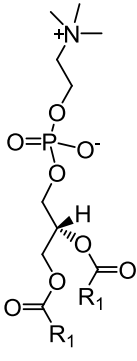
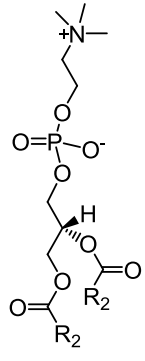
#### 3.2.1 Lipids

C18 fatty acids, such as stearic acid, (octadecenoic acid,  $\geq 95\%$ ), oleic acid (*cis*-9-octadecenoic acid,  $\geq 99\%$ ), linoleic acid (*cis*, *cis*-9,12-octadecadienoic acid,  $\geq 99\%$ ), linolenic acid (*cis*, *cis*, *cis*-9,12,15-octadecatrienoic acid,  $\geq 99\%$ ), and phospholipids, such as DPPC (1,2-dipalmitoyl-*sn*-glycero-3-phosphorylcholine, semisynthetic,  $\geq 99\%$ ), DPSC (1,2-distearoyl-*sn*-glycero-3-phosphocholine,  $\geq 99\%$ ), and DSPG (1,2-dioctadecanoyl-*sn*-glycero-3-phospho-*rac*-(1-glycerol) ammonium salt,  $\geq 98\%$ ) were purchased from Sigma-Aldrich (Palo Alto, CA, USA). SS (sucrose stearate) was purchased from Ark Pharm, Inc. (USA). The chemical structures and some of the physical properties of C18 fatty acids and phospholipids as above are listed in Table 3.1 and 3.2, respectively. 1,2-dioleoyl-*sn*-glycero-3-phosphoethanolamide-N-[methoxy(polyethyleneglycol)-2000] (ammonium salt), DOPE PEG2000 (molecular weight of 2801.47 amu) were purchased from Avanti Polar Lipids, USA. It is a white powder and kept at  $-20^{\circ}\text{C}$  freezer when not in use.

**Table 3.1:** Chemical structures of C18 fatty acids, and some of their physical properties.

Name	Stearic acid (18:0)	Oleic acid (18:1)	Linoleic acid (18:2)	Linolenic acid (18:3)
Molecular structure				
Molecular formula	$C_{18}H_{36}O_2$	$C_{18}H_{34}O_2$	$C_{18}H_{32}O_2$	$C_{18}H_{30}O_2$
Molecular weight	284.48 g mol <sup>-1</sup>	282.46 g mol <sup>-1</sup>	280.45 g mol <sup>-1</sup>	278.44 g mol <sup>-1</sup>
Physical state	Solid	liquid	liquid	liquid
Density	0.941 g ml <sup>-1</sup>	0.895 g ml <sup>-1</sup>	0.902 g ml <sup>-1</sup>	0.916 g ml <sup>-1</sup>
Boiling point	232.0°C	360.0°C	229.0°C	230.0°C
Melting point	69.3°C	13.5°C	-5.0°C	-11.0°C

**Table 3.2:** Chemical structures of lipids with same chain length but different head group, and some of their physical properties.

Name	SS	DSPG	DSPC	DPPC
Molecular structure				
Molecular formula	$C_{30}H_{56}O_{12}$	$C_{38}H_{78}NO_{10}P$	$C_{44}H_{88}NO_8P$	$C_{40}H_{80}NO_8P$
Molecular weight	608.76 g mol <sup>-1</sup>	740.00 g mol <sup>-1</sup>	790.16 g mol <sup>-1</sup>	734.039 g mol <sup>-1</sup>
Physical state	Solid	Solid	Solid	Solid

### 3.2.2 Proteins

BSA (albumin fraction V, white powder,  $\geq 98\%$ ) were purchased from Carl Roth GmbH, Karlsruhe, Germany. AS25 is supplied as an IgG fraction of antiserum (using the rabbit as host species) in 0.1 M phosphate-buffered saline, pH 7.4, containing 15 mM sodium azide as a preservative. It is stored in  $-20^{\circ}\text{C}$  freezer. BSA and anti-SNAP25 protein sequences, X-ray crystallography structure that obtained from Protein Data Bank (PDB), and their amino acid compositions are presented in Chapter 1.

### 3.2.3 Chemicals and solvents

Analytical grade chloroform was purchased from Merck, USA, and used throughout the experiment to dissolve all the lipids. Liquid chloroform ( $\text{CH}_3\text{Cl}$ ) was double-distilled at its boiling point ( $61.2^{\circ}\text{C}$ ) before use. High-performance liquid chromatography (HPLC) grade of methanol and 1-octanol were purchased from Merck and Fluka, respectively. Absolute ethanol (AnalaR NORMAPUR<sup>®</sup> VWR, Radnor, PA, USA) was double distilled at its boiling point ( $78.3^{\circ}\text{C}$ ) before we use it to prepare DPPC liposomes by ethanol injection method. Phosphate buffered saline (PBS) tablets was purchase from Sigma Aldrich. One tablet of PBS completely dissolved in 200 ml of distilled water will yields 0.01 M PBS (pH 7.4) at  $25^{\circ}\text{C}$ . Phosphotungstic acid (PTA) hydrate for transmission electron microscopy (TEM) negative staining was purchased from Fluka and stored in the desiccator when not in use.

Double-distilled water processed using NANOpure Diamond Ultrapure Water System (Barnstead International, USA) was used as water subphase throughout (Resistivity  $18\text{ M}\Omega\text{ cm}^{-1}$ ).

### 3.3 Instrumentations

#### 3.3.1 Langmuir-Blodgett technique

The Langmuir-Blodgett (LB) device is an efficient and effective instrument in investigating floating monolayer, precise deposition of monolayer (or multilayer) onto solid substrates, and also as a platform for use in observing surface chemistry in various area, such as lipid-protein interactions in the biological membrane (Brezesinski & Möhwald, 2003; Dynarowicz-Łątka, Dhanabalan, & Oliveira Jr, 2001; Hąc-Wydro & Dynarowicz-Łątka, 2008; Stefaniu, Brezesinski, & Möhwald, 2014).

Monolayers are usually produced from amphiphilic molecules. The surface pressure and mean molecular area of the monolayer are continuously measured by Wilhelmy plate-method. Throughout the experiment, the suspended Wilhelmy plate is partially immersed in the subphase. The force contributed by surface tension of the monolayer is measured by microbalance. Forces acting on the plate consist of the gravity and surface tension downward, and buoyancy due to displaced water upward.

For a rectangular Wilhelmy plate of dimensions  $l_p$ ,  $w_p$ , and  $t_p$ , of material density  $\rho_p$ , immersed to a depth  $h_l$  in a liquid of density  $\rho_l$ , the net downward force,  $F$  is given by the following equation:

$$F = \rho_p g l_p w_p t_p + 2\gamma(w_p t_p)(\cos\theta) - \rho_p g w_l t_l h_l \quad (1)$$

Where  $\gamma$  is the liquid surface tension,  $\theta$  is the contact angle of the liquid on the solid plate and  $g$  is the gravitation constant. The surface pressure is then determined by measuring the change in force for a Wilhelmy plate in a subphase only and a subphase with a monolayer present. For completely wetted plate ( $\theta_c = 0$ , therefore  $\cos\theta = 1$ ) the surface pressure can be obtained from the equation:

$$\Pi = - \gamma = \left[ \frac{-F}{2(t_p + w_p)} \right] = \left[ \frac{-F}{2w_p} \right], \text{ if } W_p \gg t_p \quad (2)$$

### 3.3.3.1 Surface pressure–mean molecular area ( $\Pi$ – $A$ ) isotherms

A computer-controlled Langmuir balance (KSV 5000, Langmuir System, Helsinki, Finland) equipped with symmetric barriers and Teflon trough was used to determine the  $\Pi$ – $A$  isotherms (Figure 3.1). The surface pressure of the films was measured to an accuracy of  $\pm 0.1 \text{ mN m}^{-1}$  using a flame cleansed high-purity platinum metal Wilhelmy plate (19.62 mm  $\times$  10 mm) of 39.80-mm total length. The trough was filled with water ( $25^\circ\text{C} \pm 0.1^\circ\text{C}$ ) serving as the subphase.

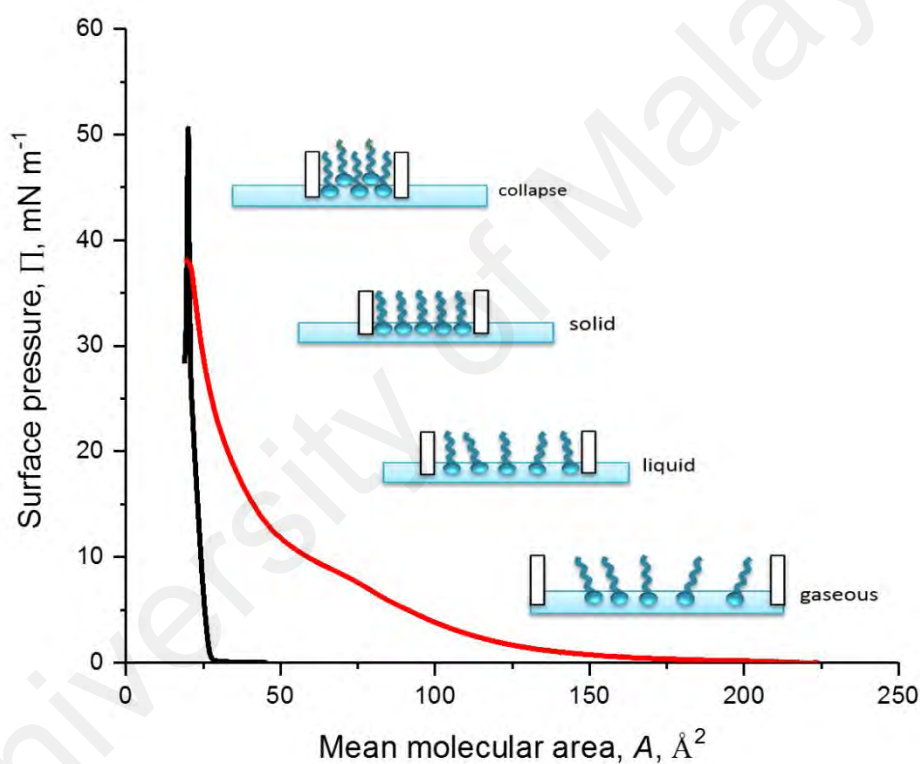


**Figure 3.1:** A schematic representation of surface pressure–mean molecular area ( $\Pi$ – $A$ ) isotherm of Langmuir film and molecular in different phases.

A simple terminology used to classify different monolayer phases of fatty acids has been proposed by W.D. Harkins as early as 1952. At large the monolayers exist in the gaseous state (G) and can on compression undergo a phase transition to the liquid-expanded state (LE). Upon further compression, the LE phase undergoes a transition to the liquid-condensed state (LC), and at even higher densities the monolayer finally

reaches the solid state (S). If the monolayer is further compressed after reaching the S state, the monolayer will collapse into three-dimensional structures. The collapse is generally seen as a rapid decrease in the surface pressure or as a horizontal break in the isotherm if the monolayer is in a liquid state (Figure 3.1).

### **3.3.1.2 Deposition of monolayer on a substrate**

LB technique is the best methods for the preparation of thin film as it enables deposition of the monolayer over large area homogenously, and multilayer structures with the same or different layer of molecules composition (Figure 3.2(a)). This is accomplished by successively dipping a solid substrate up and down through the monolayer while simultaneously keeping the surface pressure constant by a computer controlled feedback system at the desired surface pressure. Consequently, the floating monolayer is adsorbed to the solid substrate. In this way multilayer structures of hundreds of layers can be produced. These multilayer structures are commonly known as LB films.

Different kind of LB multilayers can be produced and/or obtained by successive deposition of monolayers on the same substrate (Figure 3.2(b)). The most common one is the Y-type multilayer (Figure 3.2(c)), which is produced when the monolayer deposits to the solid substrate in both up and down directions. When the monolayer deposits only in the up or down direction the multilayer structure is called either Z-type or X-type (Figure 3.2(c)).

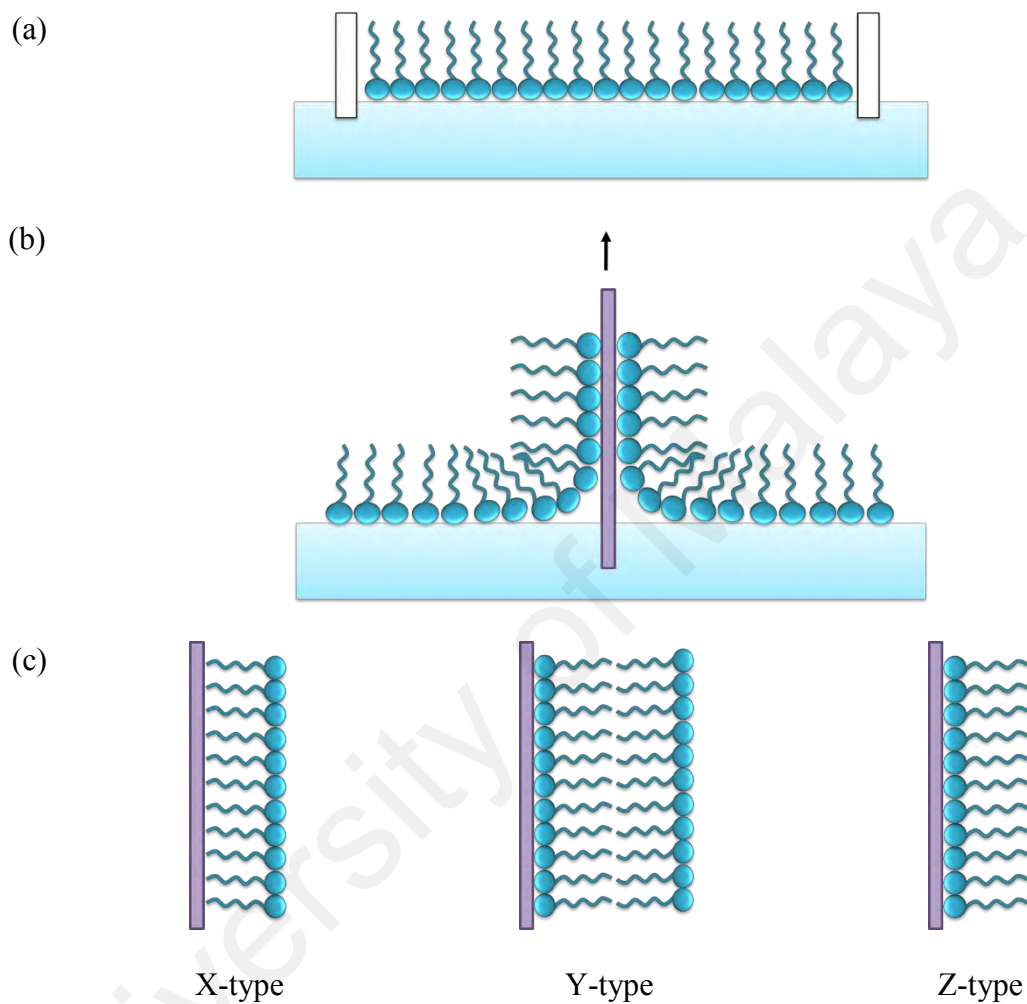


**Figure 3.2:** (a) Langmuir monolayer, (b) deposition of LB film onto solid substrate, (c) various LB deposition onto solid substrate, X-type is obtained when the sample's tails are deposited hydrophobic surface of substrate, Y- and Z-type is obtained when sample's headgroups are deposited on hydrophilic surface of substrate, in contrast Y is bilayer, and Z is monolayer.

### 3.3.1.3 Precaution steps when handling LB

- a) The microbalance is calibrated at least every six months by using a pre-weighed metal ring.
- b) While handling the trough and barriers, wear rubber gloves to minimize oils from the skin contaminating the apparatus. Clean the trough and barriers with pure ethanol using a soft brush and then rinse with NANOpure water.
- c) The most thorough way to clean the Wilhelmy platinum plate is with a hot flame (or Bunsen burner).
- d) The purity of the water in the trough can be determined by zeroing the reading of the balance at the maximum distance of the barriers and then bring them closer together. It is satisfactorily clean if the surface pressure shown does not more than  $0.3 \text{ mN m}^{-1}$ . If the water surface contains contaminants, remove them by sucking on the surface of water with an aspirator.

### 3.3.1.4 LB data analysis

The obtained  $\Pi$ - $A$  isotherms will be analyzed by the following equations (Davies & Rideal, 1963; Gaines, 1966).

Firstly, the packing density of monolayers will be evaluated and analyzed by the compression modulus  $C_s^{-1}$ , which is defined as,

$$C_s^{-1} = -A \left( \frac{d\Pi}{dA} \right) \quad (3)$$

$C_s^{-1}$  versus  $\Pi$  curves provide detailed information on the phase transitions of mixed monolayers.  $C_s^{-1}$  can be classified into various phases, namely (a) liquid-expanded (LE) phase at surface pressures in the range from 10 to 50  $\text{mN m}^{-1}$ , (b) liquid (L) phase from 50 to 100  $\text{mN m}^{-1}$ , (c) liquid-condensed (LC) phase from 100 to 250  $\text{mN m}^{-1}$ , and (d) solid (S) phase above 250  $\text{mN m}^{-1}$ . In this work, the compression moduli were obtained

by numerical calculations of the first derivative from the isotherm data points using the OriginPro 2017 program.

Secondly, the miscibility of the mixed monolayer components can be determined by calculating the mean molecular area  $A_{12}$ . For ideality of mixing,  $A_{12}$  is defined as

$$A_{12} = A_1X_1 + A_2X_2 \quad (4)$$

where  $A_1$  and  $A_2$  are the mean molecular areas of single components at the same surface pressure and  $X_1$  and  $X_2$  are the mole fractions of components 1 and 2 in the mixed film. Quantitatively these deviations can be described with the excess mean molecular area values,  $A_{ex}$

$$A_{ex} = A_{12} - (A_1X_1 + A_2X_2) \quad (5)$$

Non-linear plots of  $A_{ex}$  showed the existence of interactions between the molecules in the monolayer.

Furthermore, molecular interactions can be expressed quantitatively in the thermodynamic analysis. Total Gibbs free energy of mixing  $G_{mix}$  is defined by the following equation:

$$G_{mix} = G_{id} + G_{ex} \quad (6)$$

Where

$$G_{id} = RT(X_1 \ln X_1 + X_2 \ln X_2) \quad (7)$$

And the excess Gibbs free energy of mixing  $G_{ex}$  can be calculated from  $\Pi$ - $A$  isotherms by

$$G_{ex} = \int_0^{\Pi} [A_{12} - (X_1A_1 - X_2A_2)]d\Pi \quad (8)$$

where  $A_{12}$ ,  $A_1$  and  $A_2$  represent the area of the mixed system and respective areas of components as 1 and 2, and  $\Pi$  is the surface pressure of monolayer. If the monolayer is ideally mixed,  $G_{ex}$  should be zero.

### **3.3.2 Atomic force microscopy (AFM)**

Scanning probe techniques, namely scanning tunneling microscopy (STM) and AFM has become useful tools to characterize and fabricate nanoscale surface structures of biological surfaces. AFM provides a numerous advantage over conventional microscopy techniques, such as probe the sample and make measurements in three dimensions,  $x$ ,  $y$ , and  $z$ , thus enabling the presentation of three dimensional images of a sample surface morphology (Blanchard, 1996).

One of the widely used applications of AFM is imaging of mono- and bilayer. It can be used to investigate structural properties of LB and self-assembled films since the surface potential is strongly dependent on the molecular packing and orientation. Furthermore, useful structural information can be obtained including accurate determination of film height, elucidation of domain structure and formation (Cohen & Bitler, 2008).

The development of tapping mode enabled researchers to image fragile samples not to tolerate the lateral forces caused by contact mode, yet, use a higher scan speed than that could be obtained in non-contact mode. Tapping-mode atomic force microscopy (TM-AFM) maps topography by lightly tapping the surface with an oscillating probe tip. The cantilever's oscillation amplitude changes with sample surface topography, and the topography image is obtained by monitoring these changes and closing the  $z$  feedback loop to minimize them.

#### **3.3.2.1 The operation of tapping-mode atomic force microscopy (TM-AFM)**

In the tapping mode, the tip-sample separation is modulated while the sample is scanned by an oscillating cantilever at or near its resonance frequency (100–400 kHz) with amplitudes ranging between 10 and 100 nm. The oscillated cantilever causes the main piezoelectric tube to vibrate in the vertical  $z$  direction, in turn causing the

cantilever to vibrate by viscous coupling. Alternatively, the oscillation is induced by a small piezoelectric transducer at the fixed end of the cantilever or by an oscillating magnetic field (the cantilever must be coated with a magnetic material). The feedback control ensures a constant tip-sample interaction during imaging by keeping the oscillation amplitude constant by maintaining a constant root mean square (rms) of the oscillation signal. The oscillating cantilever touches the sample only once at each minimum at the end of its downward movement. This reduces the contact time, the friction, and the lateral forces (1 pN) considerably compared to the contact mode, making it ideal for studying soft biological samples. It overcomes the disadvantage of scanning in the contact mode as the fragile surface of the sample are often swept away by the cantilever while raster scanning the surface. When the drive frequencies is close to the resonance frequency of the cantilever, it will precisely control the cantilever oscillation; thus a high-resolution of membrane topography will be obtained.

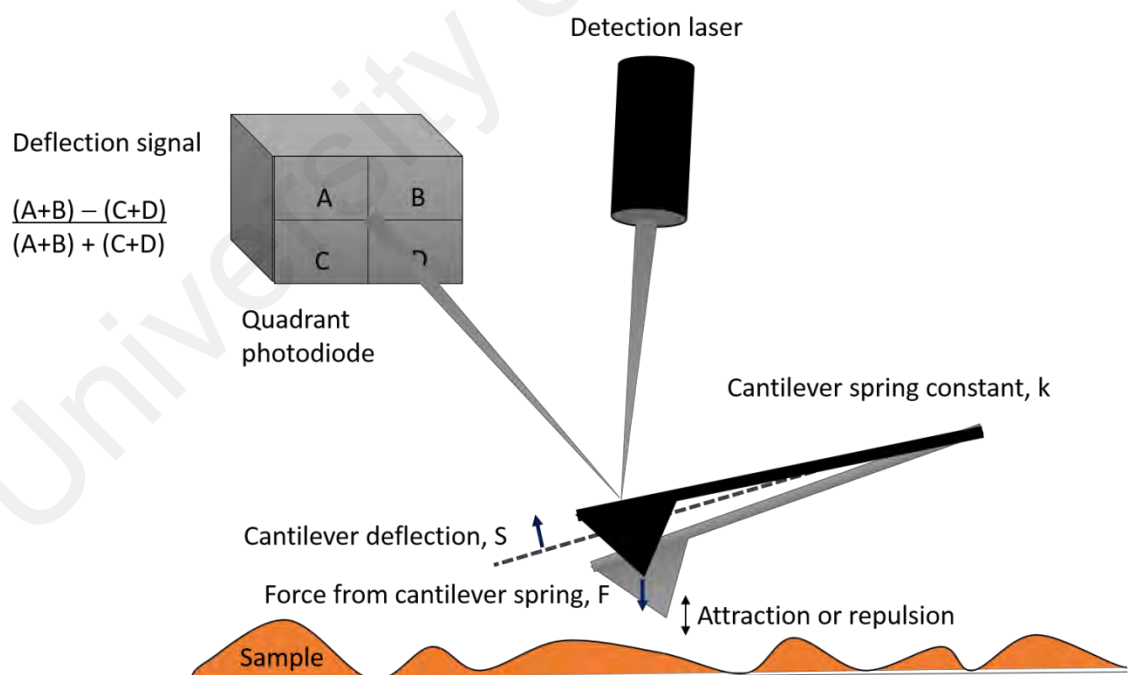


**Figure 3.3:** The AFM tip-cantilever assembly oscillates at the sample surface while the tip is scanned, thus, the tip taps lightly on the surface of the sample while imaging and only touches the sample at the bottom each oscillation. By using constant oscillation amplitude, a constant tip-sample distance is maintained until the scan is completed.

### 3.3.3.2 Cantilever and spring constants

Cantilever is the most critical part of the device; it can be thought as a plate spring.

According to Hooke's law,

$$F = -ks \quad (9)$$

Where  $F$  is the force used to extend the spring depends linearly on the distance of extended  $s$ , and  $k$  is the cantilever with spring constant between 0.005 and 40 N m<sup>-1</sup> (Figure 3.3). Different imaging mode use cantilevers with different properties. The stiffer cantilever is usually used for tapping mode, particularly in the air. The stiffer cantilever gives more stable imaging in air, since the cantilever can break free of the capillary forces when the tip touches the sample. Tapping mode cantilevers are usually with a resonant frequency of 200–400 kHz, and spring constant more than 10 N m<sup>-1</sup>.

### 3.3.3.3 AFM topography: Surface roughness

AFM topography provides a surface morphological insight into the surface interaction of molecules (Cohen & Bitler, 2008; García-Sáez & Schwill, 2010; Goksu, Vanegas, Blanchette, Lin, & Longo, 2009). One key feature we can look into is surface roughness measurements. Surface roughness is a useful parameter to characterize the features of the membrane. The mean roughness,  $R_a$ , and rms roughness,  $R_q$ , are the most commonly used parameter to characterize the surface features of the cell membrane. Both representations of  $R_a$  and  $R_q$  demonstrate valuable information of the surface morphology and surface interactions, but they are calculated using different formulas.

$R_a$  is the mean value of the surface relative to the center plane, calculated as (De Oliveira, Albuquerque, Leite, Yamaji, & Cruz, 2012):

$$R_a = \frac{1}{L} \int_0^L |Z(x)| dx \quad (10)$$

$R_q$  is the rms of surface measurements of peaks and valleys, defined as (De Oliveira et al., 2012):

$$R_q = \sqrt{\frac{1}{L} \int_0^L |Z^2(x)| dx} \quad (11)$$

where  $Z(x)$  is the function that describes the surface profile analyzed in terms of height ( $Z$ ) and position ( $x$ ) of the sample over the evaluation length of  $L$ .  $R_q$  of a surface is similar to the roughness average,  $R_a$ , with the only difference being the mean squared absolute values of surface roughness profile.

### 3.2.3 Zetasizer Nano system

Zetasizer Nano system enables us to measure particle size, zeta potential and molecular weight of particles or molecules in a liquid medium. The Zetasizer system determines the size by first measuring the Brownian motion of the particles in a sample using dynamic light scattering (DLS) and then interpret the particles size. It operates by illuminating the particles with a laser and analyze the intensity fluctuation in the scattered light. When the particles are illuminated by a 4 mW helium-neon laser light source, the particles will scatter the light in all direction. A detector is used to measure the intensity of the scattered light of particles at the position of  $173^\circ$ . The intensity of scattered beam was detected and processed using the Malvern Zetasizer NanoZS software. A DTS 1070 U-shape polycarbonate cell with gold plated electrodes was used to measure the zeta potential of liposomes using the patented M3-PALS<sup>®</sup> technique. DLS allows a quick estimation of the size distribution of liposome population in nanosize, polydispersity, and surface charge by referring to the values of zeta potential.

### 3.4 Methods

#### 3.4.1 Preparation of Langmuir monolayers/ mixed monolayers for LB measurement

Preparation of spreading solutions for Langmuir measurements was varied from mixtures to mixtures. Spreading solution of C18 fatty acids, phospholipids (SS, DSPC, and DPPC), DOPE PEG2000 was prepared by dissolving it in analytical-grade  $\text{CHCl}_3$ . DSPG was dissolved in a mixture of methanol and chloroform at 90:10, and then sonicated for 2 minutes. Various concentrations of BSA aqueous solutions were prepared. Solution of AS25 was withdrawn from the vial directly without any dilution. All mixtures of lipid-lipid and lipid-protein solutions were carefully transferred and spread randomly onto the water subphase ( $25^\circ\text{C} \pm 0.1^\circ\text{C}$ ) using a Hamilton microsyringe (precision to 0.5  $\mu\text{l}$ ).

The surface pressure of the LB films was measured by a computer-controlled Langmuir balance (KSV 5000, Langmuir System, Helsinki, Finland) equipped with symmetric barriers and Teflon trough was used to obtain the  $\Pi$ - $A$  isotherms (Figure 3.1) as described in 3.2.1.1.

The total area of trough used in each mixture is adjusted according to the mixtures, so that the gas phase of each monolayer can be recorded (Table 3.3). This is due to the lipids used in this studies are differing in size, and concentrations. For example, bigger molecules such as DOPE PEG2000, it will require a larger trough area, so that the gas phase of monolayer will be captured in the isotherms. It is inappropriate to provide a smaller trough area for lipids with bigger molecular structure or solution of lipids with higher concentrations, it will be too “crowded” and the mixture will form liquid-condensed phase immediately after spreading of solutions into the water subphase without going through gas phase and liquid-expanded phase.

In order to ensure the phase behaviours of the monolayers are comparable, all measurements in this study were obtained at an identical temperature which was 25°C  $\pm$ 0.1°C, and monolayers were compressed at a rate of 10 mm min<sup>-1</sup>.

**Table 3.3:** Trough area used for each lipid-lipid and lipid-protein mixtures.

<b>Mixtures</b>	<b>Trough area, mm<sup>2</sup></b>
C18 fatty acids	48840
C18 fatty acids–BSA	60720
C18 fatty acids–AS25	48840
C18 fatty acid–DOPE PEG2000	71640
C18 fatty acids–DOPE PEG2000–AS25	48840
SS, DPSC, DPSG–BSA	69600
SS, DPSC, DPSG–AS25	48840
DPPC–BSA	69600
DPPC–AS25	48840
DPPC–DOPE PEG2000	71640
DPPC–DOPE PEG2000–AS25	48840

#### 3.4.1.1 Mixed monolayers C18 fatty acids

The tail-to-tail interactions were studied by mixing any two C18 fatty acids in a trough with water subphase. The combinations are SA-L1, SA-L2, SA-L3, L1-L2, L1-L3 and L2-L3. SA has a saturated hydrocarbon chain; meanwhile, L1, L2 and L3 have an increasing degree of unsaturation in their respective hydrocarbon chain. Different mole ratio varying from 9:1, 8:2, 7:3 to 1:9 of each solution were transferred onto the water subphase.

#### **3.4.1.2 Mixed monolayers C18 fatty acids–BSA and phospholipids–BSA**

Lipid solutions (25  $\mu$ l) with increasing concentrations were deposited randomly. After spreading, the monolayers were left to equilibrate for about 5 min, and then 25  $\mu$ l of BSA was added onto each lipid monolayer. Various mole ratio from 9:1, 8:2, 7:3 to 1:9 of each solution were transferred onto the water subphase. The significant isotherms were selected and shown in Chapter 4.

#### **3.4.1.3 Mixed monolayers C18 fatty acids–AS25 and phospholipids–AS25**

After spreading of C18 fatty acids (or phospholipids) solution, the monolayers were left to equilibrate for about 5 min, and then an increasing volume of antibody (10  $\mu$ l, 25  $\mu$ l, 50  $\mu$ l, 75  $\mu$ l, and 100  $\mu$ l, respectively) were added onto each monolayer formed. The desired volume of antibody was withdrawn from the vial directly without any dilution. The amount of antibody used was converted into mole by using the concentration stated in the product sheet (product number: S9684), which is 9.55  $\mu$ g/ $\mu$ l for C18 fatty acid and 8.40  $\mu$ g/ $\mu$ l for phospholipid mixed systems, respectively. This mole ratio of fatty acids to antibody was used in all the plotted graphs and data analysis.

#### **3.4.1.4 Mixed monolayers C18 fatty acids–DOPE PEG2000 and DPPC–DOPE PEG2000**

Fatty acids (or DPPC) solutions (25  $\mu$ l) with increasing concentrations were deposited randomly. After spreading, the monolayers were left to equilibrate for about 5 min, and then 25  $\mu$ l of DP was added onto each monolayer of fatty acid. A small amount of PEG is predicted to be sufficient for PEG-lipid systems to obtain a long circulation effect in the blood stream. A very much lower concentration of PEG compared to the concentration of lipids is applied in this study. In this experiment, the mole ratio of fatty acids to DP was kept constant concerning increasing mole of fatty acids, 10:1, 20:1,

30:1 to 100:1. Selected isotherms (mole ratio of fatty acids to DP) which show a significant trend are plotted in graphs and data analysis in this paper.

#### **3.4.1.5 C18 fatty acids/DOPE PEG2000–AS25 and DPPC/DOPE PEG2000–AS25 mixed monolayers**

The best mole ratio of interacting mixtures of each mixture of Lipid-DP were selected by referring to the Gibbs free energy of mixing obtained in Figure 4.25(b) (C18 fatty acids/DP) and Figure 4.51(a) (DPPC/DP) in Chapter 4, and this ratio is found to be 50:1 for both C18 fatty acids/DP and DPPC/DP. A 25- $\mu$ l of C18 fatty acids (or DPPC) stock solutions in chloroform and 25  $\mu$ l of DP were injected into the water subphase. After spreading, the monolayers were left to equilibrate for about 5 min, and then an increasing volume (10  $\mu$ l, 25  $\mu$ l, 50  $\mu$ l, 75  $\mu$ l, and 100  $\mu$ l, respectively) of AS25 were added onto each mixed monolayer formed. The concentrations of AS25 were 9.55  $\mu$ g/ $\mu$ l used for C18 fatty acid and 8.40  $\mu$ g/ $\mu$ l for DPPC mixed systems, respectively. The mole AS25 added was used in all the plotted graphs and data analysis.

#### **3.4.2 Deposition of bilayer of lipid-lipid and lipid-protein mixtures on the oxidized silicon wafer for AFM imaging**

Silicon (100) wafers (Sigma-Aldrich) were cut into approximately 5 cm  $\times$  1 cm pieces and placed in a furnace (Carbolite, Watertown, WI, USA) for 8 hours at 900°C to allow oxidation. The oxidized silicon wafer was clamped vertical to the subphase and immersed into the dipping well before spreading the monolayer material. After complete evaporation of the solvent, the floating layer was compressed at a rate of 10 mm min<sup>-1</sup> to reach a target surface pressure of monolayers and kept for 15 min to attain stability for deposition. The target surface pressures for dipping are different among the mixtures. The deposition is done at the liquid-condensed phase of each of the

pure, binary or ternary monolayers. The Y-type deposition of LB film (Figure 3.2(c)) was performed at the targeted pressure with a dipping speed of  $10 \text{ mm min}^{-1}$ . All the transferred films were kept for at least three days in a dry, clean and closed container before AFM imaging.

### **3.4.3 AFM imaging**

High-resolution imaging of bilayers was obtained by AFM after transferring them from the air/water interface to a solid oxidized silicon substrate. Mixed bilayers from the Langmuir trough were transferred onto oxidized silicon substrates at the desired Wilhelmy pressure. Bilayers transferred to substrates were imaged using the NanoScope®V scanning probe microscope controller (Bruker, USA) in tapping mode under ambient conditions. Silicon probes with an aluminum coating (VISTA T190R, Canada) were used. The resonance frequency of the probe was 190 kHz, and the force constant was  $48 \text{ N m}^{-1}$ . Images in height mode were collected simultaneously with  $512 \times 512$  points at a scanning rate of 1.0 Hz per line. A series of AFM images were taken from different perspectives.

### **3.4.4 Determination of $K_{ow}$ of AS25 by reverse phase-high performance liquid chromatography (RP-HPLC)**

A 20- $\mu\text{l}$  of AS25 (concentration of  $9.55 \mu\text{g}/\mu\text{l}$ ) was added to two separate vials: (i) 1 ml of nanopure water, and (ii) mixture of 1:1 octanol-water. A series of dilution of an aqueous solution of AS25 were also prepared to enable us to plot a standard curve. Solutions were homogeneously mixed using shaker powered by an electric motor at a speed of 250 rpm for 10 minutes. The solutions were then left to stand for 30 minutes to achieve equilibrium prior to HPLC analysis.

HPLC analysis of AS25 was carried out using a Shimadzu reverse phase-high performance liquid chromatography (RP-HPLC) system with Merck Chromolith® ODS C18 HPLC column (length: 100 mm × 4.6 mm I.D., pore size: 2 µm) equipped with photodiode array detector (PDA) and auto-injector. Detection of AS25 using PDA was observed at 200 to 500 nm as the reference wavelength. The mobile phase was methanol-water (50/50, v/v). All peak areas were obtained by averaging the results of at least three independent injections (20 µl of injection volume) at a mobile phase flow rate of 1.0 ml min<sup>-1</sup>.

A standard curve of peak area against the concentration of AS25 (in µg per µl) was plotted. The unknown amount of AS25 in the mixture of octanol-water solution can be obtained from the plotted standard curve. The octanol-water model system will allow prediction of the amount of water soluble antibody interacting with the biological membrane. Octanol is best represents the biological membrane, hence octanol-water partition coefficient,  $K_{ow}$  provides useful information of the distribution of substance into two immiscible phases (Efremov et al., 2007; Han et al., 2011; Leo, Hansch, & Elkins, 1971; Sangster, 1989).

The octanol-water partition coefficient,  $K_{ow}$  is defined as (Leo et al., 1971; Sangster, 1989):

$$K_{ow} = \frac{[AS25 \text{ in octanol-water}]}{[AS25 \text{ in water}]} \quad (12)$$

where the concentration of AS25 in water and octanol-water are expressed in µM, respectively.

### **3.4.5 Preparation of liposomes**

#### **3.4.5.1 Unsaturated C18 fatty acids/AS25, C18 fatty acids/DP and C18 fatty acids/DP/AS25 liposomes**

The unsaturated C18 fatty acids (L1, L2 and L3) can form liposome solutions. L1 liposome solution of 1 mM was prepared by mixing L1 in a 1 ml of 1 M NaOH aqueous solution, and stirred for 2 hours by magnetic stirrer. The procedure for preparation of the stock solution for L2 and L3 are essentially the same. A desired volume of AS25 (10  $\mu$ l, 25  $\mu$ l, 50  $\mu$ l, 75  $\mu$ l and 100  $\mu$ l) using a Hamilton microsyringe precise to 0.5  $\mu$ l were added into 1 mM of each L1, L2 and L3 liposome solution and stirred overnight before characterization. Preparation of stealth C18 fatty-acid liposomes was carried by lipid thin-film hydration method (Samad, Sultana, & Aqil, 2007; Torchilin & Weissig, 2003). Various mole ratios of L1/DP, L2/DP and L3/DP were mixed in chloroform in a round bottom flask, respectively. Thin film of lipids formed on the flask by using rotary vacuum evaporator to remove the residue organic solvent. The dry film was then hydrated with 0.01 M PBS (pH 7.4), sonicated and multilamellar vesicles that formed will detach from the surface of the flask. The suspension will be then top up with PBS solution.

Mole ratio of stealth C18 fatty acid liposomes at 50 to 1 were selected by referring to our LB findings. The same volume of AS25 (concentration of 9.55  $\mu$ g/ $\mu$ l) as above was added to individual vials containing 5 ml of 1 mM stealth C18 fatty acids liposome solutions. Both stealth C18 fatty acids liposome and antibody-targeted stealth C18 fatty acids liposome solutions were stirred overnight before characterization.

### **3.4.5.2 DPPC, DPPC/AS25, DPPC/DP and DPPC/DP/AS25 liposomes**

DPPC liposome suspension (1 mM) was prepared by ethanol injection method (Gentine, Bourel-Bonnet, & Frisch, 2013; Jaafar-Maalej, Diab, Andrieu, Elaissari, & Fessi, 2010; Pons, Foradada, & Estelrich, 1993). A 0.5-ml of distilled ethanol was introduced into a 1.0-ml low extractable borosilicate glass vial containing weighed DPPC solid, vortex to dissolve solid completely. Ethanolic DPPC solution is injected into a magnetically stirred PBS solution on a 50°C hot plate, which is the phase transition temperature of DPPC lipid membrane. DPPC liposomes solution was then top up with PBS solution and sonicated for 2 minutes, and uniform size of liposomes will form. Unlike C18 fatty acids liposomes, a successive preparation of DPPC liposomes solution, nanoliposomes will form immediately. Therefore, it was left for an hour to reach equilibrium before characterization. The same volume of AS25 (concentration of 8.40 µg/µl) as mentioned in 3.4.5.1 were added into individual vials of DPPC liposome solution and stirred overnight before characterization. The preparation of stealth-DPPC (DPPC-DP) liposomes was carried out by lipid thin-film hydration method described as above (3.4.5.1). The same volume of AS25 as above were added to individual vials containing 5 ml of 1 mM stealth DPPC and stirred overnight before characterization.

All liposome solutions were first extruded through 0.45 µm pore diameter polycarbonate Whatman membranes filter using Lipex Biomembrane extruder prior to the measurement. It is worth mentioning here that 0.2 µm membrane filter is commonly used in many nanoliposomes preparations, however, we believe there are bigger size of liposomes formed in our lipid-protein mixtures due to the embedded proteins with larger molecular size.

### **3.4.5.3 Particle size and zeta potential measurements**

The mean vesicle size and zeta potential were measured by DLS using Malvern Nano ZS (Malvern Instruments Ltd. UK). A 1.0-ml of liposomes was carefully transferred into 1 cm path length four-sided clear fluorescent quartz cuvette using a disposable syringe and analyzed using pre-set standard operation procedure (SOP) for DLS in order to measure the average hydrodynamic size of liposomes and zeta potential measurements. A 4 mW He-Ne laser was employed to generate the laser beam which detects by the backscattered detector at  $173^\circ$  with respect to the scattering transmission beam. The scattered beam that was produced by He-Ne laser pass through the sample then directed to compensation optic at  $17^\circ$  from the scattering beam. The fluctuation in the frequency of scattered beam was detected by the detector and their intensity was analyzed by the Malvern software. All measurements were performed in triplicate at  $25^\circ\text{C}$ .

### **3.4.6 Transmission electron microscopy (TEM) imaging**

A drop of liposomes solution was placed onto the high quality formvar-coated copper grid (400 square mesh) and allowed to stand for 3 minutes. The excess of solution was blotted with filtered paper, and then stained with 1% (w/v) phosphotungstic acid for 1 minute and allow to air dry. The specimens were kept in a desiccator for 2-3 days to allow it to dry. Liposomes images were obtained by using Zeiss Libra® 120 TEM operated at accelerating voltage of 120kV.

## CHAPTER 4: RESULTS AND DISCUSSION

### 4.1 Introduction

Langmuir-Blodgett (LB) is an ideal tool for studying the thermodynamic behavior of mixed systems (Du, Wang, Ding, & Guo, 2007; Hąc-Wydro & Dynarowicz-Łątka, 2008; Phan & Shin, 2015). Parameters such as mean molecular area, modulus compressibility, and Gibbs free energy of mixing can be obtained from  $\Pi$ - $A$  isotherms to determine the miscibility and stability of the mixed system. Thermodynamic analysis will provide useful information on lipid-lipid, lipid-proteins, and protein-protein interactions. This analysis enables us to know how proteins associate to the lipid membranes, their ability to form antibody-targeted liposomes, and a precise composition of fatty acids and antibodies required for forming antibody-targeted liposomes. LB technique is best methods in the preparation of thin film with a thickness of one molecule as it enables homogenously deposition of the monolayer (or multilayers) over a large area. Deposition of floating monolayers will be performed using LB to transfer the mixed monolayers onto a solid substrate, and then observed by tapping-mode atomic force microscopy (TM-AFM). AFM topography provides a surface morphological insight into the surface interaction of molecules (Antonio, Lasalvia, Perna, & Capozzi, 2012; Q. Chen et al., 2012; Du et al., 2007).

### 4.2 Lipid-protein interactions: Effect of degree of saturation C18 fatty acids

Fatty acid is a carboxylic acid with saturated or unsaturated long aliphatic hydrocarbon chain commonly contain 12 to 22 carbon atoms. They are the building block of lipid molecules. Both saturated and unsaturated fatty acids form two chains bonded to the phosphatidyl group of phospholipid molecules, which are the basic structural element of natural bilayer membrane. Fatty acids are commonly studied for their saturation degree

hydrocarbon chain. In the first part of the experiment, saturated and unsaturated fatty acids with 18 carbon atoms, namely stearic acid (SA), oleic acid (L1), linoleic acid (L2), and linolenic acid (L3) were chosen to study their imperative intermolecular interactions.

This study is divided into several parts:

- a) Intermolecular interactions between saturated (SA) and unsaturated C18 fatty acids (L1, L2, and L3) and unsaturated C18 fatty acids mixed systems, where they have different degree of saturation in their hydrocarbon chain.
- b) Lipid-protein interactions between C18 fatty acids with an integral protein (BSA) and peripheral protein (AS25), respectively.
- c) In order to apply Langmuir monolayer studies into long circulation antibody targeted fatty-acids liposomal formulations, the effect of DOPE PEG2000 on pure C18 fatty acids monolayers and C18 fatty acids/AS25 mixed monolayers were also studied.

#### **4.2.1 $\Pi$ - $A$ Isotherms**

##### **4.2.1.1 Pure monolayers of SA, L1, L2, and L3**

The  $\Pi$ - $A$  isotherms can be used to estimate the minimum cross-sectional area of the surfactant molecules,  $A_0$ , at the interface. The limiting molecular areas of pure SA, L1, L2, and L3 monolayers were determined by extrapolating the linear slope of individual  $\Pi$ - $A$  isotherms to zero surface pressure and were found to be 21 Å<sup>2</sup>, 43 Å<sup>2</sup>, 42 Å<sup>2</sup>, and 42 Å<sup>2</sup>, respectively (Figure 4.1). The collapse pressure of SA was found to be 50 ± 2 mN m<sup>-1</sup>, which is similar to the reported collapse pressure of SA at 25°C (Kamilya, Pal, & Talapatra, 2007; Kundu & Langevin, 2008; Teixeira et al., 2007), some obtained at 55 mN m<sup>-1</sup> but at a lower temperature, which was 20°C (Hąc-Wydro, Jędrzejek, &

Dynarowicz-Lątka, 2009; Hac-Wydro, Kapusta, Jagoda, Wydro, & Dynarowicz-Latka, 2007; Wydro, Krajewska, & Hac-Wydro, 2007). In one of Iribarnegaray et al. (2000) publication, showed that the monolayers have lower collapse pressure as the temperature of water subphase increases (Seoane et al., 2000).

The unsaturated C18 fatty acids, L1, L2, and L3 form liquid-type monolayers, collapse at lower surface pressure as compared to the saturated stearic acid about 30, 25, and 26  $\text{mN m}^{-1}$ , respectively. These values are in good agreement with the previously reported values (Hac-Wydro & Wydro, 2007; Makyla & Paluch, 2009; Wydro et al., 2007). The *cis*-double bonds in L1, L2, and L3 have a kink in their molecular conformation and could therefore not pack as tightly and uniformly as SA (Hac-Wydro et al., 2009; Kanicky & Shah, 2002; Vollhardt, 2007). They are thermodynamically unstable compared to *trans* configuration. The bends and kinks in the molecular structure may interfere with the packing of the lipid monolayer which will promote fluidity.

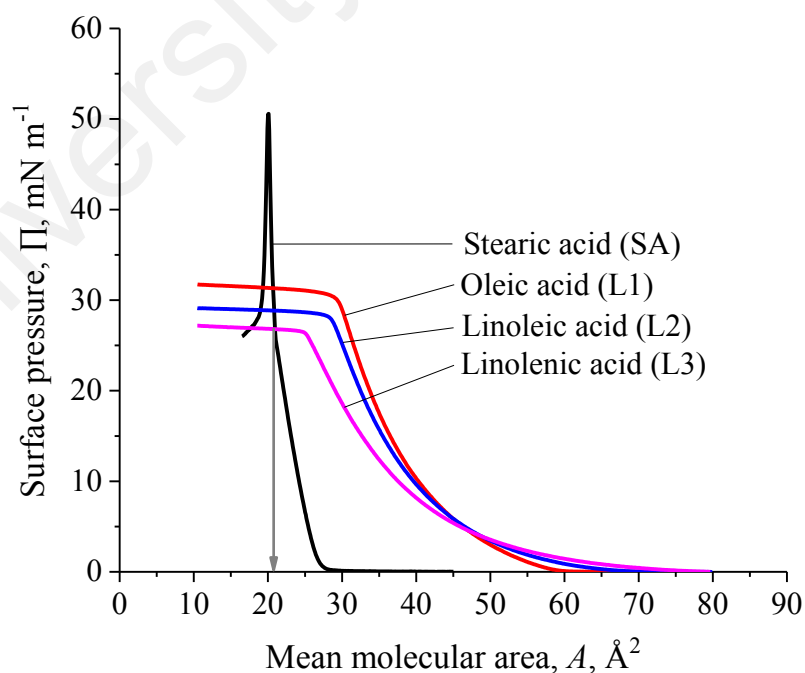


**Figure 4.1:** The surface pressure–area ( $\Pi$ – $A$ ) isotherms of C18 fatty acids (SA, L1, L2, and L3), spread on water subphase at 25°C.

#### 4.2.1.2 Mixed monolayers of C18 fatty acids: Effect of degree of saturation

Lipid-lipid interactions will affect membrane proteins functions environment. In order to study lipid-lipid interactions, any two of C18 fatty acids were mixed to form 6 binary mixtures (SA/L1, SA/L2, SA/L3, L1/L2, L1/L3, and L2/L3) to observe the effect of degree of saturation of C18 fatty acids on monolayers at air/water interface. The steric effect is greatly contributed by the interaction between unsaturated hydrocarbon chains.

The  $\Pi$ - $A$  isotherms of mixed monolayer of saturated SA with unsaturated L1, L2, and L3 shifted away from pure SA monolayer as the mole fraction of SA decreases (Figure 4.2). A typical curve of SA is observed at  $X_{SA} = 0.9$  and  $0.7$  for all the investigated systems, meanwhile typical shape of liquid-monolayers is recorded at a larger mole fraction of L1, L2, or L3, respectively. The isotherms shift to increasing mean molecular area as the mole ratio of unsaturated L1, L2, and L3 increased. At the largest mole fraction of unsaturated FA ( $0.9$ ), the isotherm increased gradually. In contrast, steeper curves were observed  $X_{SA} = 0.9$  and  $0.7$  and localized at the smaller molecular area, which reveals a closer packing of molecules in these systems like the highly condensed pure SA monolayer. SA owns saturated hydrocarbon chain, whereas L1, L2, and L3 possess one, two and three *cis* double bond(s) in its hydrocarbon chain, respectively. The presence of bending *cis*-double bond(s) in hydrocarbon chain increases the distance between the molecules and prevent close packing of molecules in the monolayer. Mixtures of unsaturated fatty acids (L1/L2, and L1/L3, L2/L3) showed similar curve as their pure monolayer isotherms (Figure 4.3). For L1/L2 and L1/L3 binary mixtures,  $\Pi$ - $A$  isotherms of mixed monolayer shift to increasing mean molecular area as  $X_{L2}$  and  $X_{L3}$  increases (Figure 4.3(a) & (b)). At the largest  $X_{L3}$  in the mixed systems, L1/L3 isotherms shifted to the larger mean molecular area as compare to SA/L3 and L2/L3 mixtures. Greater repulsion could occur in L1/L3 SA/L3 L2/L3.

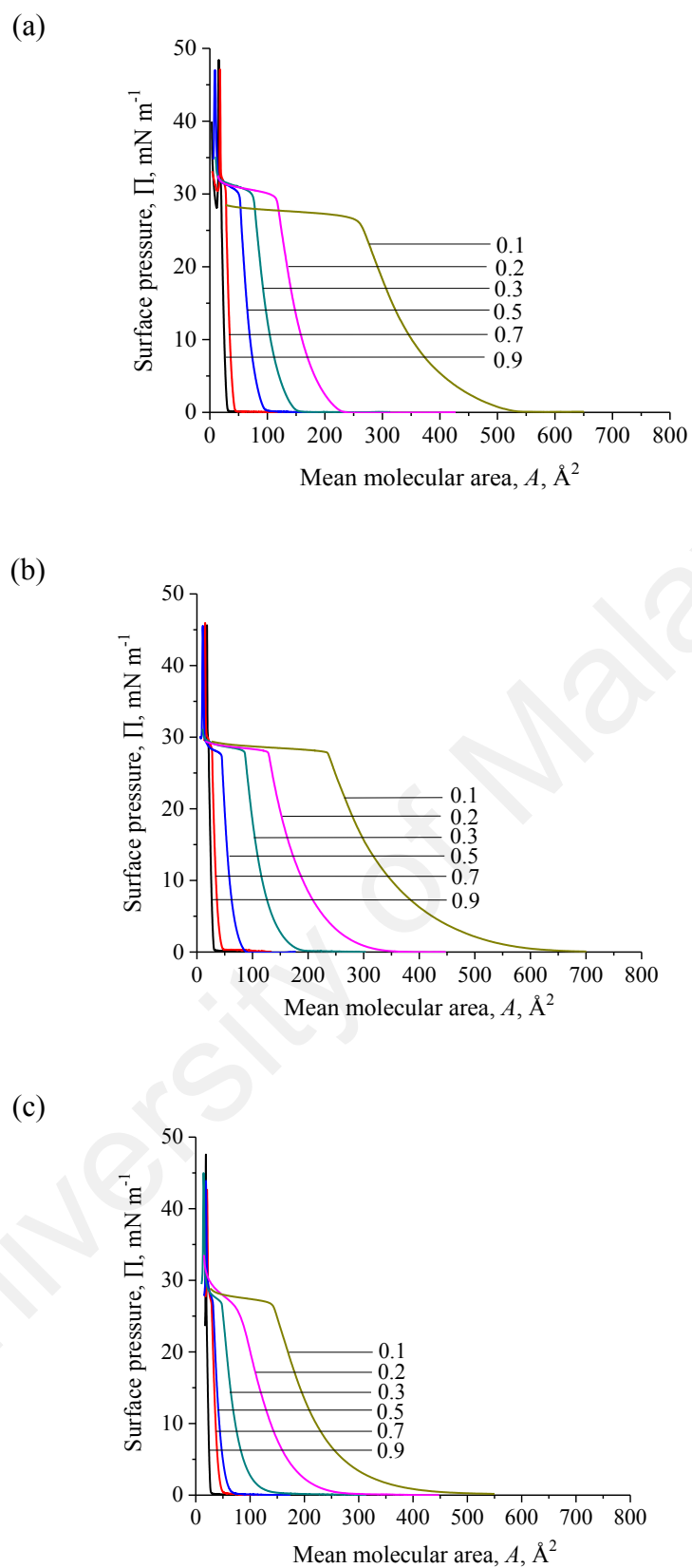


**Figure 4.2:** The surface pressure–area ( $\Pi$ – $A$ ) isotherms of mixed monolayers (plotted in mole fraction of SA): (a) SA/L1, (b) SA/L2, and (c) SA/L3 spread on a nanopure water subphase at  $25^\circ\text{C}$ .

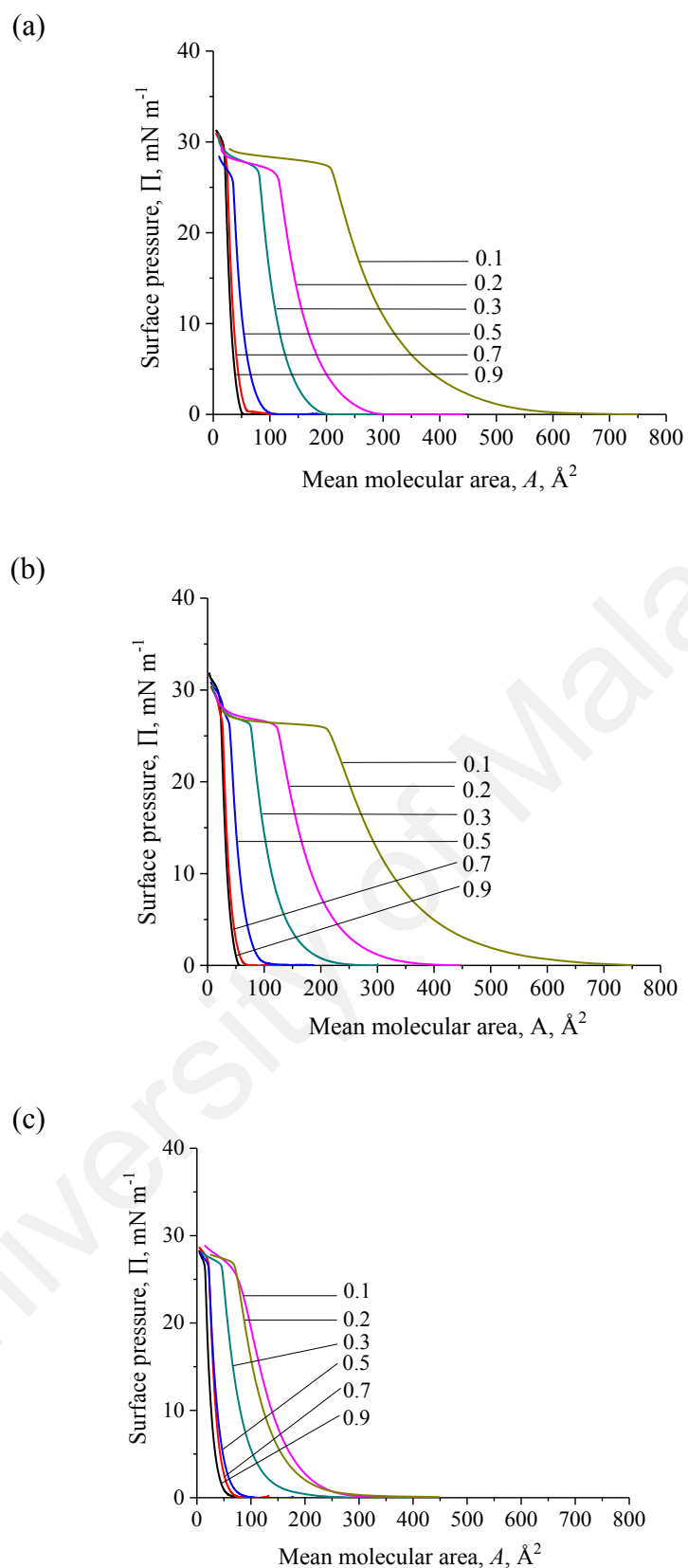


**Figure 4.3:** The surface pressure–area ( $\Pi$ – $A$ ) isotherms of mixed monolayers (plotted in mole fraction of L1 or L2): (a) L1/L2, (b) L1/L3, and (c) L2/L3 spread on a nanopure water subphase at  $25^\circ\text{C}$ .

### 4.2.1.3 Mixed monolayers of C18 Fatty acids and DP

DOPE PEG2000 (DP) has a PEG head group that consists of an average of 45 units of ethoxyl monomers, which is attached to a phospholipid with two C18 hydrocarbon chains with one *cis*-double bond on each chain (Figure 4.4(a)). The molecular structures of the C18 fatty acids are simpler, consisting of a small  $\text{-COOH}$  head-group with one 18-carbon hydrocarbon chain. Repulsions between DP and DP in the monolayer are expected to be greater than that of  $\text{-COOH}$  head groups of the C18 fatty acids because of their chemical structure. There are at least three types of interactions that occur in the pure-DP monolayer, as illustrated in Figure 4.4(b): (1) head-to-head interactions, (2) tail-to-tail interactions, and (3) head-to-tail interactions.

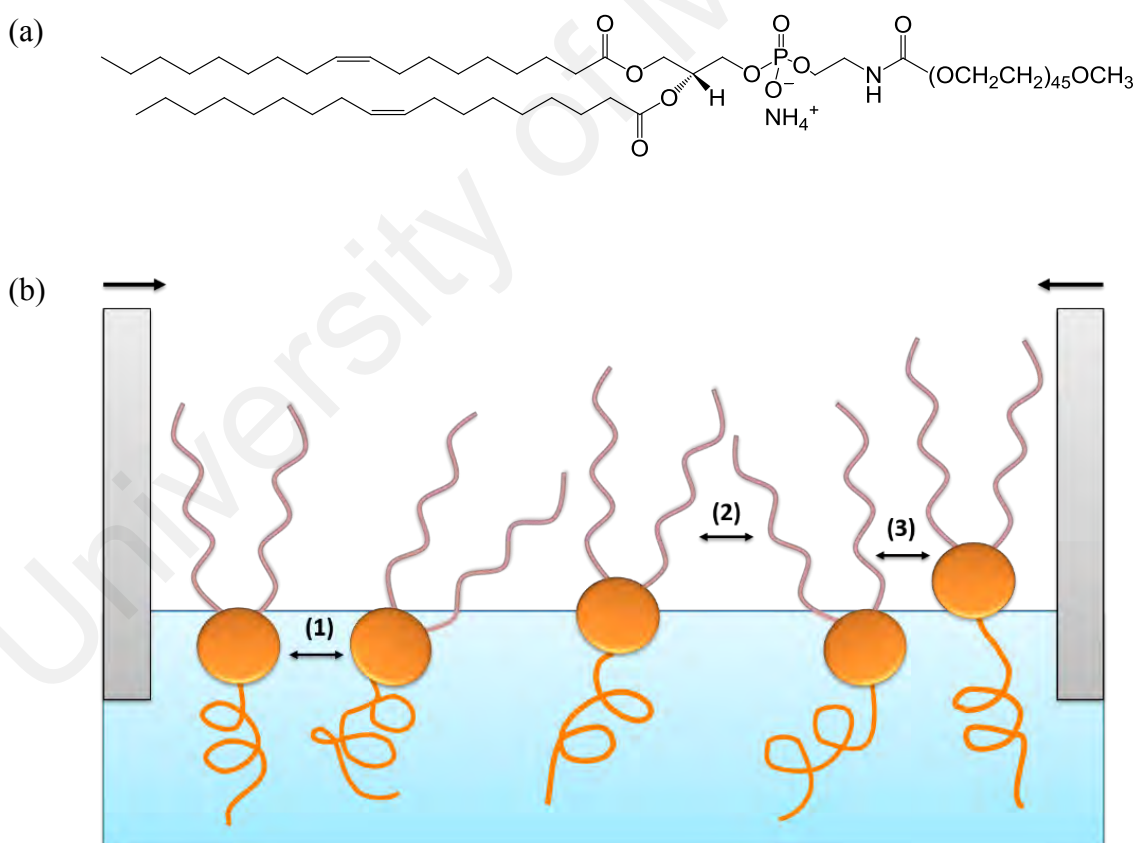


**Figure 4.4:** (a) Molecular structure of DP; (b) Three types of intermolecular interactions that occur between DP and DP: (1) Head-to-head; (2) tail-to-tail; (3) head-to-tail.

No collapse pressure was clearly observed in the DP isotherm (Figure 4.5). The limiting molecular area of DP was found to be  $594 \text{ \AA}^2$  (Figure 4.5). However, the derivative of the pure-DP  $C_s^{-1}$  versus  $\Pi$  profile (Figure 4.5) did not show a change at approximately  $12 \text{ mN m}^{-1}$ , which presumably corresponds to its collapse pressure, showing that the molecular size of DP was much larger than that of the C18 fatty acids. There are several breaks in the slopes that may indicate phase transitions, which can be observed at surface pressure of 6, 8.5, and  $10.5 \text{ mN m}^{-1}$ . This change was more obviously seen in the plot of  $C_s^{-1}$  versus  $\Pi$  (Figure 4.5), indicating that the monolayer of DP was less compressible and disordered, and the low  $C_s^{-1}$  values suggest that the DP molecular organization.

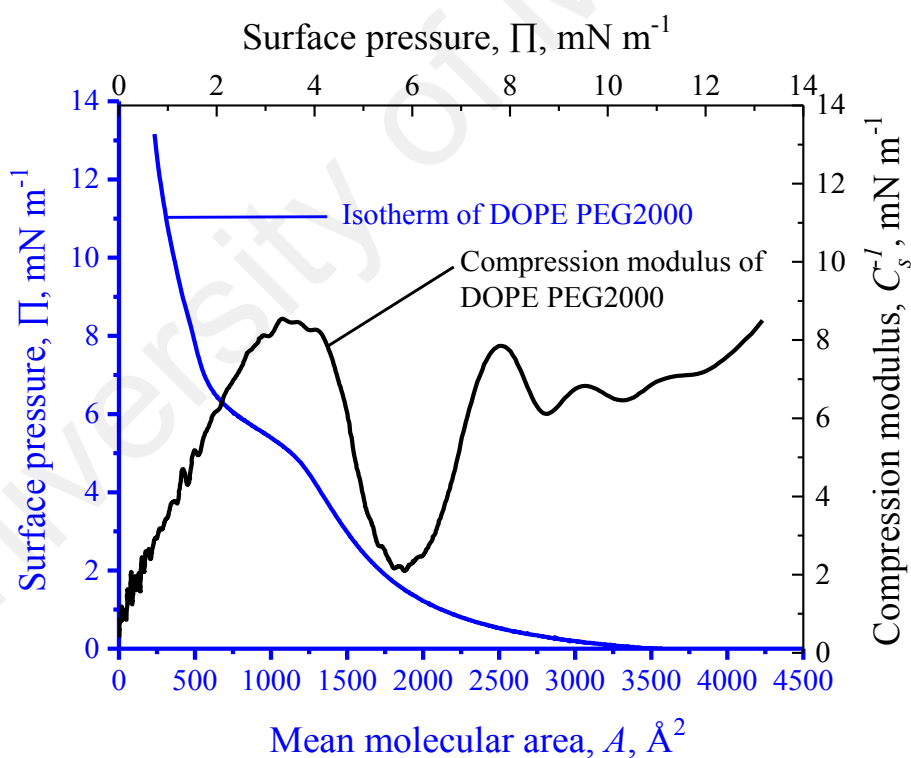


**Figure 4.5:** The surface pressure–area ( $\Pi$ – $A$ ) isotherm of DOPE PEG2000 monolayer, and its compressibility modulus ( $C_s^{-1}$ ), spread on water subphase at  $25^\circ\text{C}$ .

avored their arrangement in the liquid-expanded phase in subphase water at 25°C. Several type of interactions occurred can be predicted referring to the molecular structure of DP (Figure 4.4(a)), for example, interactions between the large PEG head group of DP and another head group of DP as illustrated in Figure 4.4(b). Additionally, the *cis*-double bonds of the DOPE hydrocarbon chains in one or two DP molecules provided kink effects that significantly influenced the molecular packing and miscibility. The isotherm of DP will be used as a reference for us to compare C18 fatty acid–PEG interactions that occur in our studies.

The  $\Pi$ – $A$  isotherms of fatty-acid monolayers and mixed monolayers of various mole ratios of C18 fatty acids (SA, L1, L2, and L3) to DP on nanopure water subphases are presented in Figure 4.6. When DP was incorporated into the SA monolayer, the mean molecular area of the mixtures increased as the content of SA increased (Figure 4.6(a)). The mixed monolayers of unsaturated fatty-acid (L1, L2, and L3) isotherms (Figures 4.6(b)–(d)) with the addition of DP shifted away from their pure fatty-acid isotherms due to the presence of PEG. While there was no noticeable difference between some of the mole ratios in the isotherms, at 5 mN m<sup>-1</sup> we observed a mixed monolayer containing <50:1 (mole ratio of unsaturated C18 fatty acids to DP) that had a larger mean molecular area compared with its respective pure monolayer. Profiles of C18 fatty acids to DP 50:1 that had a smaller mean molecular area was also observed at a surface pressure of 5 mN m<sup>-1</sup>. This showed that interactions occurred between the fatty acids and DP. The effect of DP was clearly shown from 0 to 15 mN m<sup>-1</sup> in all of the mixed system isotherms. DP–DP interactions occurred first, followed by DP–C18 fatty-acid interactions. This observation is also supported by the compressibility modulus (Figure 4.5). Similar  $C_s^{-1}$  profiles as observed in DP (Figure 4.5) can be seen in most of the binary systems in Figures 4.16 at surface pressures from 0 to 15 mN m<sup>-1</sup>, which will be discussed later.

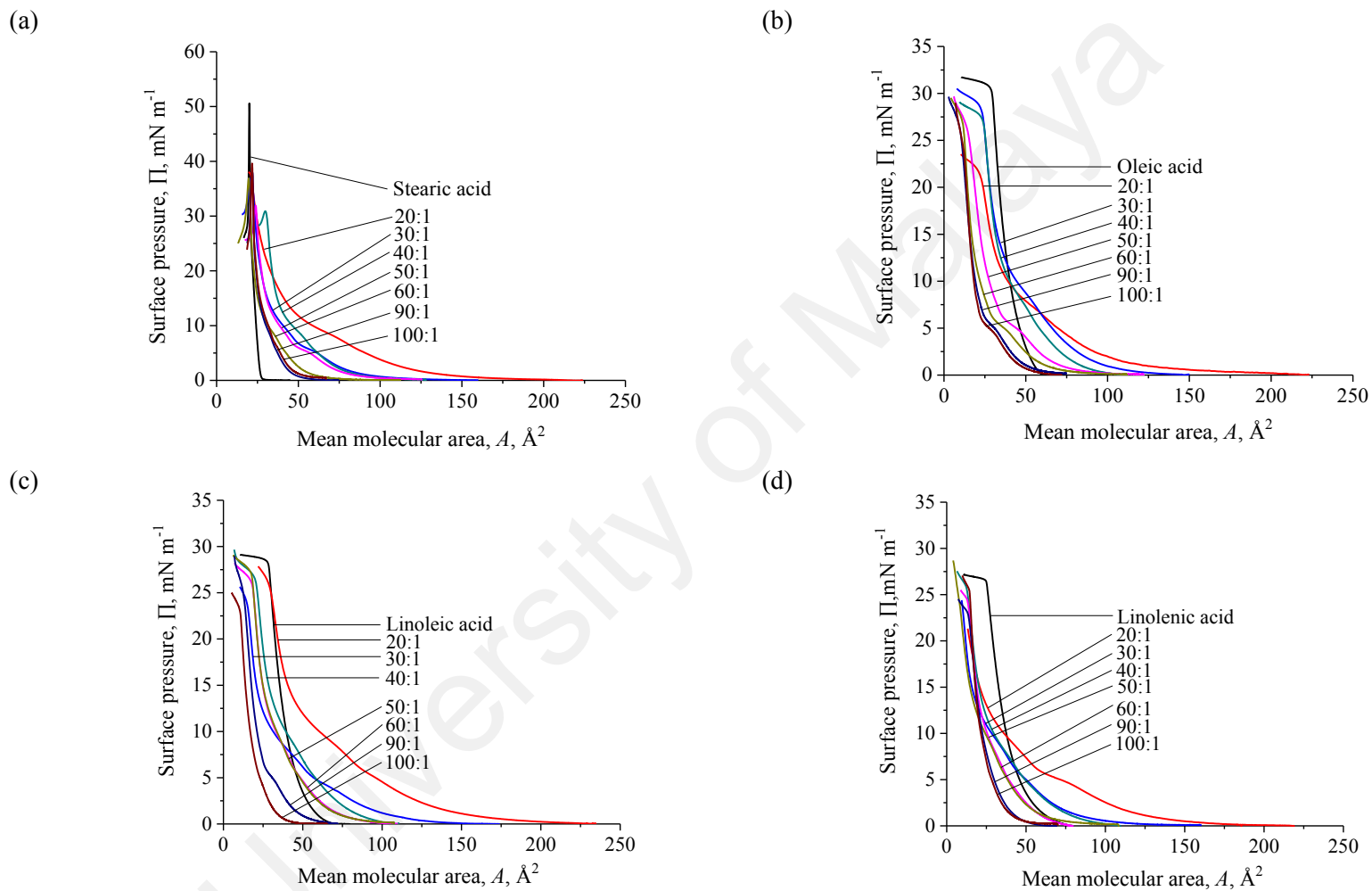


**Figure 4.6:** The surface pressure–area ( $\Pi$ – $A$ ) isotherms of mixed monolayers (plotted in mole ratio of C18 fatty acids to DOPE PEG2000): (a) SA/DOPE PEG2000, (b) L1/DOPE PEG2000, (c) L2/DOPE PEG2000, and (d) L3/DOPE PEG2000, spread on a nanopure water subphase at 25°C.

#### 4.2.1.4 Mixed monolayers of C18 fatty acids and BSA

BSA is an integral protein; it was thought to be penetrating in between the lipids molecules in the biological membrane, which has made BSA as the choice of protein in this study. C18 fatty acids were used to model the membrane in Langmuir trough to illustrate how the effect of degree of saturation C18 fatty acids affects the interaction between lipids and BSA molecules, and also to provide useful energetic data to explain lipid-protein interactions in the biological membrane.

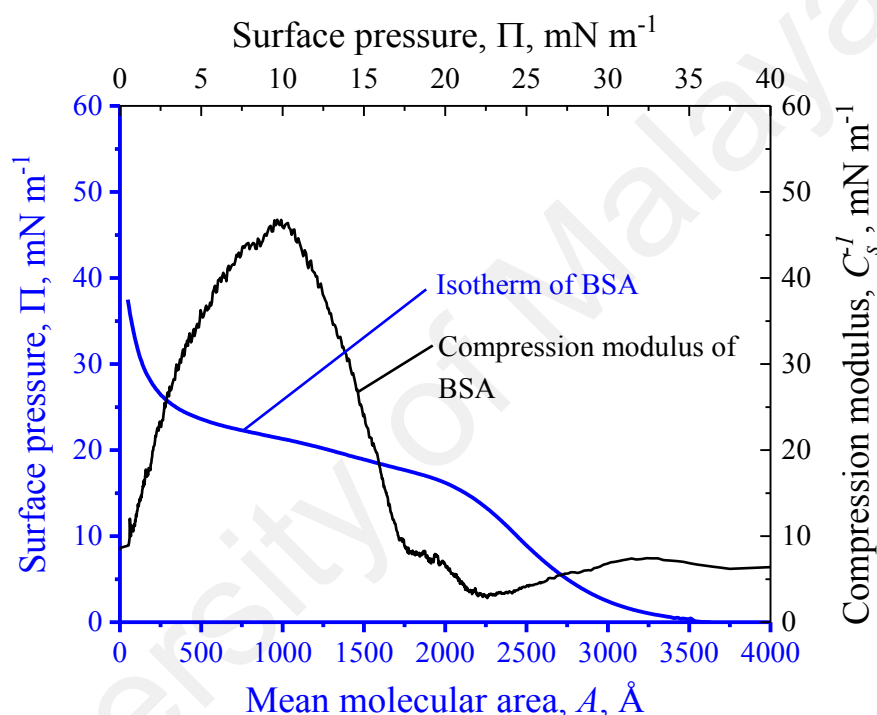


**Figure 4.7:** The surface pressure–area ( $\Pi$ – $A$ ) isotherm of BSA monolayer and, its compressibility modulus ( $C_s^{-1}$ ), spread on water subphase at 25°C.

There was no collapse pressure clearly observed in BSA isotherm (Figure 4.7). However, the derivative of the pure-BSA  $C_s^{-1}$  versus  $\Pi$  profile (Figure 4.7) showed a change at 22 mN m<sup>-1</sup> that presumably corresponds to its collapse pressure. The limiting molecular area of pure BSA monolayers was determined by extrapolating the linear slope of its  $\Pi$ – $A$  isotherms to zero surface pressure and were found to be 500 Å<sup>2</sup>. Typical collapse pressure of a monolayer (for example SA) will cause a rapid decrease in the surface pressure. However, there are some exceptions where the monolayer is in a

liquid state (such as BSA in part of the experiment), a horizontal break can be observed in the isotherm. This horizontal break of BSA can be observed at approximately  $22 \text{ mN m}^{-1}$  with the support of compressibility modulus profile (Figure 4.7), as it is not clearly shown in BSA isotherm (Figure 4.7). Compression modulus is used as a measure of phase transitions of the monolayer. The monolayer of BSA is less ordered and low compressible, where low  $C_s^{-1}$  values ( $<50 \text{ mN m}^{-1}$ ) suggests that the arrangement of BSA molecules are in LE phase in subphase water at  $25^\circ\text{C}$ . As the compression began, the molecules have larger space to lie flat on the water subphase surface. Molecules start to change their orientation from a horizontal to vertical position when further compression. The observed plateau region is due to the reorientation of molecules as the similar observation has been reported for other biological molecules such amphotericin B and nystatin (Hąc-Wydro & Dynarowicz-Lątka, 2006a, 2006b; Hąc-Wydro, Dynarowicz-Lątka, Grzybowska, & Borowski, 2005; Hąc-Wydro et al., 2007).

Intermolecular interactions between amphiphilic fatty acids and BSA molecules can be studied in depth by interpreting protein sequences in BSA to obtain better insight. BSA protein sequences are made of 607 amino acids, including 173 hydrophobic, 232 hydrophilic, 105 acidic and 97 basic amino acids (Peters, 1995). The polarity of a protein can be predicted by studying the side chain of each amino acid in the sequences, where hydrophilic amino acids will attract to the polar head-group region of fatty acids, and hydrophobic amino acids will attract to the non-polar hydrocarbon chain. However, this prediction is insufficient to explain the behavior of the protein in the membrane; their interactions are also affected by membrane fluidity which is related to the degree of saturation of the hydrocarbon chain, and also the headgroup of the lipids.

When BSA was incorporated into each of the individual C18 fatty acid monolayers, the isotherms of the mixed monolayers were shifted to dramatically high

molecular area with the increasing mole fraction of BSA (Figure 4.8) indicating the interactions have taken place between the fatty acids and the integral protein. Similar shape of isotherms in mixed systems as the pure BSA system was observed, particularly, at the beginning of the compression at surface pressure 0 to 20 mN m<sup>-1</sup>. Presumably, the interaction between BSA–BSA has taken place first, and then continued by C18 fatty acids–BSA. BSA molecules are larger than the molecules of C18 fatty acids; they will embed in between the C18 fatty acids in the monolayer. The ensuing lipid monolayer with embedded integral proteins is thermodynamically stable. The attractive interactions will be verified by referring to the analysis of free energy of mixing in the next section.

The collapse pressure of all SA/BSA mixed systems except  $X_{BSA} = 0.9$  are found to be around 50 mN m<sup>-1</sup>, which is similar to the collapse pressure of pure SA monolayer. The mixed system of SA/BSA at  $X_{BSA} = 0.9$ , which contains the highest concentration of BSA, has no obvious collapse pressure shown. The presence of BSA in SA membrane greatly affects their phase transition and molecular packing (Gew & Misran, 2014). It can be observed at surface pressure of 0 to 18 mN m<sup>-1</sup> in the isotherm of SA/BSA mixed systems, plausibly, BSA-BSA interactions is greater than SA/BSA occurred at the beginning of the compression. At surface pressure of 20 to 50 mN m<sup>-1</sup>, the shape of isotherms climbing up rapidly like isotherm of SA.

The collapse pressure of unsaturated C18 fatty acids/BSA are observed to be similar to their respective pure system, and there is no clear collapse pressure observed when the  $X_{BSA}$  is more than 0.5 for all 3 unsaturated C18 fatty acids/BSA mixed systems (Figure 4.8(b)–(d)). BSA is thought to be penetrated in between the lipid membrane by hydrophobic and van der Waal forces. The presence of BSA in the mixtures greatly affect the phase transition of the mixtures, in particularly, at the beginning of compression (at surface pressure of 0 to 18 mN m<sup>-1</sup>).

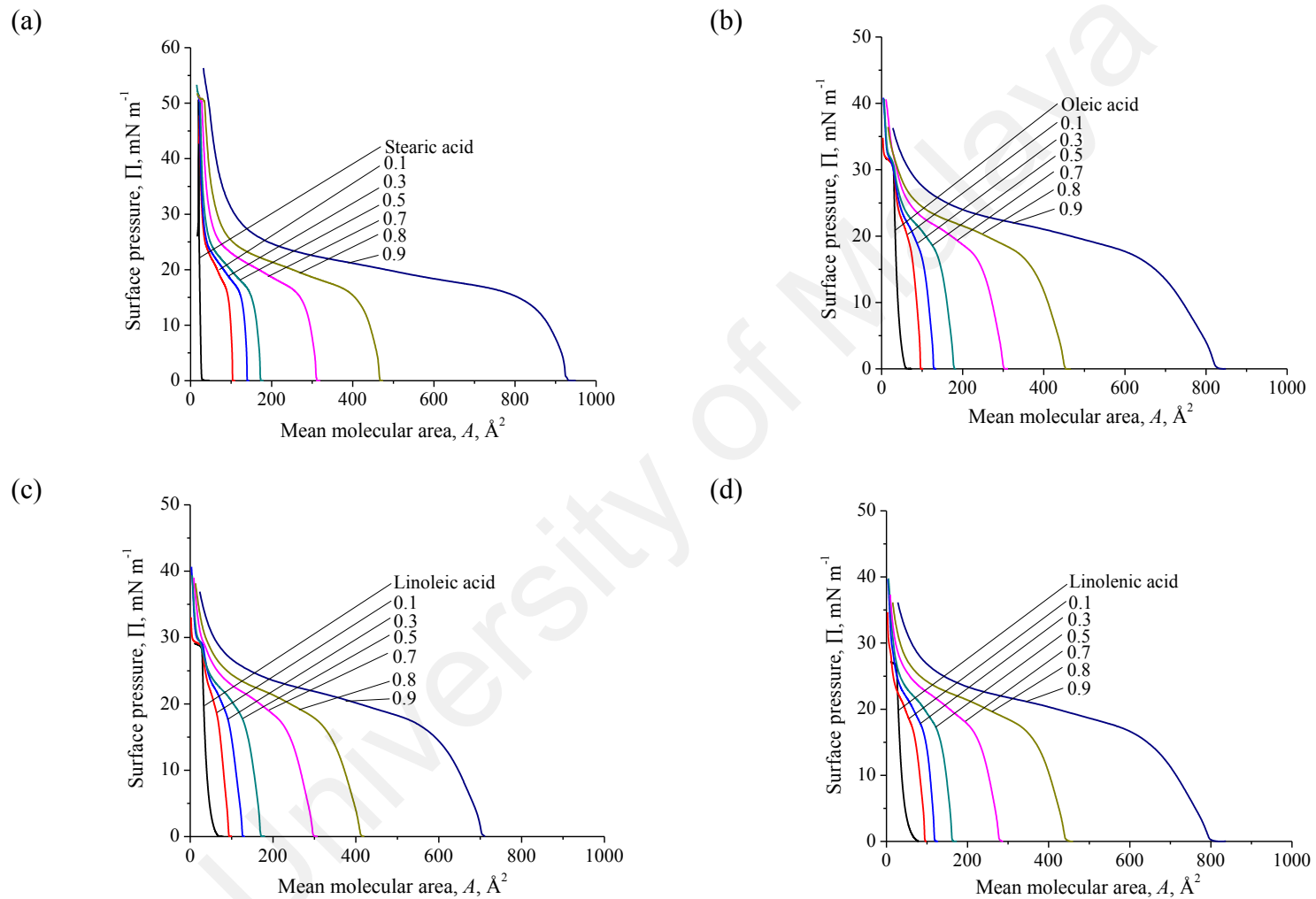


**Figure 4.8:** The surface pressure–area ( $\Pi$ – $A$ ) isotherms of mixed monolayers (plotted in mole fraction of BSA): (a) SA/BSA, (b) L1/BSA, (c) L2/BSA, and (d) L3/BSA spread on a nanopure water subphase at 25°C.

The presence of BSA improves the rigidity of the unsaturated C18 fatty acids membrane, making the membranes less fluid as compare to their respectively pure systems. As the compression increased (from 20 to 30 mN m<sup>-1</sup>), the polar BSA molecules may be sunk into the trough of water subphase, therefore the similar collapse pressure as their pure system were observed.

#### 4.2.1.5 Mixed monolayers of C18 fatty acids and AS25

There was no collapse pressure clearly observed in AS25 isotherm (Figure 4.9). However, the derivative of the pure-AS25  $C_s^{-1}$  versus  $\Pi$  profile (Figure 4.9) showed a change at 38 mN m<sup>-1</sup> that presumably corresponds to its collapse pressure. The limiting molecular area of AS25 was found to be 160 Å<sup>2</sup> (Figure 4.9), showing that AS25 molecules are much larger than C18 fatty acids. There is a change in the slope that can be observed at 28 to 30 mN m<sup>-1</sup>. This change is more obviously seen in its plot of  $C_s^{-1}$  versus  $\Pi$  (Figure 4.9), indicating that the monolayer of AS25 is low compressible and less ordered, where low  $C_s^{-1}$  values suggests that the organization of molecules of AS25 favor their arrangement in liquid-expanded phase in water subphase at 25°C. The isotherm of AS25 is used as a reference in this work to compare lipid-protein interactions and protein-protein interactions that take place in this study.

Shown in Figure 4.10 are the  $\Pi$ - $A$  isotherms of fatty-acid monolayers and mixed monolayers of C18 fatty acids (SA, L1, L2, and L3) with increasing volume of AS25 on nanopure water. When AS25 was incorporated into the SA monolayer, the isotherms of the mixed monolayers were shifted to higher mean molecular area with increasing volume of AS25 (Figure 4.10(a)). The collapse pressure of SA/AS25 mixed systems was significantly reduced from 50 mN m<sup>-1</sup> (pure SA monolayer) to about 30-35 mN m<sup>-1</sup> (Figure 4.10(a)).

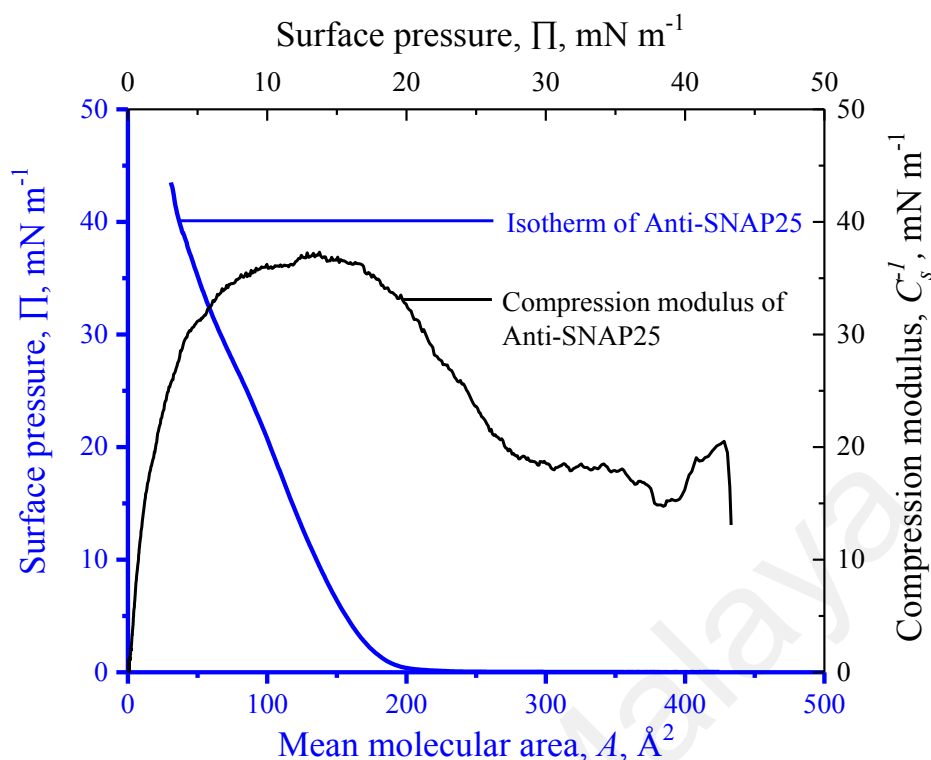


**Figure 4.9:** The surface pressure–area ( $\Pi$ – $A$ ) isotherm of Anti-SNAP25 monolayer and, its compressibility modulus ( $C_s^{-1}$ ), spread on water subphase at 25°C.

The presence of AS25 molecules in SA monolayer increase the membrane fluidity, making the molecular arrangement less well organized as compared to pure SA monolayer. The composition of a membrane will greatly affect its fluidity. There is no specific trend on the shift shown in mixed monolayers of unsaturated fatty-acid (L1, L2, and L3) isotherms (Figure 4.10(b)–(d)) with the addition of AS25, however isotherms of the L1 and L2 mixed systems are significantly shifting away (to smaller mean molecular area) from their pure fatty-acid isotherms in the presence of an antibody. This shows that interactions have taken place between the fatty acids and the antibody. The collapse pressures of unsaturated C18 fatty acids/AS25 mixed systems were lower by 5  $\text{mN m}^{-1}$  as compare to their pure monolayers. Plausibly, AS25 molecules partially embedded into the monolayer, or presence on the monolayer surface.

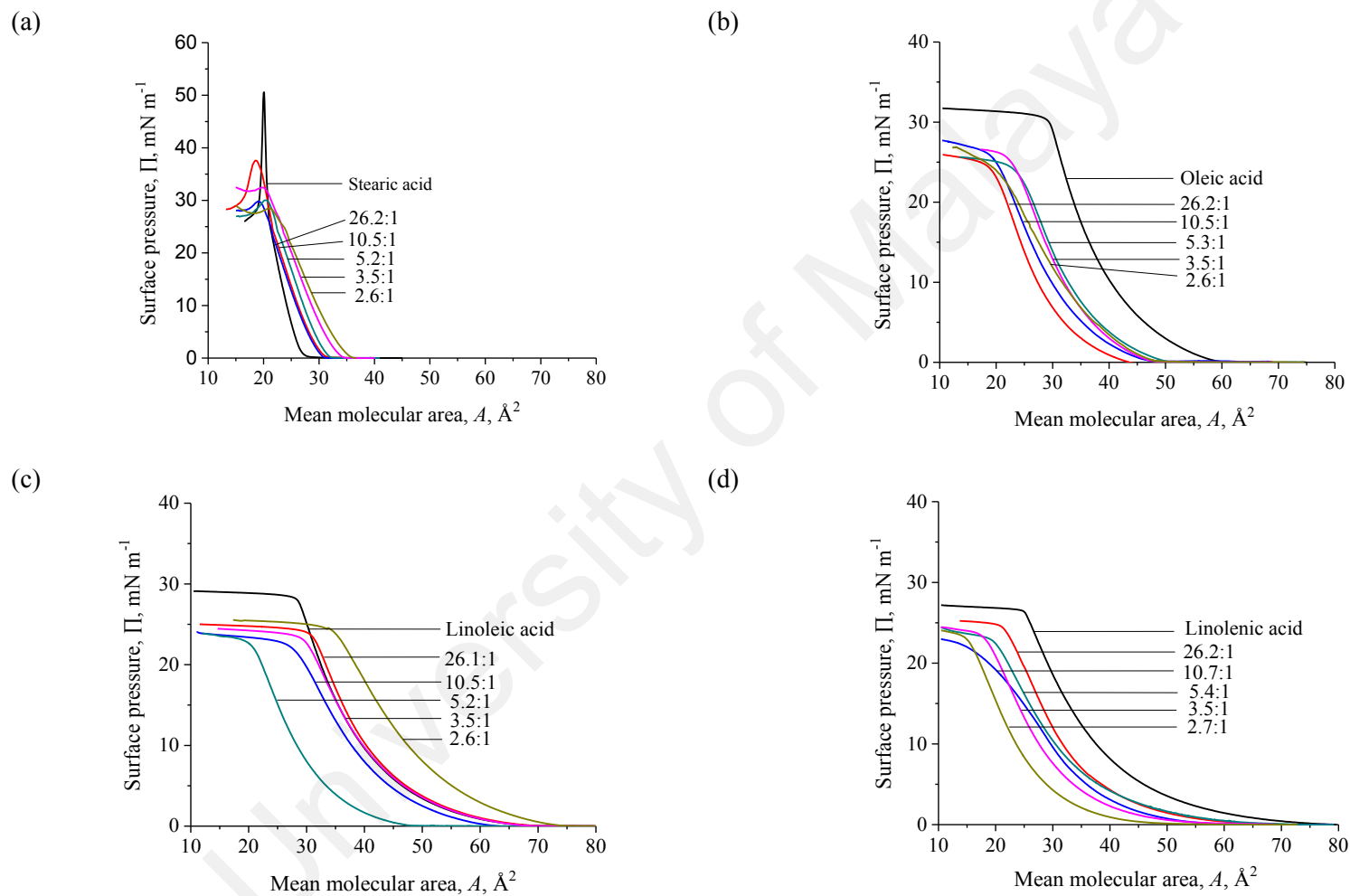


**Figure 4.10:** The surface pressure–area ( $\Pi$ – $A$ ) isotherms of mixed monolayers (plotted in mole ratio of C18 fatty acids to Anti-SNAP25): (a) SA/Anti-SNAP25, (b) L1/Anti-SNAP25, (c) L2/Anti-SNAP25, and (d) L3/Anti-SNAP25, spread on water subphase at 25°C.

#### 4.2.1.6 C18 fatty acids, DP and AS25 mixed monolayers

Prior to this experiment, experiments on C18 fatty acids/AS25 and C18 fatty acids/DP interactions were carried out and their energetic data was analyzed. The best mole ratios of each C18 fatty acid/DP were selected to be incorporated in the same amount of AS25 (as described in section 4.2.1.5) into the individual mixed system of C18 fatty acids/DP.

The incorporation of AS25 into SA/DP leads their isotherms shifted to the smaller mean molecular area and higher collapse pressure as illustrated in Figure 4.11(a). The collapse pressure of SA/DP/AS25 (45 to 50 mN m<sup>-1</sup>) is slightly higher than SA/DP (30 mN m<sup>-1</sup>). The effect of DP in the mixture was also clearly shown from 0 to 15 mN m<sup>-1</sup> in all of the mixed systems of SA/DP/AS25, which is similar to the behaviour of DP in SA monolayer. Presumably, DP–DP interactions were first to be occur, followed by DP–SA interactions, and then the incorporation of AS25 increased the rigidity of the molecular packing. The presence of unsaturated DOPE in DP interacts with saturated hydrocarbon chain of SA increases the membrane fluidity as discussed in 4.2.1.5, and yet, the incorporation of AS25 caused the formation of tightly packed monolayers. The presence of membrane protein AS25 on the surface membrane of SA/DP making it more condensed in their molecular packing. More on the phase transitions will be discussed in compression modulus (section 4.2.2.6).

In the unsaturated C18 fatty acid (L1/DP, L2/DP and L3/DP) mixed systems, the effect of AS25 in the mixed monolayer gave rise to the respectively mean molecular area (Figure 4.11(b)–(d)). There is no specific trend on the shift shown in all four mixed monolayers of C18 fatty acid/DP isotherms with the addition of AS25.

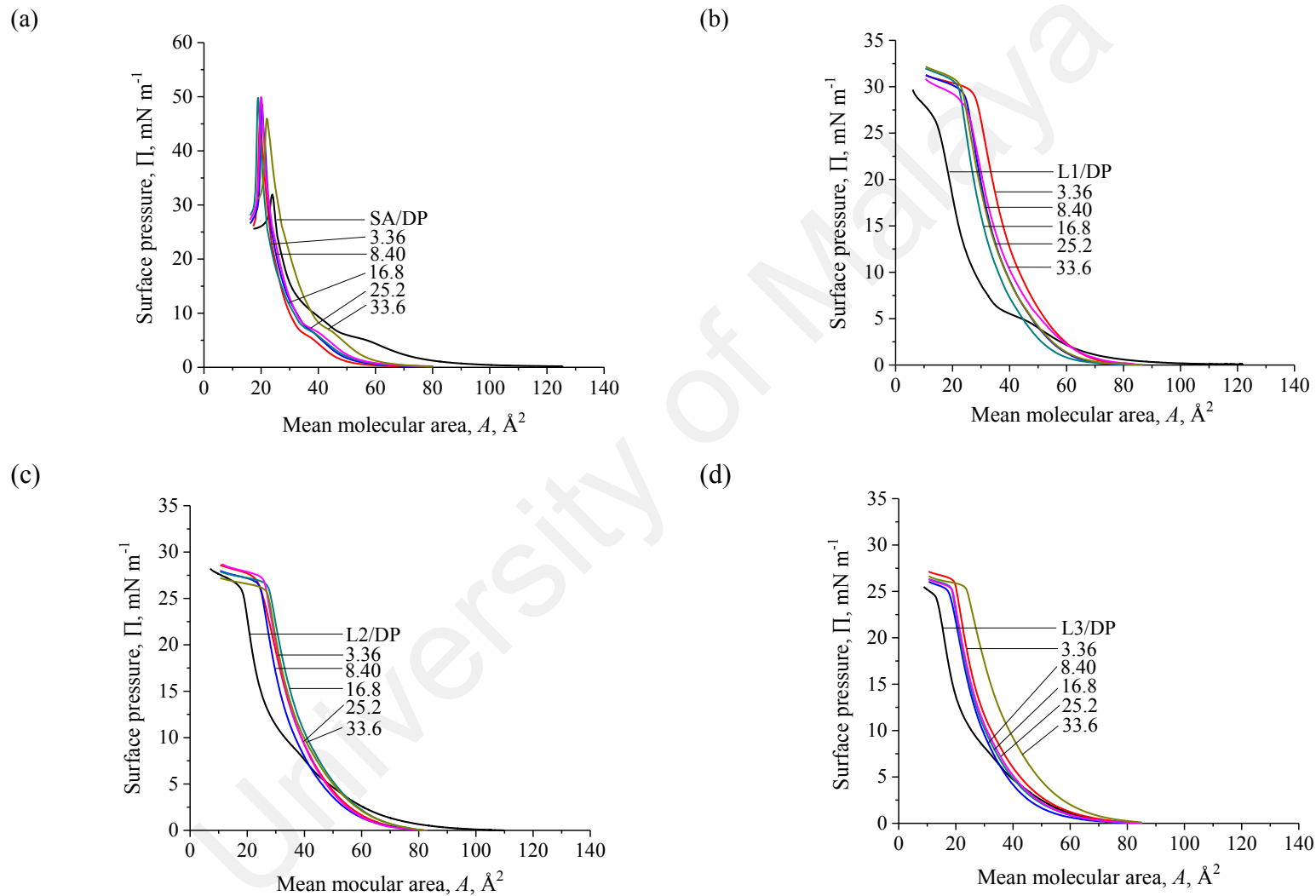


**Figure 4.11:** The surface pressure–area ( $\Pi$ – $A$ ) isotherms of mixed monolayers (plotted in nanomole of AS25): (a) SA/DP/AS25, (b) L1/DP/AS25, (c) L2/DP/AS25, and (d) L3/DP/AS25, spread on water subphase at 26°C.

However, the isotherms of the unsaturated C18 fatty acids/DP/AS25 mixed systems are noticeable shift away (to increasing mean molecular area) from their unsaturated C18 fatty acids/DP isotherms starting from the surface pressure of  $5 \text{ mN m}^{-1}$  onwards. The effect of DP in C18 fatty acids monolayer was clearly shown in their isotherms at surface pressure of 0 to  $15 \text{ mN m}^{-1}$  (Figure 4.6); however DP–DP interactions are not significantly shown in the unsaturated C18 fatty acids/DP/AS25 isotherms. This could be membrane protein AS25 interacted with the carboxyl and PEG headgroups in the mixed system, instead of the hydrocarbon chains of unsaturated C18 fatty acids and DP. The collapse pressures of unsaturated C18 fatty acids/DP/AS25 mixed systems are similar to their unsaturated C18 fatty acids/DP isotherms.

#### **4.2.2 Compressibility analysis**

##### **4.2.2.1 Pure monolayers of SA, L1, L2, and L3**

The significantly large value of compression modulus for the pure SA monolayer indicates its highly condensed phase (Figure 4.12). As the compression began at surface pressure of 0 to  $20 \text{ mN m}^{-1}$ , pure SA occurs at L phase; then a change of its slope was observed at  $25 \text{ mN m}^{-1}$ , a noticeable phase transition of pure SA occurs from L phase to S phase. The maximal  $C_s^{-1}$  value of pure SA is  $700 \text{ mN m}^{-1}$  (Gew & Misran, 2016). Molecules of SA are packed closely in favored of its saturated hydrocarbon chain due to the van der Waals interactions occur between their tails.

The maximum compression modulus values of pure-L1 and -L2 monolayers are approximately  $80 \text{ mN m}^{-1}$  and  $65 \text{ mN m}^{-1}$ , respectively, and the pure-L3 monolayer, which is an unsaturated fatty acid with three double bonds, has the lowest compression modulus value,  $45 \text{ mN m}^{-1}$  (Figure 4.12). No obvious phase transition is observed in these three unsaturated fatty acids. They are either at LE or L phase. Unsaturated fatty acids are less compressible compared to saturated fatty acids because of their *cis*-double

bonds in the hydrocarbon long chain. The presence of *cis*-bonds in hydrophobic chains affects its geometry structure: the more *cis*-double bonds, the more bent is the chain. The presence of double bonds prevents them from packing tightly together, which allows more favorable packing of the molecules in the mixed monolayer. Theoretically, LE and L phases in monolayers are ideal for proteins to be embedded in between the fatty acids (Gew & Misran, 2016).

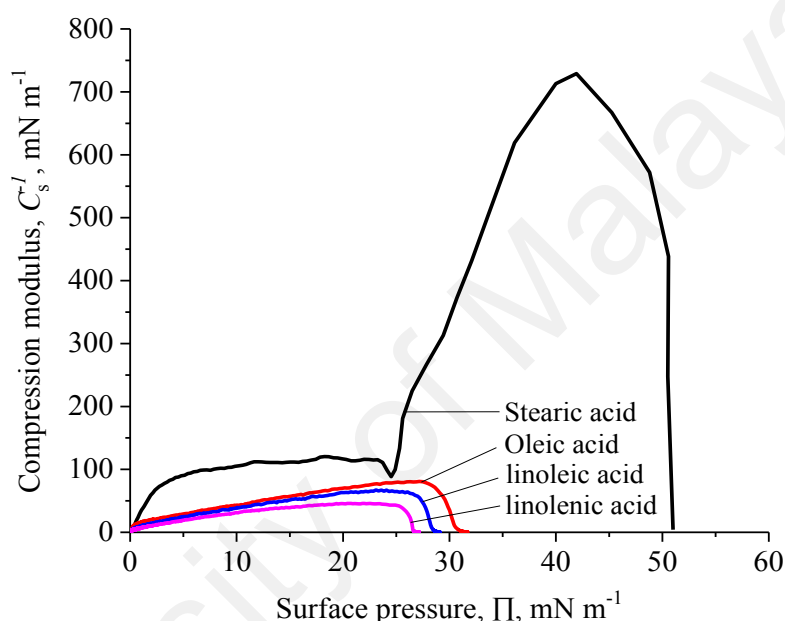


**Figure 4.12:** The compression modulus ( $C_s^{-1}$ ) of pure C18 fatty acids (stearic acid, oleic acid, linoleic acid and linolenic acid) monolayers, spread on water subphase at 25°C.

#### 4.2.2.2 Mixed monolayers of C18 fatty acids: Effect of degree of saturation

The same noticeable phase transition like pure SA is also observed in SA/L1, SA/L2 and SA/L3 mixtures (Figure 4.14). At surface pressure of 25  $\text{mN m}^{-1}$ , the phase transition changed from L to LC, and then to S phase. At  $X_{SA} = 0.9$ ,  $C_s^{-1}$  profiles of SA/L2 and SA/L3 showed higher  $C_s^{-1}$  maximal value (500  $\text{mN m}^{-1}$ ) than SA/L1 (250  $\text{mN m}^{-1}$ ) at surface pressure between 30 to 48  $\text{mN m}^{-1}$ , but lower than the  $C_s^{-1}$  maximal value of pure SA monolayer (700  $\text{mN m}^{-1}$  in Figure 4.12). When  $X_{SA} \leq 0.3$ , there is no noticeable phase transition like SA. They have the similar profile like their unsaturated

C18 fatty acids pure systems remained at L or LE phase ( $<100 \text{ mN m}^{-1}$ ). The presence of unsaturated fatty acids (L1, L2, and L3) in SA monolayer disrupts SA monolayer's condensation and increase membrane fluidity (Figure 4.13(a)). This is due to the steric effect contributed by the *cis*-double bond(s) in the mixed monolayers. As the mole fraction of unsaturated C18 fatty acids is higher than SA, the membrane fluidity increases.

The maximal  $C_s^{-1}$  values of L1/L2 and L1/L3 in L1 were smaller as compare to L1 pure monolayer (Figure 4.15(a) & (b)). All the mixtures exhibited LE phase for the entire investigated ranges. The maximal value of  $C_s^{-1}$  of L2/L3 is less than  $50 \text{ mN m}^{-1}$  (Figure 4.15(c)).  $C_s^{-1}$  Profiles of L2/L3 of the entire investigated ranges also showed LE phase. The bending of hydrocarbon chain of the *cis*-double bond(s) increases the membrane fluidity of monolayers as illustrated in Figure 4.13(b). Hence, the repulsion between the tails prevent the perfect molecular packing of molecules.

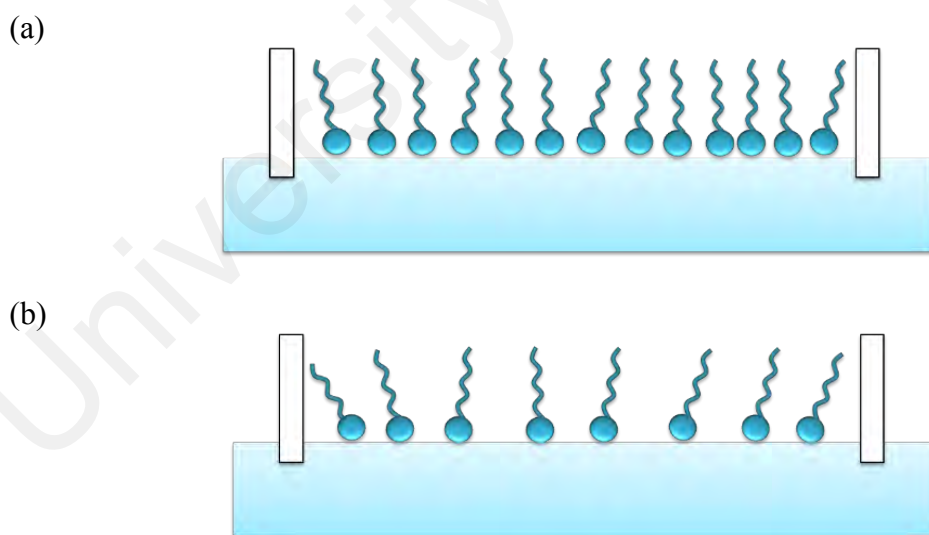


**Figure 4.13:** A schematic illustration of the molecular packing of SA/L1, and (b) L1/L2 mixed monolayers.

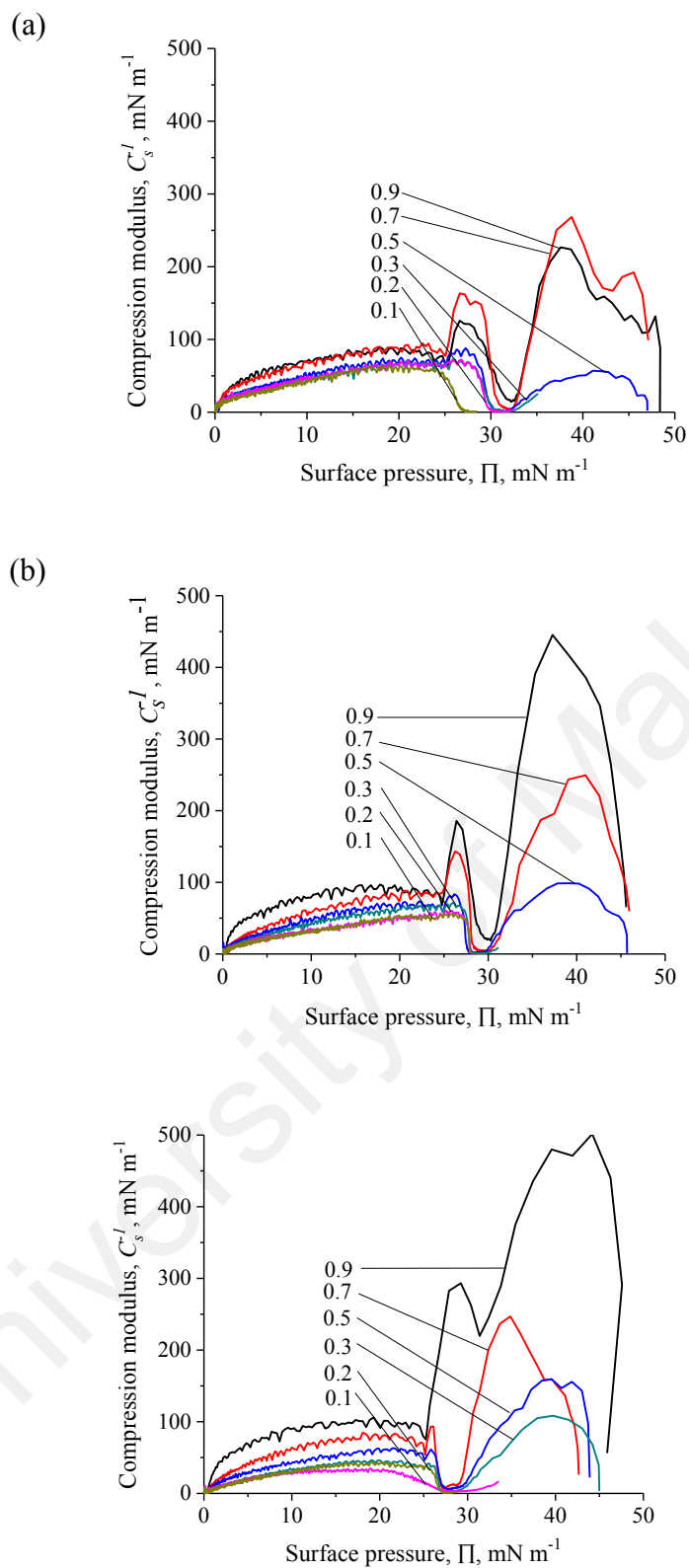


**Figure 4.14:** The compressibility modulus ( $C_s^{-1}$ ) vs surface pressure ( $\Pi$ ) of mixed monolayers (plotted in mole fraction of SA): (a) SA/L1, (b) SA/L2, and (c) SA/L3 mixed monolayers, spread on a nanopure water subphase at 25°C.

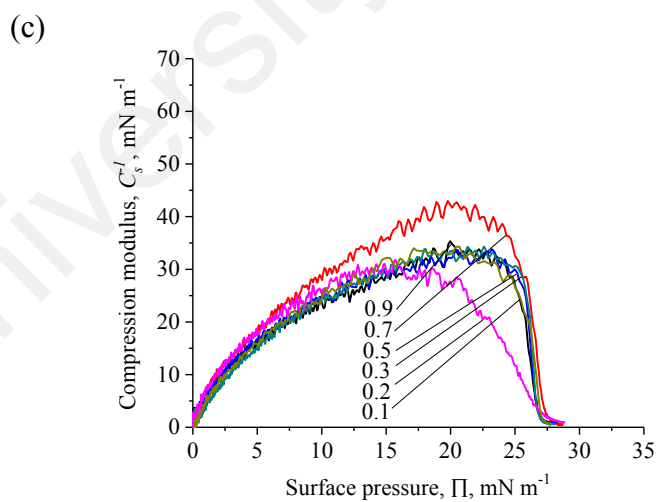
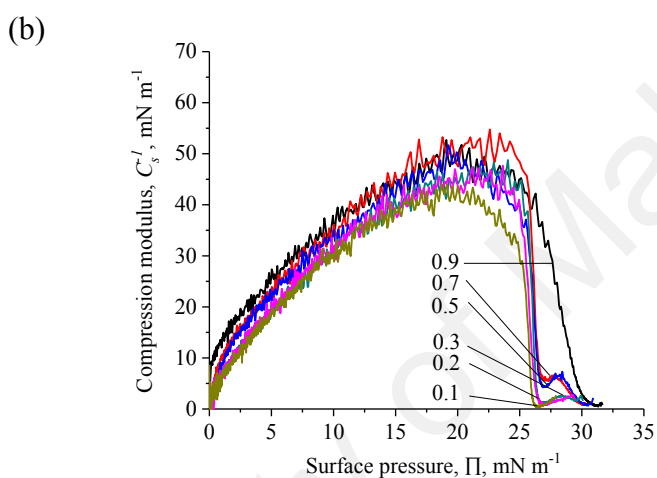
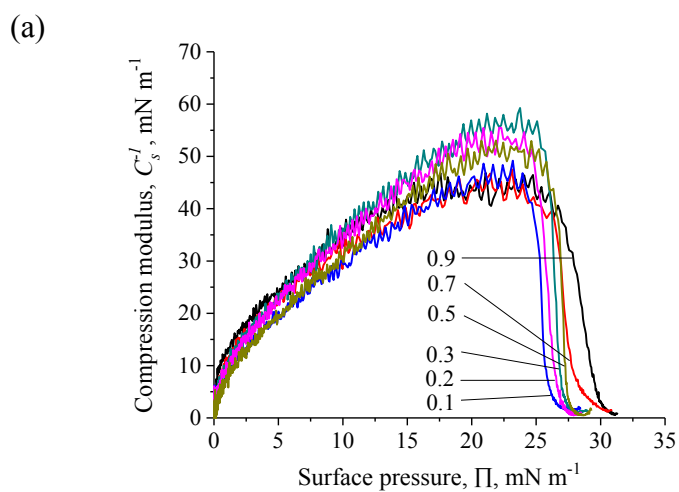


**Figure 4.15:** The compressibility modulus ( $C_s^{-1}$ ) vs surface pressure ( $\Pi$ ) of mixed monolayers (plotted in mole fraction of L1 or L2): (a) L1/L2, (b) L1/L3, and (c) L2/L3 mixed monolayers, spread on a nanopure water subphase at 25°C.

#### 4.2.2.3 Mixed monolayers of C18 fatty acids and DP

At low surface pressures (0 to 10 mN m<sup>-1</sup>), results similar to those of the DP compression moduli were observed in all of the mixed systems, as plotted in Figure 4.16. These results showed that the effect of DP was very strong in all of the mixtures; intermolecular interactions began with DP–DP interactions and then DP–FAs occurred from 10 mN m<sup>-1</sup> onwards.

SA can easily form a solid phase because it contains a saturated hydrocarbon chain. With the presence of DP in SA monolayers, its mixtures were less compressible than pure SA, consecutively forming LE, L, and LC phases. The *cis*-double bonds of DOPE in DP increased the membrane fluidity, which prevented the molecules from packing tightly and uniformly. Interestingly, the maximal values of the compression modulus for mixed systems of SA/DP of 90:1 and 100:1 were higher than those of other mixed monolayers of SA/DP (Figure 4.16(a)). The molecular packing of SA/DP was favorable when the mole ratio of SA was higher; less bend and kink effects were contributed from the *cis*-double bonds of DOPE in the DP molecular structures to the monolayers.

The *cis*-double bonds in the unsaturated C18 fatty acids in the mixed systems increased the membrane fluidity and greatly affected the compressibility of the mixed monolayer. Pure-L1, -L2, and -L3 were in L phase. Mixed systems of L1/DP, L2/DP and L3/DP had lower compression moduli compared with their pure monolayers, which were below 50 mN m<sup>-1</sup> (Figures 4.16(b)–(d)). The phases of the monolayers changed from L to LE phase. The L3/DP mixed systems had a similar compression-modulus value as the pure system. However, an exception was observed for a mole ratio of L3/DP at 100:1; its maximal value was higher than that of the pure system (Figure 4.16(d)).

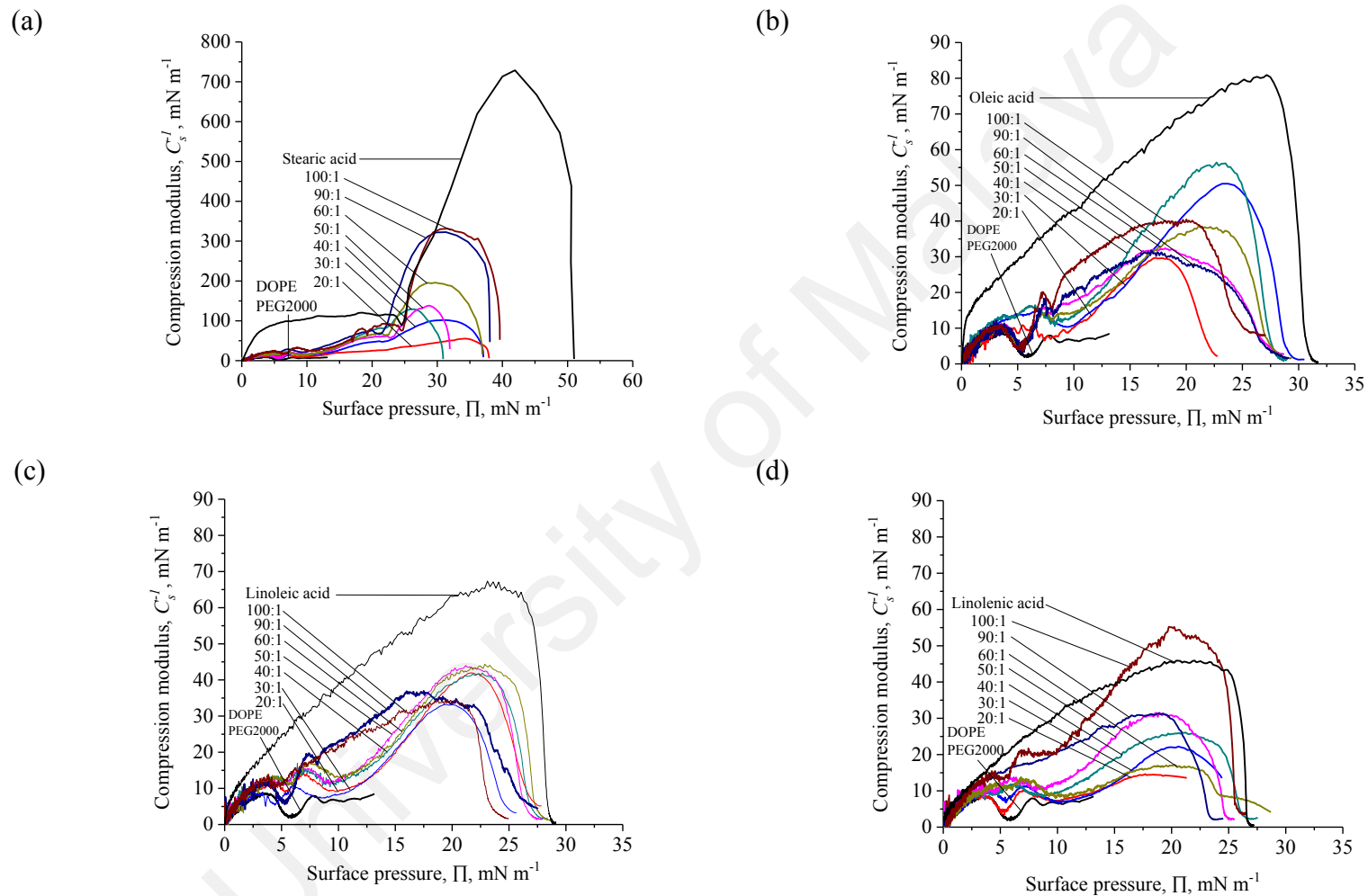


**Figure 4.16:** The compressibility modulus ( $C_s^{-1}$ ) vs surface pressure ( $\Pi$ ) of mixed monolayers (plotted in mole ratio of C18 fatty acids to DOPE PEG2000): (a) SA/DOPE PEG2000, (b) L1/DOPE PEG2000, (c) L2/DOPE PEG2000, and (d) L3/DOPE PEG2000, spread on a nanopure water subphase at 25°C.

#### 4.2.2.4 Mixed monolayers of C18 fatty acids and BSA

Two remarkable observations can be made on  $C_S^{-1}$  versus  $\Pi$  profile of C18 fatty acids/BSA binary systems (Figure 4.17). Firstly, the similar shape of pure BSA  $C_S^{-1}$  versus  $\Pi$  profile of pure BSA was observed in C18 fatty acids/BSA profile at surface pressure of 0 to 20  $\text{mN m}^{-1}$ . Presumably, the protein-protein interaction of BSA–BSA occurred when the compression first began. However, as the compression continued, protein-protein interaction is followed by lipid-protein interaction of C18 fatty acids–BSA occurred. Secondly, a similar  $C_S^{-1}$  versus  $\Pi$  profile of pure C18 fatty acids is observed at surface pressure of 25 to 50  $\text{mN m}^{-1}$ , but a lower  $C_S^{-1}$  value ( $<100 \text{ mN m}^{-1}$  for SA and  $<25 \text{ mN m}^{-1}$  for L1, L2 and L3) is obtained. At the first maximal (surface pressure of 0 to 20  $\text{mN m}^{-1}$ ), all SA/BSA mixed monolayers exist as solid crystalline phase ( $C_S^{-1}$  values are in between 500 to 700  $\text{mN m}^{-1}$ ). With the increasing of  $X_{BSA}$  in unsaturated C18 fatty acid monolayers (L1, L2 and L3), it exhibits LC phase at their first maximal. Phase transition shifted from the ordered LC phase to disordered LE phase with the increasing mole fraction of L1, L2, and L3. At surface pressure of 25 to 50  $\text{mN m}^{-1}$ , a small peak is more obvious for SA/BSA mixed systems as compare to L1/BSA, L2/BSA and L3/BSA systems.

The incorporation of BSA into SA monolayer increases the membrane fluidity and prevents the molecular packing from forming solid phase at the second maximal, unlike the second maximal pure SA monolayer is as high as 700  $\text{mN m}^{-1}$ . The presence of BSA greatly affects the phase transition and molecular packing of the mixed systems differently in term of the degree of saturations. In contrast, BSA improves the molecular packing of unsaturated C18 fatty acids from L to LC phase, enhance a better molecular packing in the mixed monolayer making it less fluid as compared to their pure monolayers.

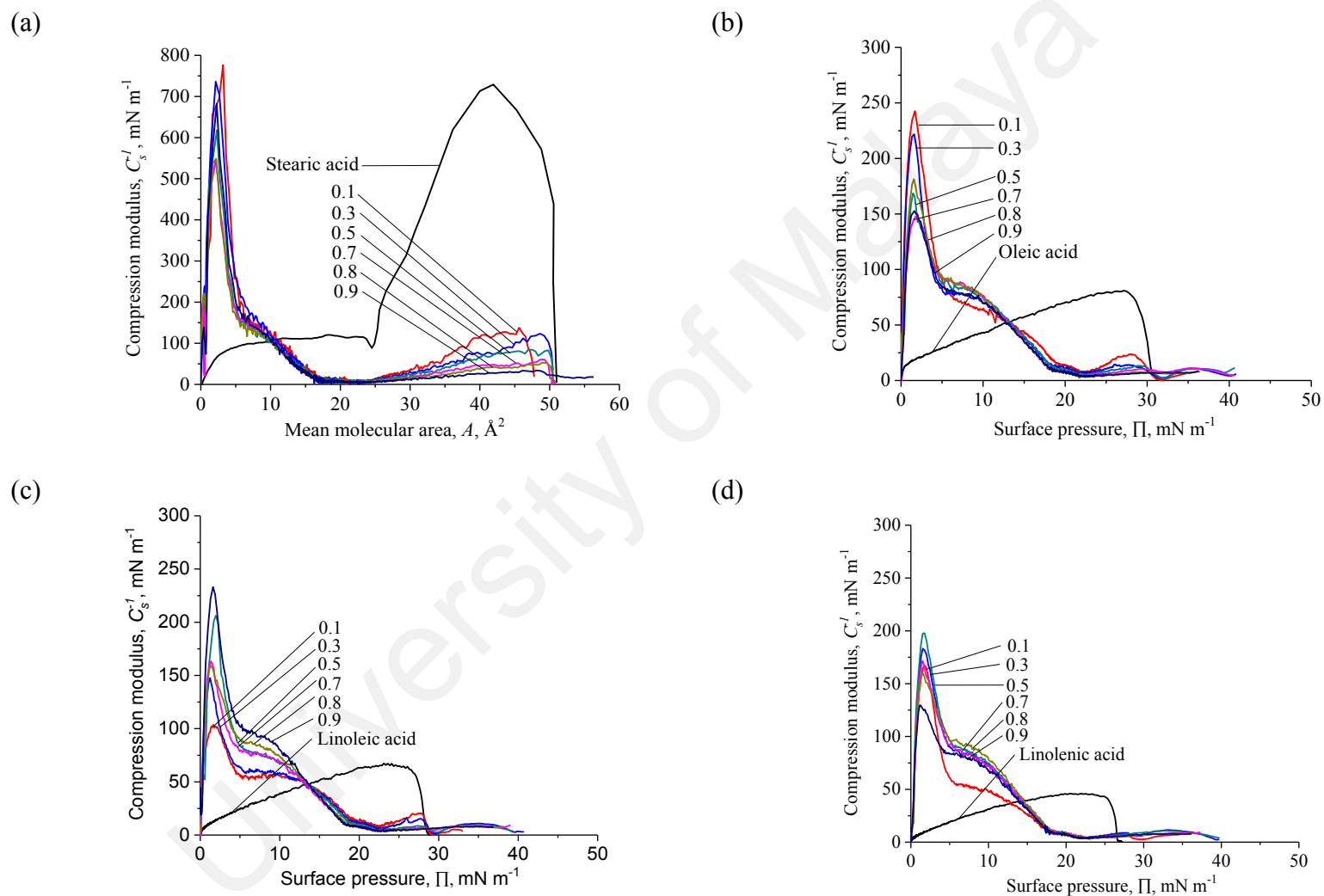


**Figure 4.17:** The compressibility modulus ( $C_s^{-1}$ ) vs surface pressure ( $\Pi$ ) of mixed monolayers (plotted in mole fraction of BSA): (a) SA/BSA, (b) L1/BSA (c) L2/BSA, (d) L3/BSA, spread on a nanopure water subphase at 25°C.

#### 4.2.2.5 Mixed monolayers of C18 fatty acids and AS25

There is an obvious difference observed in the compressibility plot of pure SA monolayers and its mixed monolayers in the presence of antibodies at lower surface pressure (Figure 4.18(a)). At higher surface pressure, there are some interesting observations obtained by comparing the compression-modulus profiles of SA/AS25 and pure AS25. The similar pattern in both curves were observed at surface pressures of 28 to 32 mN m<sup>-1</sup>. AS25 is known a membrane-bound protein; this behavior is clearly shown in the analysis of the binary mixed monolayer of SA/AS25. SA can be easily compressed to form a monolayer at solid phase because of the saturated hydrocarbon chain. Significant intermolecular repulsion has taken place between SA and AS25, as shown by a positive  $G_{mix}$  in Figure 4.29(b).

Molecular rearrangement of AS25 takes place in the mixtures during compression of barriers to accommodate the behavior of SA molecules, rod-like molecules with all *trans*-conformation in its saturated hydrocarbon chain. Once the monolayer of SA is formed and the molecules are tightly packed uniformly, AS25 interacts with SA head-group peripherally and does not interact with SA as an integral protein, interacting spontaneously with phospholipids in natural biological membranes (Gew & Misran, 2014, 2016).

Intermolecular interactions between amphiphilic fatty acids and AS25 molecules can be studied in depth by interpreting protein sequences in SNAP-25 to obtain better insight. SNAP-25 protein sequences are made of 206 amino acids (Hodel, 1998), including 63 hydrophobic, 69 hydrophilic, 44 acidic, and 30 basic amino acids. The polarity of SNAP-25 can be predicted by studying the side chain of each amino acid in the sequences, where hydrophilic amino acids will attract to the polar head-group region of fatty acids, and hydrophobic amino acids will attract to the non-polar hydrocarbon chain. However, the prediction from their protein sequences by interpreting their

polarity of amino acids is insufficient to elucidate the behaviour of AS25 in the lipid membrane as lipid-protein interactions are also affected by lipid membrane fluidity, which is related to the degree of saturation of the hydrocarbon chain and the head-group of the lipids. Thus, Gibbs free energy mixing studies is meaning in the investigations on lipid-protein interaction.

The investigated C18 fatty acids possess the same head-group, but different saturation degrees in their hydrocarbon chain. The presence of *cis*-bonds in hydrophobic chains affects its geometry structure: the more *cis*-double bonds, the more bent is the chain. The presence of double bonds prevents them from packing tightly together, which allows more favourable packing of the molecules in the mixed monolayer. The maximum compression modulus value of pure-L1 and -L2 monolayers are approximately  $80 \text{ mN m}^{-1}$  and  $65 \text{ mN m}^{-1}$  respectively, and the pure-L3 monolayer, which is an unsaturated fatty acid with three double bonds, has the lowest compression modulus value,  $45 \text{ mN m}^{-1}$  (Figure 4.18(b)–(d)). Unsaturated fatty acids are less compressible compared to saturated fatty acids due to their *cis*-double bonds in the hydrocarbon long chain. No phase transition is observed in these three unsaturated fatty acids. They are either at LE or L phase. Theoretically, LE and L phases in monolayers are ideal for antibodies to be embedded in between the fatty acids. Mixed systems of L1 and L2 have lower compression moduli compared to their pure systems, which are below  $50 \text{ mN m}^{-1}$ . The phase of the monolayers changes from L to LE phase. The L3 mixed system has a similar compression-modulus value as the pure system. The AS25 compression modulus was discussed above, was also found to be LE phase. Spontaneity between antibodies on the monolayer will be discussed in depth by looking at the thermodynamic stability analysis in the following section.

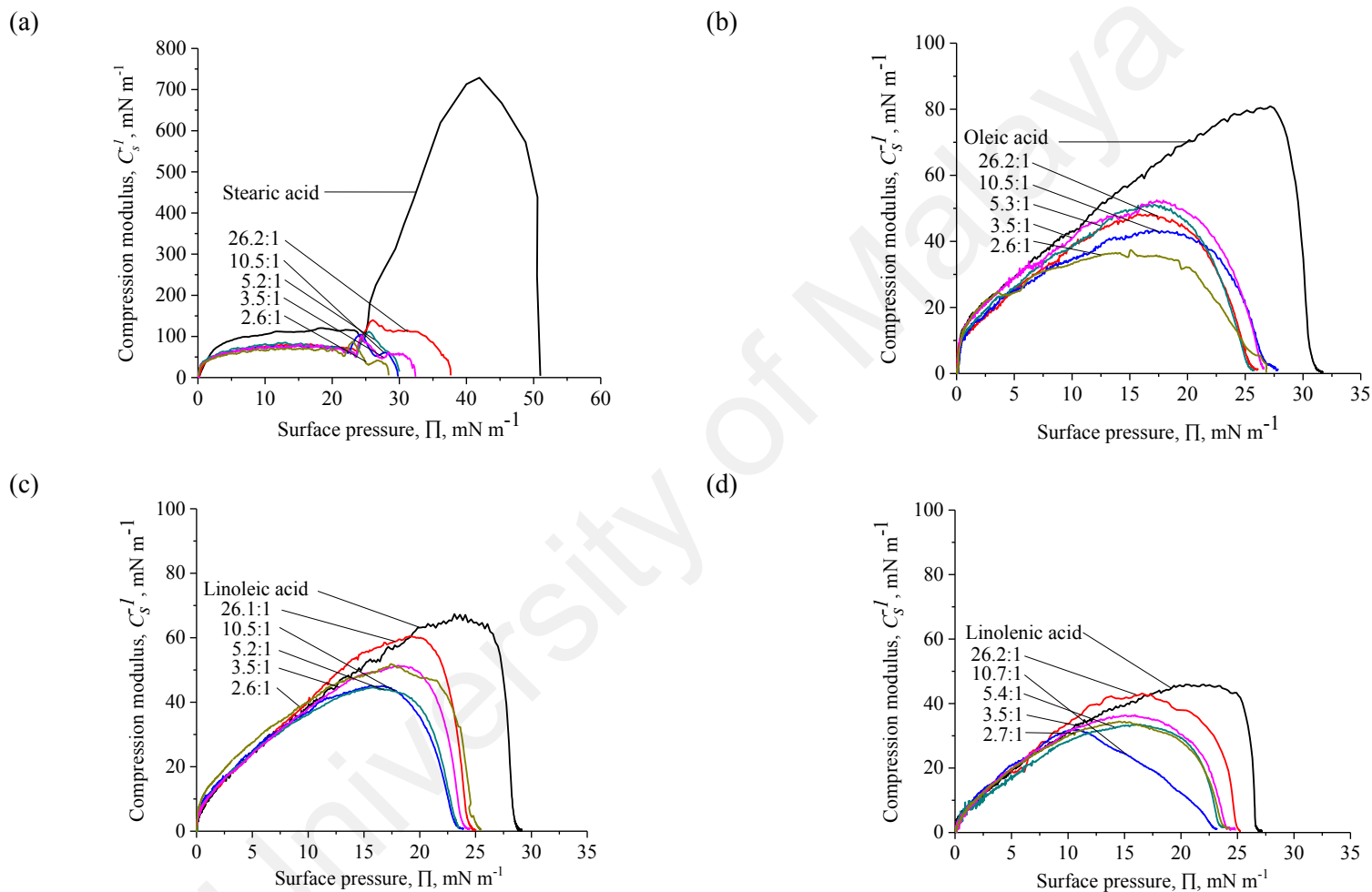


**Figure 4.18:** The compressibility modulus ( $C_s^{-1}$ ) vs surface pressure ( $\Pi$ ) of mixed monolayers (plotted in mole ratio of C18 fatty acids to Anti-SNAP25): (a) SA/Anti-SNAP25, (b) L1/Anti-SNAP25, (c) L2/Anti-SNAP25 and (d) L3/Anti-SNAP25, spread on water subphase at 25°C.

#### 4.2.2.6 C18 fatty acids, DP and AS25 mixed monolayers

As the compression started ( $0$  to  $10 \text{ mN m}^{-1}$ ), the similar shape of DP were shown in the SA/DP/AS25 isotherms (Figure 4.20(a)). This could be DP–DP interactions take place first, followed by DP-SA, then the present of AS25 molecules increases the  $C_s^{-1}$  maximal value of SA/DP/AS25 and collapsed at a higher pressure as compared to pure SA. The  $C_s^{-1}$  maximal value of SA/DP exhibits LE phase, and then changed to LC phase as the mole of AS25 in SA/DP/AS25 mixtures increased. The incorporation of AS25 into the mixed monolayer caused the molecular packing to be more rigid and densely packed. There were a few slopes can be seen at surface pressure of  $25$  to  $50 \text{ mN m}^{-1}$ . For the proteins to achieve stability on lipid membrane, the reorientation of membrane protein AS25 may occur as the compression was closer to the collapse pressure at  $50 \text{ mN m}^{-1}$  as illustrated in Figure 4.19. AS25 molecules may adsorb (i) on the carboxyl headgroup SA/DP, or (ii) in between carboxyl of SA and PEG headgroups of DP, or (iii) on the PEG headgroup of DP as shown in Figure 4.19. Energetic stability analysis in the following section will enable us to determine the precise position of AS25 molecules on the SA/DP monolayer.

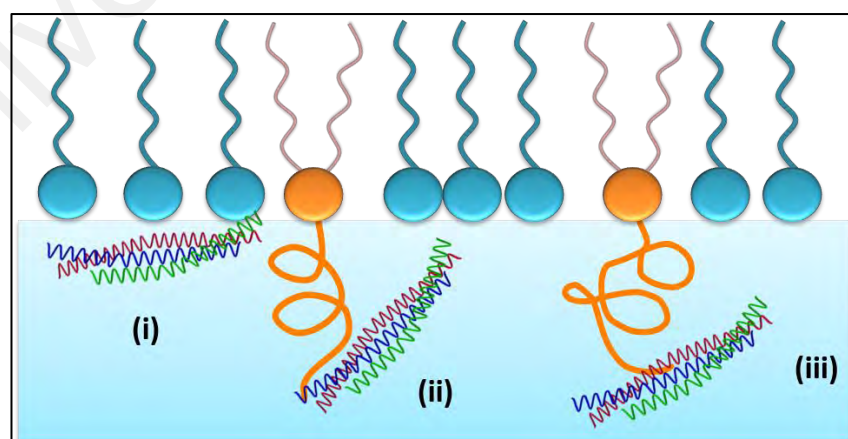


**Figure 4.19:** AS25 molecules may adsorb (i) on the carboxyl headgroup SA/DP, or (ii) in between carboxyl of SA and PEG headgroups of DP, or (iii) on the PEG headgroup of DP.

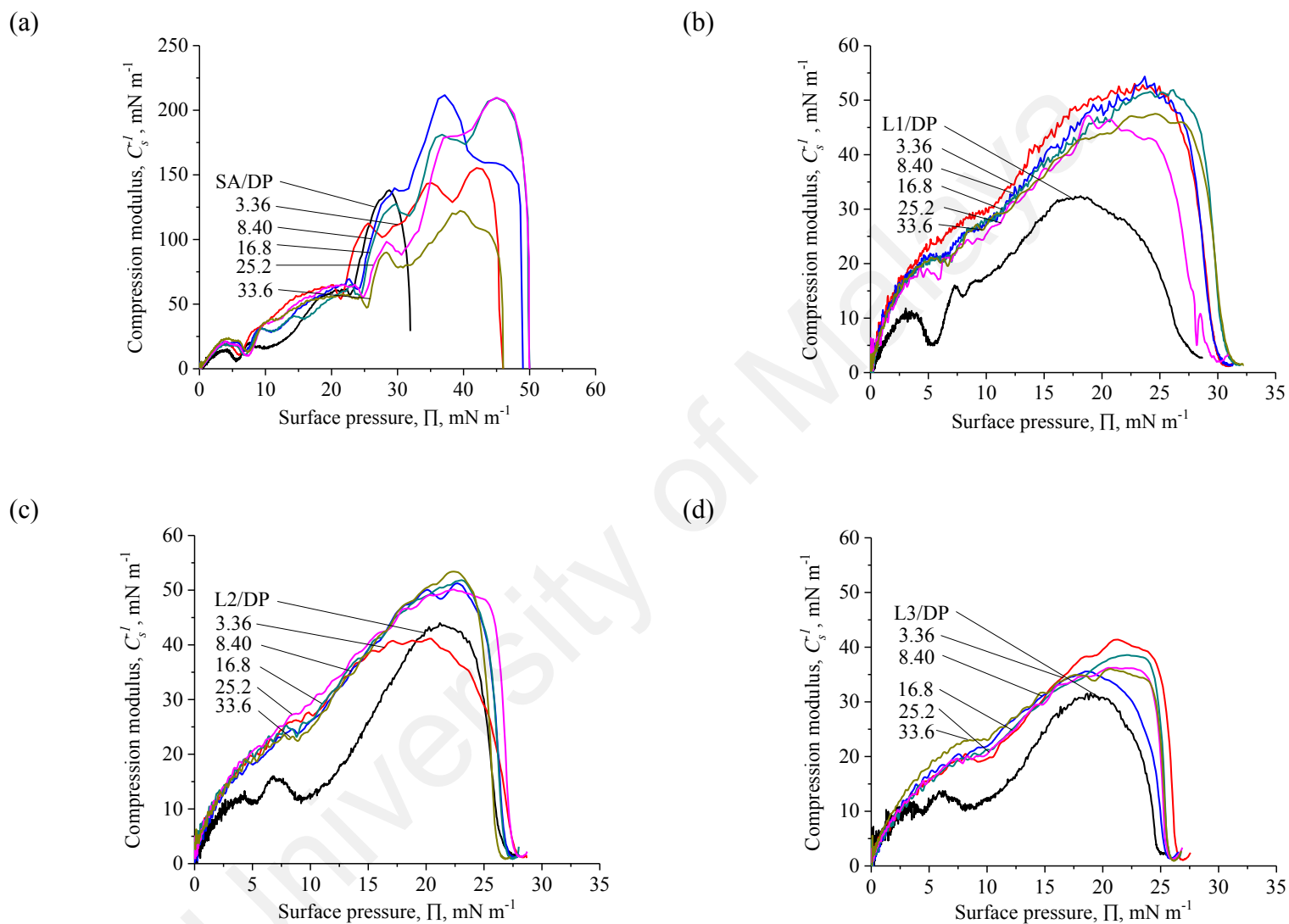


**Figure 4.20:** The compressibility modulus ( $C_s^{-1}$ ) vs surface pressure ( $\Pi$ ) of mixed monolayers (plotted in nanomole of AS25): (a) SA/DP/AS25, (b) L1/DP/AS25, (c) L2/DP/AS25, and (d) L3/DP/AS25, spread on water subphase at 25°C.

L1/DP/AS25, L2/DP/AS25 and L3/DP/AS25 mixtures shows LE phase at all range of investigation (Figure 4.20(b)–(d)). The presence of AS25 in the unsaturated C18 fatty acids/DP mixtures has higher values of  $C_s^{-1}$  as compare to the binary mixtures without AS25. There is no  $C_s^{-1}$  versus  $\Pi$  profile of DP in their mixtures at surface pressure of 0 to 10 mN m<sup>-1</sup> shown in all unsaturated C18 fatty acids/DP mixtures. Presumably, DP mixed well with unsaturated C18 fatty acids at a mole ratio of 50 to 1, forming a mixed monolayer spontaneously as shown in their energetic stability analysis (Figure 4.25(b)). AS25 molecules interact with the surface of unsaturated C18 fatty acids/DP membrane, unlike in  $C_s^{-1}$  versus  $\Pi$  profile of SA/DP/AS25 has several slopes were observed at higher surface pressure (30 to 50 mN m<sup>-1</sup>). The unsaturated C18 fatty acids/DP mixed monolayers are more fluid and less ordered will promote the incorporation of AS25 as compare to the saturated monolayer. The reorientation of AS25 may also occur in the LE phase of unsaturated C18 fatty acids/DP mixed monolayer, however the reorientation of AS25 may be able to be accommodated by the fluid membrane therefore it is not clearly captured in the isotherms and  $C_s^{-1}$  profile.

### **4.2.3 Energetic stability of mixed monolayers**

#### **4.2.3.1 Mixed monolayers of C18 fatty acids: Effect of degree of saturation**

In Figure 4.21, the mean molecular area  $A_{ex}$  is presented against mole fractions of SA mixed monolayers of C18 fatty acids at different surface pressures (5, 10, 15, 20 and 25 mN m<sup>-1</sup>). A positive deviation from linearity was attributed to the immiscibility of both components interacting with each other at the interface. The mean molecular area declined as the surface pressure increased. There were only slight deviations from ideality observed at  $X_{SA} = 0.1$  and  $0.2$  at selected surface pressures, indicating immiscibility between both components in a mixed monolayer (Figure 4.21). At  $X_{SA} = 0.2$  to  $0.9$ , a remarkable negative deviation indicated strong attractions between the

molecules in the mixed monolayer as compared with the interactions in their respective pure films. Large negative deviation observed at  $X_{SA} = 0.2, 0.3$  and  $0.5$  for the selected surface pressures showed a significant influence on the molecular packing and favorable interactions between molecules in the mixed monolayers. Negative deviations of  $A_{ex}$  revealed non-ideal behavior and showed that the monolayer components were miscible. This observation was also supported by the negative values obtained for  $G_{mix}$  (Figure 4.22), which showed that strong intermolecular attractions occurred between SA and unsaturated C18 fatty acids (L1, L2 and L3) at  $X_{SA} = 0.5$  and  $0.7$ .

Negative values of  $G_{mix}$  in the entire range of the SA and unsaturated C18 fatty acids monolayer composition except  $X_{SA} = 0.1$ , indicated strong attractions between molecules in the mixed system (Figure 4.22).  $G_{mix}$  values became more negative with the increasing mole fraction of unsaturated C18 fatty acids. This could be the effect of the *cis*-double bond(s) of polyunsaturated fatty acids promote the membrane fluidity. The most stable intermolecular interaction was observed at  $X_{SA} = 0.5$  for SA/L3 and  $0.7$  for SA/L1 and SA/L2 at discrete surface pressures. It was also supported by the  $A_{ex}$  and  $C_s^{-1}$  measurements as discussed earlier.

In Figure 4.23, the mean molecular area  $A_{ex}$  is presented against mole fractions of unsaturated C18 fatty acids mixed monolayers (L1/L2, L1/L3, and L2/L3) at surface pressures of 5, 10, 15, 20 and 25  $\text{mN m}^{-1}$ . A negative deviation from linearity was also observed in the unsaturated mixtures showing the immiscibility of both unsaturated components interacting with each other at the interface. The mean molecular area declined as the surface pressure increased. A slight deviation from ideality was observed at  $X_{LI} = 0.1$  and  $0.2$  at selected surface pressures, indicating immiscibility and weak interactions in a mixed monolayer (Figure 4.23(a) & (b)). At  $X_{LI} = 0.3$  to  $0.7$ , a noteworthy deviation indicated strong attractions between L1 and L2 (or L3) molecules in the mixed monolayer as compared with the interactions in their respective pure films.

$A_{ex}$  values of L2/L3 is slightly smaller than L1/L2 and L1/L3 mixed systems in the entire investigation range showed that L2 and L3 are energetically stable in a monolayer (Figure 4.23(c)). At  $X_{L2} = 0.1$  (Figure 4.24(c)), small positive values of  $G_{mix}$  were obtained for L2/L3 as compare to L1/L2 and L1/L3, indicating poor repulsion occurred between L2 and L3 when  $X_{L2} = 0.1$  at the selected surface pressure. It showed a significant influence on the molecular packing and favorable interactions between molecules in the mixed monolayers. The increasing *cis*-double bonds disrupt the molecular packing, hence increase membrane fluidity. Negative deviations of  $A_{ex}$  revealed non-ideal behavior and showed that the monolayer components were miscible. This observation was also supported by the negative values obtained for  $G_{mix}$  (Figure 4.24), which showed that strong intermolecular attractions occurred in unsaturated C18 fatty acids mixtures (L1/L2, L1/L3 and L2/L3).

There is a slight recovery of  $G_{mix}$  at  $X_{SA} = 0.9$  (Figure 4.22) in the mixed monolayers of SA/L1, SA/L2 and SA/L3, as less attractive interactions were observed when the highest  $X_{SA}$  (0.9) present in the mixtures as compared to  $X_{SA} = 0.7$ . Similar observation were shown in L1/L2, L1/L3, and L2/L3 mixed monolayers (Figure 4.24). There is a slight increase of  $G_{mix}$  values at  $X_{L1} = 0.9$  (Figure 4.24(a)-(b)) and  $X_{L2} = 0.9$  (Figure 4.24 (c)),  $G_{mix}$  is less negative than the respective mole fraction of 0.5 and 0.7.

Among the mixtures of C18 fatty acids, L2/L3 is considered as the energetically stable. The optimum amount of  $X_{L2}$  and  $X_{L3}$  is 0.5 respectively, at all discrete surface pressure.

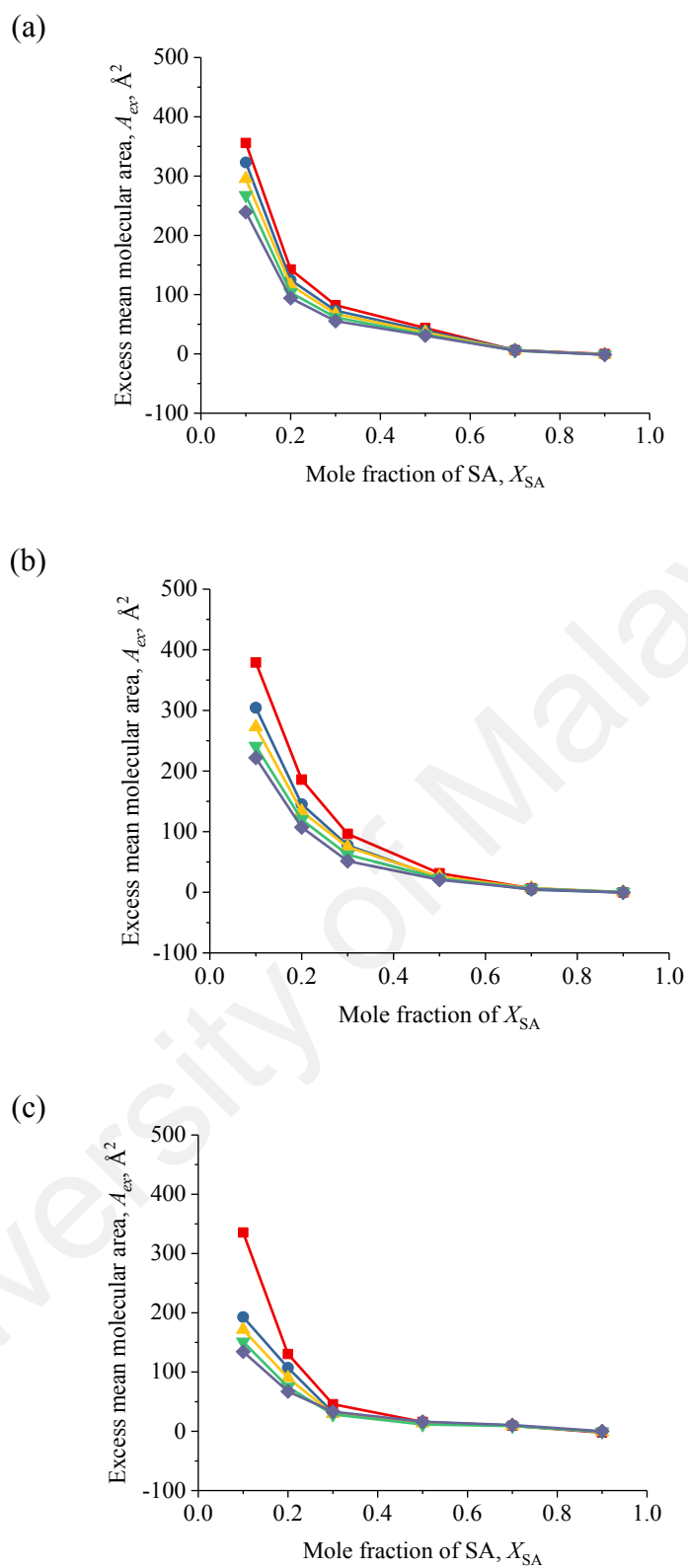


**Figure 4.21:** Mean molecular area of C18 fatty acids mixed monolayers vs  $X_{SA}$  of (a) SA/L1, (b) SA/L2 and (c) SA/L3 on pure water subphase at 25°C. For discrete surface pressure of  $\blacksquare = 5 \text{ mN m}^{-1}$ ,  $\bullet = 10 \text{ mN m}^{-1}$ ,  $\blacktriangle = 15 \text{ mN m}^{-1}$ ,  $\blacktriangledown = 20 \text{ mN m}^{-1}$  and  $\blacklozenge = 25 \text{ mN m}^{-1}$ .

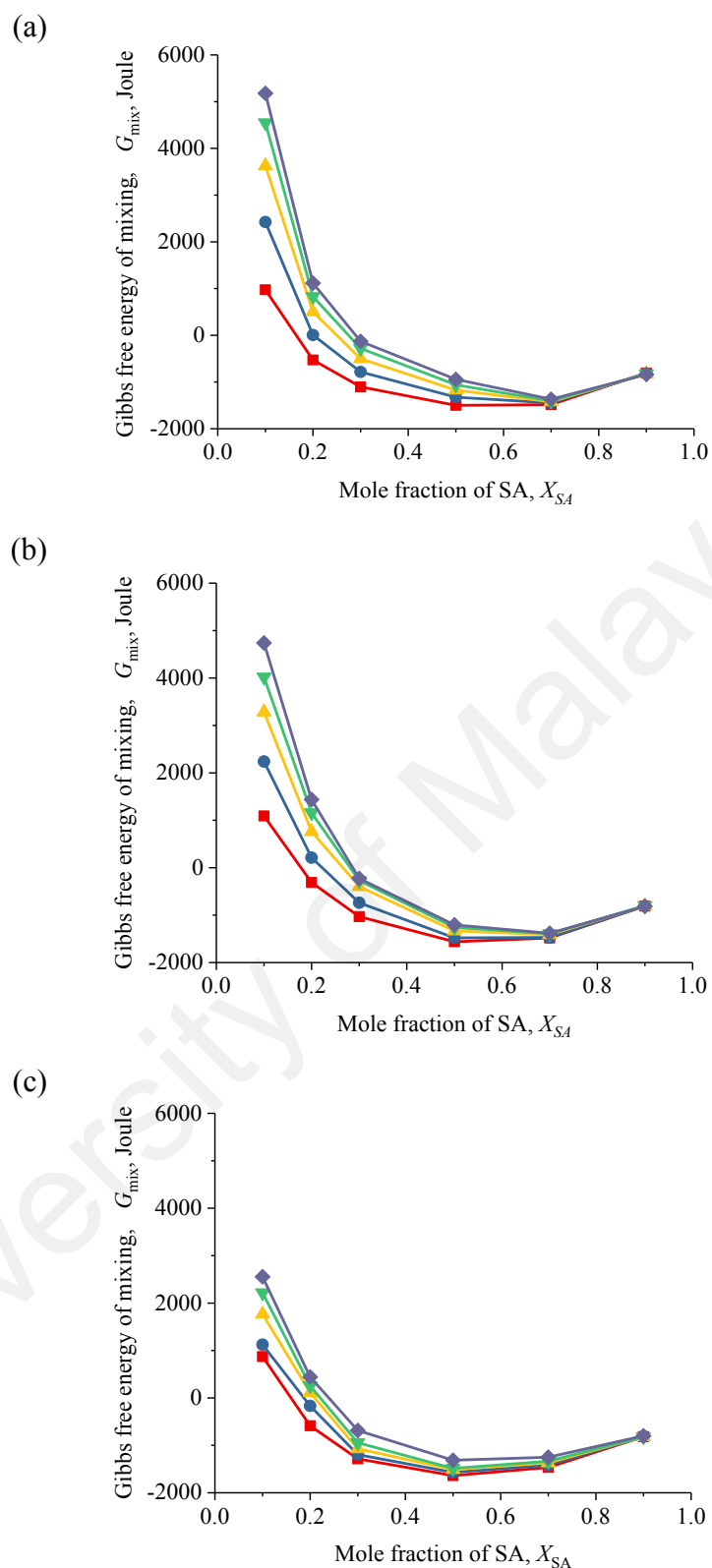


**Figure 4.22:** Gibbs free excess energy  $G_{mix}$  of C18 fatty acids mixed monolayers vs  $X_{SA}$  of (a) SA/L1, (b) SA/L2 and (c) SA/L3 on pure water subphase at 25°C. For discrete surface pressure of  $\blacksquare = 5 \text{ mN m}^{-1}$ ,  $\bullet = 10 \text{ mN m}^{-1}$ ,  $\blacktriangle = 15 \text{ mN m}^{-1}$ ,  $\blacktriangledown = 20 \text{ mN m}^{-1}$  and  $\blacklozenge = 25 \text{ mN m}^{-1}$ .

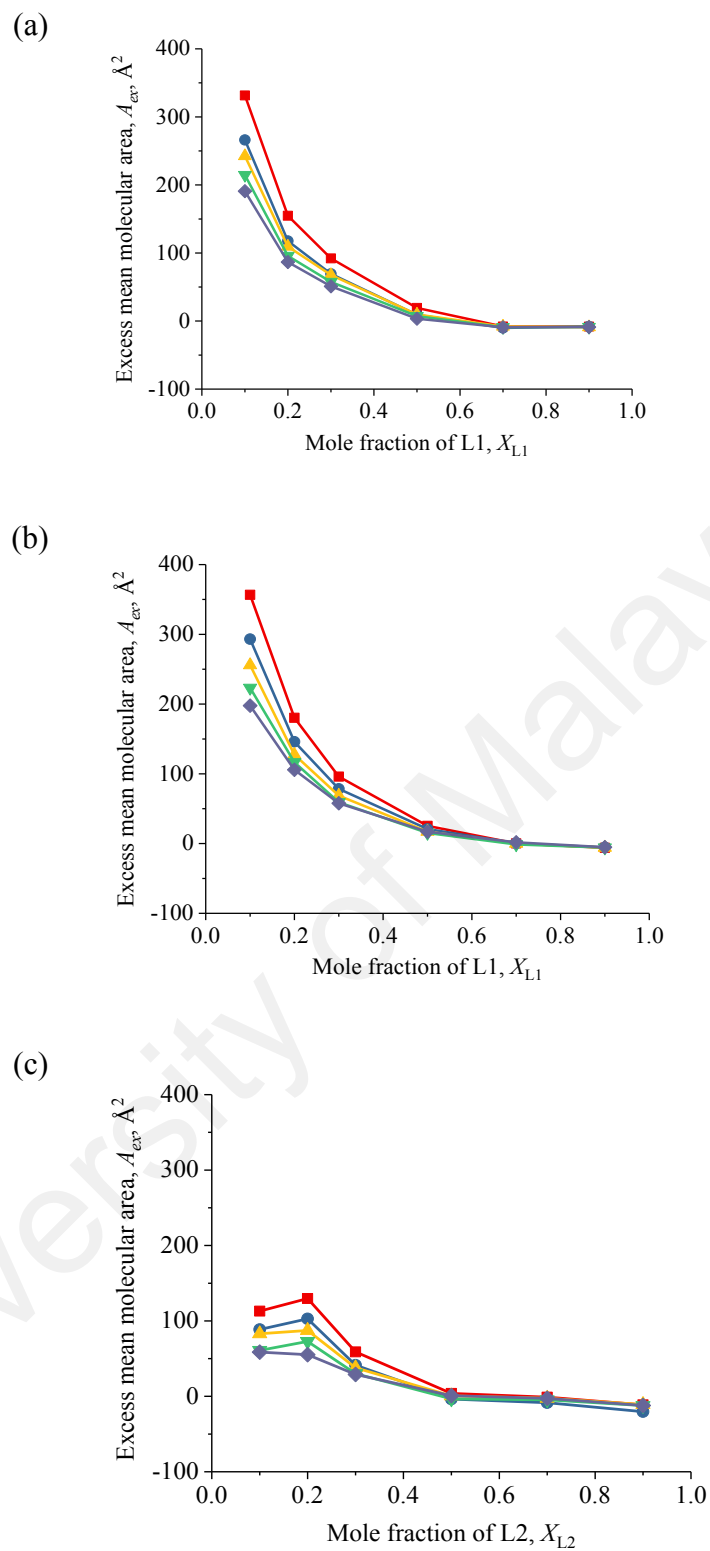


**Figure 4.23:** Mean molecular area of C18 fatty acids monolayers vs mole fraction of L1 or L2: (a) L1/L2, (b) L1/L3 and (c) L2/L3 on pure water subphase at 25°C. For discrete surface pressure of  $\blacksquare = 5 \text{ mN m}^{-1}$ ,  $\bullet = 10 \text{ mN m}^{-1}$ ,  $\blacktriangle = 15 \text{ mN m}^{-1}$ ,  $\blacktriangledown = 20 \text{ mN m}^{-1}$  and  $\blacklozenge = 25 \text{ mN m}^{-1}$ .

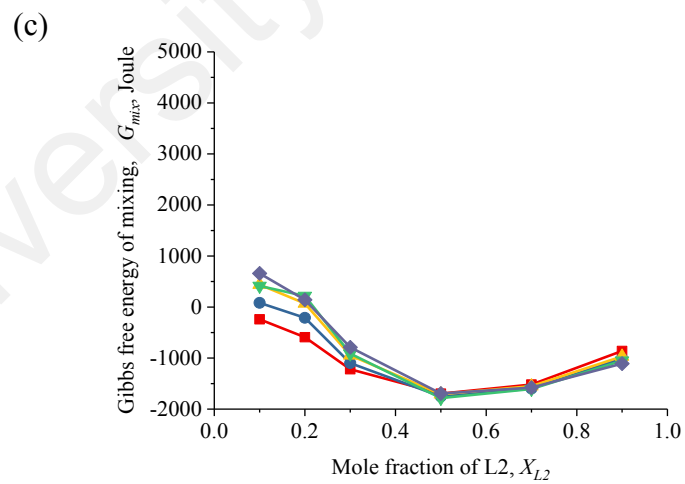
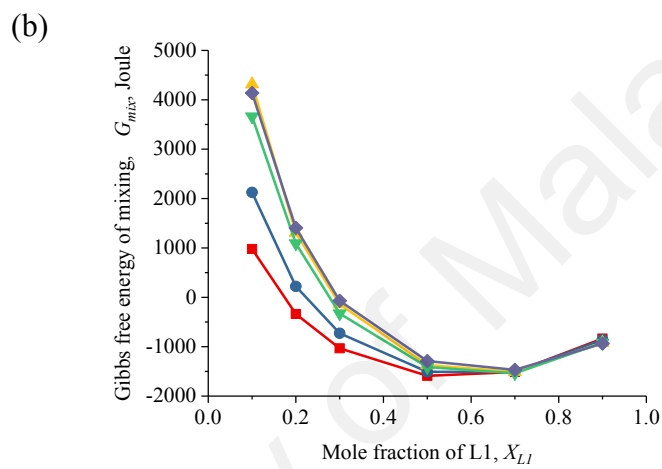
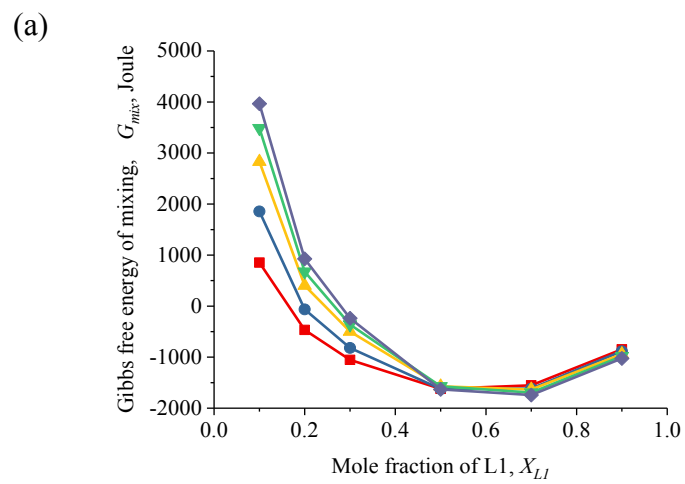


**Figure 4.24:** Gibbs free excess energy  $G_{mix}$  of C18 fatty acids monolayers vs mole fraction of L1 or L2: (a) L1/L2, (b) L1/L3 and (c) L2/L3 on pure water subphase at 25°C. For discrete surface pressure of  $\blacksquare = 5 \text{ mN m}^{-1}$ ,  $\bullet = 10 \text{ mN m}^{-1}$ ,  $\blacktriangle = 15 \text{ mN m}^{-1}$ ,  $\blacktriangledown = 20 \text{ mN m}^{-1}$  and  $\blacklozenge = 25 \text{ mN m}^{-1}$ .

#### 4.2.3.2 Mixed monolayers of C18 fatty acids and DP

Due to the low collapsed pressure of DP ( $12 \text{ mN m}^{-1}$ ) as shown in Figure 4.5, the mean molecular area of DP ( $A_{DP}$ ) at higher pressure are not available to be substituted into Equation 5 as stated in Chapter 3. Davies (1963) and Gaines (1966) defined  $A_{12} = A_1X_1 + A_2X_2$ , where  $A_1$  and  $A_2$  are the mean molecular areas of single components at the same surface pressure and  $X_1$  and  $X_2$  are the mole fractions of components 1 and 2 in the mixed film. Hence, some useful information on surface pressure higher than  $12 \text{ mN m}^{-1}$  (the DP collapsed pressure) will be missed if using this equation for this study. Presumably, pure DP monolayer collapsed at  $12 \text{ mN m}^{-1}$ ; however DP may not collapse at such low surface pressure in a mixed system as DP may be embedded or bounded to the lipid membrane. In order to generate useful information, the limiting molecular area of single components will be used for calculations in all the mixtures that containing DP.

Negative deviation of  $A_{ex}$  from ideal behavior were obtained for SA/DP (Figure 4.25(a)) over most of the ranges investigated. The two components of SA and DP were miscible and formed a nonideally mixed monolayer at the air/water interface. Exceptions were observed when the mole ratio of SA/DP was 90:1 and 100:1, where position deviation occurred. SA/DP mixtures were immiscible at mole ratio of 90:1 and 100:1. DP molecules poorly interacted with SA molecules. It showed that the introduction of high DP into the SA monolayer caused instability of the monolayer. This observation was consistent with the positive values of  $G_{mix}$  obtained (Figure 4.25(b)).

Negative values were observed in unsaturated fatty acids (L1, L2, and L3) for all of their mixed systems. These deviations revealed non-ideal behavior and showed that the monolayer components were miscible. The negative values also supported observation obtained for  $G_{mix}$  (Fig. 4.25(b)), which showed that strong intermolecular

attractions occurred between unsaturated fatty acids and DP. These results will be further discussed in the following section regarding the thermodynamic stability of the mixed monolayer.

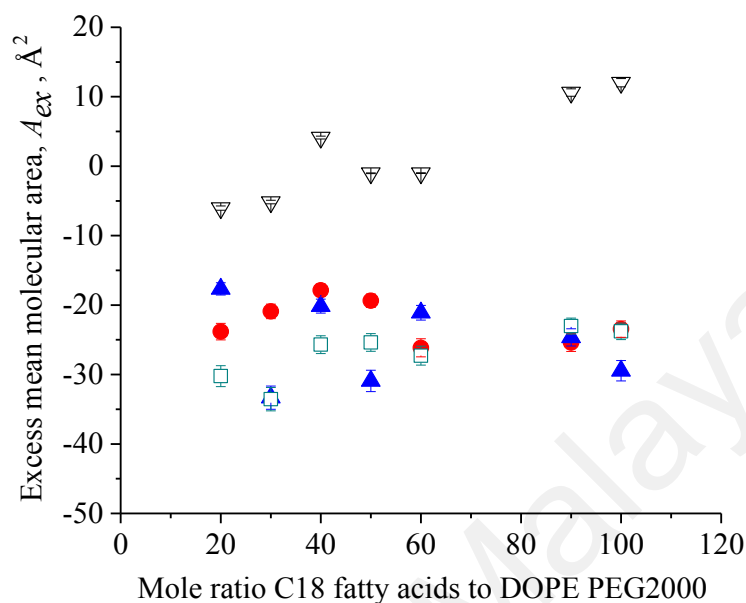
The values of  $G_{mix}$  of SA/DP mixtures were close to negative throughout the tested ranges of the binary systems (Figure 4.25(b)). Exceptions were observed at the two highest mole ratios of SA/DP, which were 90:1 and 100:1. A similar observation was apparent in their compression-modulus plot (Figure 4.16(a)). Strong repulsions are expected when SA molecules are packed tightly and uniformly. This also suggests that DP molecules were attracted to the hydrophobic head group of SA in these two mixtures.

The lower negative free energy of mixing values were obtained throughout the range of the unsaturated C18 fatty acid (L1, L2, and L3) mixed systems compared with the saturated SA mixed systems (Figure 4.25(b)), indicating that very strong attractions occurred between the molecules in the monolayers. This observation was expected because the bend and kink effects from the *cis*-double bond(s) in the hydrocarbon chains affect the molecular packing of the monolayers. Greater interactions occurred between the unsaturated hydrocarbon chains of the fatty acids and the unsaturated DOPE in DP.

L1, L2 and L3 showed similar trends, becoming less negative as the moles of fatty acid were increased. Intermolecular interactions were greater when unsaturated C18 fatty acids interacted with DP. By extrapolating the curves of L1/DP, L2/DP and L3/DP, we obtained 50:1 as the intersection point. This ratio is suggested to be employed in preparing pegylated L1, L2 and L3 nanoliposomes; at this composition, the mixed systems are thermodynamically the most stable. Increasing the number of double bonds in the hydrocarbon chains of the fatty acids did not significantly contribute to

interactions in the binary systems. As the moles of unsaturated C18 fatty acids increased (from 60:1 and higher),  $G_{mix}$  had predominantly similar negative values.

(a)



(b)

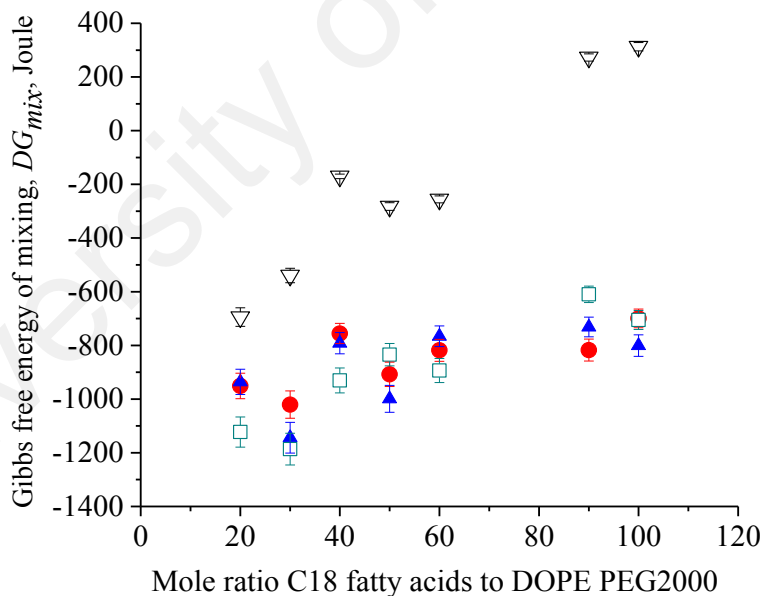


**Figure 4.25:** (a) Excess mean molecular area ( $A_{ex}$ ), (b) Gibbs free energy of mixing ( $G_{mix}$ ) vs mole ratio of C18 fatty acids to DOPE PEG2000 mixed monolayers: ∇ = stearic acid/DOPE PEG2000, ● = oleic acid/DOPE PEG2000, ▲ = linoleic acid/DOPE PEG2000, and □ = linolenic acid/DOPE PEG2000, spread on a nanopure water subphase at 25°C.

### 4.2.3.3 Mixed monolayers of C18 fatty acids and BSA

In Figure 4.26, the mean molecular area  $A_{ex}$  is presented against mole fraction of C18 fatty acids ( $X_{FA}$ ) at different surface pressures (5, 10, 15, 20 and 25  $\text{mN m}^{-1}$ ). A negative deviation from linearity was attributed to the miscibility of both components interacting with each other at the interface. The mean molecular area inclined as the surface pressure increased. There were only slight deviations from ideality at 25  $\text{mN m}^{-1}$ , indicating poor miscibility and weak interactions in a mixed monolayer. When the compression began at surface pressure of 5  $\text{mN m}^{-1}$ , a marked negative deviation indicated strong attractions between the molecules in the mixed monolayer as compared with the interactions in their respective pure films. Large deviation observed at  $X_{BSA} = 0.8$  for the selected surface pressures showed a significant influence on the molecular packing and favorable interactions between molecules in the mixed monolayers. Negative deviations of  $A_{ex}$  revealed non-ideal behavior and showed that the monolayer components were miscible. This observation was also supported by the negative values obtained for  $G_{mix}$  (Figure 4.27), which showed that strong intermolecular attractions occurred between C18 fatty acids and BSA.

Negative values of  $G_{mix}$  in the entire range of the C18 fatty acids/BSA monolayer composition indicated very strong attractions between molecules in the mixed system.  $G_{mix}$  gradually decreased as the concentration of BSA rose. Greater attraction occurs with increasing amount of protein in the C18 fatty acids/BSA mixtures. The results showed that the C18 fatty acids/BSA mixed monolayers were thermodynamically stable. At  $X_{BSA} = 0.1$ ,  $G_{mix}$  values were nearly zero for all surface pressures. The most energetically stable intermolecular interaction was observed at  $X_{BSA} = 0.8$  for C18 fatty acids/BSA at surface pressure of 15  $\text{mN m}^{-1}$  as the most  $G_{mix}$  values (-20 to -22 kJ) were obtained, suggesting

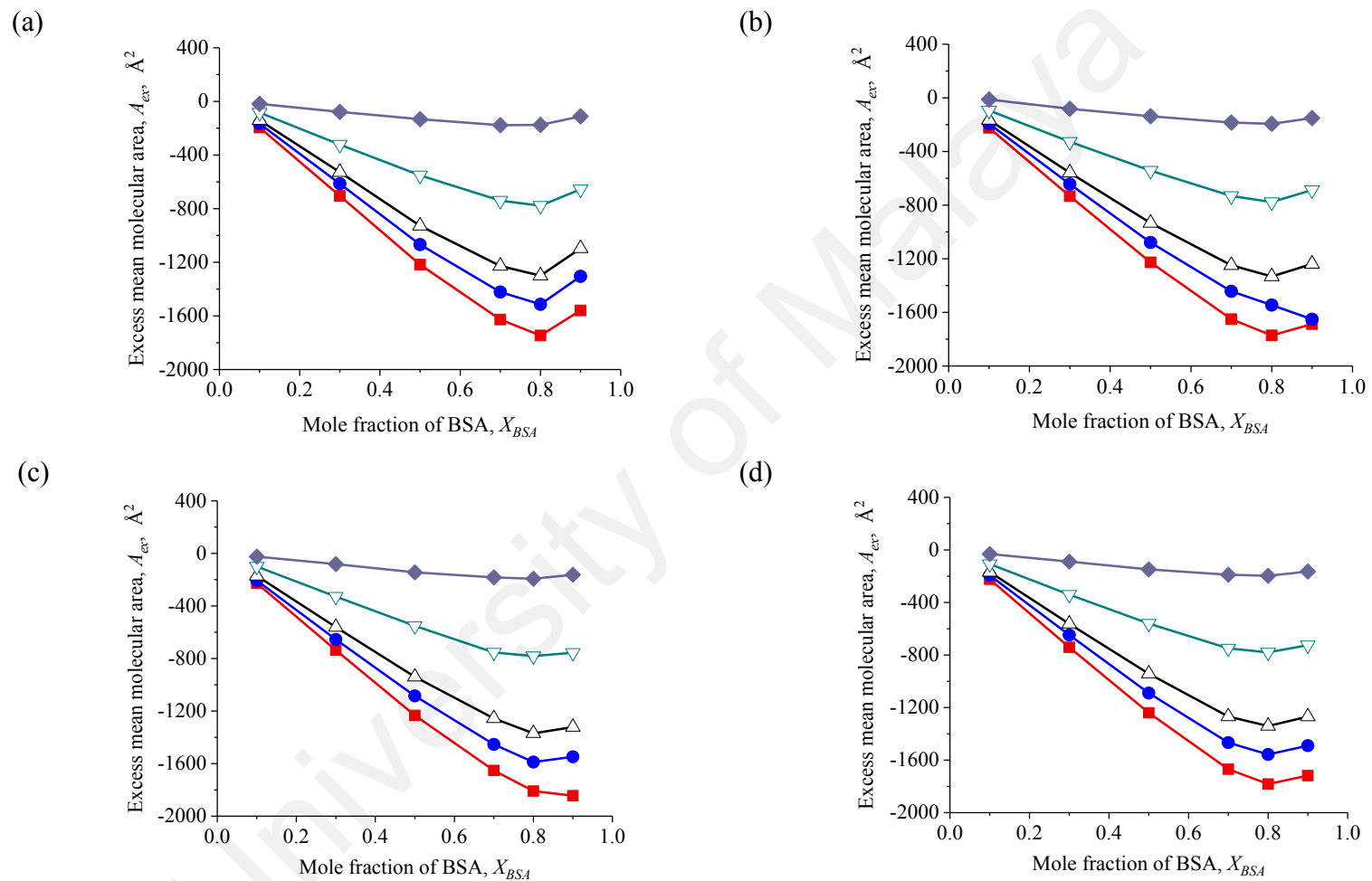


**Figure 4.26:** Mean molecular area of C18 fatty acids/BSA monolayers vs  $X_{BSA}$ : (a) SA/BSA, (b) L1/BSA, (c) L2/BSA, and (d) L3/BSA on pure water subphase at 25°C. For discrete surface pressure of  $\blacksquare = 5 \text{ mN m}^{-1}$ ,  $\bullet = 10 \text{ mN m}^{-1}$ ,  $\blacktriangle = 15 \text{ mN m}^{-1}$ ,  $\nabla = 20 \text{ mN m}^{-1}$  and  $\blacklozenge = 25 \text{ mN m}^{-1}$ .

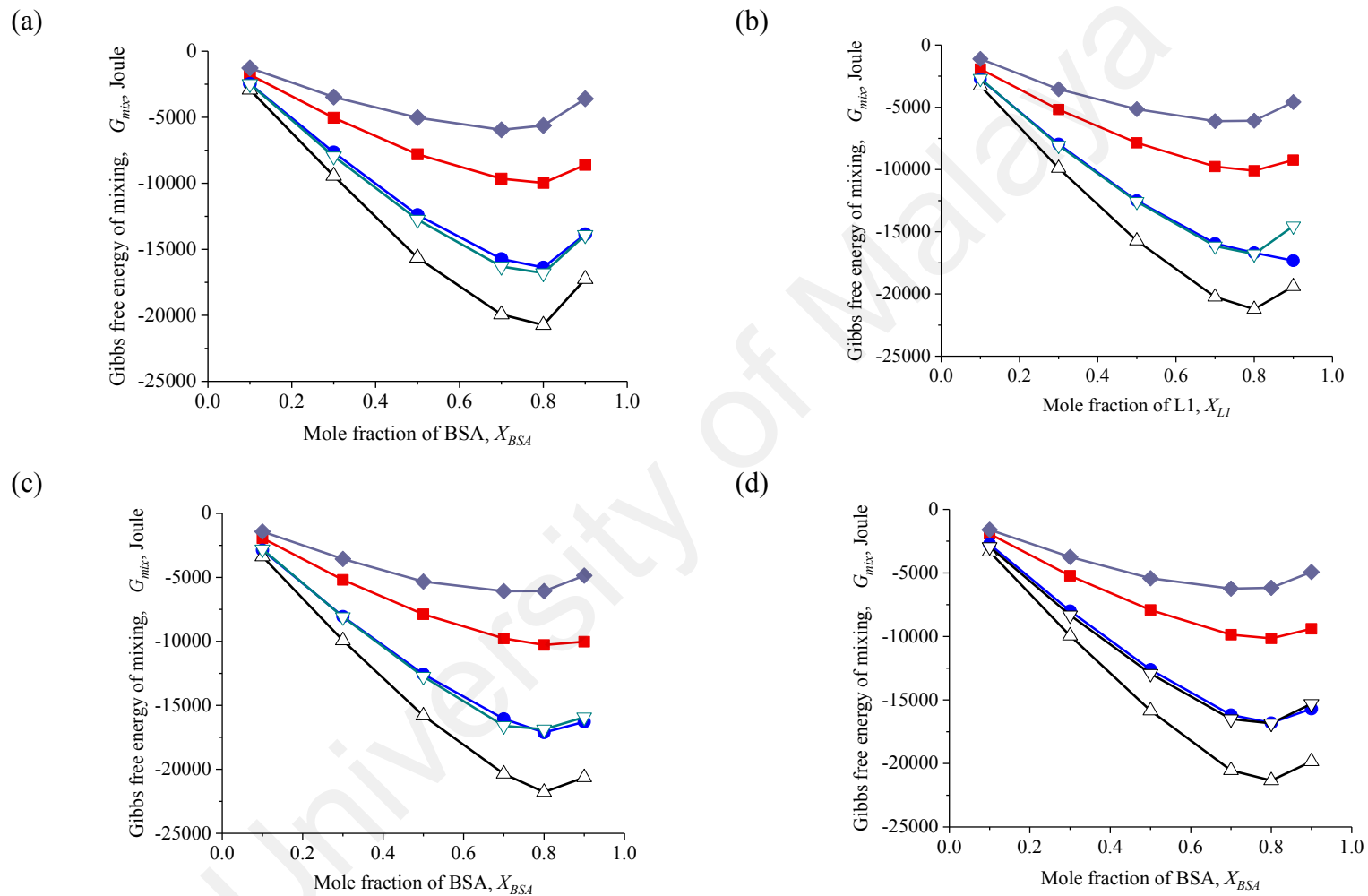


**Figure 4.27:** Gibbs free excess energy  $G_{mix}$  of C18 fatty acids/BSA monolayers vs  $X_{BSA}$ : (a) SA/BSA, (b) L1/BSA, (c) L2/BSA, and (d) L3/BSA on pure water subphase at 25°C. For discrete surface pressure of  $\blacksquare = 5 \text{ mN m}^{-1}$ ,  $\bullet = 10 \text{ mN m}^{-1}$ ,  $\blacktriangle = 15 \text{ mN m}^{-1}$ ,  $\nabla = 20 \text{ mN m}^{-1}$  and  $\blacklozenge = 25 \text{ mN m}^{-1}$ .

that C18 fatty acids interacted strongly with BSA molecules and were miscible in this specific mole ratio of 8 to 2 and surface pressure.

There was a slight recovery of  $G_{mix}$  at  $X_{BSA} = 0.9$  for C18 fatty acids/BSA. This might be due to intermolecular repulsion occurring in the mixed monolayer system when the concentration of BSA was saturated in the system. This observation was supported by the  $A_{ex}$  and  $C_s^{-1}$  measurements as discussed above.  $C_s^{-1}$  versus  $\Pi$  profiles of C18 fatty acids/BSA showed that favorable for protein-protein interaction than lipid-protein interaction. The most compatible mixture of C18 fatty acids/BSA mixed monolayers is  $X_{BSA} = 0.8$ .

Lipid binding is dominated by acyl chain interactions with the protein, the interactions are stabilized by hydrophobic effects of the wide range of amino acid side chains of BSA that are hydrophobic (Figure 4.28). Acyl chains of the lipids may be bound on the surface of the transmembrane domain of the protein. They may be bounded to more than one subunit, thus contribute to the stability of the protein structure. The acyl chains of the lipids may penetrate the globular transmembrane domain of the protein.

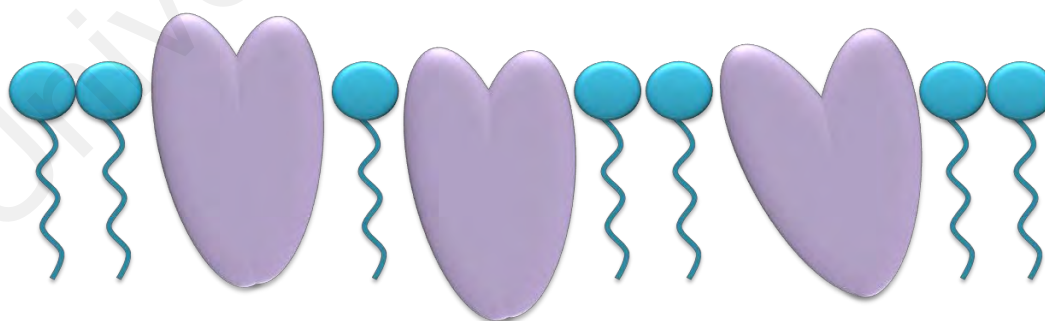


**Figure 4.28:** A cartoon illustration to describe the interactions between C18 fatty acids and BSA.

#### 4.2.3.4 Mixed monolayers of C18 fatty acids and AS25

Non-linear plots of  $A_{ex}$  show the existence of interactions between the monolayer components (Figure 4.29(a)). The strength of these interactions will also be verified based on  $G_{mix}$  (Figure 4.29(b)). Negative deviations of  $A_{ex}$  from ideality are observed in all the mixed systems (Figure 4.29(a)). These deviations indicate that the monolayer components are miscible and reveal non-ideal behavior. The mixture is increasingly miscible as the amount of AS25 added increased. Antibody-antibody interactions are preferable over the lipid-antibody interactions in the mixed systems. With the increasingly mole of C18 fatty acids in mixtures, a greater repulsion between the molecules are observed in the mixed system, showing AS25 interacts weakly with C18 fatty-acid molecules. The similar trend of intermolecular interactions occurred are also supported by the obtained  $G_{mix}$ , which will be discussed further in the section concerning the thermodynamic stability of the mixed monolayer.

The presence of AS25 in the monolayer appears to be energetically consistent in all four investigated C18 fatty acids mixed systems (Figure 4.29(b)). The negative values of free energy of mixing of SA/AS25, L1/AS25, L2/AS25 and L3/AS25 confirm the spontaneity interaction of AS25 molecules on the C18 fatty acids monolayers. The amount of AS25 incorporated into the monolayer strongly affected the thermodynamic properties of the lipid monolayers. With the increasing amount of AS25 in the lipid systems, the more negative  $G_{mix}$  values were obtained. Repulsion between the molecules is weaker as the amount of antibody is higher. Antibody-antibody interaction is preferable over lipid-antibody interaction. Interestingly, the most thermodynamically stable mixed system is observed when it contains the largest amount of antibody investigated,  $G_{mix}$  becomes more negative with increasing amount of antibody incorporated onto the monolayer. The most negative  $G_{mix}$  was found when the mixed monolayer comprises the largest amount of AS25. Aggregation of proteins is

energetically favorable when the concentrations of protein are high. Increasing lipid compositions of the membrane may change the system from protein-aggregation to a protein-distributed state (Gil et al., 1998; L Armstrong, Sandqvist, & C Rheinstadter, 2011; Sperotto, May, & Baumgaertner, 2006).

From the obtained  $G_{mix}$ , the degree of unsaturation on the hydrocarbon chain did not significantly influence the intermolecular interaction between AS25 molecules on the lipid monolayer. AS25 is a membrane-bound protein, and a membrane-bound protein is prone to be on the membrane surface interacting with the headgroup of fatty acids, unlike integral protein that interact directly with the hydrocarbon chain.

In comparison to all the four C18 fatty acids, the strongest intermolecular interaction is observed in L1 at the investigated ranges. This is supported by the negative  $G_{mix}$  value obtained. L1 is the most suitable C18 fatty acid to be used as a targeted drug-delivery carrier, where a minimal amount of antibody is required for the strongest attraction between fatty acids and antibody to take place. This finding certainly has economic significance for researches since antibodies are very costly.

The negative  $G_{mix}$  values obtained are very small negative values (approximately -0.05 to -0.25 kJ). Molecules of AS25 bound strongly on the surface of C18 fatty acids monolayer. These values are as expected as the role of antibodies in target delivery is as a facilitator to deliver the encapsulated drugs only to the targeted site without harming the human body (Hamrock, 2006; Hansel, Kropshofer, Singer, Mitchell, & George, 2010; Harris, 2004; Nydegger & Sturzenegger, 1999). Antibodies should interact with membranes and bind firmly to their surface like a peripheral protein in lipid-protein interactions.

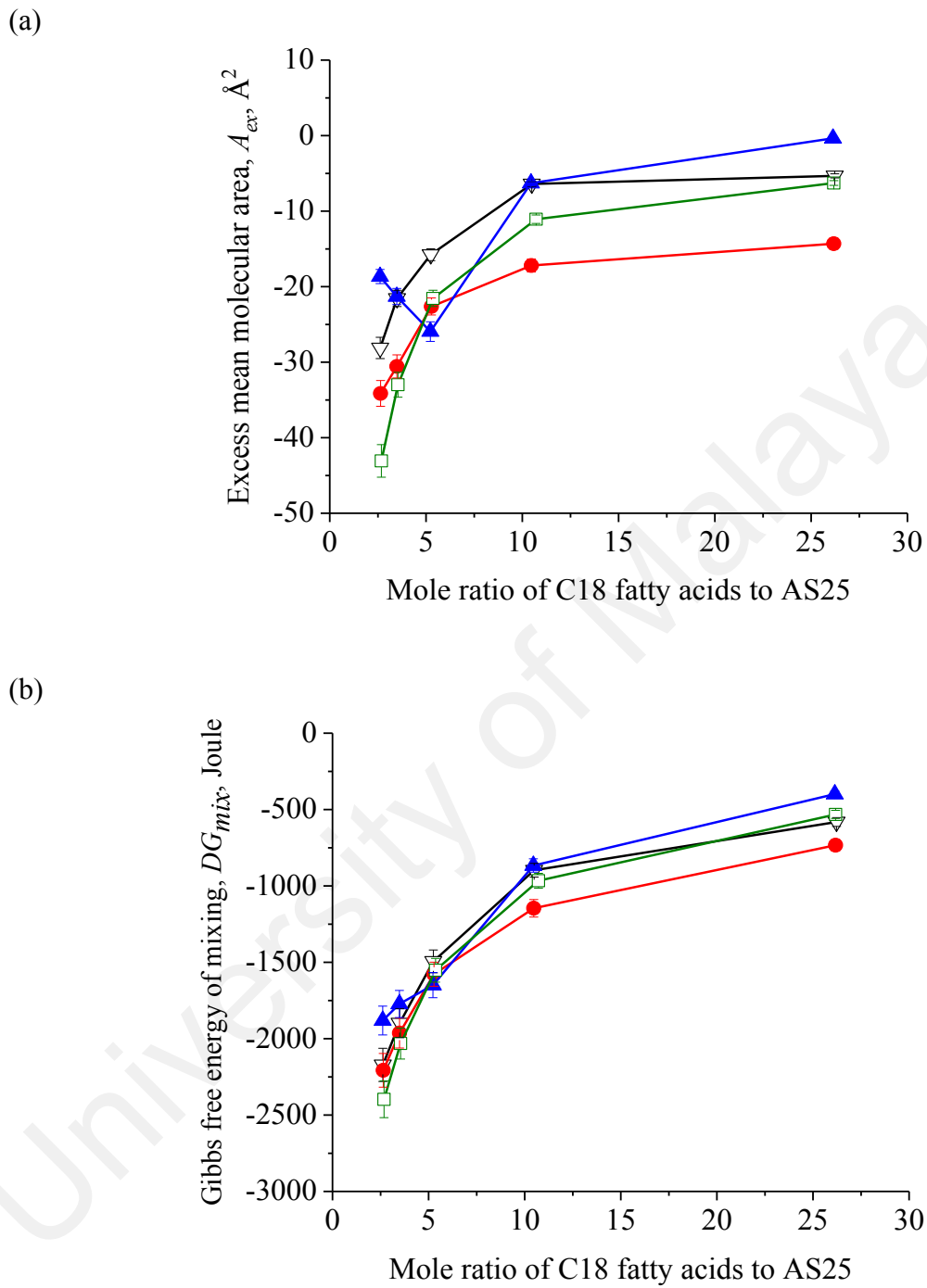


**Figure 4.29:** (a) Excess mean molecular area ( $A_{ex}$ ), (b) Gibbs free energy of mixing ( $G_{mix}$ ) vs mole ratio of C18 fatty acids to Anti-SNAP25 for mixed systems: ■ = stearic acid/Anti-SNAP25, ● = oleic acid/Anti-SNAP25, □ = linoleic acid/Anti-SNAP25, and ▽ = linolenic acid/Anti-SNAP25, spread on water subphase at 25°C.

In addition to support  $G_{mix}$  findings, it was found that only 20% of AS25 interacting with the fatty acid monolayer (i) like an integral protein, or (ii) AS25 is partially embedded into the monolayer. And the remaining 80% are (iii) presence on the monolayer surface, interacting with the head-group of fatty acids, or (iv) excess antibody remaining in the water subphase. From the quantitative energetic studies as above, the most potential intermolecular interactions take place in the mixed monolayer systems are (ii) and (iii). It also important to note that  $K_{ow}$  corresponds only to the hydrophobic properties of AS25 on the membrane (Boroujerdi, 2015).

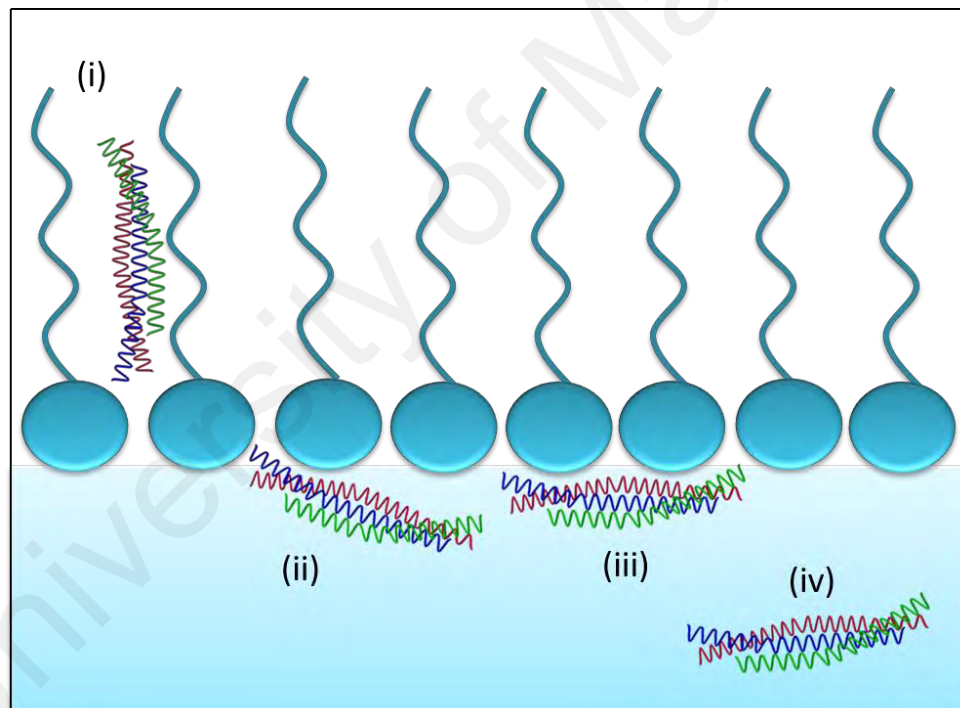


**Figure 4.30:** The possibilities of AS25 molecules interacting with the fatty acid monolayer: (i) like an integral protein, (ii) AS25 is partially embedded into the monolayer, (iii) presence on the monolayer surface, interacting with the head-group of fatty acids, or (iv) excess antibody remaining in the water subphase.

#### 4.2.3.5 C18 fatty acids, DP and AS25 mixed monolayers

Negative deviations of  $A_{ex}$  for the entire investigated range of SA/DP/AS25 and L3/DP/AS25. This showed that AS25 molecules are miscible in SA/DP and L3/DP binary mixtures respectively. However, some mole ratios of L1/DP/AS25 and L2/DP/AS25 ternary mixtures were positively deviated. Positive deviation showed AS25 molecules poorly interact with L1/DP and L2/DP binary mixtures (Figure 4.31(a)).

This observation was also supported by the obtained  $G_{mix}$  values, which showed the dissimilar intermolecular attractions occurred between AS25 in individual C18 fatty acids/DP binary mixtures (Figure 4.31(b)). These results will be further discussed in the following section regarding the thermodynamic stability of the mixed monolayer. In Figure 4.31(b), negative values of  $G_{mix}$  were obtained for SA/DP/AS25 and L3/DP/AS25 for the entire investigated ranges. Surprisingly, more negatives values were obtained for the saturated C18 fatty acids mixture, indicating a preferential interaction with the saturated C18 rather than unsaturated C18 fatty acids in the presence of DP. AS25 molecules interacted strongly with SA and DP molecules in the same trough of water subphase at 26°C. The kink and bent effect induced by the *cis*-double bond(s) of unsaturated hydrocarbon chain of L1, L2 or L3 and DOPE in DP are greater than the effect produced by the saturated hydrocarbon chain of SA and unsaturated DOPE in DP, resulting a greater repulsion prevents the binding of AS25 molecules with the L1, L2 or L3 and DP mixed monolayers. The large PEG headgroup of DP also contributed some repulsion energy in the mixtures.

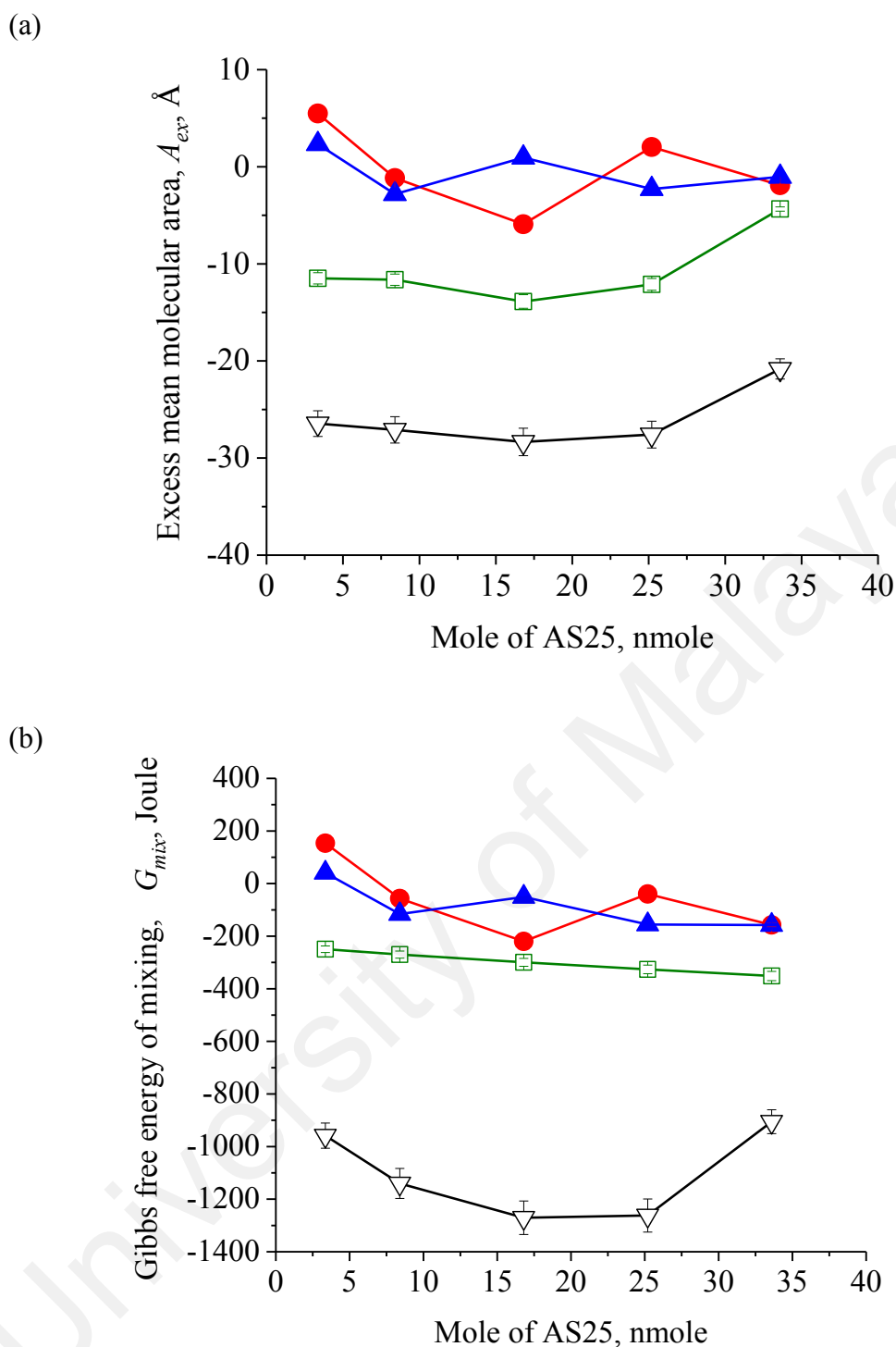


**Figure 4.31:** (a) Excess mean molecular area ( $A_{ex}$ ), (b) Gibbs free energy of mixing ( $G_{mix}$ ) vs mole ratio C18 fatty acids/DP to Anti-SNAP25 for mixed systems:  $\nabla$  = SA/DP/AS25,  $\bullet$  = L1/DP/AS25,  $\blacktriangle$  = L2/DP/AS25, and  $\square$  = L3/DP/AS25, spread on water subphase at 25°C.

### 4.3 Lipid-protein interactions: Effect of headgroups

Phospholipid has a phosphate polar head-group bonded to two nonpolar hydrocarbon chains which usually are fatty acids between 14-24 carbon atoms. The length and degree of saturation of fatty acid tails will influence the ability of phospholipid in molecules packing, subsequently, will affect the fluidity of the membrane.

In this section, lipid-protein interactions between phospholipids such as SS, DSPC, and DSPG (Table 3.1) with integral protein (BSA) and peripheral protein (AS25), respectively were carried out. SS, DSPC and DSPG consist of two saturated C18 hydrocarbon chains, but possess different headgroups with different size and charge (Table 3.2). The intermolecular interactions of SA/BSA and SA/AS25 mixed monolayer were also included in this section as a comparison of the effect of the headgroups size in lipid-protein interactions, as SA has a small carboxyl (-COOH) group.

#### 4.3.1 $\Pi$ - $A$ Isotherms

##### 4.3.1.1 Pure monolayers SS, DSPC, and DSPG

SS is a biodegradable and fully digestible surfactant (Garofalakis & Murray, 2002) poses a sucrose headgroup bonded to a C18 saturated hydrocarbon chain. Based on the chemical structure of sucrose stearate, it can bring water-soluble and oil-soluble ingredients together. Langmuir monolayer of SS is not commonly studied (Garofalakis & Murray, 2002). The limiting molecular areas of pure monolayer of SS, monolayers were determined by extrapolating the linear slope of individual  $\Pi$ - $A$  isotherms to zero surface pressure and were found  $68 \pm 2 \text{ \AA}^2$  and collapsed at surface pressure of  $40 \text{ mN m}^{-1}$  (Figure 4.32), which is the same as published by Murray et al.

Both DSPC and DSPG are commonly studied phospholipids, the isotherm of DSPC monolayer obtained is similar to those published by some researchers and

isotherm of DSPG monolayer obtained was similar as published (Bos & Nylander, 1996; Colqui Quiroga, Monzón, & Yudi, 2010). For DSPC, the transition from G to LC phase occurred at mean molecular area of  $55 \text{ \AA}^2$  and collapsed at surface pressure of  $50 \text{ mN m}^{-1}$  (Figure 4.32). The G to LC transition of DSPG isotherm took place at  $40 \text{ \AA}^2$  and collapsed at surface pressure of  $55 \text{ mN m}^{-1}$  (Figure 4.32). The increasing number of hydroxyl ( $-\text{OH}$ ) group in the head group has a larger limiting molecular area. SS has 6 hydroxyl groups and DSPG has 2. This is due to the increasing number of  $-\text{OH}$  group forming hydrogen bond with the water molecules in the subphase and occupy a larger area, thus larger limited molecular area was recorded for SS as compare to DSPC and DSPG.

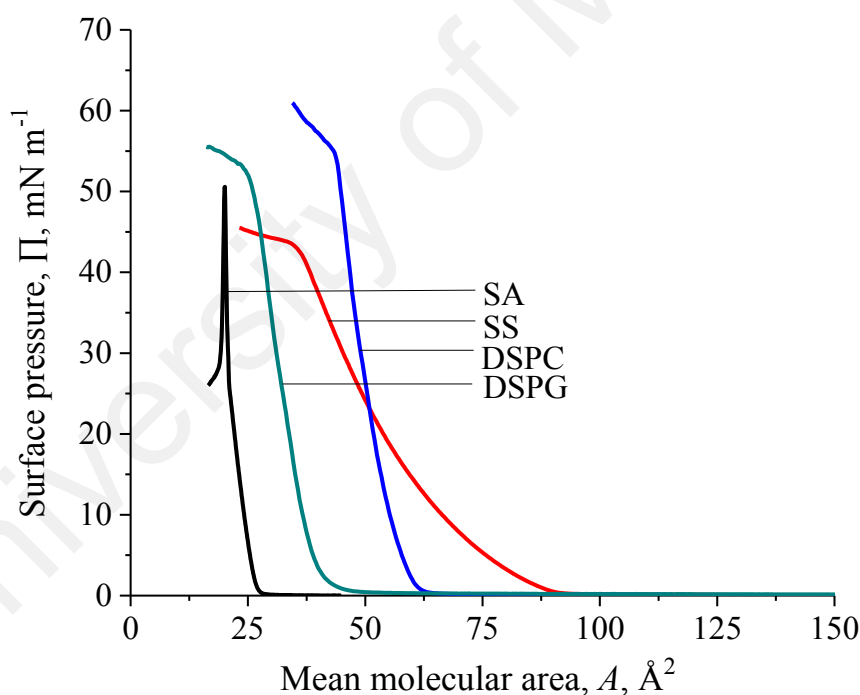


**Figure 4.32:** The surface pressure–area ( $\Pi$ – $A$ ) isotherms of pure monolayer of SA, SS, DSPC and DSPG, spread on a nanopure water subphase at  $25^\circ\text{C}$ .

#### 4.3.1.2 Mixed monolayers of SS, DSPC and DSPG and BSA

The  $\Pi$ - $A$  isotherms of SA/BSA films are presented as well as the mixed monolayer of BSA-phospholipids in Figure 4.33. With the increasing mole fraction of BSA ( $X_{BSA}$ ) in the mixed monolayers, isotherms of mixtures shifted away (to increasing mean molecular area) from their pure phospholipids respectively. In the mixtures containing the largest  $X_{BSA}$  which is 0.9, SA/BSA has the smallest mean molecular area (approximately  $925 \text{ \AA}^2$ ), whereas  $1750 \text{ \AA}^2$  and  $2200 \text{ \AA}^2$  for SS/BSA and DSPG/BSA (Figure 4.33(b) & (d)) respectively. The isotherm of DSPC/BSA ( $X_{BSA} = 0.9$ ) shifted dramatically to a very large mean molecular area ( $2500 \text{ \AA}^2$ ). Globular protein BSA molecules are much bigger than lipids such as fatty acids and phospholipids, however, the mean molecular area is also affected by the size of phospholipids and also the intermolecular interactions occur between the molecules. Plausibly, a greater repulsion occurred between DSPC and BSA molecules as compared to SA/BSA, SS/BSA and DSPG/BSA. Hydrogen bonds formed between BSA and the headgroups of SS and DSPG that are rich with hydroxyl (-OH) groups, produce an attractive force that keeps the mixtures closer to each, less repulsion occurs as compare to DSPC/BSA. SA has the smallest headgroup, giving the smallest mean molecular area as compare to phospholipids such as SS, DSPC, and DSPG.

The collapse pressure of the mixtures is found to be similar as their respective pure monolayer, however, no collapse is observed in SS/BSA and DSPC/BSA mixed monolayer at  $X_{BSA} = 0.9$ .

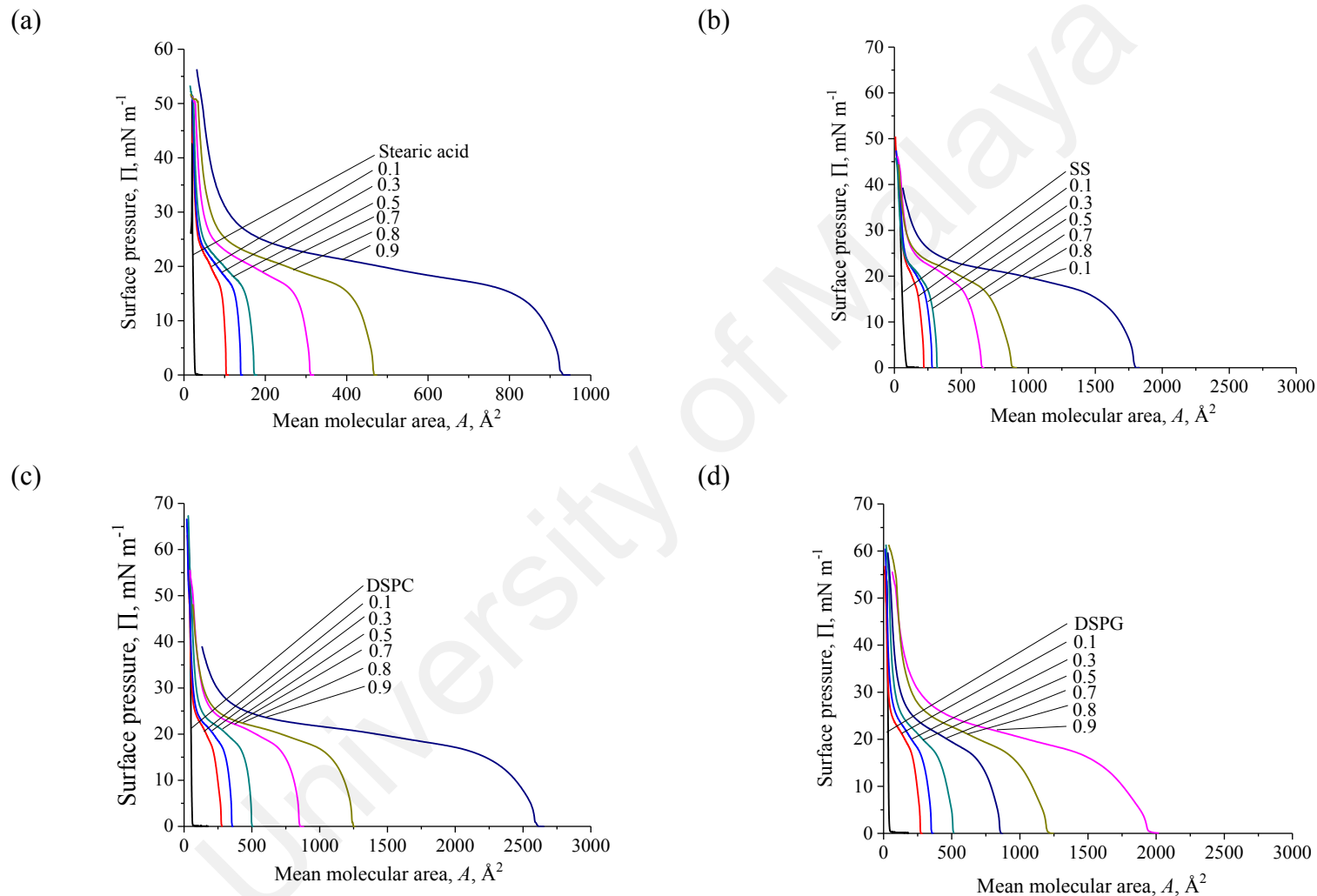


**Figure 4.33:** The surface pressure–area ( $\Pi$ – $A$ ) isotherms of mixed monolayers (plotted in mole fraction of BSA): (a) SA/BSA, (b) SS/BSA, (c) DSPC/BSA, and (d) DSPG/BSA spread on a nanopure water subphase at 25°C.

### 4.3.1.3 Mixed monolayers of SS, DSPC and DSPG and AS25

The same volume of AS25 as C18 fatty acids/AS25 (in section 4.2.2.5) was added into the phospholipids monolayer respectively, and then we converted the volumes of AS25 into mole ratio to each phospholipid. For comparison purpose, the isotherm of SA/AS25 is included in Figure 4.29. The isotherms of AS25–phospholipids mixtures shifted to the right (increasing mean molecular area) with the addition of AS25 into the phospholipids monolayers (Figure 4.34).

The isotherms of mole ratio of SS/AS25 at 5.08:1 and 12.7:1 are close to each other, presumably, a similar strength of interactions occurred between SS and AS25 at both mole ratios. Increasing mole of SS may reduce the membrane fluidity upon compression of the mixed monolayers. The increasing volume of AS25 increases in SS/AS25 and DSPG/AS25 mixed monolayers; isotherms shifted to increasing mean molecular area (Figure 4.34(b)). Isotherm of DSPC/AS25 at a mole ratio of 8.51:1 shifted slightly away from DSPC pure monolayer. As for the isotherm of DSPC/AS25 at 3.42:1 and 1.71:1, 1.14:1 and 0.85:1, they are overlapping on each other and shifted to increasing mean molecular area. All the isotherms of AS25–phospholipids have the similar collapse pressure as their respective pure monolayers.

The reason isotherms of BSA-phospholipids shifted to a larger mean molecular area than AS25–phospholipids is the molecular size of BSA is bigger than AS25. It can be proven by their limiting molecular area that we determined earlier. The limiting molecular area of pure BSA monolayer is found to be  $500 \text{ \AA}^2$  (Figure 4.7), and AS25 is  $160 \text{ \AA}^2$  (Figure 4.9). The size of protein molecule will also affect the compression modulus value which will be discussed in the next section.

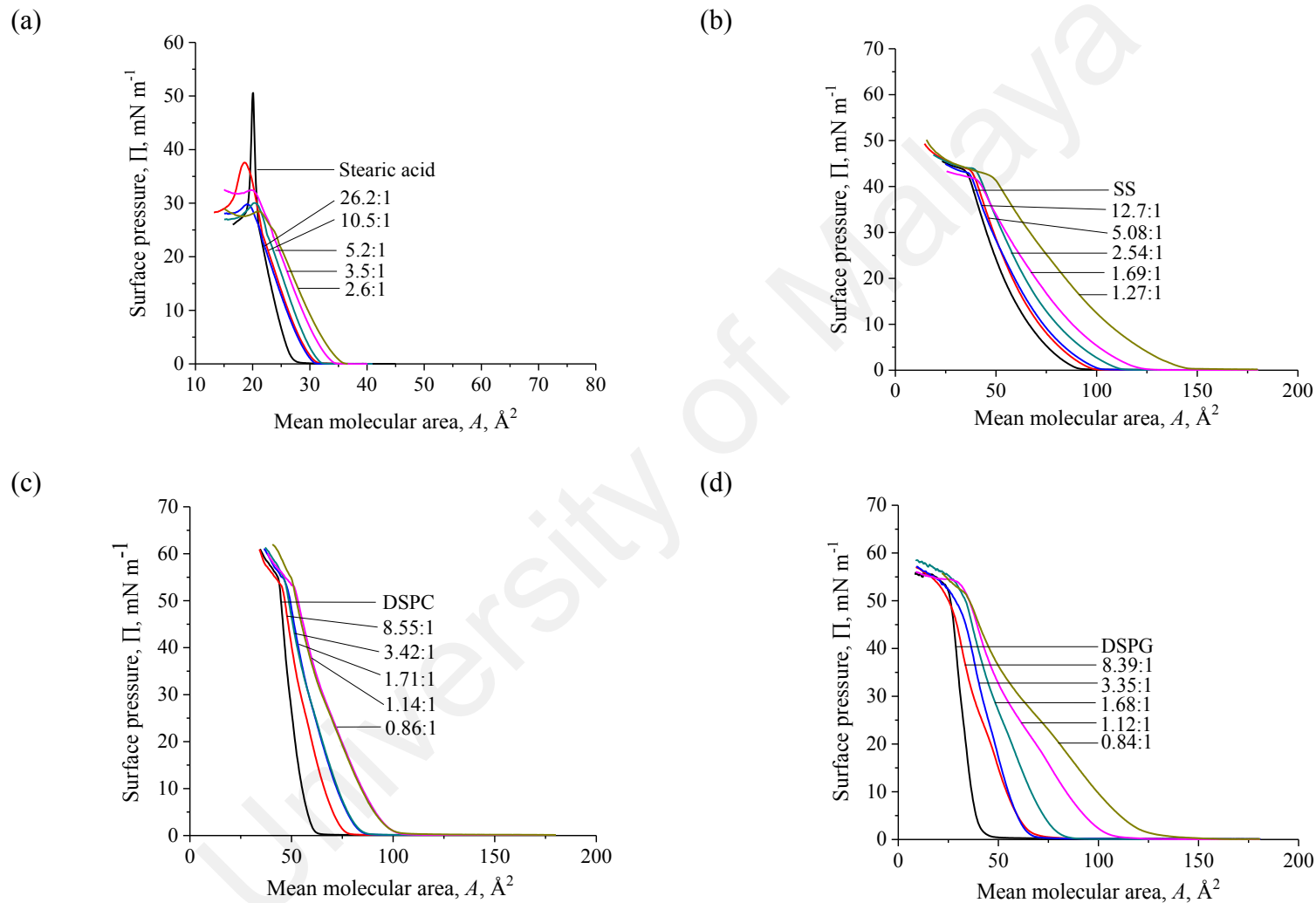


**Figure 4.34:** The surface pressure–area ( $\Pi$ – $A$ ) isotherms of mixed monolayers (plotted in mole ratio of phospholipids to AS25) : (a) SA/AS25 (b) SS/AS25 (c) DSPC/AS25 (d) DSPG/AS25. spread on a nanopure water subphase at 25°C.

### 4.3.2 Compressibility analysis

#### 4.3.2.1 Pure monolayers of SS, DSPC and DSPG

The  $C_s^{-1}$  profile of pure monolayer of SS, DSPC and DSPG is presented in Figure 4.35, the profile of SA was also included for comparison. The  $C_s^{-1}$  profile of SS showed LE phase, and as DSPC and DSPG are LC phase throughout the compression. Unlike SA, the bulky headgroup of phospholipids prevent the molecules to form S phase. The carboxyl head group of SA is very much smaller as we compare it to the head group of SS, DSPC, and DSPG. The molecules of SA can easily form S phase as the compression approaching its collapse pressure, whereas the large head group of phospholipids repels from each other in their respective monolayer at a/w interface prevent them from forming S phase. The maximal of  $C_s^{-1}$  of DSPC is approximately  $250 \text{ mN m}^{-1}$  at surface pressure of  $40$  to  $45 \text{ mN m}^{-1}$ . Presumably, S phase is observed in DSPC monolayer. The same observation is also observed in DPPC's  $C_s^{-1}$  profile; they have the same maximal of  $C_s^{-1}$  at the similar surface pressure. It is worth to mention that DPPC has the same headgroup as DSPC but shorter by 2 carbons in their hydrocarbon chains length. DPPC will be discussed in the next section 4.4 in this chapter.

The potential of molecules in molecular packing in their respective monolayer were observed  $\text{SS} < \text{DSPG} < \text{DSPC} < \text{SA}$ . SS molecules have the least potential to pack tightly as compare to DSPG, DSPC and SA. The  $-\text{OH}$  groups in the chemical structure of sucrose-headgroup of SS, it forms hydrogen bonds to the water molecules in subphase as compare to DSPC and DSPG. SS headgroups span horizontally on the monolayer caused a great repulsion between the headgroups of each SS molecules occurred in the system. This prevents a close molecular packing that results SS monolayer exist as LE phase.

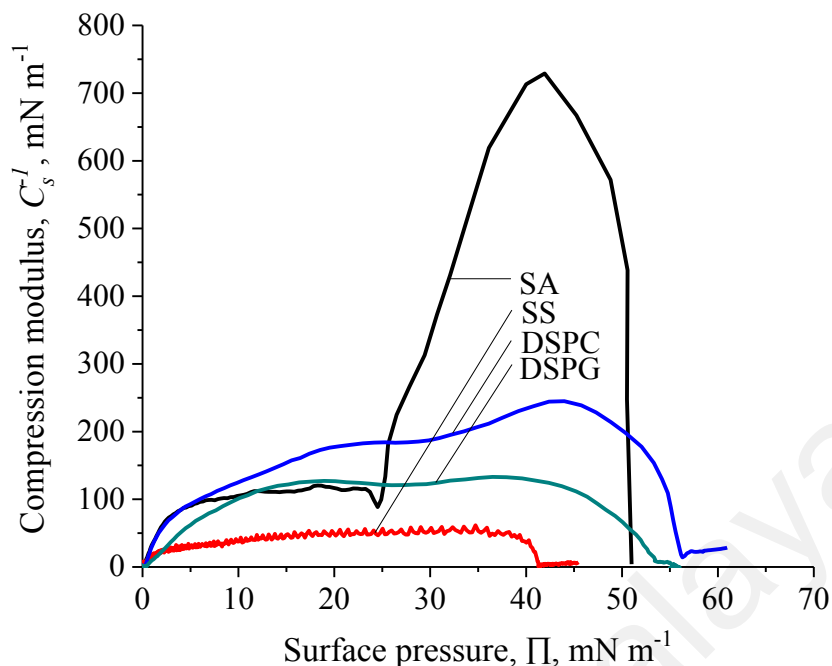


**Figure 4.35:** The compression modulus ( $C_s^{-1}$ ) vs surface pressure ( $\Pi$ ) of mixed monolayers of SA, SS, DSPC and DSPG, spread on a nanopure water subphase at 25°C.

The repulsive energy between the headgroup of DSPG as the molecules contact to each other in their monolayer is less than SS, where the maximal of DSPG (approximately 135  $\text{mN m}^{-1}$ ) is higher than SS (55  $\text{mN m}^{-1}$ ). There are 2 maximals observed in DSPG  $C_s^{-1}$  profile; they are 125  $\text{mN m}^{-1}$  (at surface pressure of 15 to 20  $\text{mN m}^{-1}$ ) and 135 (at surface pressure of 35 to 40  $\text{mN m}^{-1}$ ). This could be the reorientation of DSPG molecules occur in the monolayer. DSPG is a negatively charged molecule; it has several functional groups such as hydroxyl (-OH), carbonyl (C=O), and phosphate ( $\text{PO}_4^{3-}$ ) groups. The reorientation of the PG headgroup might be caused by the several hydrogen bonding formed between oxygen atom in -OH, C=O or/and P=O to the water structure at the surface.

DSPC is a zwitterion, it carries a positive charge at the ammonium ion and a negative charged at phosphate ion that presents in its phosphatidylcholines head group (Seelig, Gally, & Wohlgemuth, 1977). DSPC is considered as the least polar as compared to SS and DSPG who have many -OH group. A gradual increase to the first

maximal at surface pressure of 25 mN m<sup>-1</sup> in C<sub>s</sub><sup>-1</sup> profile, then a slight decrease on the curve at 28 mN m<sup>-1</sup>, and then rapidly increased to the second maximal at 45 mN m<sup>-1</sup>. The rearrangement of the PC headgroup occurred that the phase transition of DSPC monolayer change from LC to S phase at 45 mN m<sup>-1</sup>.

#### 4.3.2.2 Mixed monolayers of SS, DSPC and DSPG and BSA

At surface pressure of 0 to 5 mN m<sup>-1</sup>, all the lipids–BSA mixtures (Figure 4.36) exist at S phase ( < 250mN m<sup>-1</sup>), and then a dramatic collapse is observed after 5 mN m<sup>-1</sup>. The self-assembly of globular protein BSA into S phase can be clearly observed (McManus, Charbonneau, Zaccarelli, & Asherie, 2016) in C<sub>s</sub><sup>-1</sup> profiles. SS, DSPC and DSPG have the same saturated carbon-18 chain like SA, have higher maximal of C<sub>s</sub><sup>-1</sup> (about 700 mN m<sup>-1</sup>) unlike the unsaturated C18 fatty acids, maximal of C<sub>s</sub><sup>-1</sup> is about 250 to 300 mN m<sup>-1</sup>. The *cis*-double bond(s) increase the penetration of BSA into the membrane, in contrast, the *trans* configurations of saturated hydrocarbon chains forming a closely packed and less fluid membrane that prevents the dispersion of BSA into the membrane. As the surface pressure increases, the solid phase membrane collapsed and formed L or LE phase. Presumably, most of the BSA molecules had solubilized in the water subphase or sink to the bottom of the trough. None of the C<sub>s</sub><sup>-1</sup> profile of mixed systems exhibits the profile of their respective pure system. All the mixed monolayers form LE and L at higher surface pressure ( > 20 mN m<sup>-1</sup>), unlike DSPC formed S phase, DSPG formed LC phase in their pure monolayer. The pure BSA monolayer exhibits LE phase (Figure 4.7), however, a phase transition occurs from LE to S phase when the saturated phospholipids incorporated into BSA monolayers, the molecules become more tightly packed.

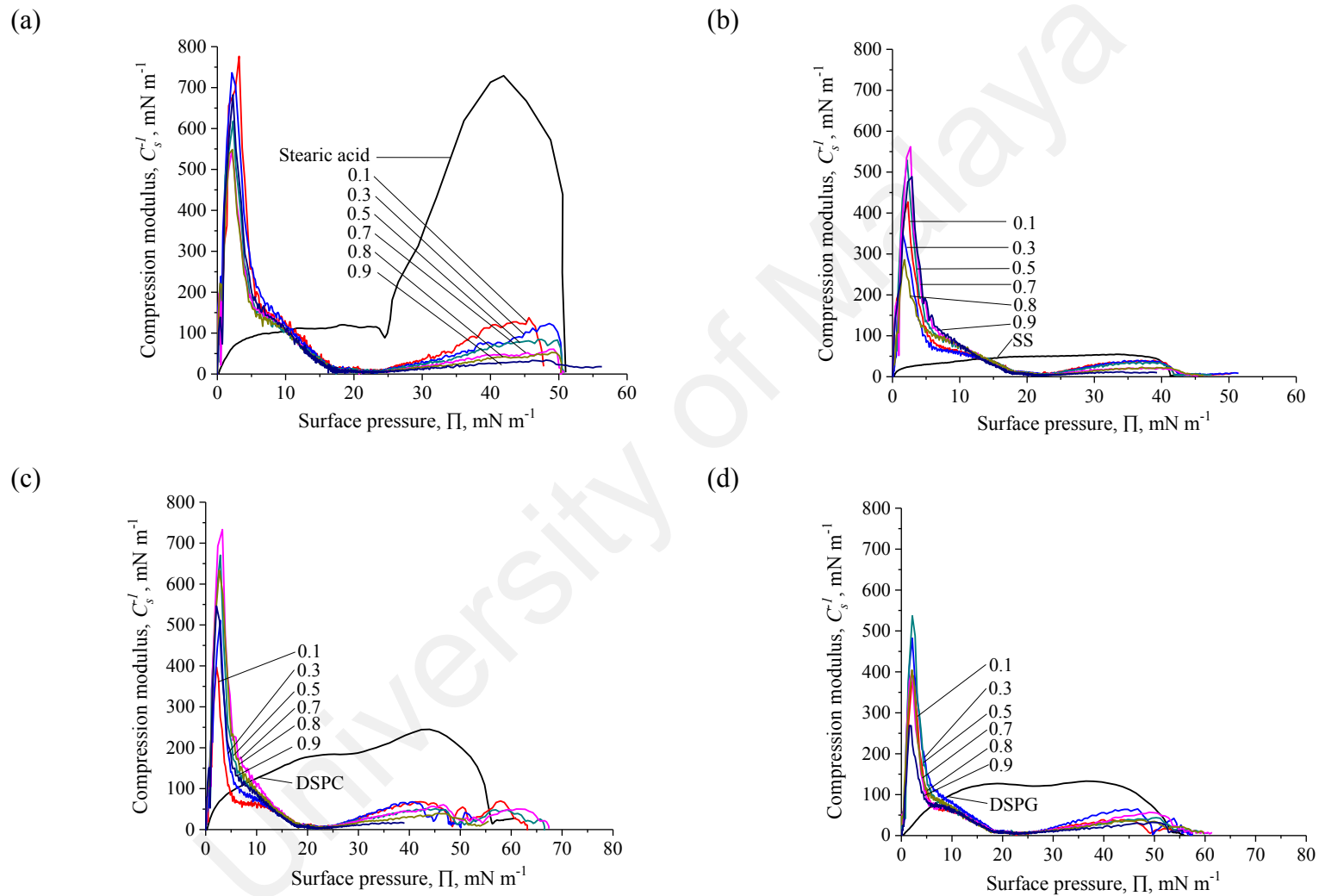


**Figure 4.36:** The compression modulus ( $C_s^{-1}$ ) vs surface pressure ( $\Pi$ ) of mixed monolayers (plotted in  $X_{BSA}$ ): (a) SA/BSA, (b) SS/BSA, (c) DSPC/BSA, and (d) DSPG/BSA, spread on a nanopure water subphase at 25°C.

In the mixtures of lipid-protein, molecular packing of phospholipids/BSA mixed systems is more compact than the pure system of BSA. The condensing effect of BSA on phospholipids monolayer is greatly influenced by their molecular packing as the surface pressure increases due to the compression of the barrier.

#### 4.3.2.3 Mixed monolayers of SS, DSPC and DSPG and AS25

The  $C_s^{-1}$  profile of phospholipids/AS25 mixed systems has the similar curve as their respective pure phospholipids monolayer (Figure 4.37), but with smaller  $C_s^{-1}$  values. In  $C_s^{-1}$  profile of SS/AS25, there was a decline of  $C_s^{-1}$  values value at surface pressure of  $30 \text{ mN m}^{-1}$  in mixed systems of 5.4:1, 2.54:1 and 1.27:1, however all of SS/AS25 mixed systems remained in LE phase at all the investigated ranges. In the mixed system of DSPG/AS25,  $C_s^{-1}$  is observed to be below  $80 \text{ mN m}^{-1}$  for the entire range of AS25 mole ratios, this being indicative of the formation of LE phase. This implied that the incorporation of AS25 into DSPG monolayers reduced their molecular packing as compared to pure DSPG monolayer. A change of its slope was observed in DSPG/AS25 mixed systems at  $25 \text{ mN m}^{-1}$  (Figure 4.37(c)), and  $30 \text{ mN m}^{-1}$  for DSPC/AS25 (Figure 4.37(d)). This observation is consistent with the plateau region existing in the  $\Pi$ -A isotherm of their pure system (Figure 4.32). The presence of AS25 in DSPC monolayer increases the fluidity of the membrane. The phase transition changed from LC to L and LE with the increasing amount of AS25 in the mixed systems of DSPC/S25. Lipid molecules interact with a protein in a different way. Favorable interactions occurred between the hydroxyl groups of SS and DSPG with polar region of AS25 molecules.

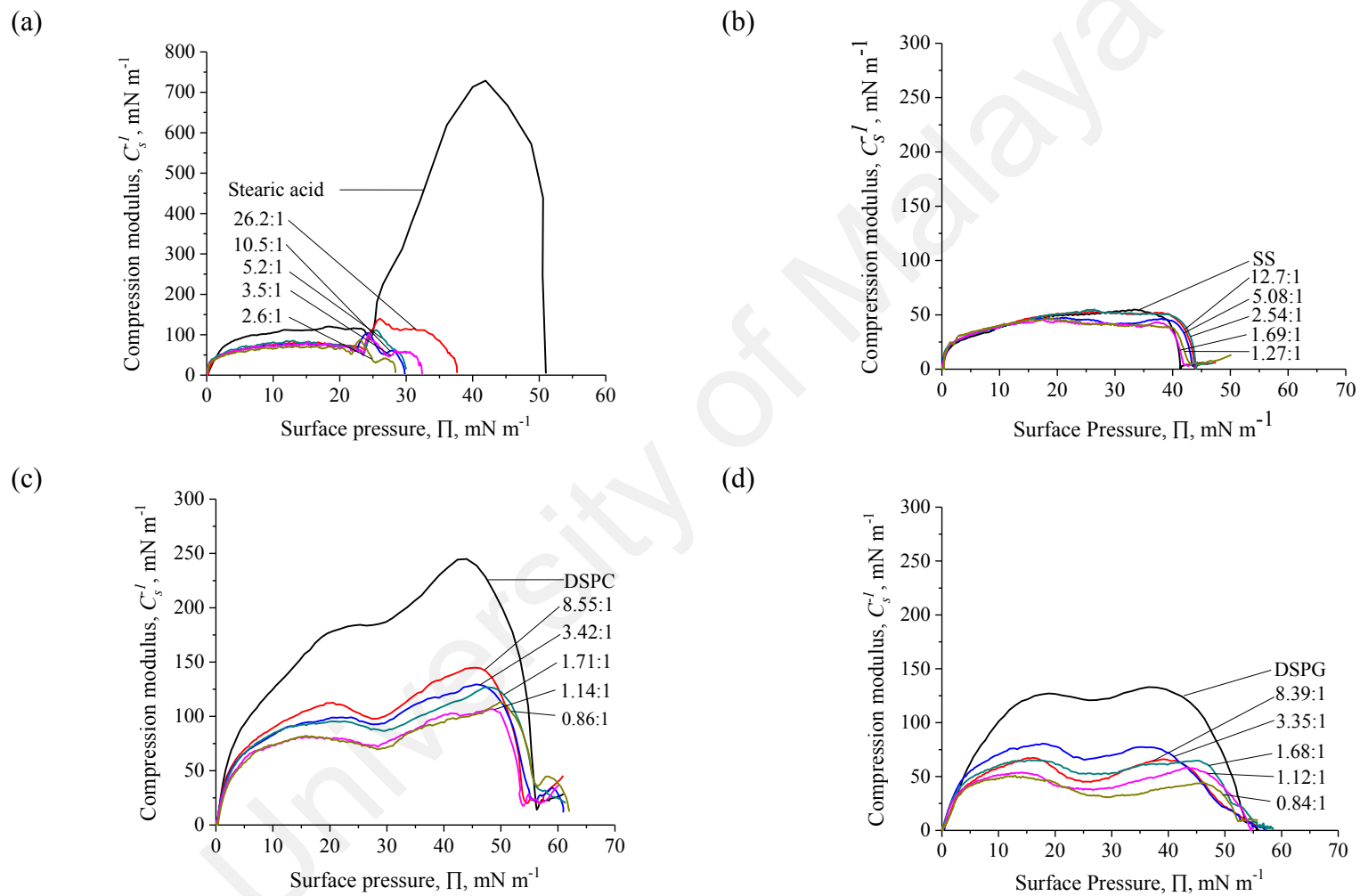


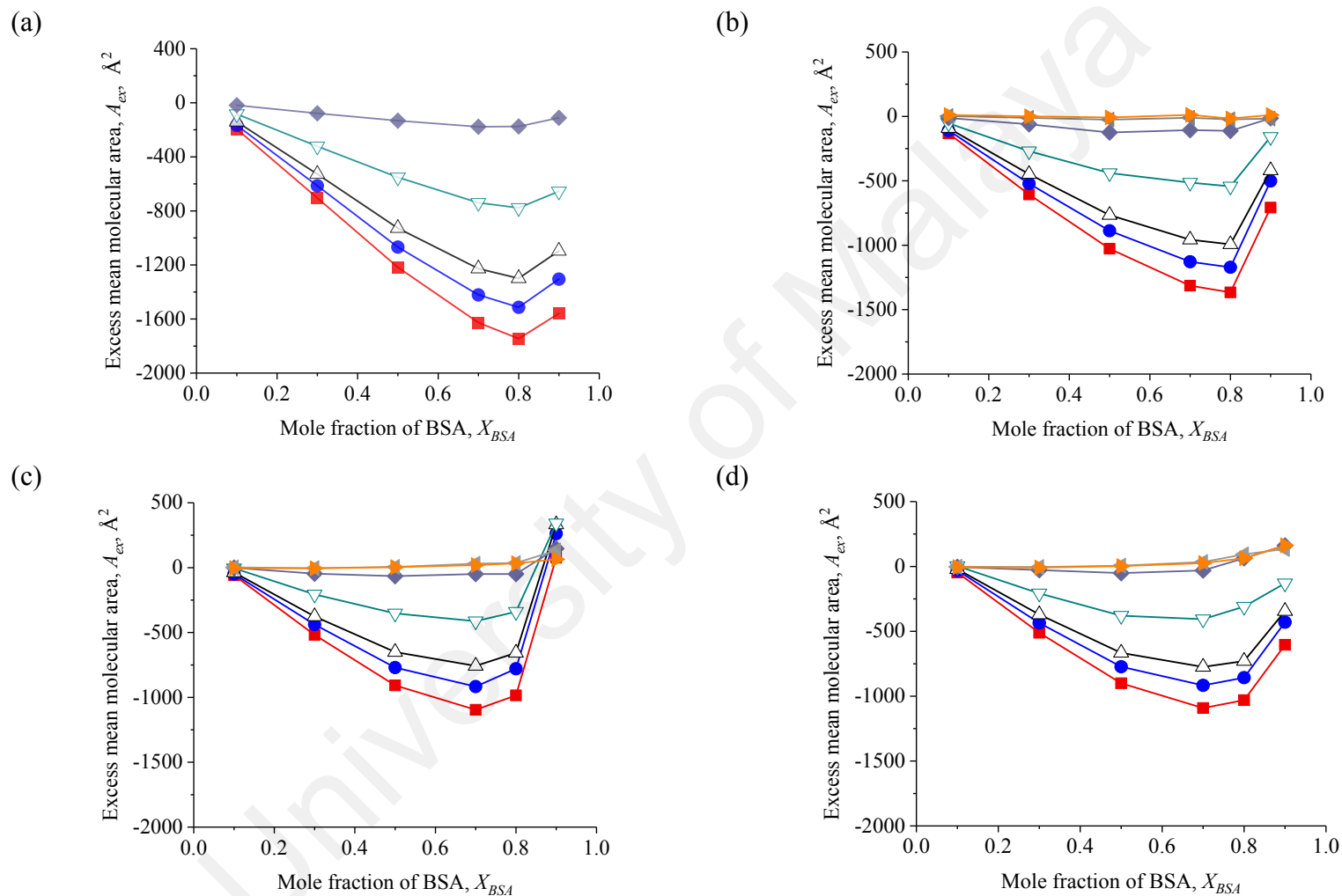
**Figure 4.37:** The compression modulus ( $C_s^{-1}$ ) vs surface pressure ( $\Pi$ ) of mixed monolayers (plotted in mole ratio of phospholipids to AS25): (a) SA/AS25 (b) SS/AS25 (c) DSPC/AS25 (d) DSPG/AS25, spread on a nanopure water subphase at 25°C.

### 4.3.3 Energetic stability of mixed monolayers

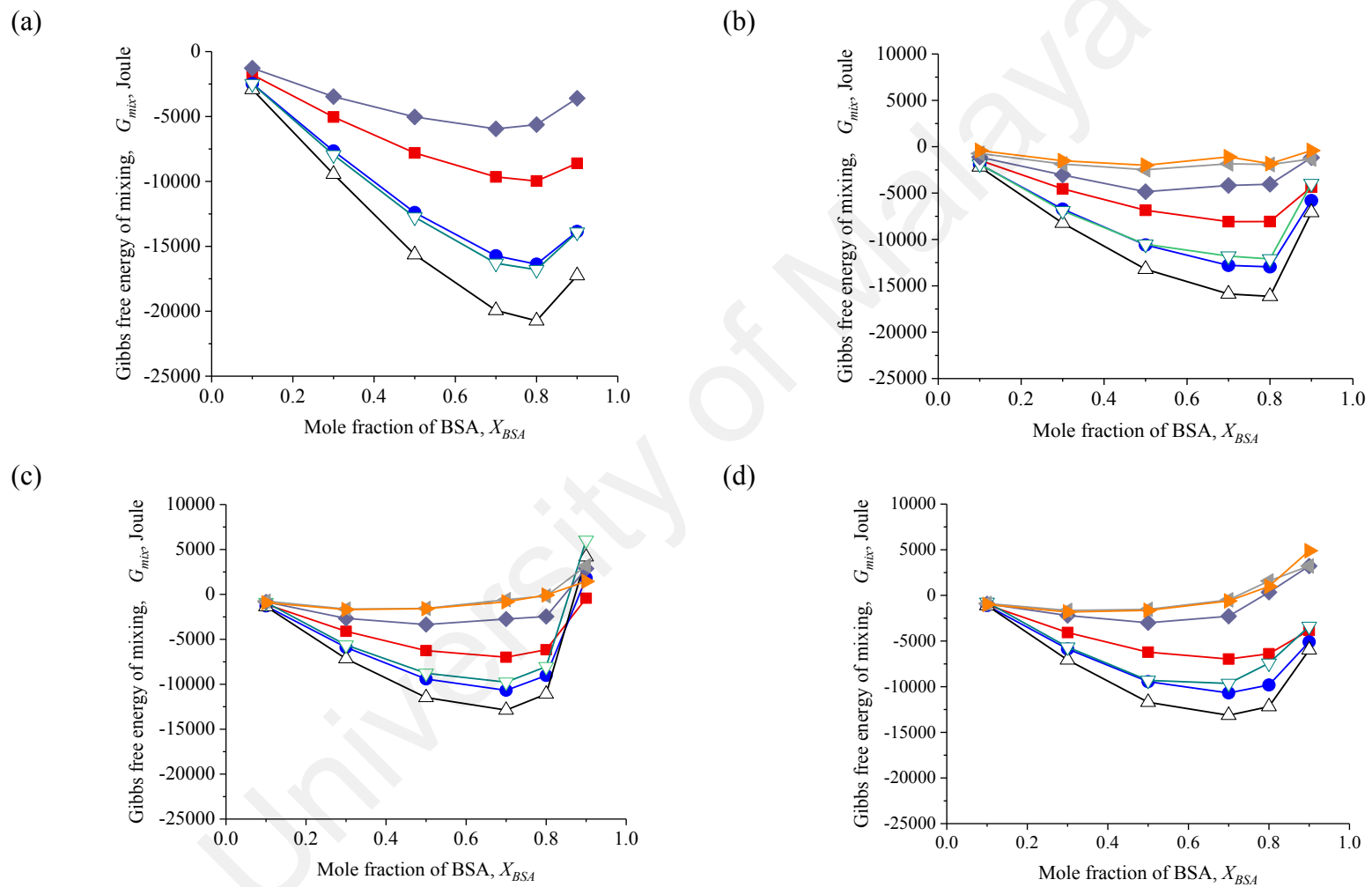
#### 4.3.3.1 Mixed monolayers of SA, SS, DSPC and DSPG and BSA

Figure 4.38 showed that mean molecular area  $A_{ex}$  is presented against mole fractions of phospholipids (SS, DSPC, and DPG) to BSA mixed monolayers at different surface pressures (5, 10, 15, 20, 25, 30 and 35 mN m<sup>-1</sup>). The mean molecular area increased as the surface pressure increased. Negative deviations of  $A_{ex}$  shown for all profiles of phospholipids/BSA, except at  $X_{BSA} = 0.9$  in DSPC/BSA mixture, a positive value of  $A_{ex}$  was obtained. PC headgroup is the least favored in BSA mixtures as compared to PG and sucrose headgroup of SS which showed negative deviations throughout the whole investigated range, in particularly,  $X_{BSA} = 0.9$  in DSPC/BSA mixed system.  $A_{ex}$  values of DSPG/BSA and SS/BSA became more negative with increasing  $X_{SS}$  and  $X_{DSPG}$ . The  $A_{ex}$  values of SA/BSA are more negative than phospholipids/BSA. This showed that the size of headgroup and functional groups in lipids' headgroup are greatly influenced the intermolecular interactions in the lipid-protein interactions.

A similar trend of  $G_{mix}$  was shown in all three mixtures of phospholipids/BSA mixed systems in Figure 4.39.  $G_{mix}$  gradually increased negative as  $X_{BSA}$  from 0.1 to 0.8, and then a slight recovered at  $X_{BSA} = 0.9$ . The most negative  $G_{mix}$  values were observed at  $X_{BSA} = 0.8$  for SS/BSA, and 0.9 for DSPC/BSA and DSPG/BSA mixed system at surface pressure of 15 mN m<sup>-1</sup>, it is certainly clear that the most energetically stable mixture of phospholipids/BSA is  $X_{BSA} = 0.7$  and 0.8. So it appears that generous amount phospholipids are required in the lipid-protein mixtures for an attractive interaction between phospholipids and BSA to be occurred (Figure 4.40).



**Figure 4.38:** Excess mean molecular area of phospholipids/BSA mixed monolayers vs mole fraction of BSA on pure water subphase at 25°C. For discrete surface pressure of  $\blacksquare = 5 \text{ mN m}^{-1}$ ,  $\bullet = 10 \text{ mN m}^{-1}$ ,  $\blacktriangle = 15 \text{ mN m}^{-1}$ ,  $\nabla = 20 \text{ mN m}^{-1}$  and  $\blacklozenge = 25 \text{ mN m}^{-1}$ .  $\blacktriangleleft = 30 \text{ mN m}^{-1}$  and  $\blacktriangleright = 35 \text{ mN m}^{-1}$ .



**Figure 4.39:** Free excess energy  $G_{mix}$  of phospholipids/BSA monolayers vs mole fraction of BSA on pure water subphase at 25°C. For discrete surface pressure of  $\blacksquare = 5 \text{ mN m}^{-1}$ ,  $\bullet = 10 \text{ mN m}^{-1}$ ,  $\blacklozenge = 15 \text{ mN m}^{-1}$ ,  $\nabla = 20 \text{ mN m}^{-1}$  and  $\blacklozenge = 25 \text{ mN m}^{-1}$ .  $\blacktriangleleft = 30 \text{ mN m}^{-1}$  and  $\blacktriangleright = 35 \text{ mN m}^{-1}$ .

Negative values of  $G_{mix}$  for the entire investigated range of the mixed system of SS/BSA were obtained (Figure 4.39(b)). A considerable large positive  $G_{mix}$  value was observed in DSPC/BSA mixed system at  $X_{BSA} = 0.9$  indicating great repulsion occurred between protein-protein molecules in the lipid-protein mixtures at surface pressure of 5 to 35  $\text{mN m}^{-1}$  (Figure 4.39(c)). Positive values of  $G_{mix}$  value was observed at  $X_{BSA} = 0.9$  for DSPG/BSA mixed systems at surface pressure of 25, 30 and 35  $\text{mNm}^{-1}$ . (Figure 4.39(d)). SS/BSA and DSPG/SS have the similar plots of  $A_{ex}$  and  $G_{mix}$ . This showed that the preferences of BSA molecules in SS monolayer over DSPC and DSPG at the entire investigated mole ratios. This could be due to the polar amino acids composition of BSA interacting with SS's sucrose headgroup which contains a number of hydroxyl groups.

$G_{mix}$  values of SA/BSA mixed systems were more negative than phospholipids/BSA. The size of lipids' headgroup will cause a greater repulsion in the mixed systems. SA/BSA is energetically preferred than phospholipids/BSA. This study will serve as a reference in lipid-protein research and prodrug research as albumin is widely used as drug delivery carrier. In the selection of phospholipids in designing DDS formulations, it is important for us to look into the insight of quantitative energetic stability in each mixture.

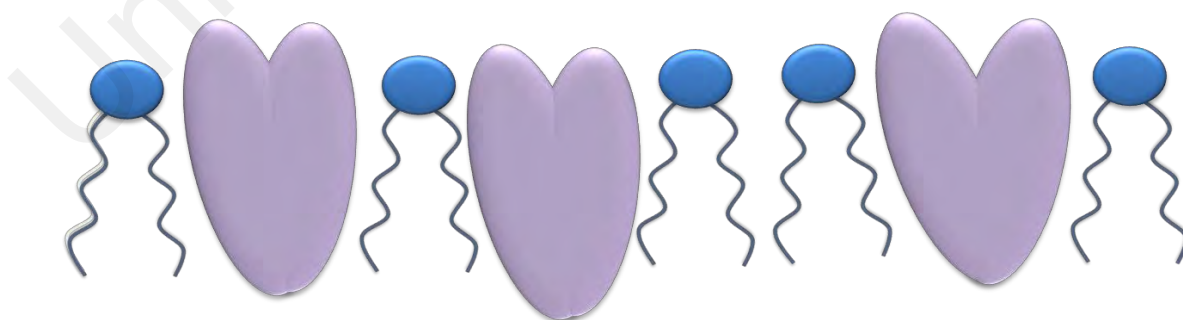


**Figure 4.40:** A cartoon illustration to describe the interactions of BSA and phospholipids.

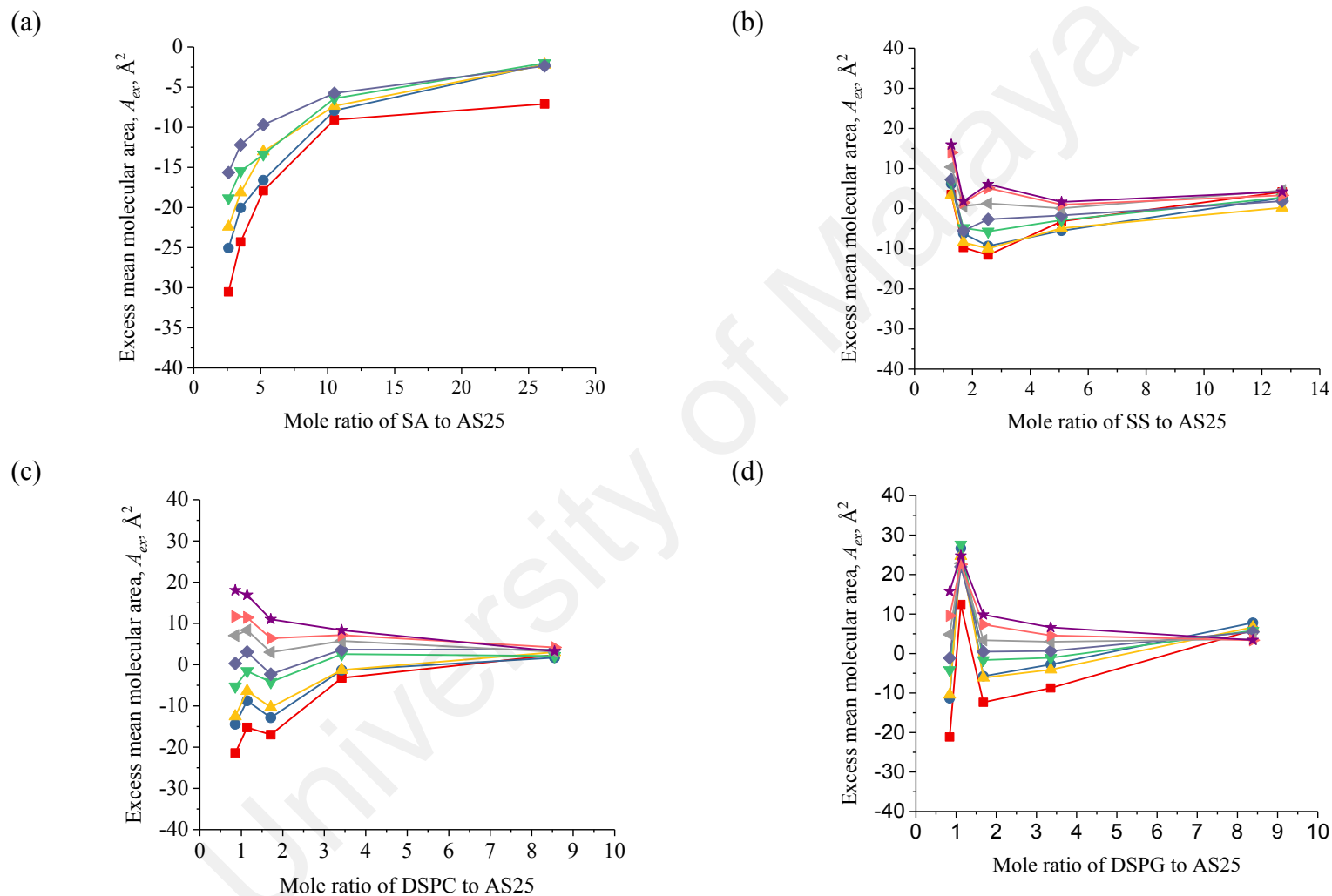
#### 4.3.3.2 Mixed monolayers of SS, DSPC and DSPG and AS25

Figure 4.41 showed mean molecular area  $A_{ex}$  is presented against mole fractions of phospholipids (SS, DSPC and DPG) to AS25 mixed monolayers at different surface pressures (5, 10, 15, 20, 25, 30, 35 and 40 mN m<sup>-1</sup>). The mean molecular area increased with the increasing surface pressure. Negative deviations were also observed in phospholipids/AS25  $A_{ex}$  profiles; however the values of  $A_{ex}$  is less negative as compared to phospholipids/BSA in Figure 4.38. This is due to AS25 is a membrane-bound protein, it will interact on the surface of phospholipids membrane; in contrast, integral protein BSA will interact in between the phospholipids molecules in a membrane. The mixture of phospholipids/BSA is more miscible than with AS25 in the mixtures.

The  $A_{ex}$  profile of SS/AS25 mixtures are observed to be positive and some values are near to zero, positive values of  $A_{ex}$  were observed at the lowest (1.27 to 1) and highest (12.7 to 1) mole ratios. At the highest mole of DSPG (8.39 to 1), repulsions occurred between AS25 and DSPG molecules in the mixed system.

The Gibbs free energy plots of SA/AS25, SS/AS25 and DSPG/AS25 are found to have negative  $G_{mix}$  values in the whole investigated mole ratios, and their  $G_{mix}$  values are in between -500 to -1900 Joules (Figure 4.42(b)). They have the similar interactions energy with AS25 in their lipid systems.

The small and negative charged carboxyl headgroup of SA is readily formed an ordered molecular packing as compared to the phospholipids with large headgroup. Thus, the positive charged surface of AS25 will be easily embedded on the ordered surface of negatively charged SA membrane. In contrast, a greater repulsion between the headgroup of phospholipids molecules will occur during the molecular packing in their pure monolayers as compared to pure SA monolayer.



**Figure 4.41:** Excess mean molecular area of phospholipids/AS25 mixed monolayers vs mole ratio of phospholipids to AS25 on pure water subphase at 25°C. For discrete surface pressure of  $\blacksquare$  = 5  $\text{mN m}^{-1}$ ,  $\bullet$  = 10  $\text{mN m}^{-1}$ ,  $\blacktriangle$  = 15  $\text{mN m}^{-1}$ ,  $\blacktriangledown$  = 20  $\text{mN m}^{-1}$ ,  $\blacklozenge$  = 25  $\text{mN m}^{-1}$  (diamond),  $\blacktriangleleft$  = 30  $\text{mN m}^{-1}$ ,  $\blacktriangleright$  = 35  $\text{mN m}^{-1}$  and  $*$  = 40  $\text{mN m}^{-1}$ .

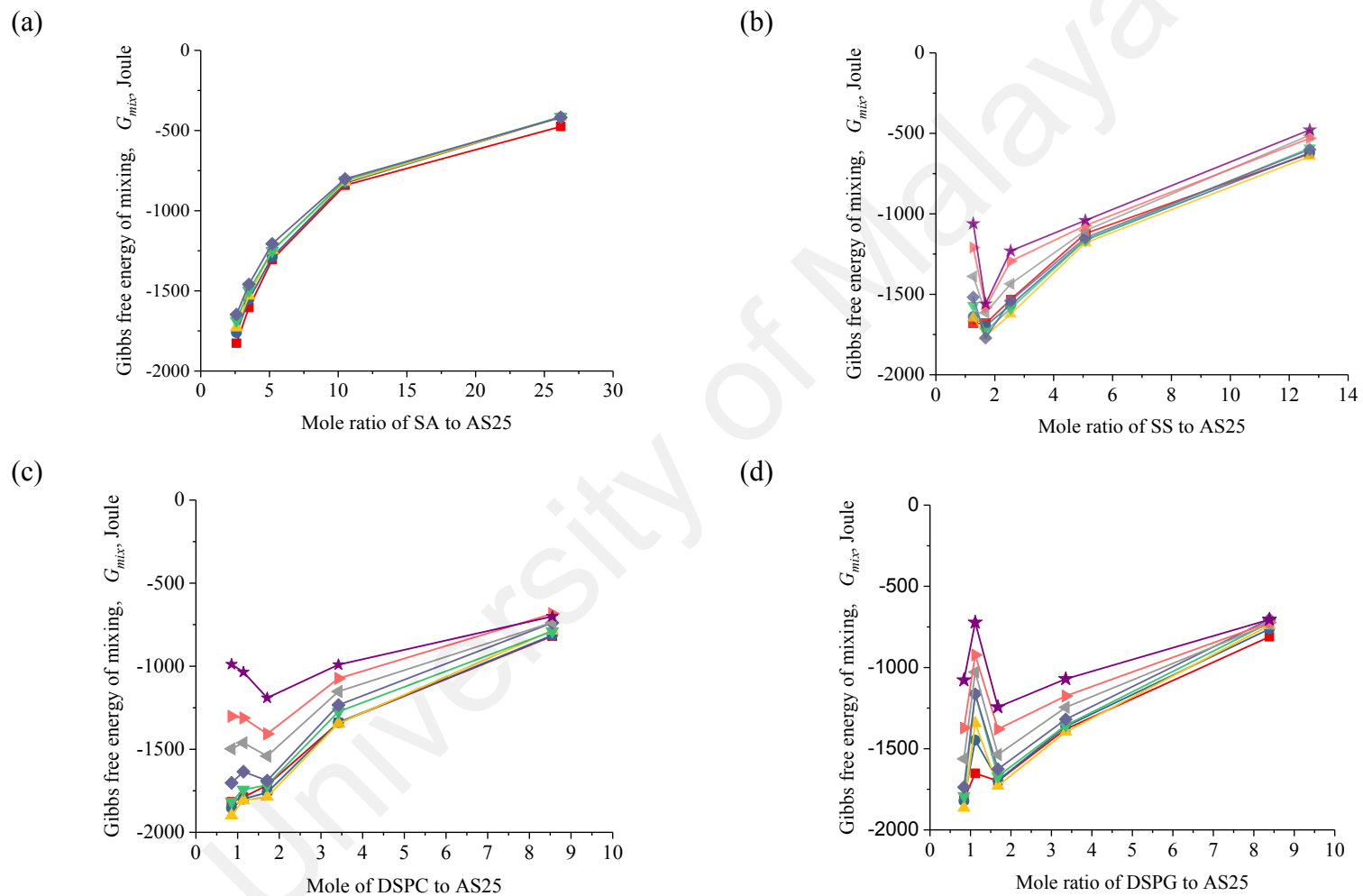


**Figure 4.42:** Gibbs free energy of mixing  $G_{mix}$  of phospholipids/AS25 monolayers vs mole ratio of phospholipids to AS25 on pure water subphase at 25°C. For discrete surface pressure of  $\blacksquare$  = 5 mN m<sup>-1</sup>,  $\bullet$  = 10 mN m<sup>-1</sup>,  $\blacktriangle$  = 15 mN m<sup>-1</sup>,  $\blacktriangledown$  = 20 mN m<sup>-1</sup>,  $\blacklozenge$  = 25 mN m<sup>-1</sup> (diamond),  $\blacktriangleleft$  = 30 mN m<sup>-1</sup>,  $\blacktriangleright$  = 35 mN m<sup>-1</sup> and  $*$  = 40 mN m<sup>-1</sup>.

Hence, the repulsion between headgroup of phospholipids in lipid membrane will affect the conjugation of AS25 on the surface of phospholipid membrane, and also considering the preferences of each amino acid in AS25 protein sequences interacting with the functional groups in each headgroup of phospholipids.

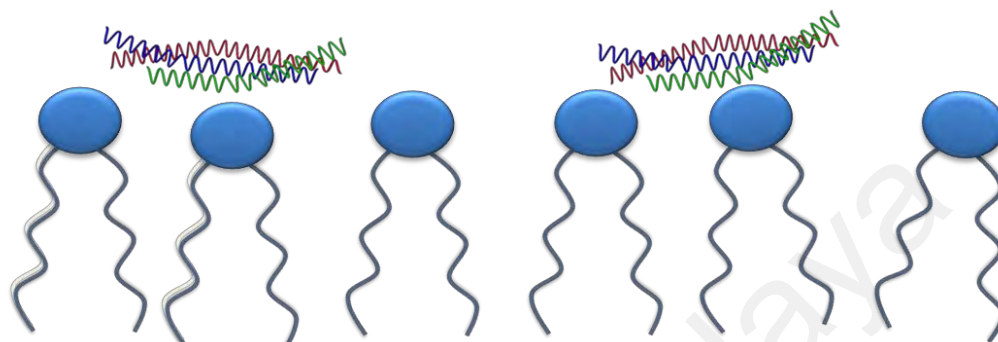


**Figure 4.43:** A cartoon illustration to describe interactions of AS25 on the surface of phospholipid membrane.

#### 4.4.Lipid-protein interactions: DPPC

##### 4.4.1 $\Pi$ -A Isotherms

DPPC exist as a zwitterion, in its phosphatidylcholines head group consist of a positive charged at ammonium ion and a negative charged at phosphate ion (Gally, Niederberger, & Seelig, 1975; Seelig et al., 1977). The general phases assigned for the phospholipid are G phase, coexistence of gas phase and liquid expanded phase (G-LE), LE phase, coexistence liquid-expanded phase and liquid condensed phase (LE-LC), LC phase, and S phase as collapse phases (Figure 4.44). DPPC molecules are packed loosely in the gas phase at the water surface. As the monolayer is being compressed, the first plateau to the far right in the isotherm at (surface pressure of 0 to 10 mN m<sup>-1</sup>) shows G-LE transition is formed. In the LE phase, the organizations of molecules are like a two-dimensional liquid surface and are not as fluid as to move about compare to in the gas phase. Further compression results LE-LC phase transition (the second plateau shifting from right to left in the isotherm) occurred. LE-LC phase transition occurs at about 15 mN m<sup>-1</sup> for DPPC. In LC phase, molecules are packed more closely

than the liquid-expanded film. At a surface pressure of  $60 \text{ mN m}^{-1}$ , a curve appears in the isotherm indicating the collapse of DPPC film. Similar limiting molecular area of  $55 \text{ \AA}^2$  were reported by several colloid researchers (Hąc-Wydro & Dynarowicz-Łątka, 2006a; Hąc-Wydro et al., 2005; Hąc-Wydro et al., 2007; Kamilya et al., 2007; Moghaddam et al., 2011).

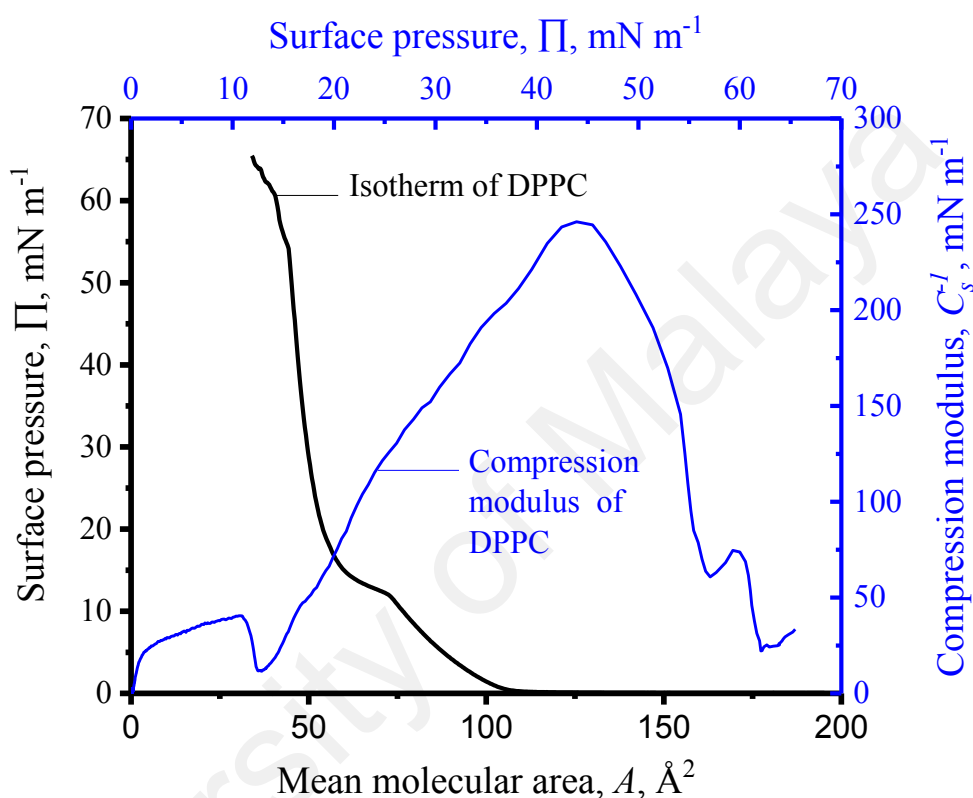


**Figure 4.44:** The surface pressure–area ( $\Pi$ – $A$ ) isotherm of DPPC monolayer, and its compressibility modulus ( $C_s^{-1}$ ), spread on water subphase at  $25^\circ\text{C}$ .

#### 4.4.1.1 Mixed monolayers of DPPC and BSA

The interaction of DPPC and BSA was also performed to obtain the valuable thermodynamic data to elucidate the lipid-protein interactions between an integral protein and phospholipids, and also as a comparison to a membrane bound protein such as AS25. BSA is the best selection of integral protein to be used to illustrate the lipid-protein interactions in the biological membrane model.

The isotherms of DPPC/BSA shift to the right (increasing molecular area) as the mole fraction of BSA increases (Figure 4.45). All the mixtures' isotherms have the

same shape as the isotherm of BSA when the compression first started. The same observation also observed in their compression modulus profile. Plausibly, intermolecular interaction between BSA and BSA first occur, and then followed by BSA and DPPC interacting with each other. Protein-protein interaction is more likely preferable compared to lipid-protein interactions.

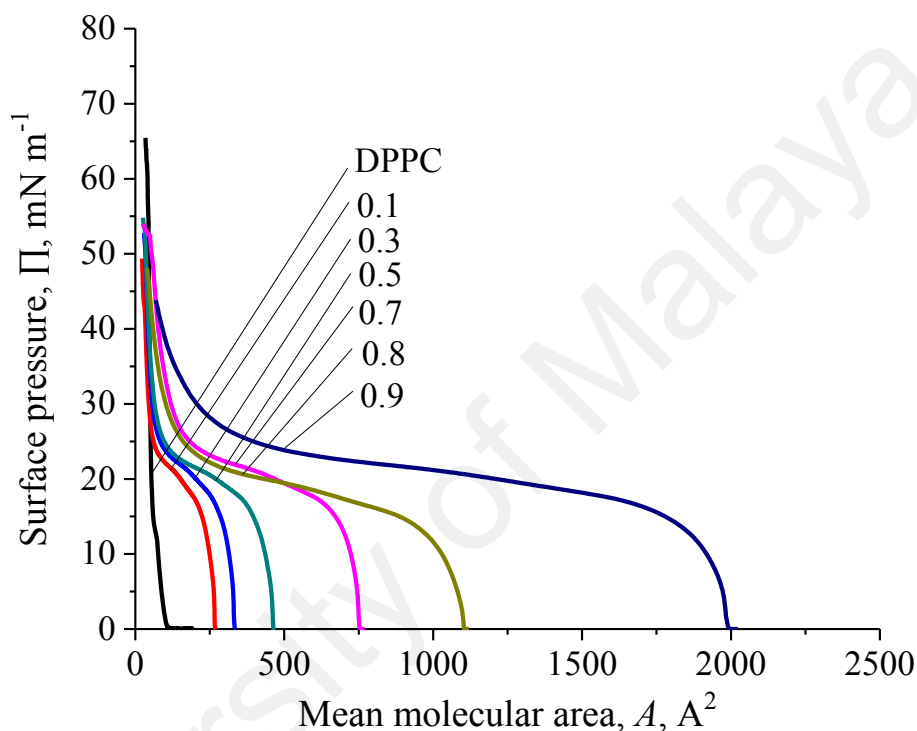


**Figure 4.45:** The surface pressure–area ( $\Pi$ – $A$ ) isotherms of DPPC/BSA mixed monolayers (plotted in  $X_{BSA}$ ), spread on a nanopure water subphase at 25°C.

#### 4.4.1.2 Mixed monolayers of DPPC/AS25, DPPC/ DP and DPPC/ DP/AS25

Figure 4.46 shows the  $\Pi$ – $A$  isotherms of DPPC and DPPC/AS25 at 25°C on a nanopure water subphase. The objectives of the following studies are to learn the effect of DP in DPPC/AS25 mixed monolayers. The molecular compatibility of DPPC and DP were firstly studied and the best mole ratio of DPPC/DP will be subsequently used to create a mixed monolayer for incorporation of AS25. The energetic findings will facilitate the preparation of nanoliposomes at their most stable form.

The isotherms of DPPC/DP mixed system shifted to the left (decreasing molecular area) as denoted in Figure 4.46(a). The effect of DP on DPPC monolayer was noticeably shown from 0 to 15 mN m<sup>-1</sup> in the mixed systems' isotherms, where there is a broad similar broad shape of  $\Pi$ - $A$  isotherm of DP can be observed in the mixed systems (Figure 4.5). This could be DP-DP interactions occurred first, and then followed by DP-DPPC interactions. Comparing the pure system of DPPC and mixed systems DPPC/DP, DPPC isotherm increases rapidly at zero surface pressure from a smaller mean molecular area (125 Å<sup>2</sup>), whereas, the isotherm of DPPC/DP (such as mole ratio of 100:1) increased gradually starting from a larger mean molecular area (300 Å<sup>2</sup>). DP molecules disrupted the molecular packing of DPPC, as the headgroup of DP is larger than DPPC headgroup. Presumably, the presence of DP in the mixtures create a noteworthy repulsion between the molecules as compared to the pure DPPC system, only one type of molecule present in the monolayer. When AS25 was incorporated into DPPC monolayers, the isotherms of the mixed monolayers of DPPC/AS25 were shifted to the higher molecular area with the increasing volume of AS25 (Figure 4.46(b)). The collapse pressures of DPPC/AS25 mixed systems are slightly lower than pure DPPC, which is about 55 mN m<sup>-1</sup>.

Referring to the energetic stability data (  $G_{mix}$  ) of DPPC/DP, the mole ratio of 50:1 is chosen as the best mole ratio to be used to mimic a part of stealth nanoliposomes membrane. Subsequently, the incorporation of AS25 into DPPC/DP mixed monolayer to be carried out. The isotherms of ternary mixtures of DPPC/DP/AS25 shifted dramatically to the right, increasing mean molecular area for the entire investigated range (Figure 4.6(c)). A greater interaction is taken place between 3 types of molecules in the same trough area. However similar collapse pressure was observed for all ternary mixtures.

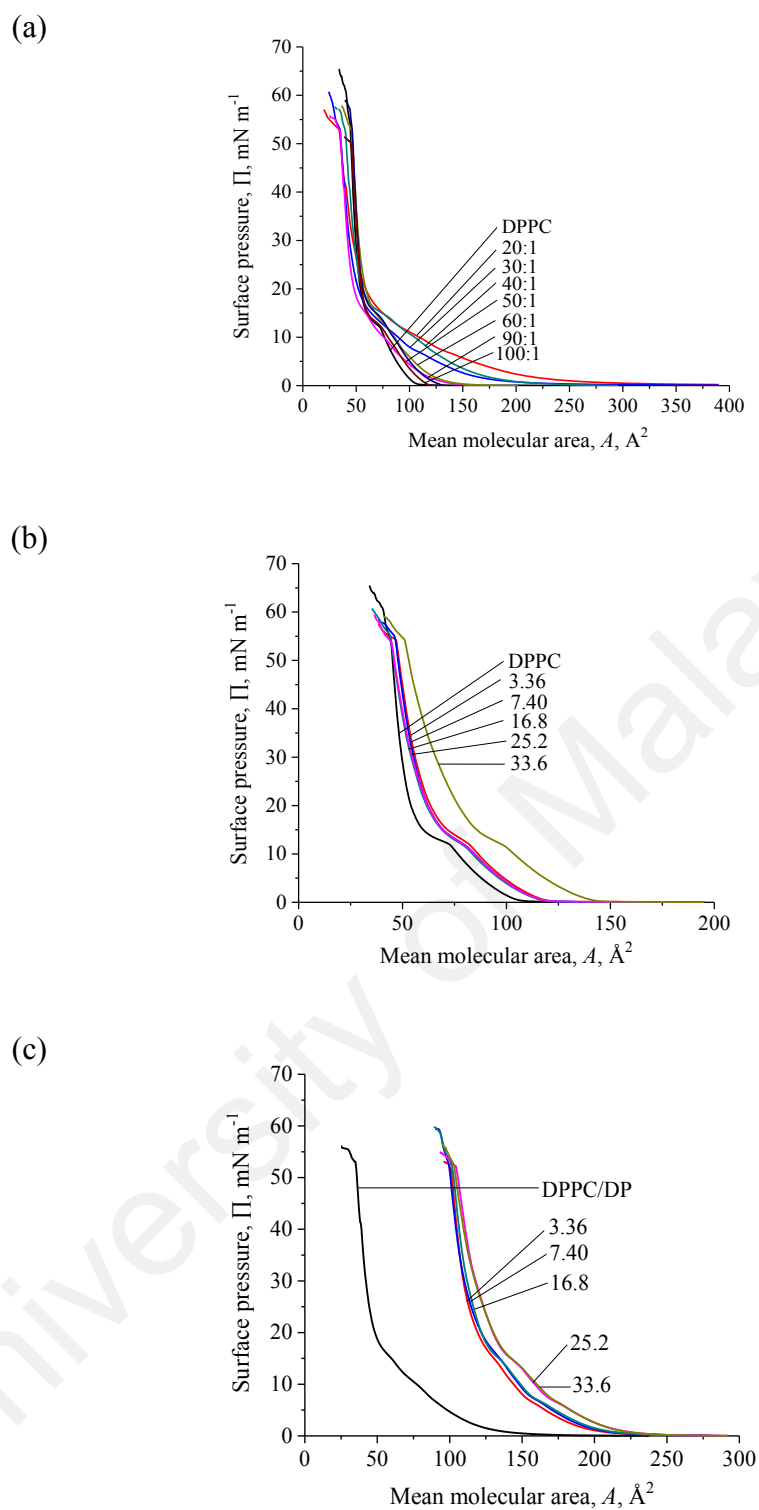


**Figure 4.46:** The surface pressure–area ( $\Pi$ – $A$ ) isotherms of mixed monolayers of: (a) DPPC/DP (plotted in mole fraction of DPPC to DP), (b) DPPC/AS25 (mole of AS25), and (c) DPPC/DP/AS25 (plotted in nmole of AS25), spread on a nanopure water subphase at 25°C.

#### 4.4.2 Compressibility analysis

##### 4.4.2.1 Mixed monolayers of DPPC and BSA

Mixtures of DPPC/BSA are highly condensed, the maximal values of  $C_s^{-1}$  are much higher than the respective single system of DPPC (250 mN m<sup>-1</sup>) and BSA (50 mN m<sup>-1</sup>). Monolayer of BSA without DPPC exhibits LE phase, meanwhile, monolayer of DPPC without BSA exhibits LC phase (Figure 4.47). Interestingly, solid crystalline domain formed when DPPC and BSA are mixed together in the same trough of water subphase. Two pronounced observations can be made on  $C_s^{-1}$  versus  $\Pi$  profile of DPPC/BSA binary systems. First, at surface pressure of 0 to 20 mN m<sup>-1</sup>, the similar shape of pure BSA  $C_s^{-1}$  versus  $\Pi$  profile appeared in DPPC/BSA profile. This could be BSA–BSA interaction takes place first when the compression began. However, as the compression continued, protein-protein interaction is tailed by the lipid-protein interaction of DPPC–BSA occurred. Second, a similar  $C_s^{-1}$  versus  $\Pi$  profile of pure DPPC is observed at surface pressure of 25 to 50 mN m<sup>-1</sup>, but at a lower  $C_s^{-1}$  value (<100 mN m<sup>-1</sup>) is obtained. This can be explained by the presence of BSA in DPPC monolayer prevents the molecule packing of DPPC from forming LC phase.

##### 4.4.2.2 Mixed monolayers of DPPC/AS25, DPPC/ DP and DPPC/ DP/AS25

Pure DPPC monolayers are highly condensed as supported by the large value of compression modulus owing to both of its saturated hydrocarbon chains. A noticeable phase transition of pure DPPC occurs from liquid phase (at 10 to 15 mN m<sup>-1</sup>) to LC phase (at 15 to 55 mN m<sup>-1</sup>); and the same phase transition is observed in the  $C_s^{-1}$  versus  $\Pi$  plot for all its mixed systems (including DPPC/AS25, DPPC/DP, and DPPC/DP/AS25) for the entire compression (Figure 4.48).

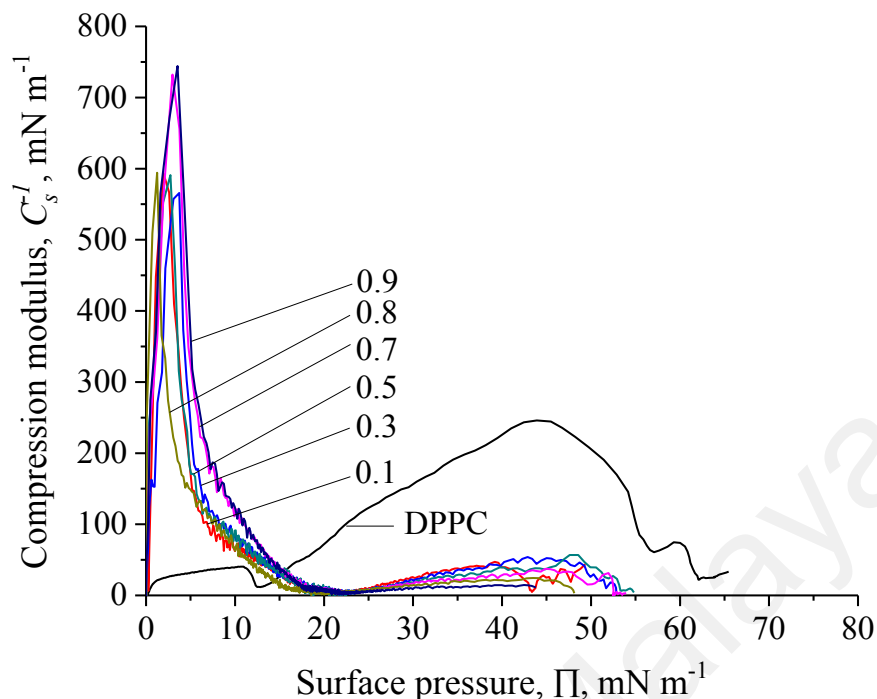


**Figure 4.47:** The compression modulus ( $C_s^{-1}$ ) vs surface pressure ( $\Pi$ ) of mixed monolayers of DPPC/BSA (plotted in mole fraction of BSA), spread on a nanopure water subphase at 25°C.

The presence of AS25 in DPPC monolayers caused the mixtures become less compressible than pure DPPC, sequentially forming LE, L, and LC phases with increasing volume of AS25 incorporated into the membrane. AS25 molecules perturb the perfect molecular packing of DPPC monolayer that will lead to a greater repulsion between the molecules preventing the molecules from packing tightly. Membrane fluidity increases as the arrangement of molecules are less ordered and less compressible. DPPC/AS25 is less condensed compare to pure DPPC monolayer, as the maximal compression modulus values are lower ( $<200 \text{ mN m}^{-1}$ ) than pure DPPC ( $\pm 250 \text{ mN m}^{-1}$ ).

At low surface pressures (0 to  $10 \text{ mN m}^{-1}$ ), results similar to those of the DP compression moduli (Figure 4.5) were observed in the mixed systems of DPPC/DP and DPPC/DP/AS25, as plotted in Figure 4.47. These results showed that the effect of DP

was very strong in all of the mixtures; intermolecular interactions began with DP–DP interactions and then DP–DPPC (or DP–DPPC–AS25) occurred from 10 mN m<sup>-1</sup> onward.  $C_S^{-1}$  value rapidly increases from surface pressure of 15 to 35 mN m<sup>-1</sup>, plausibly, a great interaction of DPPC–DP occurred as the molecules are trying to position themselves in the most stable form. Then, there is a slight decrease in compression modulus value at 40 to 45 mN m<sup>-1</sup> for the mixtures; this could be the initiation of DPPC–DPCC intermolecular interactions. At a lower mole ratio of DPPC, such as 20:1, the mixture forms LE phase, as we compare to a higher mole of DPPC in DPPC/DP mixture, the mixture forms LC phase. Increasing mole of DPPC will enhance compressibility and a more ordered molecular packing will form to achieve LC phase.

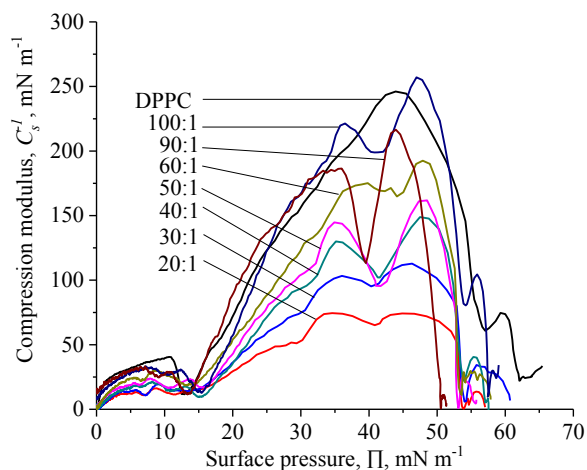
As mentioned earlier, AS25 was incorporated into DPPC/DP mixed monolayer at mole ratio of 50 to 1.  $C_S^{-1}$  values decrease as the mole of AS25 increase. At the smallest mole of AS25 incorporated in the mixture (3.36 nmole), a highly condensed phase formed. However, at the highest mole of AS25 in the mixture, LC phase formed as a greater repulsion occurs between the molecules when a large amount of AS25 present in DPPC/DP mixed system. The presence of AS25 in DPPC/DP mixed system improves the molecular packing, as compared to the molecular packing of DPPC/AS25 and DPPC/DP.

#### **4.4.3 Energetic stability of mixed monolayers**

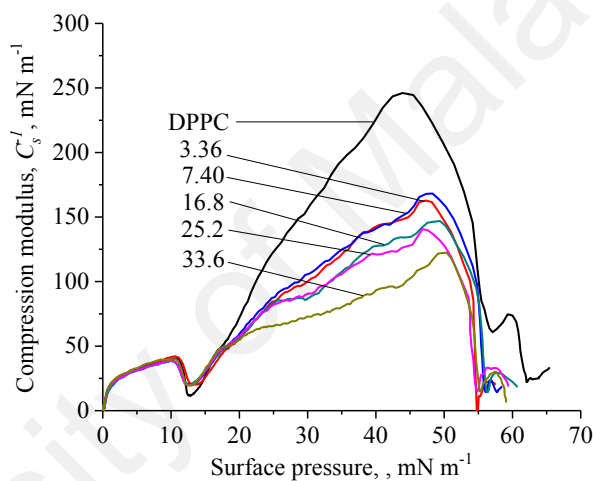
##### **4.4.3.1 Mixed monolayers of DPPC and BSA**

Non-linear plots of  $A_{ex}$  show the existence of interactions between the monolayers components at different surface pressures of 5, 10, 15, 20, 25, 30 and 35 mN m<sup>-1</sup> (Figure 4.49(a)). Negative deviations of  $A_{ex}$  from ideality predominate, and showed that the monolayer components were miscible (Figure 4.49(a)).

(a)



(b)



(c)

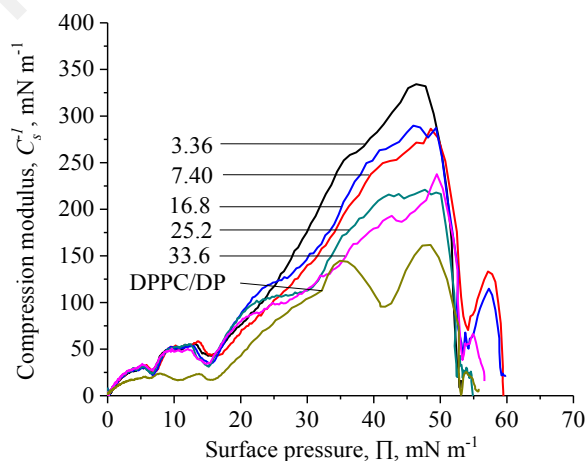


**Figure 4.48:** The compressibility modulus ( $C_s^{-1}$ ) vs surface pressure ( $\Pi$ ) of mixed monolayers of: (a) DPPC/DP (plotted in mole fraction of DPPC to DP), (b) DPPC/AS25 (mole of AS25), and (c) DPPC/DP/AS25 (plotted in nmole of AS25), spread on a nanopure water subphase at 25°C.

This observation was also supported by the negative values obtained for  $G_{mix}$  (Figure 4.49(b)), which showed that strong intermolecular attractions occurred between DPPC and BSA.

The excess mean molecular area,  $A_{ex}$  increased as the surface pressure increased. There were only slight deviations from ideality observed at surface pressures of 30 and 35  $\text{mN m}^{-1}$ , indicating immiscibility and weak interactions in a mixed monolayer. A change of slope was observed in  $C_S^{-1}$  versus  $\Pi$  profile of DPPC/BSA, corresponding to the phase transition of the mixture from S to LC phase at 20 to 25  $\text{mN m}^{-1}$  (Figure 4.47). For 25  $\text{mN m}^{-1}$  onwards, BSA may be solubilized in water subphase or sunk below the monolayer surface.

Theoretically, BSA is an integral protein known to interact strongly with lipids in the biological membrane. However, no proper collection of quantitative thermodynamic assessment of each individual phospholipids–BSA interactions can be adopted as a good reference of lipid-protein interaction. Negative values of  $G_{mix}$  were observed in the entire investigated range (except  $X_{BSA} = 0.9$  at 30 and 35  $\text{mN m}^{-1}$ ) indicated that very strong interactions between DPPC and BSA in the mixed monolayer forming stable films at their satisfactory molecular organization.  $G_{mix}$  is more negative with increasing  $X_{BSA}$ . The most negative  $G_{mix}$  value is found at  $X_{BSA} = 0.8$  at 15  $\text{mN m}^{-1}$ , this could be the most favorable interaction of the protein-enriched lipid domain.

$G_{mix}$  values are less negative in  $X_{BSA} = 0.9$  indicating repulsion is greater when large amount of BSA present in the DPPC/BSA mixtures. The presence of DPPC in the mixture will lead to a more ordered and closer molecular packing. Protein-protein interaction is favorable when they are surrounded by the lipids raft, such as mole ratio of protein to lipids at 8:2. It is a good agreement supporting the lipid raft hypothesis. Substantial amounts of lipid environment will promote the stability of protein films.

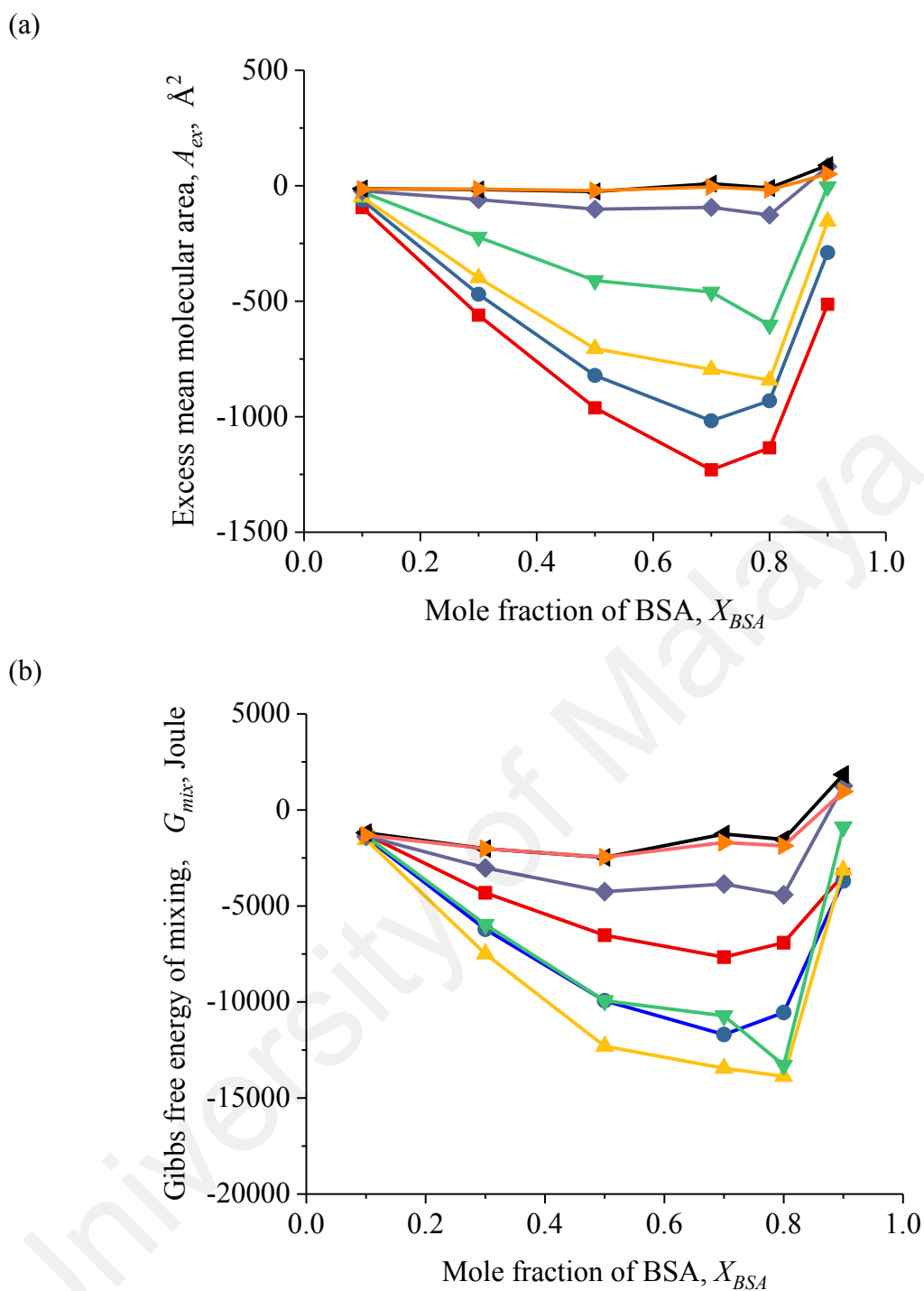


**Figure 4.49:** (a) Excess mean molecular area, and (b) Gibbs free energy of mixing of DPPC/BSA mixed monolayers vs  $X_{BSA}$  on pure water subphase at 25°C. For discrete surface pressure of  $\blacksquare = 5 \text{ mN m}^{-1}$ ,  $\bullet = 10 \text{ mN m}^{-1}$ ,  $\blacktriangle = 15 \text{ mN m}^{-1}$ ,  $\blacktriangledown = 20 \text{ mN m}^{-1}$ ,  $\blacklozenge = 25 \text{ mN m}^{-1}$ ,  $\blacktriangleleft = 30 \text{ mN m}^{-1}$  and  $\blacktriangleright = 35 \text{ mN m}^{-1}$ .

$G_{mix}$  values of DPPC/BSA (-11 kJ) is less negative than DSPC/BSA (-14 kJ) at surface pressure of  $15 \text{ mN m}^{-1}$ . DPPC and DSPC consist of same PC headgroup but different hydrocarbon chain length by 2 carbons. The intermolecular interactions of both phospholipids (DPPC and DSPC) and BSA are greatly affected by their headgroup and also the hydrocarbon chain length.

#### 4.4.3.2 Mixed monolayers of DPPC/ DP, DPPC/AS25 and DPPC/ DP/AS25

Negative deviations of  $A_{ex}$  were observed in DPPC/DP for all of their mixed systems (Figure 4.50(a)). These deviations indicated that non-ideal behavior and showed that both components in monolayer were miscible. This observation was also supported by the negative values obtained for  $G_{mix}$  (Figure 4.51(a)), which showed that strong intermolecular attractions occurred between DPPC and DP.

A slight negative deviation of  $A_{ex}$  from ideal behavior were obtained for DPPC/AS25 (Figure 4.50(b)) over most of the ranges investigated, except at the smallest mole of AS25 (3.36 nmole) introduced into the membrane. The presence of DP makes a significant change to the miscibility of DPPC and AS25. Poor miscibility between DPPC and AS25 molecules occurred without the DP being in the mixtures. A substantial negative deviation from ideal behavior was obtained for DPPC/DP/AS25 show 3 components are miscible in the ternary monolayer. The strengths of these interactions were verified based on  $G_{mix}$  (Figure 4.51(b)).

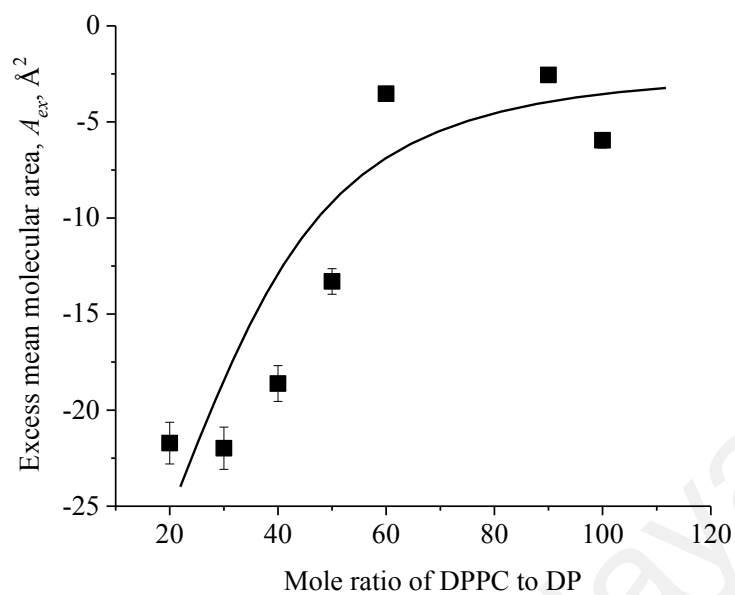
The values of  $G_{mix}$  of DPPC/DP mixtures were negative throughout the entire tested ranges of the binary systems (Figure 4.51(a)). By extrapolating the curves of DPPC/DP, we obtained 50:1 as the intersection point. This mole ratio can be used to prepare pegylated nanoliposomes, as they are thermodynamically stable at this mole composition. As the moles of DPPC increased (from 60:1 and higher),  $G_{mix}$  values were essentially constant. The *cis*-double bonds in both hydrocarbon chains of DOPE in

DP created an imperfection on the membrane structure of lipid-drug delivery systems, which is expected to enhance lipid-based systems for antibody conjugation and drug encapsulation.

As shown in Figure 4.51(b) that  $G_{mix}$  is more negative in DPPC/DP/AS25 mixed systems (with the presence of DP) compare to DPPC/AS25 without DP. AS25 molecules attract stronger in DPPC/DP mixed monolayer compare to pure DPPC monolayer. The bend and kink effect of the *cis*-double bonds of 1,2-dioleoyl-*sn*-glycero-3-phosphoethanolamide (DOPE) in DP increased the membrane fluidity, which prevented the molecules from packing tightly and uniformly. The molecules of DPPC/DP are packed loosely compared to DPPC, gives AS25 a better penetration into the phospholipid membrane. Less bend and kink effects were contributed from DPPC molecules; this could be the molecular structure of DPPC consist of two C16 saturated hydrocarbon chains. DPPC molecules are most likely packed closely, and AS25 molecules are bounded on the DPPC headgroup. As the mole of AS25 introduced into the pure DPPC monolayer increased (from 16.8 nmole onwards),  $G_{mix}$  values become slightly more negative, however, the curve exhibits an optimum of amount AS25 attracted to DPPC monolayer (Figure 4.51(b)). In the preparation of antibody-conjugated DPPC/AS25 liposomes, only a small amount of AS25 (such as 16.7 nmole of AS25) is required to avoid excessive introduction of the antibody into human body which eventually will cause an adverse effect.

However,  $G_{mix}$  values become more negative with the increasing AS25 molecules in DPPC/DP/AS25 mixed systems. The largest mole of AS25 which is 33.6 nmole incorporated into DPPC/DP monolayer exhibit the largest negative  $G_{mix}$  value.

(a)



(b)

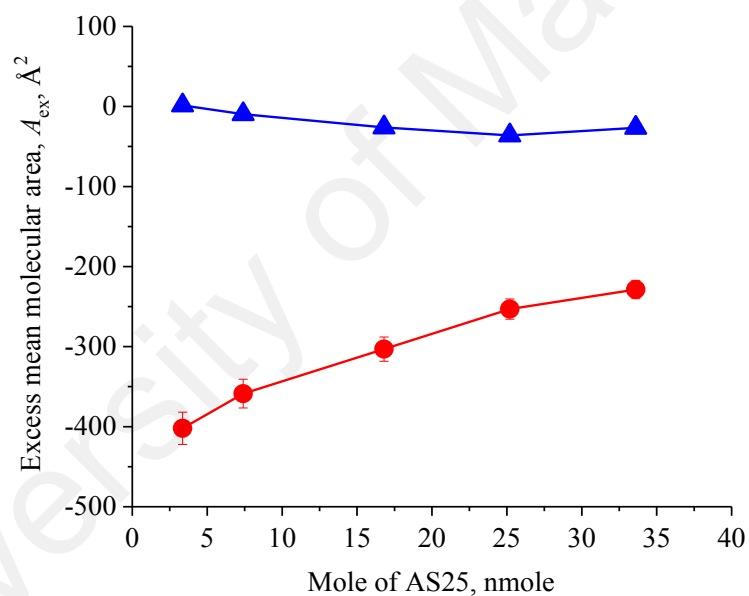
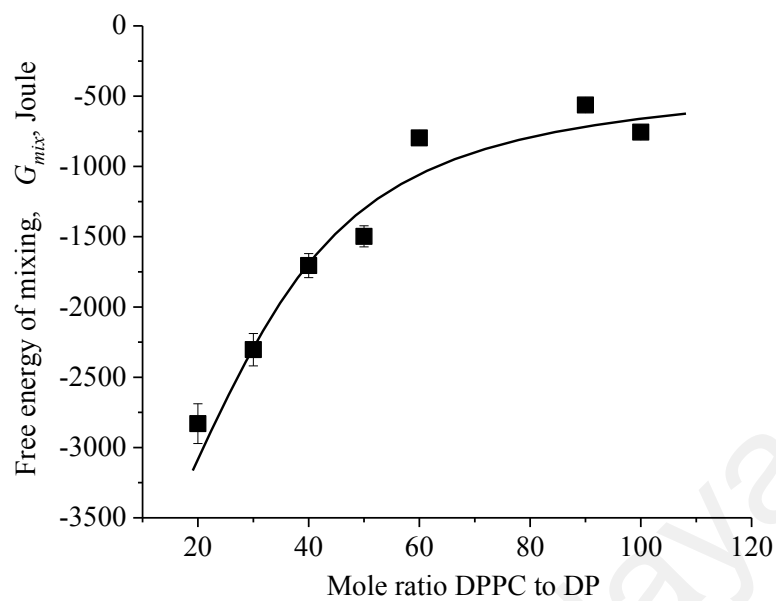


**Figure. 4.50:** Excess mean molecular area ( $A_{ex}$ ) of (a)  $\blacksquare$  = DPPC/DP (b)  $\blacktriangle$  = DPPC/AS25 (plotted in nmole of AS25), and (c)  $\bullet$  = DPPC/DP/AS25 (plotted in nmole of AS25), spread on a nanopure water subphase at 25°C.

(a)



(b)

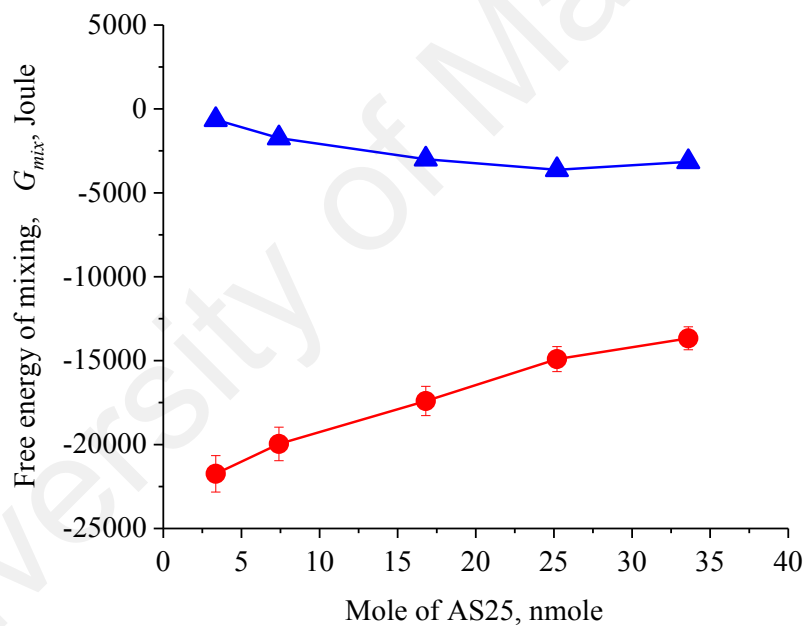


**Figure. 4.51:** Gibbs free energy of mixing ( $G_{mix}$ ) of (a)  $\blacksquare$  = DPPC/DOPE PEG2000 (plotted in mole ratio of DPPC to DP), (b)  $\blacktriangle$  = DPPC/AS25 (plotted in nmole of AS25), and  $\bullet$  = DPPC/DP/AS25 (plotted in nmole of AS25), spread on a nanopure water subphase at 25°C.

## 4.5 AFM observations

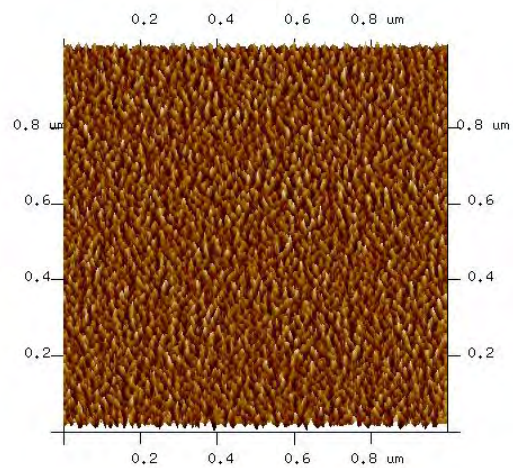
### 4.5.1 Lipid-protein interactions: Effect of degree of saturation C18 fatty acids

AFM topography provides a surface morphological insight into the surface interaction of pure C18 fatty acids (Figure 4.52), pure DP (Figure 4.53), mixed systems of C18 fatty acids/DP (Figure 4.54), pure BSA (Figure 4.56), mixed systems of C18 fatty acids/BSA (Figure 4.57), pure AS25 (Figure 4.58) the, mixed systems of C18 fatty acids/AS25 (Figure 4.59) and C18 fatty acids/DP/AS25 (Figure 4.60). AFM surface roughness measurements of pure C18 fatty acids, DP, BSA, AS25 and their mixtures studied are tabulated in Table 4.1 to support the LB quantitative analysis.

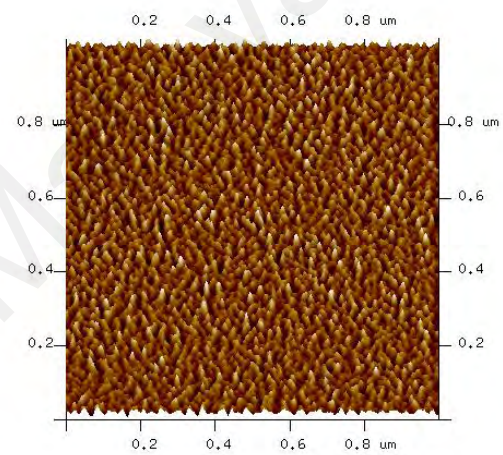
#### 4.5.1.1 Pure monolayers of SA, L1, L2, and L3

Similar surface images were obtained for C18 fatty acids as they have the same carboxyl headgroup (Figure 4.52). The values of  $R_a$  and  $R_q$  of pure C18 fatty acids increase with the increasing degree of saturation of C18 fatty acids (Table 4.1). Deposition of SA onto the solid substrate was carried out at surface pressure of  $45 \text{ mN m}^{-1}$  (solid phase), and unsaturated C18 fatty acids were performed at liquid phase due to the present of *cis*-double bond(s) in their respective chemical structures. These values are relatively low as compared to all the mixed systems that containing C18 fatty acids.  $R_q$  increases by about 0.1 to the respective  $R_a$  values, presumably, the surface of pure C18 fatty acids are comparatively flat.  $R_a$  and  $R_q$  values of pure C18 fatty acids system serve as a reference or comparison to their respective mixed systems.

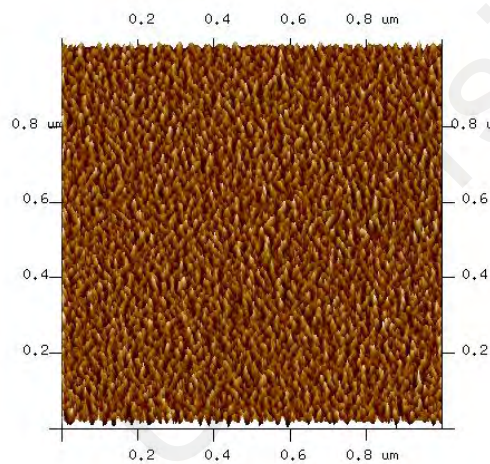
(a)



(b)



(c)



(d)

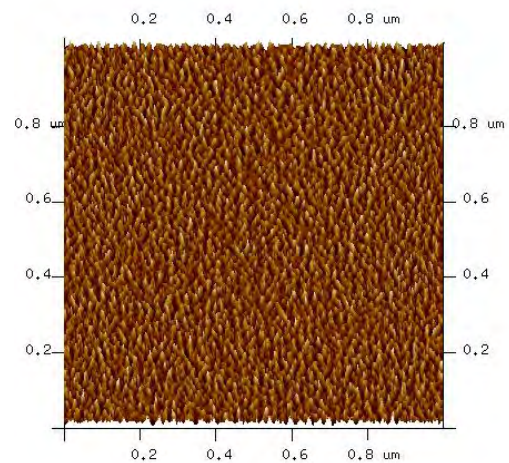


**Figure 4.52:** AFM images of pure C18 fatty-acids bilayer deposited on oxidized silicon wafer at scan size of  $1 \mu\text{m} \times 1 \mu\text{m}$  with a data scale of 25 nm for: (a) stearic acid, (b) oleic acid, (c) linoleic acid, and (d) linolenic acid.

#### 4.5.1.2 Mixed monolayers of C18 fatty acids and DP

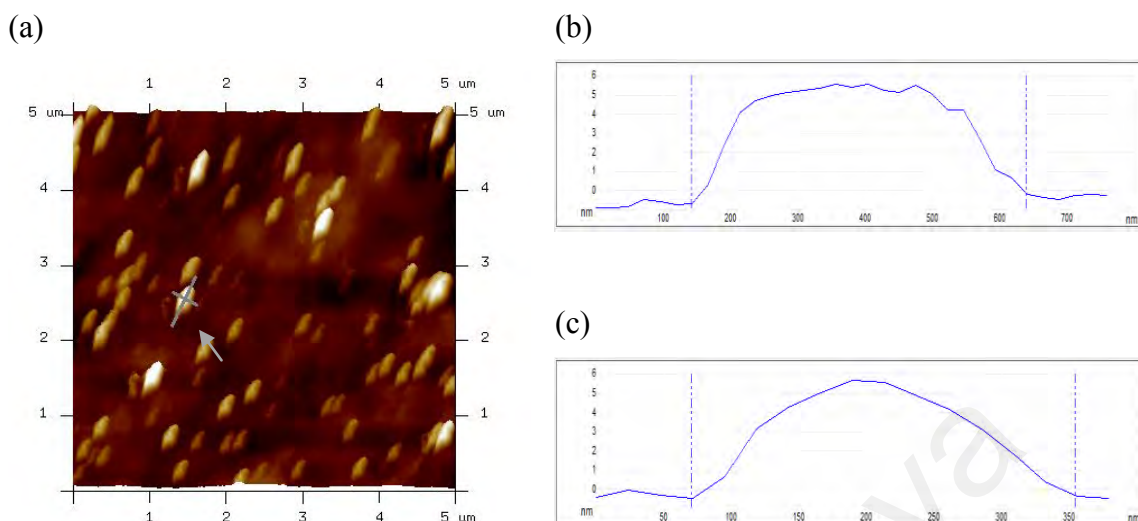


**Figure 4.53:** AFM images of pure DOPE PEG2000 bilayer deposited on oxidized silicon wafer obtained in scan size of (a) 5 μm × 5 μm with a data scale of 25 nm. A cross section was drawn on a selected DP molecule incorporated on the membrane depicted in (a) to obtain more information of the height and width of AS25 molecule. The height and width of this PEG were found to be approximately 500 nm × 286 nm, respectively as shown in (b) and (c).

The difference between  $R_a$  to the respective  $R_q$  of the mixed systems of C18 fatty acid/DP (about 0.15 to 0.2) is slightly bigger than the relatively flat pure surface of C18 fatty acids (about 0.1). While  $R_a$  and  $R_q$  values of DP is much higher owing to its large headgroup, and the difference between its  $R_a$  and  $R_q$  is 0.35 as more valley and peak is distributed on the surface morphology of pure DP. This could be the big PEG headgroups of DP span on the solid substrate as observed in Figure 4.54(a). The deposition was performed at liquid-expanded phase (due to the nature of DP chemical structure); hence, the monolayer of DP was less compressible and disordered as illustrated in Figure 4.54(b). A lot of identical spots are randomly distributed on the surface morphology of mixed systems of C18 fatty acids/DP (Figure 4.54), presumably, those spots are the PEG headgroups of DP. The molecules are arranged in a better manner as the monolayer was transferred from the water subphase onto solid substrate at LC phase.

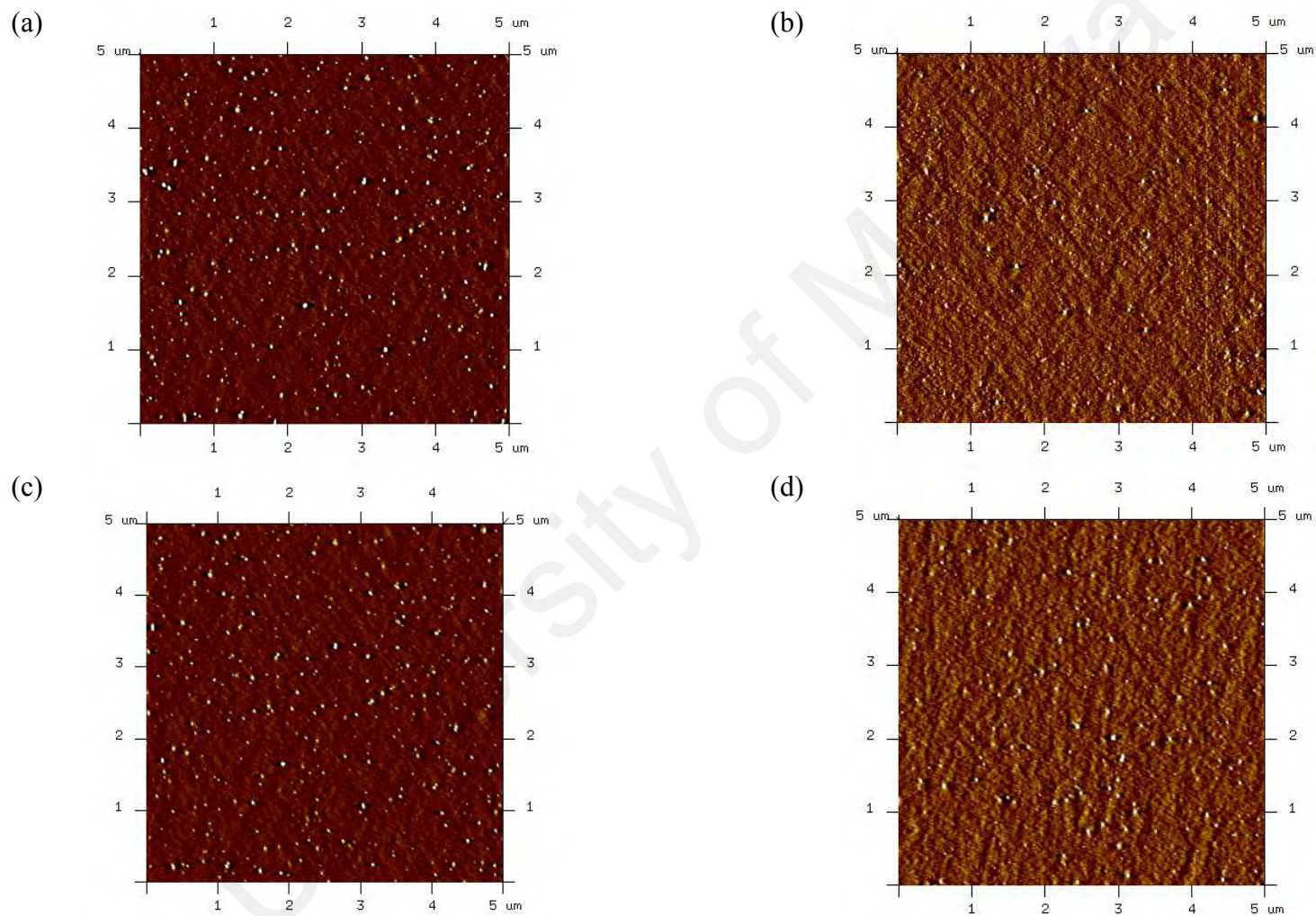


**Figure 4.54:** AFM images of mixed monolayers of C18 fatty acids/DP (mole ratio of 50:1) bilayer deposited on oxidized silicon wafer obtained in a 5.0 μm × 5.0 μm scan area with a data scale of 25 nm for: (a) stearic acid/DP, (b) oleic acid/DP, (c) linoleic acid/DP, and (d) linolenic acid/DP.

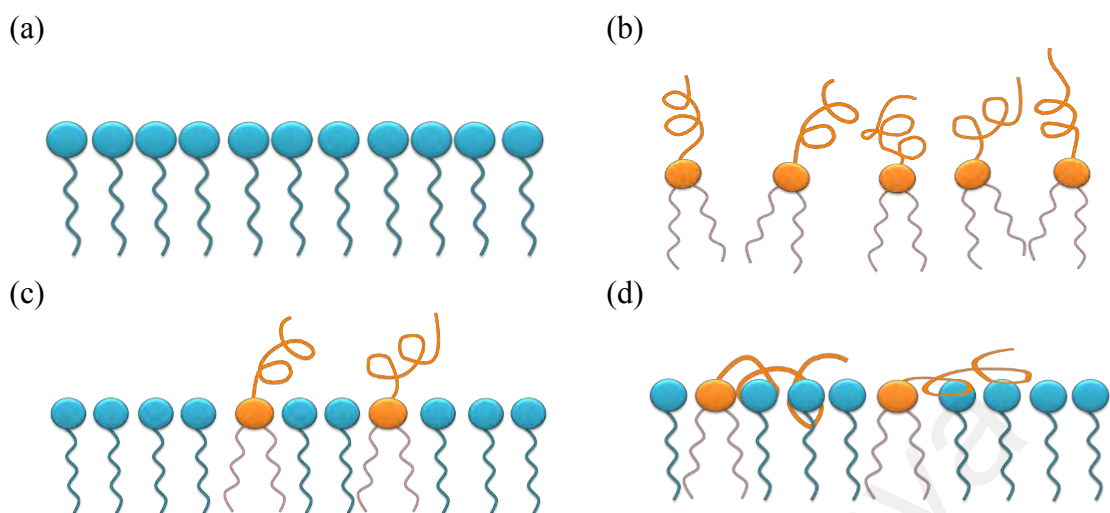


**Figure 4.55:** A cartoon illustration of surface topography to describe the surface roughness values,  $R_a$  and  $R_q$  in Table 4.1. (a) A flat surface of pure C18 fatty acids, owing to the identical of carboxyl head-groups of fatty acid; (b) pure DP, that PEG head-groups tend to fold on itself; (c) saturated C18 fatty acid (SA/DP), the present of PEG head-group on SA bilayer membrane creating the *globular*-like structure on the membrane surface; and (d) unsaturated C18 fatty acids (L3/DP), the polar PEG head-groups cloak around L3 polar carboxyl head-group in the membrane.

For SA (a saturated C18 fatty acid),  $R_a$  value changes dramatically from 0.215 (pure SA) to 0.602 nm (mixed system of SA/DP), on the other hand, there is a slight change of  $R_a$  value of unsaturated C18 fatty acid (such as L3) is observed, which from 0.460 (pure L3) to 0.556 nm (L3/DP). This observation is due to the PEG headgroup of DP is creating a *globular*-like structure on the saturated SA membrane surface (as illustrated in Figure 4.55(c)) after mixed, causing an increase of  $R_a$  value as the pure SA surface is relatively flat as mentioned earlier. As for L3 membrane, the unsaturation induces greater penetration of PEG headgroup into the bilayer membrane. The polar PEG head-groups cloak around L3 polar carboxyl head-group in the membrane, therefore only a slight change of  $R_a$  is observed (Figure 4.55(d)).  $R_a$  and  $R_q$  values of SA/DP are slightly bigger than the unsaturated fatty acids. The differences between  $R_a$  and  $R_q$  values are about 0.15 to 0.2, these values support our energetic studies, as negative  $G_{mix}$  values were obtained at mole ratio of 50:1 for all C18 fatty acid/DP

mixtures. The intermolecular interaction of DP with respective C18 fatty acid in the membrane is not greatly affected by the degree of saturation.

#### 4.5.1.3 Mixed monolayers of C18 fatty acids and BSA

Globular BSA molecules spread evenly on the solid substrate, give a smooth spongy-surface look on the AFM surface morphology of BSA (Figure 4.56). Smooth surface will not significantly affect  $R_q$  value. The different between  $R_a$  and  $R_q$  values of BSA is by 0.1 (Table 4.1).

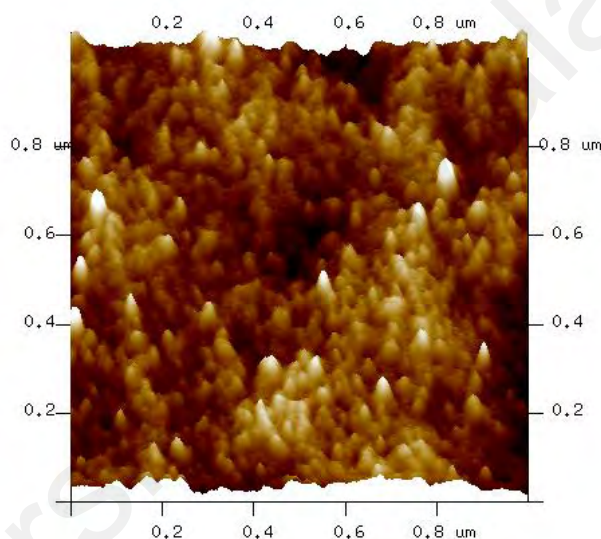


**Figure 4.56:** AFM images of pure BSA bilayer deposited on oxidized silicon wafer obtained in a  $1.0 \mu\text{m} \times 1.0 \mu\text{m}$  scan area with a data scale of 25 nm.

Both  $R_a$  and  $R_q$  values of C18 fatty acids/BSA is slightly larger than their respective pure monolayer.  $R_a$  and  $R_q$  values become larger as degree of saturations increases. The difference between  $R_a$  and  $R_q$  is smaller for saturated SA (less than 0.1) as compare to the unsaturated fatty acids (about 0.1 to 0.15). Less peaks and valleys are observed in surface morphology of C18 fatty acids/BSA (Figure 4.57).

Lipids may cause a change in protein conformation; hydrophobic surfaces of the membrane protein will penetrate into the hydrophobic interior of the membrane lipid bilayer.

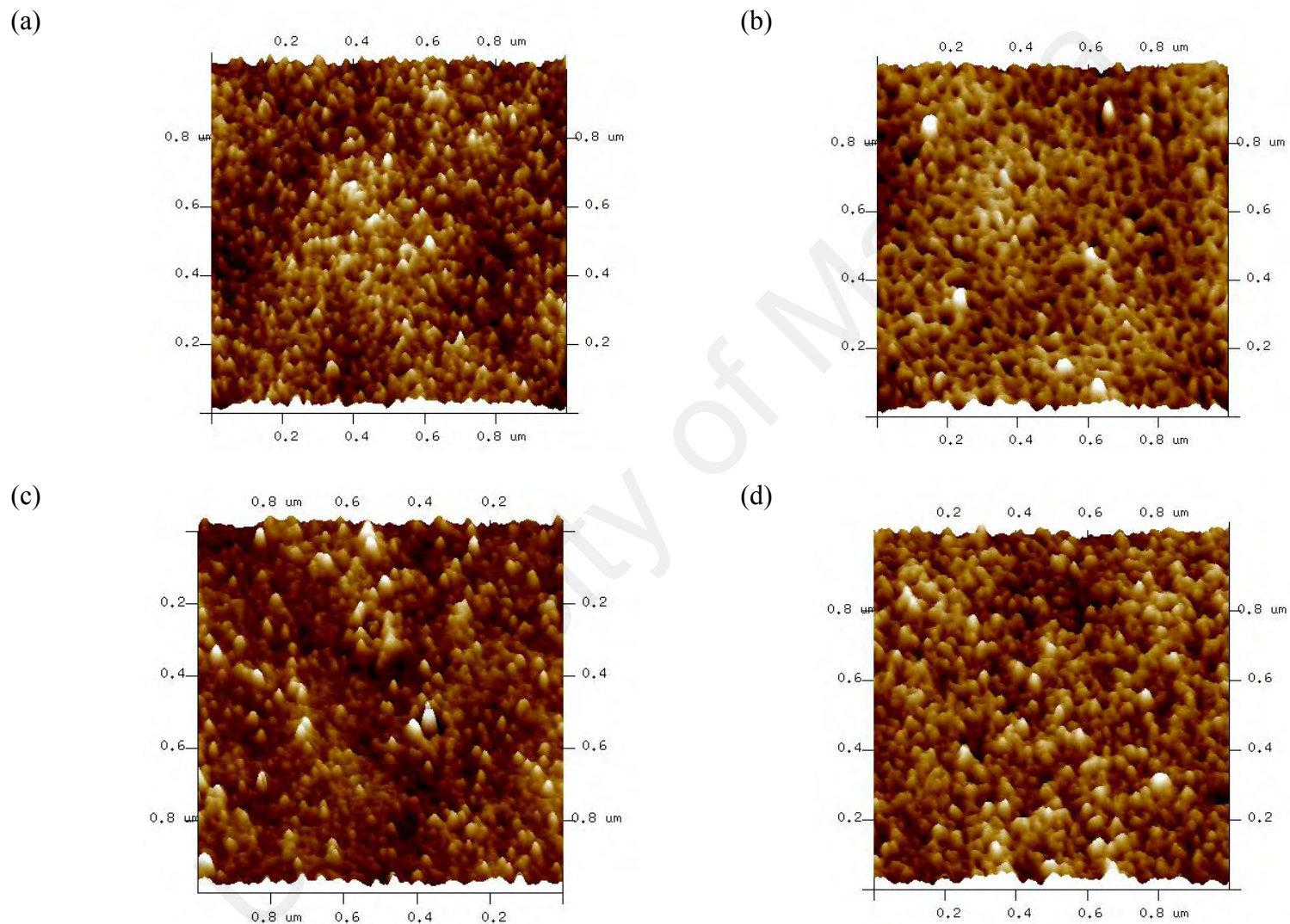


**Figure 4.57:** AFM images of C18 fatty acids/BSA bilayer deposited on oxidized silicon wafer obtained in a  $1 \mu\text{m} \times 1 \mu\text{m}$  scan area with a data scale of 25 nm for: (a) SA/BSA, (b) L1/BSA, (c) L2/BSA, and (d) L3/BSA.

When the integral protein BSA span on in a lipid bilayer, it alters its conformation to better accommodate the hydrophobic portion of the bilayer. There is also a possibility for the lipid bilayer may be distorted to cover the hydrophobic surface on the transmembrane protein. Binding of these lipids can induce changes in membrane protein conformation and consequently changes in membrane function. Integral protein BSA molecules bury into the respective bilayer of C18 fatty acids; however, AS25 is a membrane-bound protein will bound on the surface of C18 fatty acids membrane.  $R_a$  and  $R_q$  values of C18 fatty acids/BSA is slightly lower than C18 fatty acids/AS25, except L3. The differences of  $R_a$  and  $R_q$  values in L3/BSA and L3/AS25 mixed systems are very small. This could be the three *cis*-double bonds in its hydrocarbon chain of L3 caused a loosely packed configuration of L3 membrane and allowed AS25 molecules to be incorporated in between the carboxyl headgroup of L3.

#### 4.5.1.4 Mixed monolayers of C18 fatty acids and AS25

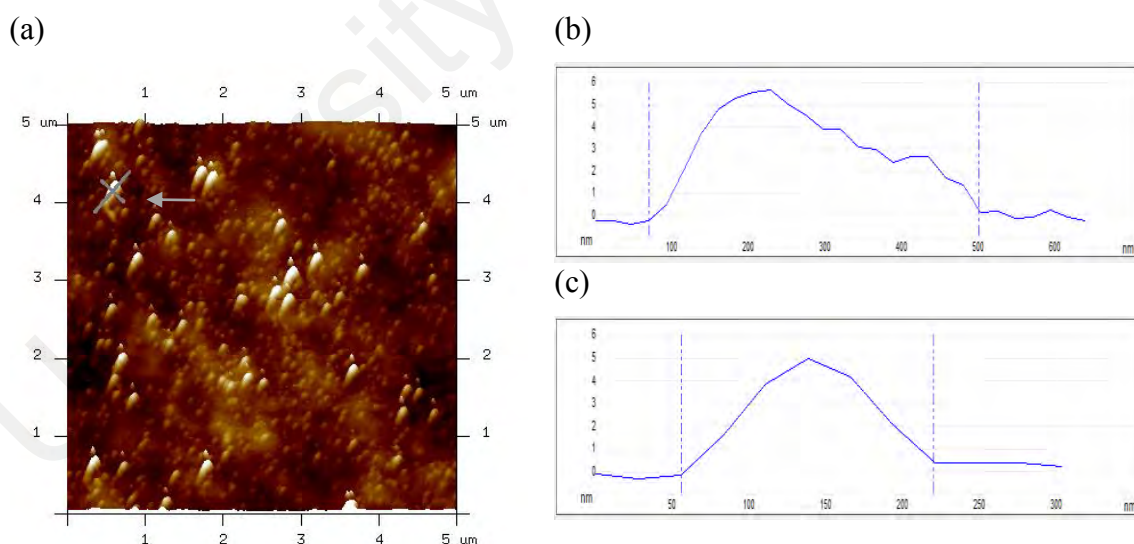


**Figure 4.58:** AFM images of pure Anti-SNAP25 bilayer deposited on oxidized silicon wafer obtained in scan size of (a)  $5 \mu\text{m} \times 5 \mu\text{m}$  with a data scale of 25 nm. A cross section was drawn on a selected AS25 molecule incorporated on the membrane depicted in (a) to obtain more information of the height and width of AS25 molecule. The height (b) and width (c) of this membrane bound protein were found to be  $453 \text{ nm} \times 166 \text{ nm}$ , respectively. Protein structure predictions of AS25 from its protein sequences that it is a coiled-coil structure as illustrated in Figure 4.30 [29], and our scanned images as above showed the shape of AS25 is true as predicted.

Both parameters  $R_a$  and  $R_q$  decrease with the increasing double bonds in their hydrocarbon chains in the mixed systems of C18 fatty acid/AS25. The degree of saturations induces greater penetration of AS25 on the lipid bilayers. In the pure system of SA (a saturated fatty acid) and mixed system of SA/AS25,  $R_a$  values increase dramatically from 0.215 to 0.721 nm. On the contrary, only a slight increase of  $R_a$  is observed for L3 (unsaturated fatty acid) and L3/AS225, which is from 0.460 to 0.493 nm.

More peaks and valleys are observed in the mixed systems of C18 fatty acids/AS25 (Figure 4.59),  $R_q$  is found to be much larger than  $R_a$ , as  $R_q$  values will be significantly affected (more than  $R_a$ ) when the surface contains a large number of peaks and valleys in the mixtures, owing to the squaring of the amplitude in the calculation. The values of  $R_a$  and  $R_q$  of mixed systems of C18 fatty acids/AS25 are greatly affected by the degree of saturation of C18 fatty acids. The differences between  $R_a$  and  $R_q$  value of saturated SA/AS25 is 0.28 (as  $R_a$  is 0.721 and  $R_q$  is 1.010), while unsaturated L1/AS25, L2/AS25 and L3/AS25 are only different by about 0.15. This could be more peaks and valleys appeared on the surface of SA/AS25 as more AS25 molecules were bounded on the saturated SA membrane surface.  $R_q$  of SA/AS25 is found to be larger than AS25; this shows more AS25 molecules are bounded on the surface as a result from the tightly packed of saturated SA bilayer. The energetic studies,  $G_{mix}$  of all mixed systems are not remarkably affected by the degree of saturation of C18 fatty acids' hydrocarbon chain. However, AFM surface roughness analysis support the hypothesis on how the membrane-bound AS25 antibody interacts with C18 fatty acids with different degree of saturation. In the mixed systems of unsaturated L1/AS25, L2/AS25 and L3/AS25, the *cis*-double bond(s) prevent the tight and rigid molecular packing enable AS25 molecules partially embedded into the bilayer membrane as

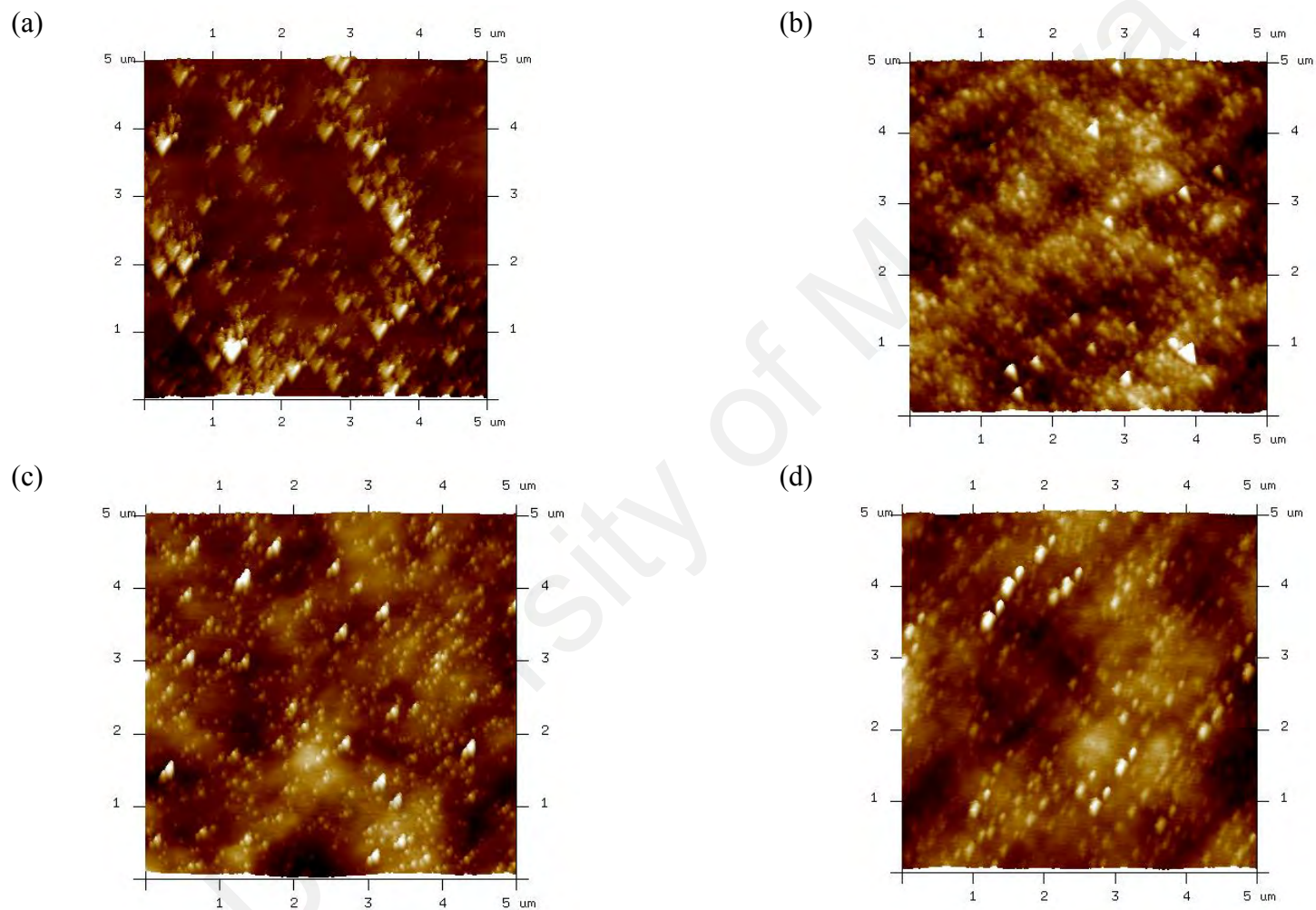


**Figure 4.59:** AFM images of binary mixture of C18 fatty acids/AS25 bilayer deposited on oxidized silicon wafer obtained in a  $5.0\ \mu\text{m} \times 5.0\ \mu\text{m}$  scan area with a data scale of 25 nm for: (a) SA/AS25, (b) L1/AS25, (c) L2/AS25, and (d) L3/AS25.

illustrated in Figure 4.58. Thus, less peaks and valleys are observed as we compare them to SA/AS25 mixed system. In conclusion, AS25 molecules are bounded on saturated SA's carboxyl headgroup, but partially inserted into unsaturated C18 fatty acids membrane.

#### 4.5.1.5 C18 fatty acids, DP and AS25 mixed monolayers

The incorporation of DP into C18 fatty acids membrane increases the membrane fluidity as the great repulsion occurred between unsaturated DOPE hydrocarbon chains of DP and C18 fatty acids' hydrocarbon chain varying degree of saturation due to the bent and kink of the molecular structure and higher cohesive energy, prevent the closely packed molecules. The large PEG headgroup of DP also contributes certain amount of repulsion in the mixtures. Molecular compositions of lipid membrane will affect the membrane fluidity. Mixtures of C18 fatty acids/DP increase the membrane fluidity and make the conjugation of antibody AS25 to the imperfect membrane become easier. AS25 molecules are distributed in between the C18 fatty acids and DP molecules. A combination of tiny dots and coiled-coil like structures were observed in Figure 4.59.

The presence of DP in SA/AS25 mixtures have lower surface roughness values, their  $R_a$  and  $R_q$  values are 0.455 and 0.664 respectively, as compared to mixtures of SA/AS25 without DP (Figure 4.60(a)).  $G_{mix}$  values of SA/DP/AS25 were found to be more negative than the unsaturated C18 fatty acids/DP/AS25. AS25 molecules may tend to embedded on SA bilayer surface as pure SA monolayer formed solid phase easily. The presence of DP increases the fluidity of SA bilayer that may cause AS25 molecules embedded in between the PEG headgroup of DP, hence, give a lower surface roughness values. The  $R_a$  and  $R_q$  values of L1/DP/AS25 (which are 0.677 and 0.936, respectively) and L2/DP/AS25 (which are 0.730 and 0.998, respectively) are larger than their respective mixtures with DP and AS25 (Table 4.1). More peaks and valleys are being

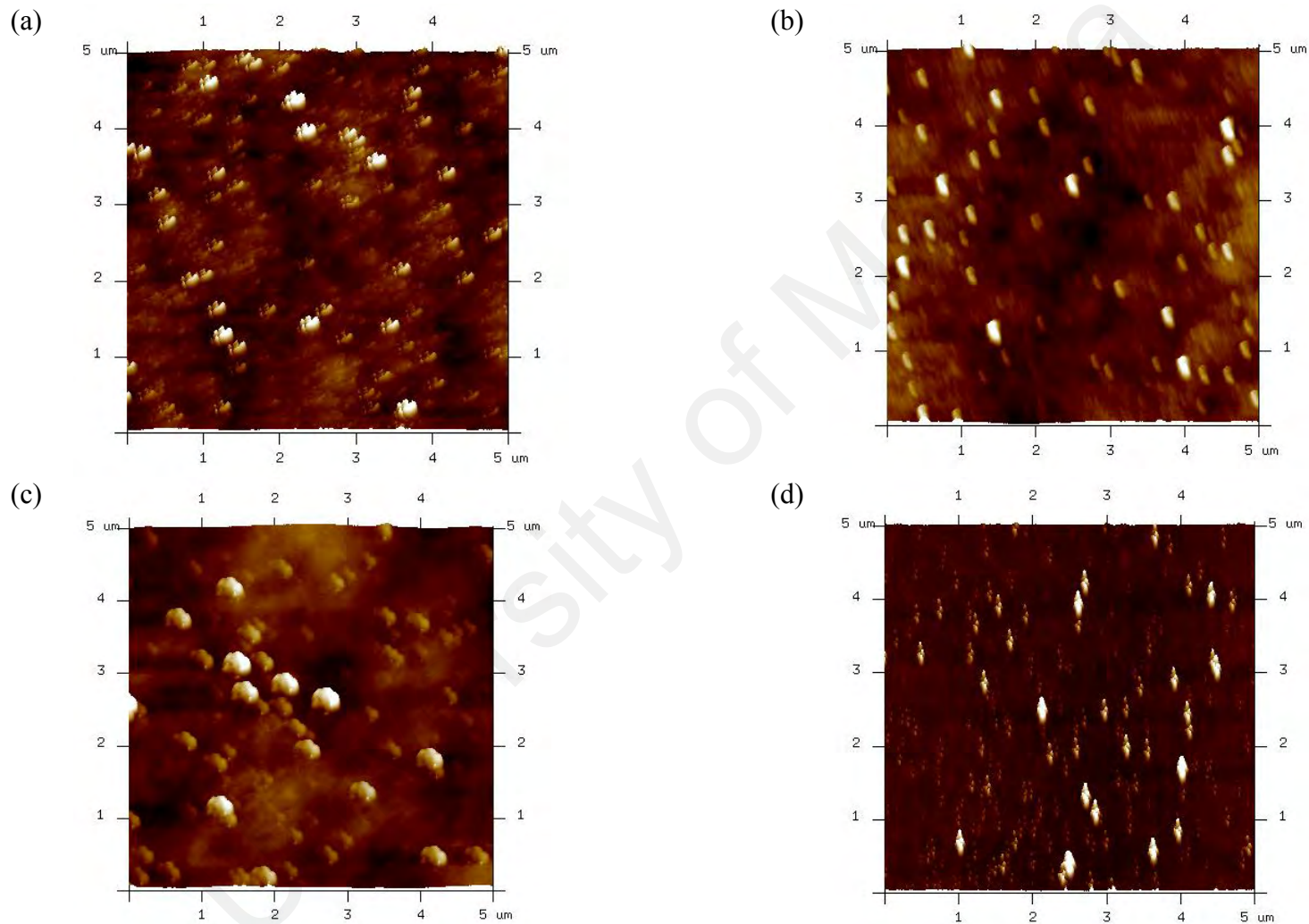


**Figure 4.60:** AFM images of binary mixture of C18 fatty acids/DP/AS25 bilayer deposited on oxidized silicon wafer obtained in a  $5.0 \mu\text{m} \times 5.0 \mu\text{m}$  scan area with a data scale of 25 nm for: (a) SA/DP/AS25, (b) L1/DP/AS25, (c) L2/DP/AS25, and (d) L3/DP/AS25.

**Table 4.1:** Surface roughness,  $R_a$  of pure C18 fatty acids, DP, BSA, AS25, binary systems of C18 fatty acids/BSA, C18 fatty acids/DP, C18 fatty acids/AS25 and ternary systems of C18 fatty acids/DP/AS25 (obtained using NanoScope Analysis 1.5)

Pure systems	Surface roughness, nm		Mixed systems	Surface roughness, nm										
	$R_a$	$R_q$		$R_a$	$R_q$		$R_a$	$R_q$		$R_a$	$R_q$		$R_a$	$R_q$
SA	0.215	0.286	SA/DP	0.602	0.806	SA/BSA	0.367	0.465	SA/AS25	0.721	1.010	SA/DP/AS25	0.455	0.664
L1	0.249	0.303	L1/DP	0.594	0.746	L1/BSA	0.397	0.515	L1/AS25	0.543	0.701	L1//DP/AS25	0.677	0.936
L2	0.282	0.578	L2/DP	0.583	0.783	L2/BSA	0.456	0.609	L2/AS25	0.528	0.584	L2/DP/AS25	0.730	0.998
L3	0.460	0.575	L3/DP	0.556	0.708	L3/BSA	0.520	0.657	L3/AS25	0.493	0.630	L3/DP/AS25	0.192	0.372
DP	0.818	1.170												
BSA	0.356	0.456												
AS25	0.566	0.789												

seen in Figure 4.60(b) and (c). L3/DP/AS25mixture has the lowest  $R_a$  and  $R_q$  values, which are 0.192 and 0.372. Less AS25 molecules were embedded on the surface of L3/DP as can be seen in Figure 4.60(d).

#### **4.5.2 Lipid-protein interactions: Effect of headgroup**

AFM topography provides a surface morphological insight into the surface interaction of pure SS, DSPC and DSPG (Figure 4.61), mixed systems of SS/BSA, DSPC/BSA and DSPG/BSA (Figure 4.62), and SS/AS25, DSPC/AS25 and DSPG/AS25 (Figure 4.63), AFM surface roughness measurements of pure phospholipids and their mixtures studied are presented in Table 4.2 to support LB quantitative analysis and also to prove the hypothesis.

$R_a$  and  $R_q$  values of phospholipids that are under studied (Table 4.2) are larger than SA with the smallest carboxyl headgroup.  $R_q$  values of SS, DSPC and DSPG (which are 0.249, 0.282, and 0.460) are larger than their respective  $R_a$  (which are 0.604, 0.644, and 0.624).  $R_q$  is found to be much larger than  $R_a$ , as  $R_q$  values will be significantly affected (more than  $R_a$ ) when the surface contains a large number of peaks and valleys in the mixtures, owing to the squaring of the amplitude in the calculation. Their values of  $R_q$  showed an agreement with their topography in Figure 4.61, where many small spots were observed on the SS, DSPC and DSPG surface topography, plausibly; those are the headgroups of SS, DSPC and DSPG, respectively.

##### **4.5.2.1 Mixed monolayers of SS, DSPC, DSPG and proteins (BSA and AS25)**

Lipid protein interactions can be observed by comparing their intermolecular interaction with integral protein BSA and membrane-bound protein AS25. Surface roughness measurements of phospholipids/AS25 mixtures are larger than phospholipids/BSA. The differences of  $R_a$  and  $R_q$  values of phospholipids/AS25 mixtures is also found to be

larger than phospholipids/BSA mixed systems. Globular protein BSA penetrated into the nonpolar region of phospholipid bilayer (Figure 4.62) and produced a spongy surface. In contrast,

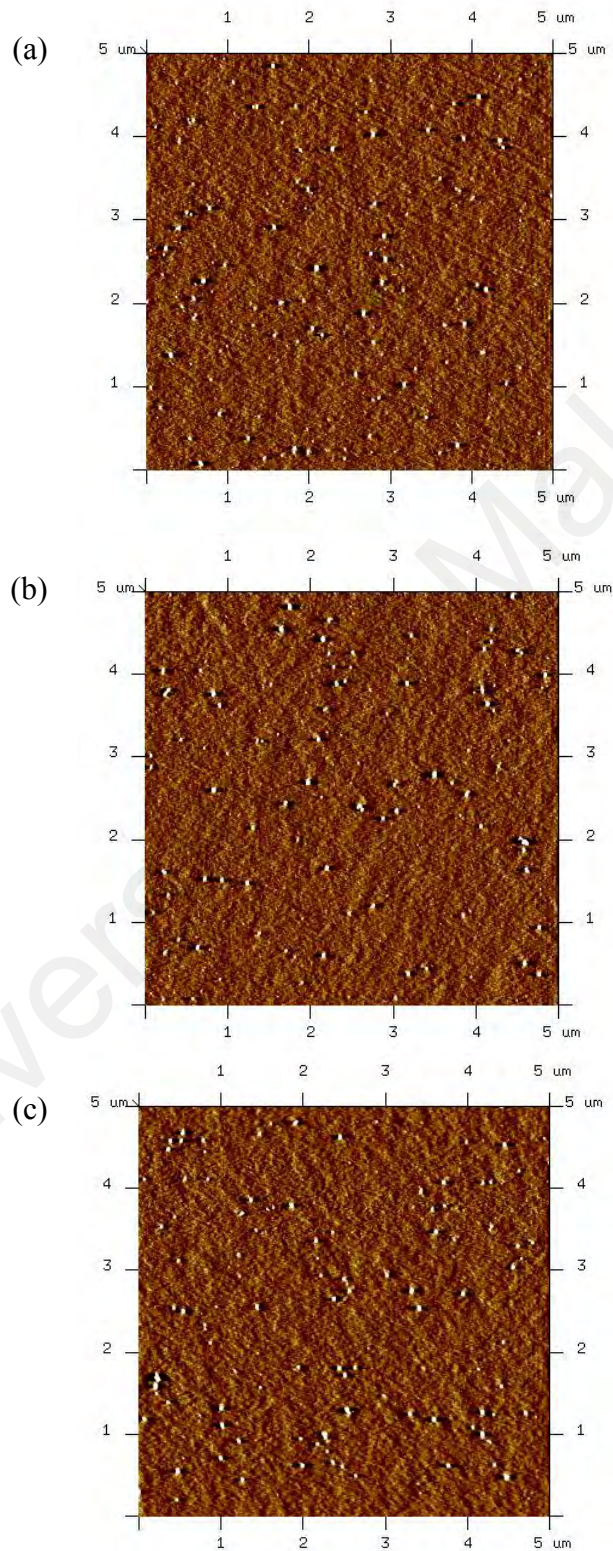


**Figure 4.61:** AFM images of binary mixture of (a) SS, (b) DSPC, and (c) DSPG bilayer deposited on oxidized silicon wafer obtained in a  $5.0 \mu\text{m} \times 5.0 \mu\text{m}$  scan area with a data scale of 25 nm.

AS25 molecules were embedded on the surface of phospholipids monolayer, caused more peaks and valleys forming on the solid substrate (Figure 4.63).

The surface roughness measurements of DSPG/BSA and DSPC/BSA is much higher than SS/BSA. At  $X_{BSA}$  is 0.5 (where the deposition of mixtures were carried out), negatives  $G_{mix}$  values of DSPG/BSA > SS/BSA > DSPC/BSA. However, AFM surface roughness measurements of  $R_a$  and  $R_q$  in Table 4.2 do not show the similar trend as their respective  $G_{mix}$  values. More BSA are appeared on the surface of DSPG and DSPC as compare to SS bilayer, BSA is more spread out and all over on the substrate (Figure 4.62).  $R_a$  and  $R_q$  values of SS are found to be 0.561 and 0.713 respective which were smaller than DSPC/BSA and DSPG/BSA, but larger than SA/BSA. In Figure 4.62, more peak and valleys are observed in DSPC/BSA and DSPG/BSA. The presence of sucrose headgroup in SS may increase the preferential of binding of BSA to the phospholipid bilayer.  $R_a$  and  $R_q$  values of DSPC/BSA are 0.951 and 1.190, and as for DSPG/BSA are 0.994 and 1.300, respectively.

The binding of AS25 is greatly influenced by the headgroup of phospholipids, as shown in  $G_{mix}$  values of SS/AS25 and DSPG/AS25, which were more negative than DSPC/AS25. The sucrose headgroup of SS is more polar than glycerol headgroup of DSPG, choline headgroup is the least polar as compare to SS and DSPG and as well as carboxyl headgroup of SA. AFM surface roughness analyses support LB thermodynamics quantitative data,  $R_a$  and  $R_q$  values of SS/AS25 (which were 0.715 and 1.000) was close to DSPG/AS25 (0.666 and 0.871), but lower than DSPC/AS25 (Table 4.2). More AS25 molecules were found on the surface morphology of SS/AS25 and DSPG/AS25 as compare to DSPC/AS25 (Figure 4.63).

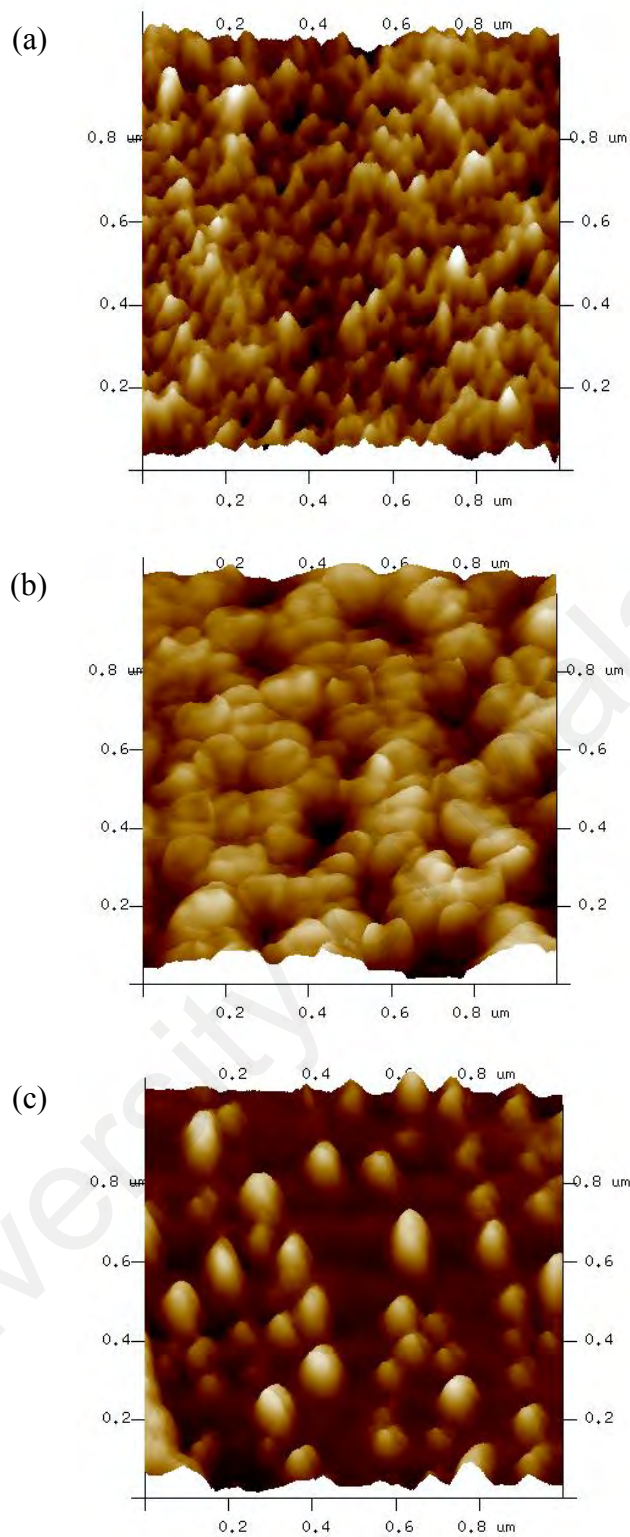


**Figure 4.62:** AFM images of binary mixture of (a) SS/BSA, (b) DSPC/BSA, and (c) DSPG/BSA bilayer deposited on oxidized silicon wafer obtained in a  $5.0 \mu\text{m} \times 5.0 \mu\text{m}$  scan area with a data scale of 25 nm.

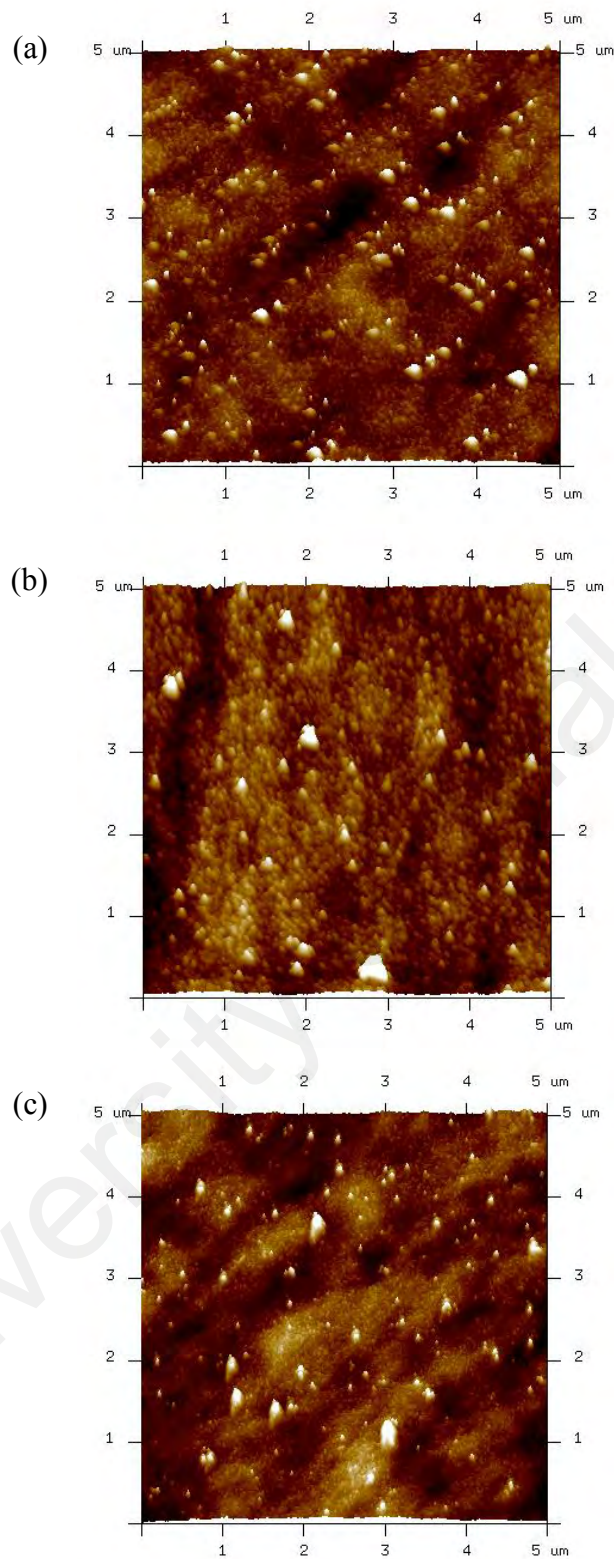


**Figure 4.63:** AFM images of binary mixture of (a) SS/AS25, (b) DSPC/AS25, and (c) DSPG/AS25 bilayer deposited on oxidized silicon wafer obtained in a  $5.0 \mu\text{m} \times 5.0 \mu\text{m}$  scan area with a data scale of 25 nm.

**Table 4.2:** Surface roughness,  $R_a$  of pure phospholipids, AS25, BSA, mixed systems of phospholipids/AS25 and phospholipids/BSA (obtained using NanoScope Analysis 1.5).

Pure systems	Surface roughness, nm		Mixed systems	Surface roughness, nm		Mixed systems	Surface roughness, nm	
	$R_a$	$R_q$		$R_a$	$R_q$		$R_a$	$R_q$
SA	0.215	0.286	SA/BSA	0.367	0.465	SA/AS25	0.721	1.010
SS	0.249	0.604	SS/BSA	0.561	0.713	SS/AS25	0.715	1.000
DSPC	0.282	0.644	DSPC/BSA	0.951	1.190	DSPC/AS25	0.834	1.190
DSPG	0.460	0.624	DSPG/BSA	0.994	1.300	DSPG/AS25	0.666	0.871
BSA	0.356	0.789						
AS25	0.566	0.456						

### 4.5.3 Lipid-protein interactions: DPPC

AFM topography provides a surface morphological insight into the surface interaction of pure DPPC (Figure 4.64(a)), mixed systems of DPPC/DP (Figure 4.64(b)), mixed systems of DPPC/ BSA (Figure 4.65), mixed systems of DPPC/AS25 (Figure 4.66(a)) and DPPC/DP/AS25 (Figure 4.66(b)). AFM surface roughness measurements of pure DPPC and their mixtures studied are tabulated in Table 4.3.

Many small spots were observed on AFM image of DPPC (Figure 4.64(a)); presumably, those are the headgroups of DPPC. DPPC surface morphology has a moderate number of peaks and valley that caused  $R_a$  and  $R_q$  different by  $\pm 0.2$  (Table 4.3). However, less spots were found in AFM image of DPPC/DP as compared to DPPC, hence  $R_a$  and  $R_q$  different by  $\pm 0.14$ . This could be great repulsion occurs between the headgroups of DP and DPPC that make them far apart from each other.

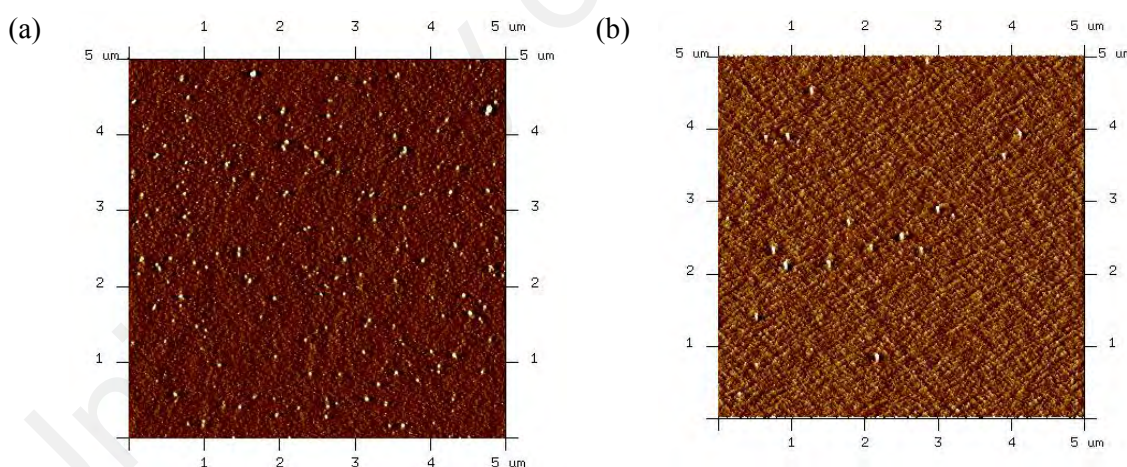


**Figure 4.64:** AFM images of (a) DPPC, (b) DPPC/DOPE PEG2000 bilayer deposited on oxidized silicon wafer obtained in a  $5.0 \mu\text{m} \times 5.0 \mu\text{m}$  scan area with a data scale of 25 nm.

#### 4.5.3.1 Mixed monolayers of DPPC and proteins (BSA and AS25)

The presence of BSA or AS25 in DPPC greatly increases the both  $R_a$  and  $R_q$  values as compared to the pure DPPC, the lipid-protein interaction can be noted as DPPC/AS25

DPPC/BSA (Table 4.3). Integral protein BSA molecules are embedded into the hydrophobic region of DPPC bilayer membrane, which makes its  $R_a$  and  $R_q$  values (0.817 and 1.020 respectively) which is slightly smaller than DPPC/AS25. In contrary, peripheral protein AS25 bounded on the surface of DPPC membrane that gives rise to  $R_a$  and  $R_q$  values (0.967 and 1.320, respectively). The difference between  $R_a$  and  $R_q$  values of DPPC/AS25 (0.44) also found to be much larger than DPPC/BSA (0.20). More bumps are found on DPPC/AS25 surface morphology as compared to smoother spongy-like surface morphology of DPPC/BSA (Figure 4.65 and 4.66). Similar observation can be seen in C18 fatty acids. The incorporation of DP into DPPC/AS25 mixtures reduces both  $R_a$  and  $R_q$  as compare to DPPC/AS25 mixed system without DP, a similar observation is observed in C18 fatty acids too.

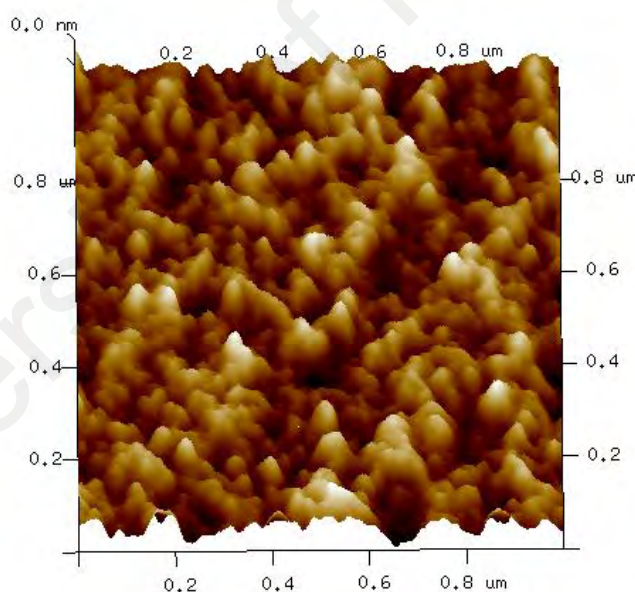


**Fig. 4.65:** AFM images of binary mixture of DPPC/BSA bilayer deposited on oxidized silicon wafer obtained in a  $1.0 \mu\text{m} \times 1.0 \mu\text{m}$  scan area with a data scale of 25 nm.

Phospholipids of DPPC and DSPC have the same polar choline headgroup, but different hydrocarbon chains length. Carbon-18 DSPC has additional two carbons on both their hydrocarbon tails as compare to carbon-16 DPPC. When both phospholipids mixed with integral protein BSA, both surface roughness measurements of DPPC/BSA

is found to be slightly lower than DSPC/BSA, presumably more hydrophobic region of BSA were embedded into the nonpolar bilayer of phospholipids with longer chain length forming the most stable form of lipid-protein mixtures. In contrast, surface roughness values of DPPC/AS25 is slightly larger than DSPC/AS25 for phospholipid/AS25 mixtures. It is the nature of AS25 molecules absorbed on the surface of phospholipids membrane; thus the binding of AS25 on the surface is not affected by the hydrocarbon chain length.

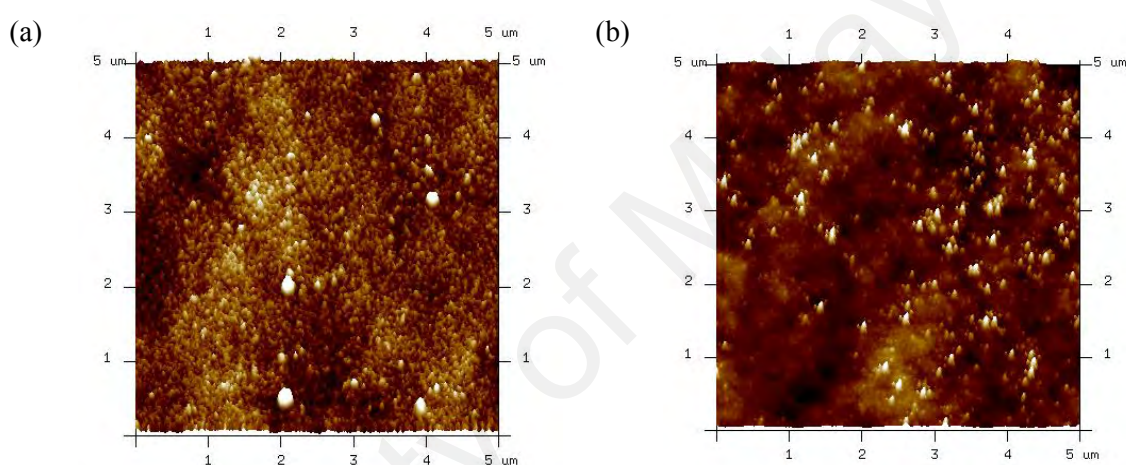


**Figure 4.66:** AFM images of (a) DPPC/AS25, and (b) DPPC/DP/AS25 bilayer deposited on oxidized silicon wafer obtained in a  $5.0 \mu\text{m} \times 5.0 \mu\text{m}$  scan area with a data scale of 25 nm.

**Table 4.3:** Surface roughness,  $R_a$  of pure DPPC, AS25, and BSA, mixed systems of DPPC/DP, DPPC/BSA, DPPC/AS25, and DPPC/DP/AS25 (obtained using NanoScope Analysis 1.5).

Pure systems	Surface roughness, nm		Mixed systems	Surface roughness, nm	
	$R_a$	$R_q$		$R_a$	$R_q$
DPPC	0.377	0.556	DPPC/DP	0.512	0.656
DP	0.818	1.170	DPPC/BSA	0.817	1.020
BSA	0.356	0.456	DPPC/AS25	0.967	1.320
AS25	0.566	0.789	DPPC/DP/AS25	0.504	0.694

## 4.6 Liposomes

### 4.6.1 Particle size and zeta potential

#### 4.6.1.1 C18 fatty acids liposomes

Phospholipids are commonly used in preparing nanoliposomes due to its stability that increases encapsulated drugs shelf life-span (Baek, Dinh Phan, Lee, & Shin, 2016; Chen et al., 2014; Fujisawa, Kadoma, Ishihara, Atsumi, & Yokoe, 2004). However, phospholipids are rather costly. In a long run, it will prominently influence the cost of cancer treatment using the liposomal drug and eventually become unaffordable and burden to the society. Cancer research should also have considered in making cancer treatment an affordable one to all in the future. Alternatively, fatty acids are also a good choice of lipid to prepare liposomes (Teo, Misran, Low & Zain, 2011; Morigaki & Walde, 2007). They are inexpensive, biocompatible, nontoxic and readily available. Moreover, the *cis*-double bond(s) of unsaturated fatty acids has made them the best choice of starting material to prepare liposomes. The presence of *cis*-double bond will prevent the molecule packing that increases the membrane fluidity in the liposomes. Membrane fluidity will allow drug encapsulation and conjugation of antibody. There were some publications from our group on preparation of stealth and nonstealth fatty acids liposomes and their capability in drugs encapsulation (Tan & Misran, 2012; Teo, Misran, & Low, 2012 & 2014a). One of the drawbacks of fatty acids liposomes is physical and chemical instabilities during the storage. In fact, this is a general drawback of most of the liposomal formulations, including some phospholipids liposomes. In order to stabilize fatty acid formulations, therefore membrane-bound antibody and PEG will be conjugated to pure C18 fatty acids liposomes solution (as illustrated in Figure 4.67) as lipid-protein interactions are naturally taking place in the biological membrane. This work also can serve as a reference or improve fatty acid liposomes formulations that are currently understudied.

Mean particle size of liposomes, zeta potential and polydispersity index (PDI) are some of the commonly monitored parameters. In general, for monomodal, reasonable narrow and spherical samples, PDI will be less than the value of 0.1, and more than 0.5 for a broader distributions sample.

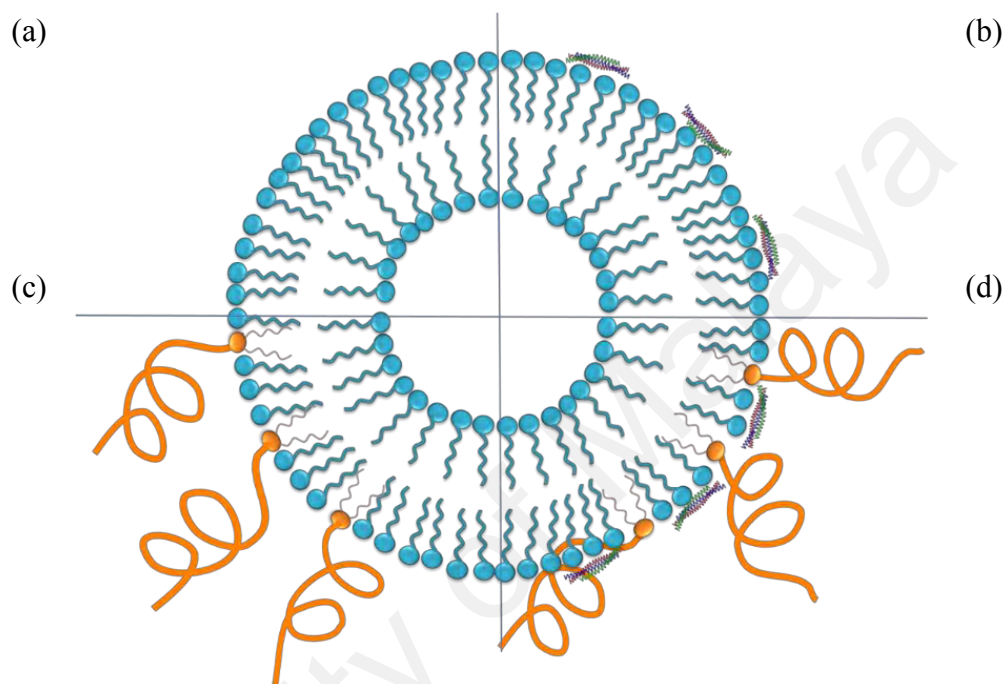


**Figure 4.67:** A schematic diagram illustrates the surface of (a) liposomes, (b) antibody-targeted liposomes, (c) stealth liposomes, and (d) stealth antibody-targeted liposomes.

#### 4.6.1.2 L1/DP, L2/DP, L3/DP liposomes

The mean particle size of pure L1, L2 and L3 liposomes in 1 mM PBS solution (pH 7.4) are 125, 129, and 122 nm, respectively (Figure 4.68). Their PDI values are 0.28, 0.21, and 0.40, respectively. The stability assessment on pure liposomes solutions demonstrated that the particle size was stable, where they remained less than 200 nm in 28 days. Their zeta potential is a large negative value of -45 mV due to their anionic carboxylate headgroup. Zeta potential magnitudes of L2 and L3 increased to -25 mN m<sup>-1</sup> and -10 mN m<sup>-1</sup> respectively over 14 days of monitoring (Figure 4.69).

The presence of PEG increases the circulation time up to hours or several days by reducing serum proteins binding, subsequently will slow down the rate of drug

release from the nanocarrier. PEG also increases vascular penetrability to liposomes enabling increased accumulation of drug containing liposomes in tumor/cancer tissue (Cattel, Ceruti, & Dosio, 2002; Immordino, Dosio, & Cattel, 2006; Moghimia & Szebenib, 2003; Nag & Awasthi, 2013; Working et al., 1994). The incorporation of DP into fatty acids liposomes did not entirely improve the particle size and zeta potential stability. The 28 days of mean particle size measurement of L2/DP were found to be more stable than L1/DP and L3/DP (Figure 4.68), the mean particle size of L2/DP varying closely within 50 to 200 nm, in contrast, inconsistency in particle size of L1/DP and L3/DP liposomes was observed fluctuating from 50 to 350 nm. Significant irregularity in particle size was observed in L3/DP at the highest mole ratio of DP (0.05) in the investigation range. The highest mole of DP (in the investigation range) caused the instability of liposomes in 28 days. Zeta potential measurements decreased dramatically (Figure 4.69) when DP is incorporated into pure fatty acid liposomes, as DP is less negative charged unlike fatty acid has an overall negative net charge. From zeta potential measurements, L1/DP is more stable compare to L2/DP and L3/DP.

PEG with saturated lipids, such as 1,2 dipalmitoyl-*sn*-glycero-3-phosphoethanolamine-N-[methoxy(polyethylene glycol)-2000] (DPPE PEG2000) (Teo, Misran, & Low, 2012, 2014a & 2014b) and 1,2-distearoyl-*sn*-glycero-3-phosphoethanolamine-N-[amino(polyethylene glycol)-2000] (DSPE PEG2000) (Kroon, Metselaar, Storm, & Pluijm, 2014; Yan et al., 2013), is commonly used in numerous preparations of stealth liposome (or immunoliposome) formulations for *in vivo* and *in vitro* cancer therapeutic studies. PEGs with saturated lipids have no bends or kinks in their saturated lipid molecular structures that promote molecular packing, so they should be easily inserted into the liposome membrane. Many applications of stealth/nonstealth liposomes (or immunoliposomes) in cancer/tumor research have been performed (Chou, Lin, & Liu, 2015; Niu et al., 2015; Wibroe, Ahmadvand, Oghabian,

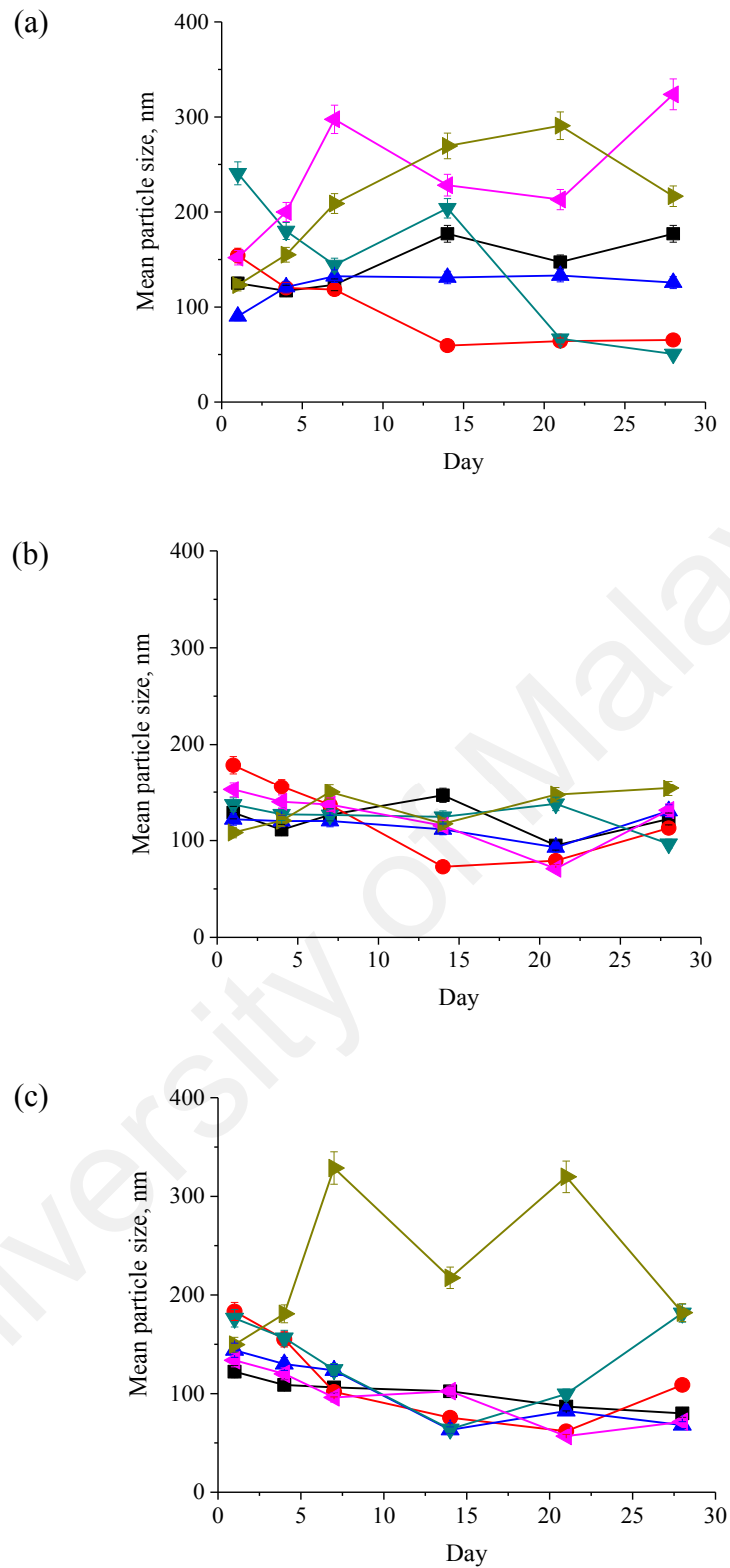


**Figure 4.68:** Mean particle size of C18 FA/DP liposomes: (a) L1/DP, (b) L2/DP, and (c) L3/DP for 28 days at 30°C. For ■ = C18 fatty acids liposomes; the mole ratio of DP to C18 fatty acids: ● = 0.01, ▲ = 0.02, ▼ = 0.03, ◄ = 0.04, and ► = 0.05 incorporated into liposomes.

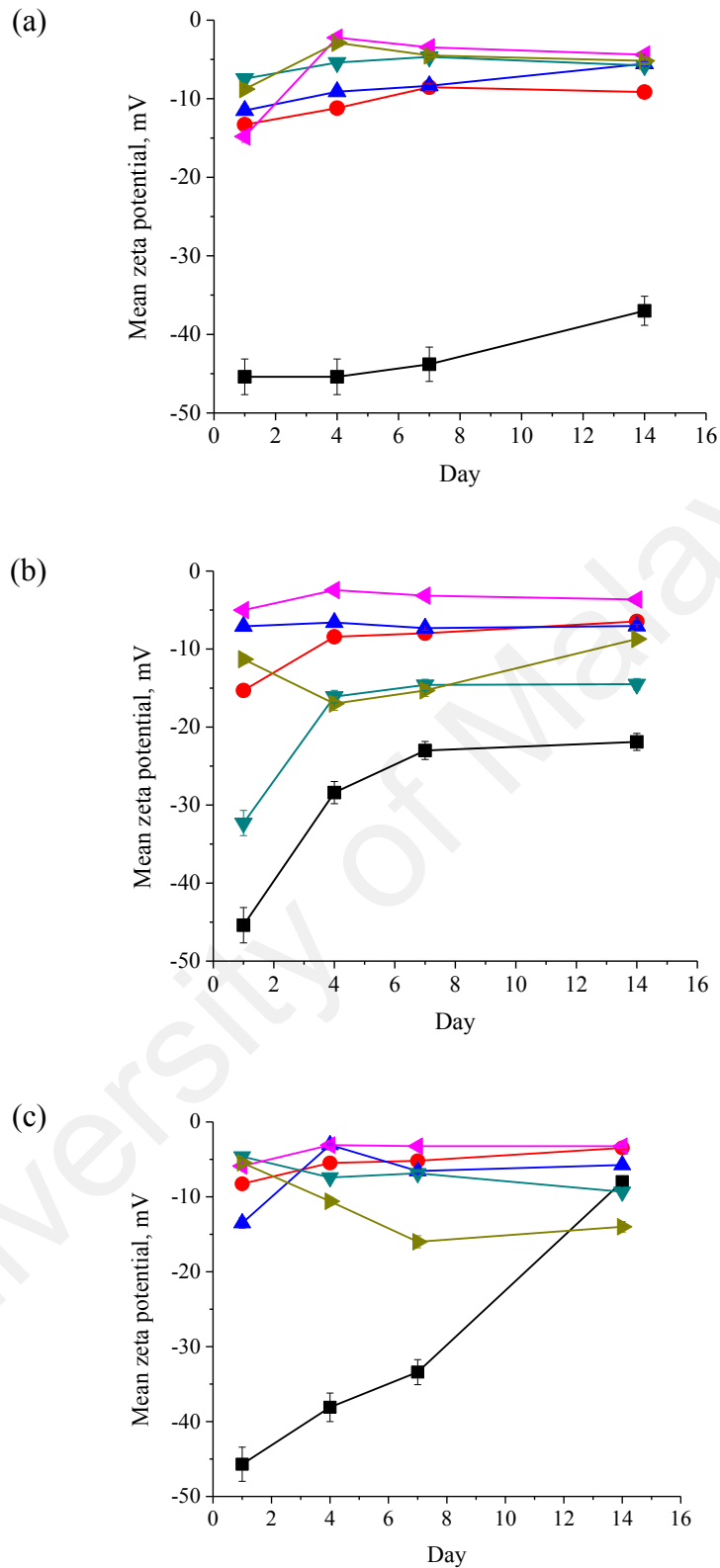


**Figure 4.69:** Mean zeta potential of C18 FA/DP liposomes, (a) L1/DP, (b) L2/DP, and (c) L3/DP for 14 days at 30°C. For ■ = C18 fatty acids liposomes; the mole ratio of DP to C18 fatty acids: ● = 0.01, ▲ = 0.02, ▼ = 0.03, ◀ = 0.04, and ▶ = 0.05 incorporated into liposomes.

Yaghmur, & Moghimi, 2016; Xia, Tian, & Chen, 2016; Yoshizawa, Kono, Ogawara, Kimura, & Higaki, 2011), but LB studies that have reported on the fundamental of intermolecular interactions between PEG on lipid Langmuir monolayers are very limited (Teo et al., 2014b).

Fatty acid liposomes that incorporated with unsaturated DOPE-PEG2000 are slightly larger than liposomes incorporated with saturated DPPE-PEG2000 (Teo et al., 2012). This is an advantage to encapsulate drugs with larger molecule size, and also increase the drug encapsulation efficiency into the nanocarriers. Both of unsaturated DOPE hydrocarbon chains of DP increase the repulsion in the molecular packing of liposomes due to the effect from *cis*-double bonds of DOPE, ultimately increase the size of liposomes.

#### **4.6.1.3 L1/AS25, L2/AS25, L3/AS25 liposomes**

The charged amino-acids that presence on the entire surface of protein will ionize or deionize depending on pH, making it a charged particle in the aqueous solution. The surface charge of a protein is not static, as the charged groups are acids and bases predominate that constantly exchange protons with water, thus they are in dynamic equilibrium with their uncharged states. Surface charge of the protein is important as the right surface charge of their active site will greatly influence the specific substrate binding. Zeta potential measurement of AS25 in PBS solution of pH 7.4 was found to be  $-6.72 (\pm 0.15)$ .

Irregularity in particle size measurement was shown in C18 fatty acids/AS25 liposomes (Figure 4.70). The particle size of L1/AS25 increases with the increasing volume of AS25 incorporated, in contrast, L2/AS25 and L3/AS25 did not show any specific trend of increasing or decreasing the amount of AS25 incorporated (Figure 4.70). The particle size of all the mixture decreased to less than 100 nm in 14 days of

stability. Presumably, it hydrolyzed into salt solutions during the storage. The carboxyl headgroup of C18 fatty acids is rather unstable. PDI of each mixture are slightly larger than their pure liposomes. Zeta potential of C18 fatty acids/AS25 liposome solutions were found to be less negative as compared to their highly negative charged pure liposomes solutions respectively. Surface charge of AS25 molecules is much lower than C18 fatty acids liposomes solutions, therefore when AS25 molecules are bounded to the negatively charged surface of C18 fatty acids liposomes, that will lead to increase the surface charge to less negative. When 3.36 nmole of AS25 was incorporated into L1 liposomes solution, an incline of zeta potential of L1/AS25 from -45 to -28 mV were observed. As the amount of AS25 (8.40, 16.8 and 25.2 nmole) added into L1 liposomes solution increased, zeta potential increases to -5 to -10 mV (Figure 4.71). Measurement of zeta potential in 14 days, it also remained at -5 to -10 mV. Zeta potential measurements of L3/AS25 for 14 days showed that the liposomes solution was stable, where their zeta potential remained between -5 to -15 mV. However, zeta potential measurements of L1/AS25 and L3/AS25 liposome solutions were more stable than L2/AS25 for 14 days, except L2/AS25 containing 25.2 nmole of AS25 remained constant at about -5 mV for 14 days.

#### **4.6.1.4 L1/DP/AS25, L2/DP/AS25 and L3/DP/AS25 liposomes**

The combination of active-targeting drug delivery with PEGylation was proven to reduce the rate of drug clearance in the blood circulation, modify the drug distribution, or even enhance the delivery of therapeutic materials.

The incorporation of AS25 into PEGylated L1, L2, and L3 liposome solutions stabilized their mean particle size and zeta potential measurements for 30 days and 14 days respectively (Figure 4.72 and 4.73). The mean particle size of L1/DP/AS25 varied from 75 nm to 125 nm, and they remained constant for 14 days. The zeta potential

measurement of L1/DP/AS25 is less negative than L1/DP of mole ratio of 50:1, which varies from -12 mV to -7.5 mV. This could be the more negative surface charge was determined when the AS25 molecules bounded to L1/DP surface as AS25 is more negative than DP. Irregularity of particle size of L2/DP/AS25 were found on the third days of measurement, and then size reduced to less than 75 nm (day 7) then increased again to 125 nm (day 14). Hydrolysis may occur within 7 days, and then transform into oil droplets in day 14. Zeta potential measurements of L2/DP/AS25 were found to be more negative than L2/DP of mole ratio of 50:1. Presumably, more AS25 molecules conjugated on L2/DP liposome surface, or AS25 molecules were conjugated to the polymer headgroup of DP. Mean particle size of L3/DP/AS25 liposome solutions were found to be slightly lower than L3/DP of mole ratio of 50:1, varies from 125 nm to 100 nm, whereas particle size of L3/DP is about 150 nm. In 14 days of particle size monitoring, their particle size reduced to less than 50 nm. This showed that L3/DP liposome solutions (containing the most *cis*-double bonds) has poor stability and has a shorter shelf-life span. Other than the carboxyl headgroup of L3 undergo hydrolysis, the *cis*-double bonds are also easily oxidized. Precipitations in the vials were observed for L2/DP/AS25 and L3/DP/AS25 liposomes solution is an indication of instability. Zeta potential measurements of L3/DP/AS25 were found to be less negative than L3/DP, except the liposomes solutions containing 3.36 nmole of AS25. Their zeta potential measurements were found to be significantly less negative on the third day of monitoring, and then remained constant in between -2.5 to -7.5 mV till day 14 for each respective mixture.

The PDI values of PEGylated C18 fatty acids/AS25 liposomes were found to be similar to C18 fatty acids/AS25, which in between 0.40 to 0.55, but larger than PEGylated C18 fatty acids (0.30 to 0.40), as aggregation will occur when protein molecules are present in the liposomes solutions.

#### 4.6.1.5 DPPC/DP, DPPC/AS25 and DPPC/DP/AS25 liposomes

Phospholipid such as DPPC is commonly used to prepare liposomes. Owing to its well-known stability, DPPC liposomes were chosen as a comparison to the unestablished and infamous fatty acid liposomal formulations.

On account of low concentration of DPPC liposomes solution (1 mM), the particle size is smaller than some published work; however most of them reported less than 100 nm. The mean particle size of DPPC liposomes was 77.5 ( $\pm 0.5$ ) nm with PDI of 0.18, and then gradually increased to 106 ( $\pm 0.25$ ) nm in 28 days (Figure 4.74(a)). The mean particles size is greatly affected by the molar concentration of liposome solutions and their method of preparation. The molecular packing of phospholipid in the bilayer of liposomes is loose and less rigid at a lower concentration.

Ethanol injection is the best choice to obtain homogenous distributions of phospholipid liposomes with low PDI value. Its zeta potential remained at about -1 mV for 28 days (Figure 4.75(a)), this value is similar to most of the published work. DPPC liposomes solution is considerable stable in 28 days of storage in term of their particle size and zeta potential.

The addition of DP into DPPC increases the size of liposomes. Mean particle size vary from 77 to 150 nm throughout 28 days. After 24 hours of liposomes formed, particle size increases with the increasing amount of DP in DPPC. The bend of *cis*-double bonds of DOPE in DP produce a kink in the mixture, and ultimately increase the liposomes size. The particle size of DPPC/DP were considerable stable for 28 days, no significant increase or reduce in size is observed. Their zeta potential falls in between -0.5 to -2 mV in 28 days.

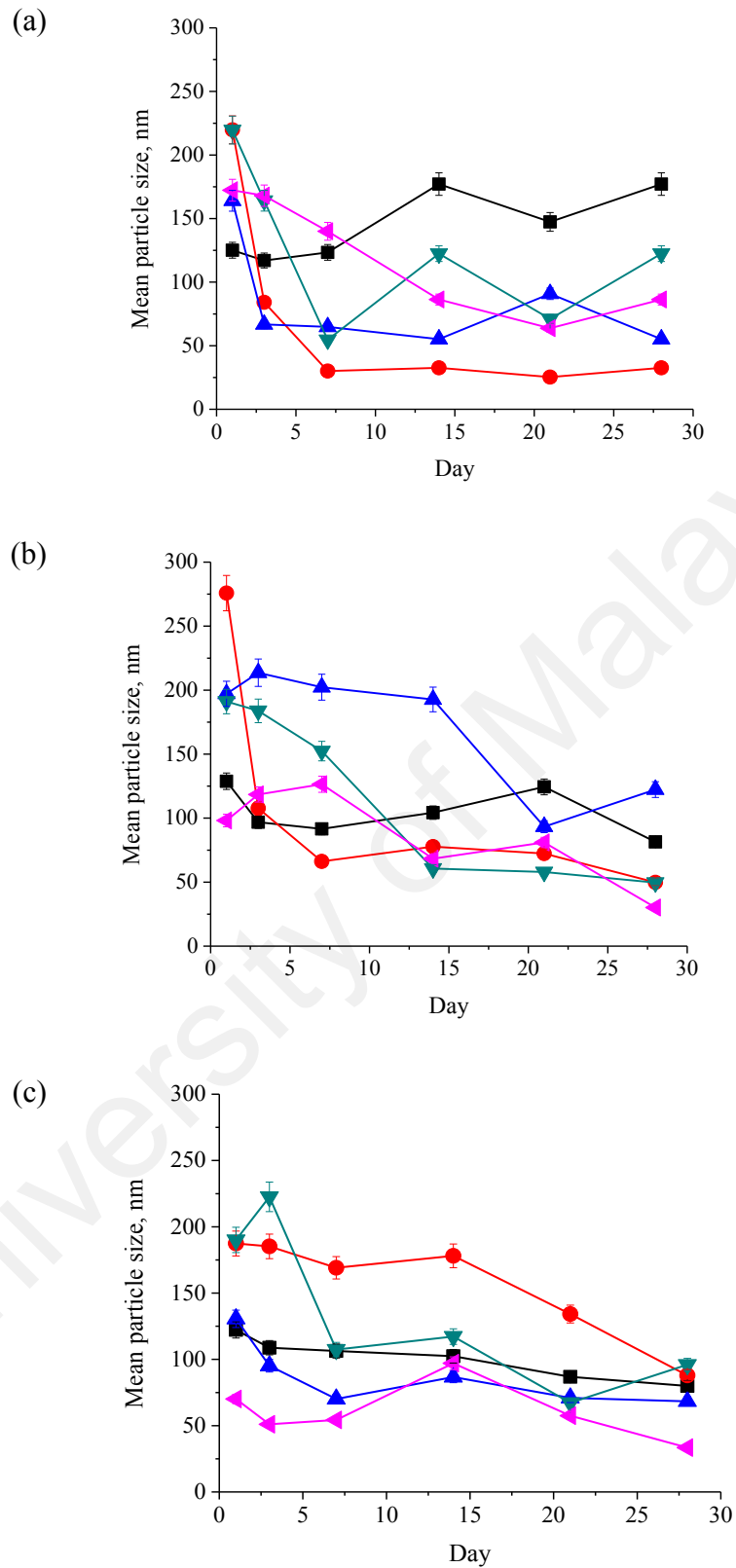


**Figure 4.70:** Mean particle size of C18 fatty acids/AS25 liposomes: (a) L1/AS25, (b) L2/AS25, and (c) L3/AS25 for 28 days at 30°C. For ■ = C18 fatty acids liposomes; the amount of AS25: ● = 3.36 nmole, ▲ = 7.40 nmole, ▼ = 16.8 nmole, ◄ = 25.2 nmole incorporated into liposomes.

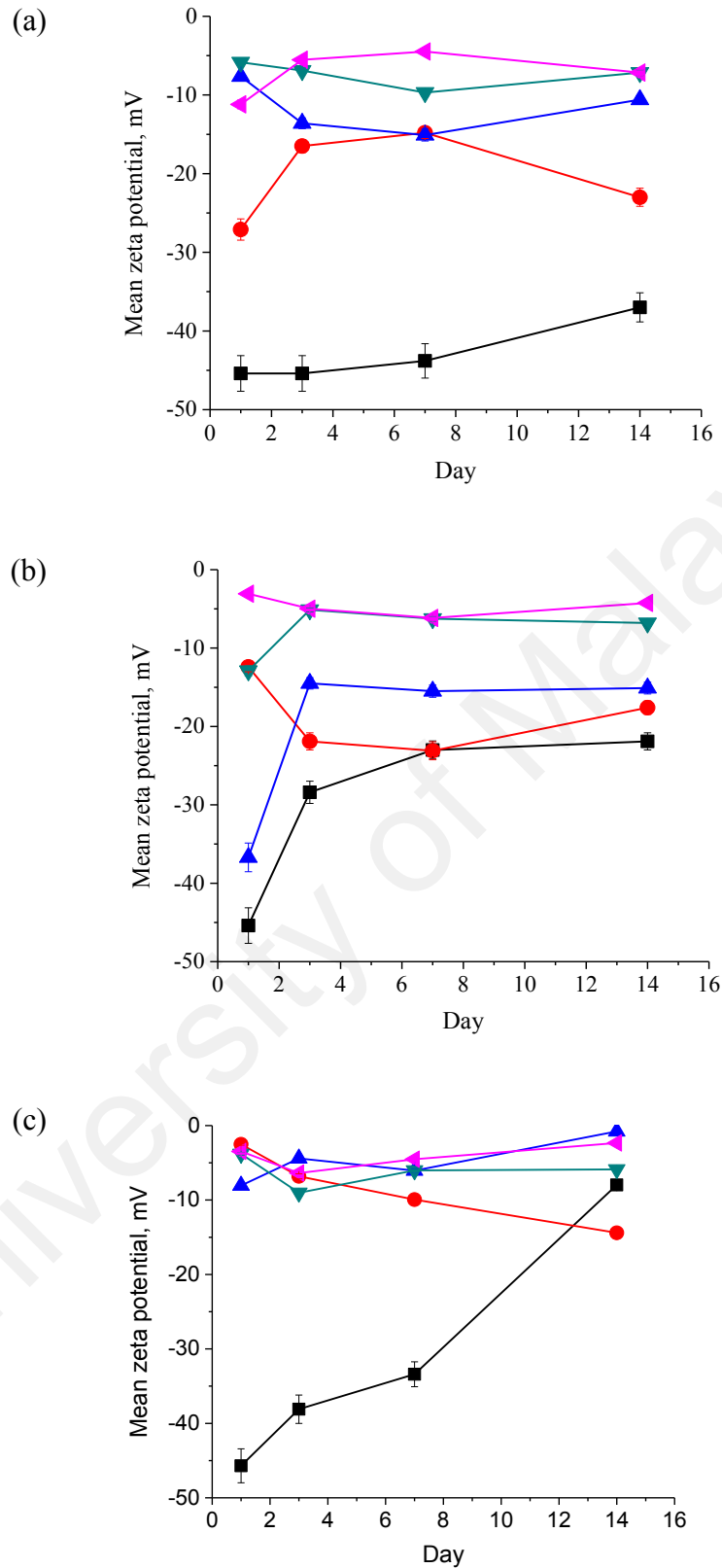


**Figure 4.71:** Mean zeta potential of C18 fatty acids/AS25 liposomes, (a) L1/AS25, (b) L2/AS25, and (c) L3/AS25 for 14 days at 30°C. For ■ = C18 fatty acids liposomes; the amount of AS25: ● = 3.36 nmole, ▲ = 7.40 nmole, ▼ = 16.8 nmole, ◀ = 25.2 nmole incorporated into liposomes.

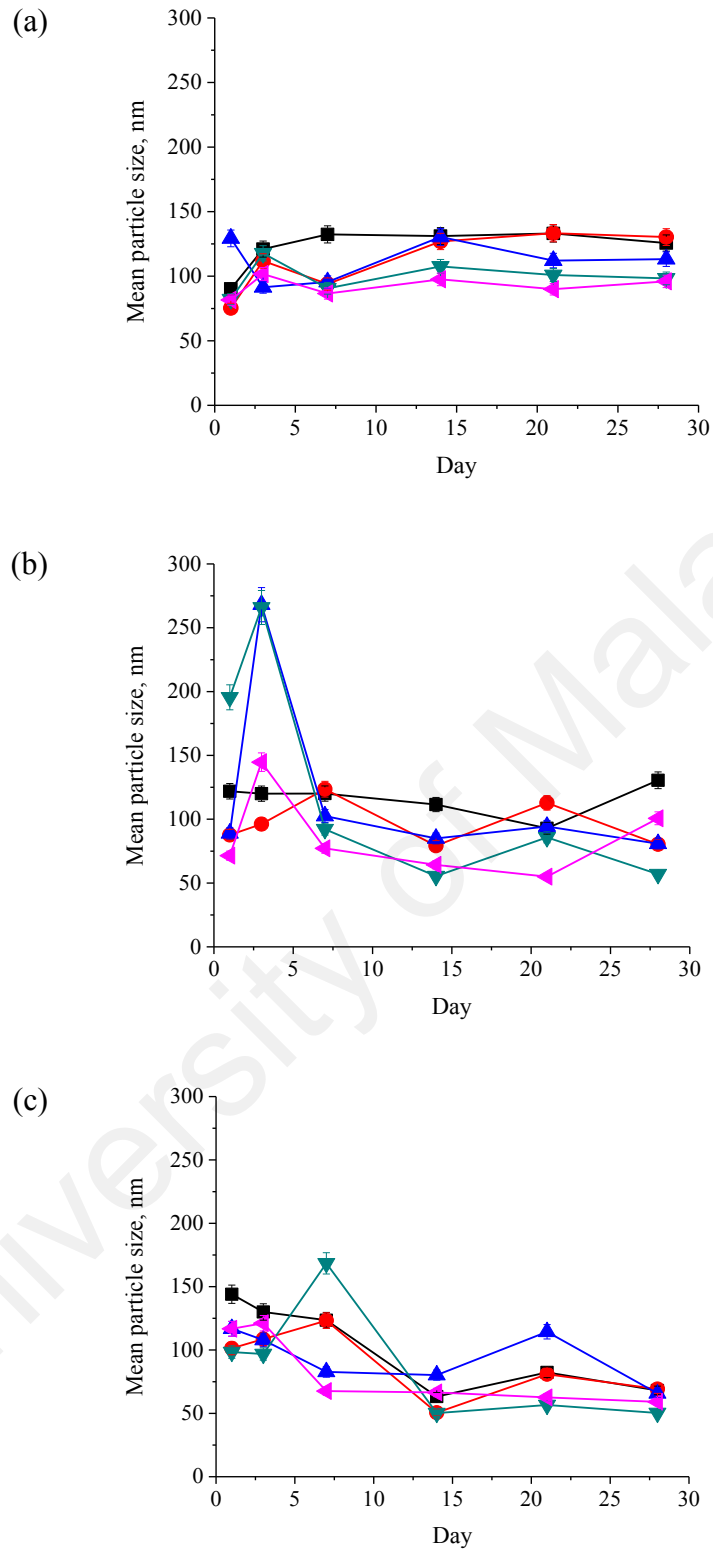


**Figure 4.72:** Mean particle size of C18 fatty acids/DP/AS25 liposomes: (a) L1/DP/AS25, (b) L2/DP/AS25, and (c) L3/DP/AS25 for 28 days at 30°C. For ■ = C18 fatty acids/DP liposomes; the amount of AS25: ● = 3.36 nmole, ▲ = 7.40 nmole, ▼ = 16.8 nmole, ◀ = 25.2 nmole incorporated into liposomes.

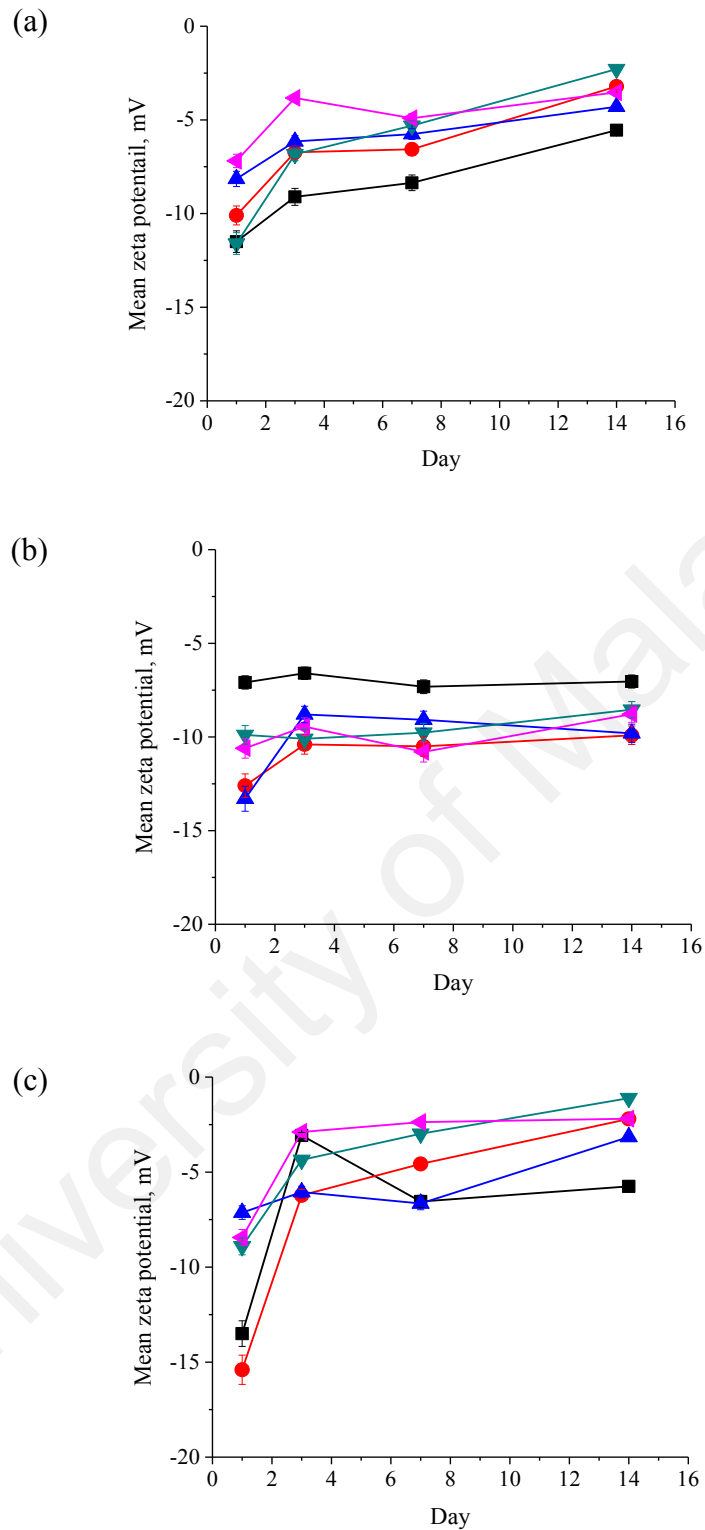


**Figure 4.73:** Mean zeta potential of C18 fatty acids/DP/AS25 liposomes, (a) L1/DP/AS25, (b) L2/DP/AS25, and (c) L3/DP/AS25 for 14 days at 30°C. For ■ = C18 fatty acids/DP liposomes; the amount of AS25: ● = 3.36 nmole, ▲ = 7.40 nmole, ▼ = 16.8 nmole, ◄ = 25.2 nmole incorporated into liposomes.

The mean particle size of DPPC/AS25 increased with increasing mole of AS25 incorporated (Figure 4.74(b)). The mean particle size of DPPC/AS25 liposomes is larger than DPPC liposomes. Interestingly, the presence of DP in DPPC/AS25 aided in stabilizes the particle size for 28 days (Figure 4.74(c)). The particle size of DPPC/DP/AS25 are found to be in between 100 to 125 nm, and remained constant for 28 days. This finding is consistent with the energetic studies, where the presence of DP in DPPC/AS25 monolayer has larger negative  $G_{mix}$  values than DPPC/AS25 without DP.

Zeta potential of DPPC/AS25 and DPPC/DP/AS25 is more negative as compare to DPPC/DP (Figure 4.75(b) & (c)). This shows that negative charged surface of AS25 are facing outward, as the positive charged surface of AS25 are conjugated to negative charged DPPC phosphate headgroup. Zeta potential is found to be more negative with the increasing mole of AS25 in the liposomes. The zeta potential of DPPC liposomes and DPPC/AS25 liposomes containing 3.36 nmole of AS25 has the same trend during 28 days of monitoring their stability. As for DPPC/AS25 liposome solutions containing 8.40, 16.8 and 25.2 nmole, their zeta potential measurements decreased with increasing number of days from -1.5 to -3.5 mV in 28 days.

Zeta potential measurement of DPPC/DP/AS25 liposomes showed that they more stable than DPPC/AS25 in 28 days, their changes is in between -1 to -2 mV. DPPC/DP/AS25 with 10ul has the most negative zeta potential values and then slightly less negative when 3.36 nmole of AS25 is incorporated into DPPC/DP liposomes. Presumably, liposomes with 10ul may have more AS25 molecules conjugated to the surface of DPPC/DP liposomes.

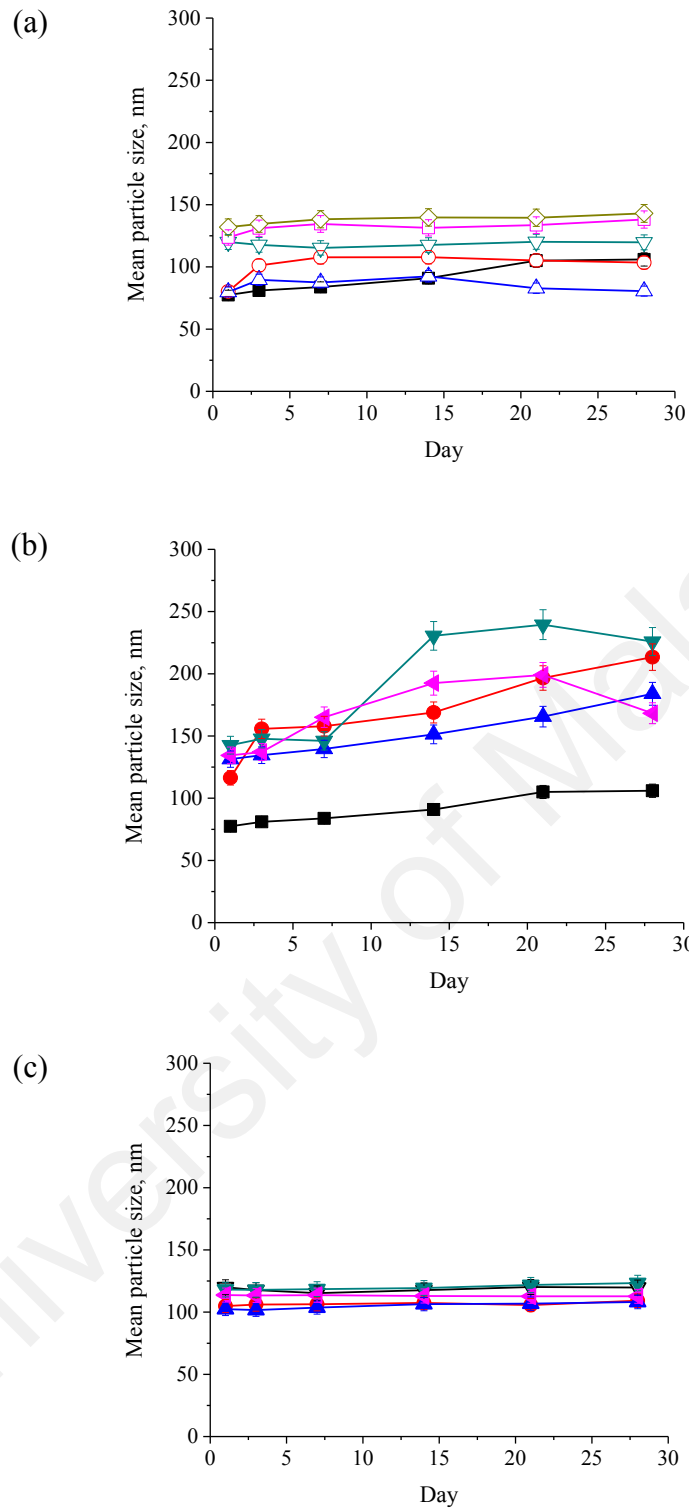


**Figure 4.74:** Mean particle size of DPPC/DP, DPPC/AS25, DPPC/DP/AS25 liposomes for 28 days at 30°C. For ■ = DPPC liposomes; (a) the mole ratio of DPPC to DP are ○ = 20:1, ● = 35:1, ▽ = 50:1, ◻ = 75:1, ◊ = 100:1. (b) and (c) the amount of AS25: ● = 3.36 nmole, ▲ = 7.40 nmole, ▼ = 16.8 nmole, ◀ = 25.2 nmole incorporated into DPPC and DPPC/DP liposomes respectively.

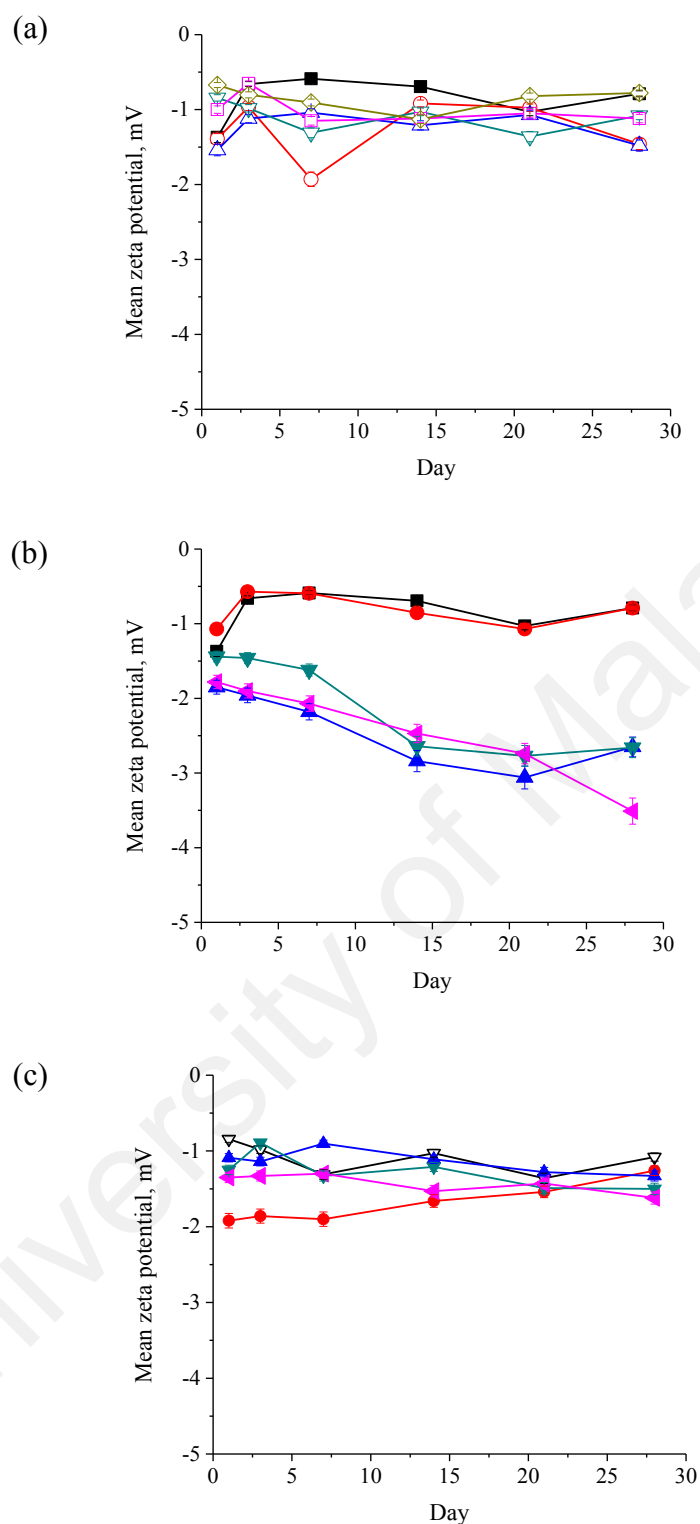


**Figure 4.75:** Mean zeta potential of DPPC/DP, DPPC/AS25, DPPC/DP/AS25 liposomes for 28 days at 30°C. For ■ = DPPC liposomes; (a) the mole ratio of DPPC to DP are ○ = 20:1, ▽ = 35:1, ▽ = 50:1, ◻ = 75:1, ◇ = 100:1. (b) and (c) the amount of AS25: ● = 3.36 nmole, ▲ = 7.40 nmole, ▼ = 16.8 nmole, ◄ = 25.2 nmole incorporated into DPPC and DPPC/DP liposomes respectively.

#### 4.6.2 Transmission electron microscopy (TEM) micrographs

TEM technique is the best available option to observe the presences of liposomes in the solution. This is due to the liposomes produced using the methods stated in Chapter 3 were below 500 nm which could not be viewed using light or polarizing microscope. Transmission electron microscopy (TEM) micrographs of 1 mM of pure L1, L2, L3 and their PEGylated liposomes (Figure 4.76), antibody-conjugated C18 fatty acids liposomes and PEGylated antibody-conjugated liposomes (Figure 4.77) and liposomes of DPPC (Figure 4.78).

Negative staining using phosphotungstic acid (PTA) solution is an easy and widely used method for examining liposomes structure at electron microscopy level. However, it involves the deposition of heavy atom stains (in this case is tungsten) that will cause flattening of spherical or cylindrical of liposomes structure are commonly observed. PTA stained liposomes represents bilayer moiety due to its strong affinity to PTA and then become very electron dense (Résois-Grégoire, 1967).

The images of liposomes were observed on the fluorescence screen which is placed at position 180°C from the electron source produced by the projection of electrons being scattered as they pass through the liposomes. As the electron beam travels through the liposome, they interact with the atoms in the membrane and travelling through membrane with different thickness. The longer the distance the electron travels, the more interaction may occur with the atoms in the membrane and hence more electrons will be diffracted. When lower electron phase density reaches the fluorescent screen, the darker image will be observed compared to the background, while the lighter areas of the image represent the area of sample which more electrons were transmitted through. This caused the variation of electron phase density around liposome and generates the contrast between the sample and background.

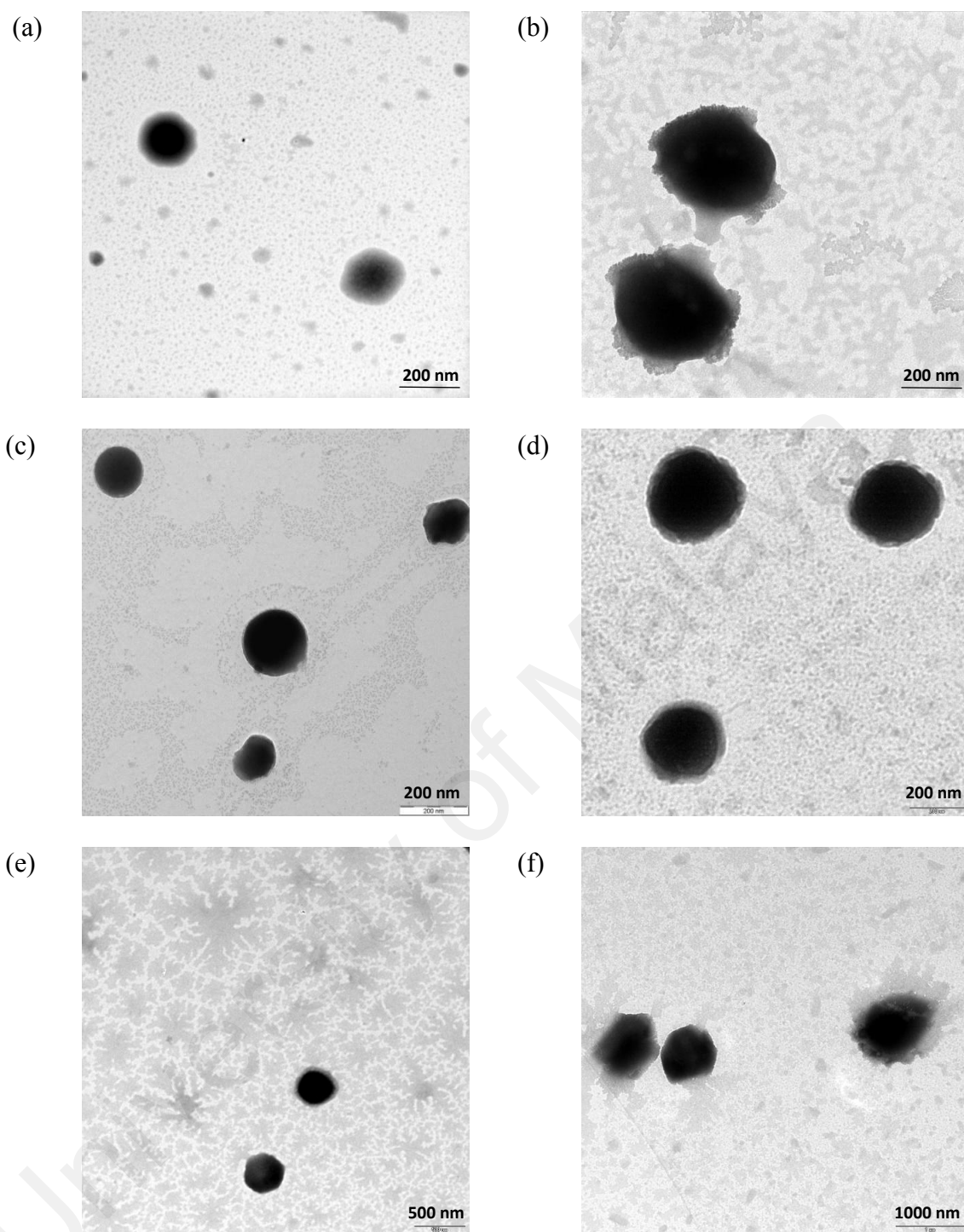


**Figure 4.76:** Transmission electron micrographs of: (a) 1 mM L1, (b) L1/DP, (c) 1 mM L2, (d) L2/DP, (e) 1 mM L3, (f) L3/DP liposomes at pH 7.4.

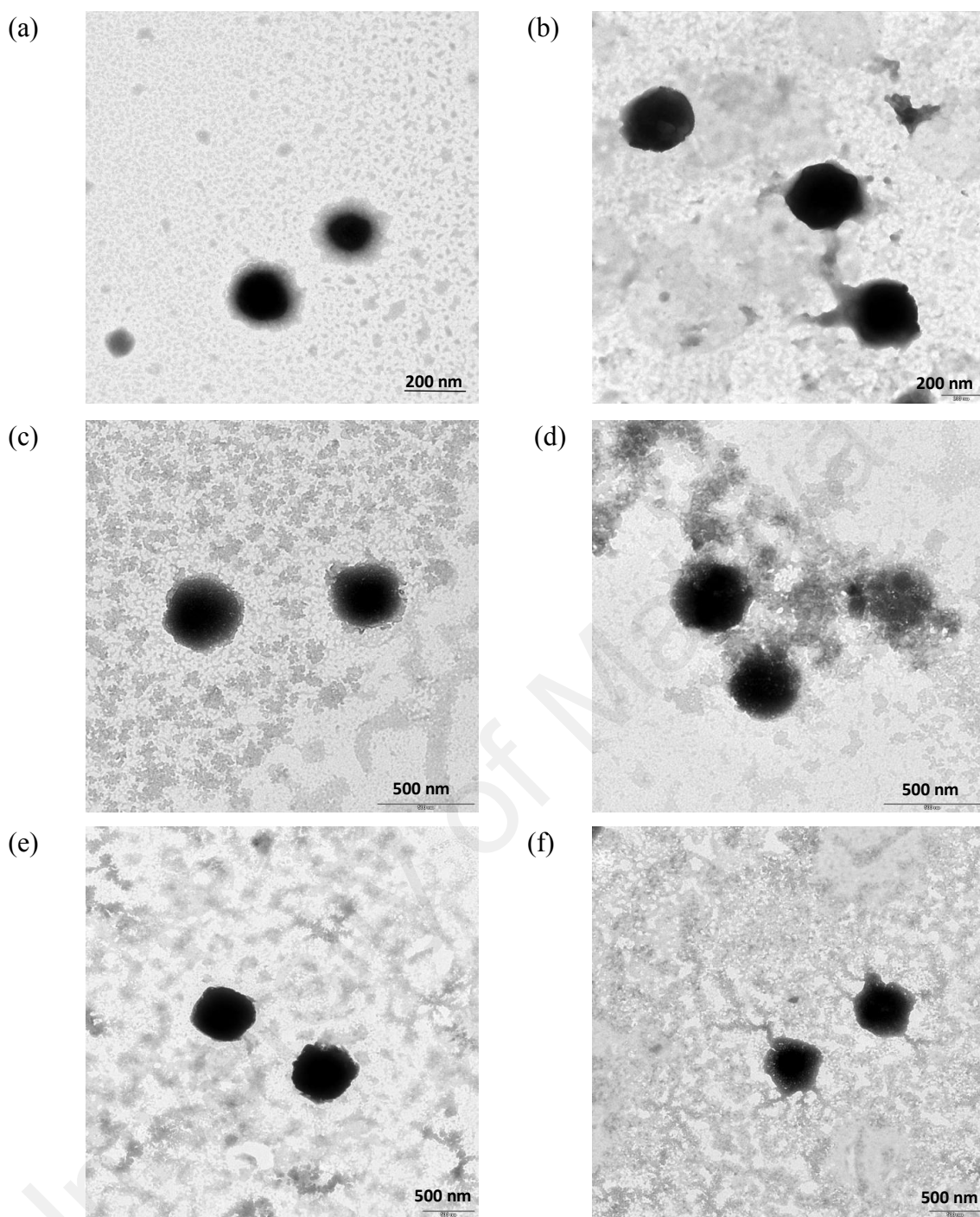


**Figure 4.77:** Transmission electron micrographs of: (a) 1mM L1/AS25, (b) L1/DP/AS25, (c) 1 mM L2/AS25, (d) L2/DP/AS25, (e) 1 mM L3/AS25, (f) L3/DP/AS25 liposomes at pH 7.4.

The particle size of PEGylated liposomes (L1/DP, L2/DP, and L3/DP) was slightly larger than their pure liposomes (Figure 4.76). The imperfection of outer membrane was observed in Figure 4.77, and Figure 4.78(b)-(d) showed that the incorporation of PEG headgroup of DP and AS25 on unsaturated c18 fatty acid and DPPC liposomes were successful. The particles sizes of liposomes containing AS25 are non-homogenous as shown in Figure 4.77 and 4.78. This is due to sonication was not performed during the preparation after adding membrane protein AS25. Sonication of proteins may cause aggregation and cell lysis.

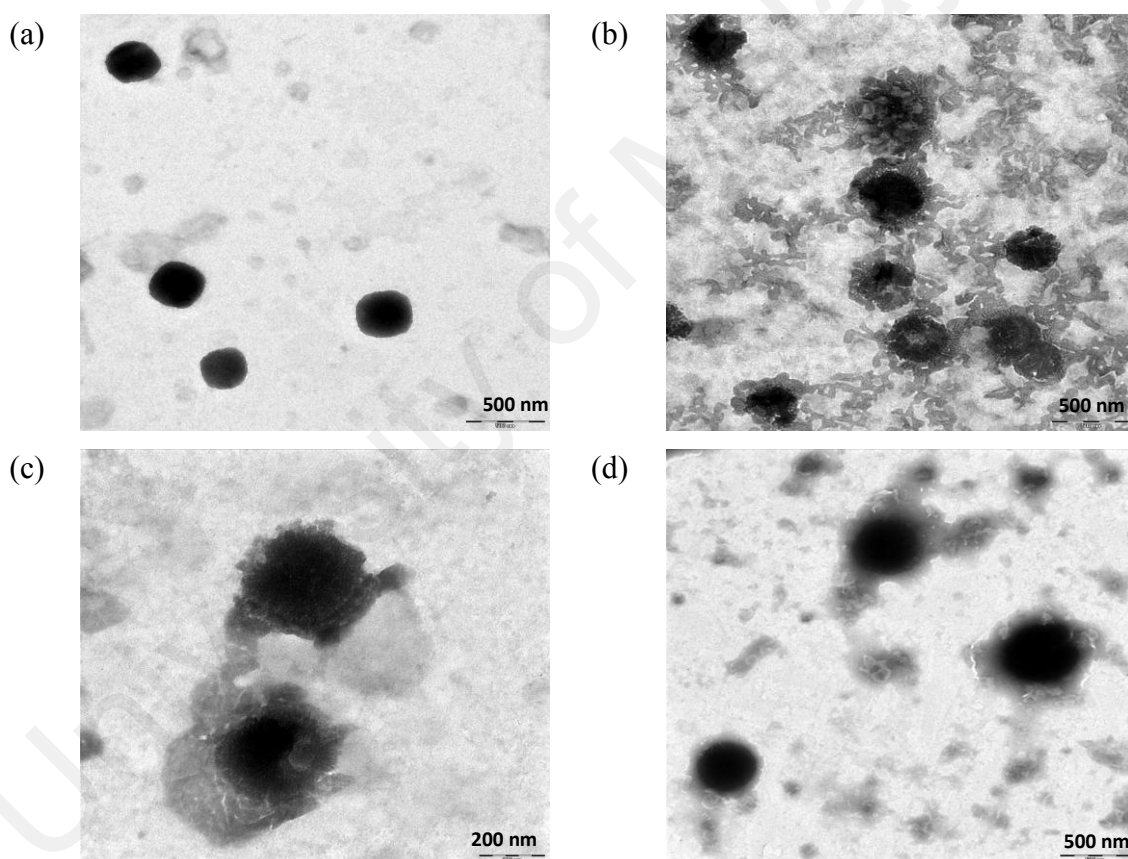


**Figure 4.78:** Transmission electron micrographs of: (a) 1 mM DPPC, (b) DPPC/DP at mole ratio of 50:1, (c) DP/AS25, and (d) DPPC/DP/AS25 liposomes at pH 7.4.

## CHAPTER 5: CONCLUSION

Lipid-protein interactions are crucial in developing targeted liposomal DDS formulations. The composition ratio of lipids and antibodies in forming DDS can be determined precisely from the LB energetic stability study of the mixed systems, which will also allow us to ensure antibodies are successfully incorporated into the lipid-carrier system. Moreover, proteins' preference for specific lipid membranes were investigated.

Bovine serum albumin (BSA), an integral protein, and anti-SNAP25 (AS25), a membrane bound protein, have become the choices of proteins to explore lipid-protein interactions. In this study, the interactions of integral and peripheral proteins with C18 fatty acids (SA, L1, L2, and L3) and phospholipids (SS, DSPC, DSPG, and DPPC) with the support of thermodynamic quantitative data, as both are the essential structural elements of biological membranes. Langmuir monolayers of lipid-protein mixed systems were successfully used to illustrate the lipid-protein interactions occurring in natural biological membranes. The energetic investigation of BSA–C18 fatty acids (and BSA–phospholipids) and AS25–C18 fatty acids (and AS25–phospholipids) mixtures enabled us to conclude that BSA molecules bound stronger on the lipid monolayers than AS25, with the support of RP-HPLC and AFM analysis. BSA is an integral protein which embedded in between lipid monolayer by hydrophobic forces and hydrophilic interactions occurred between the hydrophilic amino acid groups of BSA and lipids. The most negative values of Gibbs free energy of mixing ( $G_{mix}$ ) were found at  $X_{BSA}$  for C18 fatty acids, SS and DPPC, and 7:3 for DSPC and DSPG at surface pressure of  $15 \text{ mN m}^{-1}$  (as shown in Table 5.1).  $G_{mix}$  values of unsaturated C18 fatty acids/BSA are more negative than SA/BSA and phospholipids/BSA (Table 5.1); however SA/BSA is more negative than phospholipids/BSA that have the same hydrocarbon chain length.

The relative strength of intermolecular interactions between phospholipids and BSA molecules are SS/BSA > DSPG/BSA > DSPC/BSA and DPPC/BSA > DSPC/BSA (from strong to weak). The degree of saturation of hydrocarbon chain and headgroup of fatty acids or phospholipids are greatly influenced lipid-protein interactions in the model membrane.

**Table 5.1:** Gibbs free energy of mixing ( $G_{mix}$ ) values of C18 fatty acids/BSA and phospholipids/BSA at surface pressure at 15 mN m<sup>-1</sup>.

$G_{mix}$ of C18 fatty acids/BSA, kJ				$G_{mix}$ of phospholipids/BSA, kJ			
SA	L1	L2	L3	SS	DSPC	DSPG	DPPC
-20.7	-21.2	-21.8	-21.3	-16.1	-11.5	-13.1	-13.9

Meanwhile, AS25 is a membrane bound protein that presents on the surface of lipid monolayers, as the obtained  $G_{mix}$  values were less negative as compared to BSA. The amount of proteins incorporated into the monolayer greatly affected the thermodynamic properties of the lipid monolayers. L1 can be considered the best C18 fatty acid that interacted with AS25 in a binary system. A very small amount of AS25 incorporated into the L1 membrane model caused the strongest interactions to take place, where the mole ratio of L1/AS25 was 26 to 1. This L1/AS25 ratio mimicking a half bilayer membrane is a useful reference for our future studies in preparing fatty acid nanoliposomes as targeted drug-delivery vehicles. L1 is rather less expensive compared to the other two unsaturated lipids investigated. It is also important for us to note that not excessive amounts of antibodies should be introduced into human body. A large amount of antibodies will harm the human body, and it is not economically feasible as the cost of antibodies is extremely expensive, even at very small volumes. Less negative

$G_{mix}$  values were obtained for unsaturated C18 fatty acids/DP/AS25 showed AS25 molecules poorly adsorbed on the PEG headgroup of DP instead of C18 fatty acids carboxyl headgroup. In contrast, more negative  $G_{mix}$  values were obtained for

DPPC/DP/AS25 than DPPC/A25. The incorporation of DP into DPPC monolayer increased the membrane fluidity and strengthens the binding AS25 to the surface.

Langmuir monolayers of lipid–DP mixed systems were also successfully used to illustrate one aspect of pegylated fatty acid liposomes. The investigation of DP–C18 fatty acids (or DP–DPPC) mixtures allowed us to understand the stability of DP in saturated and unsaturated fatty-acid membranes in the PEGylated lipid-based drug-delivery system. The most thermodynamically stable composition of unsaturated C18 fatty acids (or DPPC) and DP was 50:1. This is the best mole ratio to use for preparing DP–C18 fatty acid (or DP–DPPC) and targeted DP–C18 fatty acid (or DP–DPPC) nanoliposomes; hence the incorporated AS25 into DP–C18 fatty acid (or DP–DPPC) at mole ratio of 50:1. The *cis*-double bonds in the hydrocarbon chains of DOPE in DP introduced imperfections to the membrane structure, causing the molecular packing to become less compressible and increasing membrane fluidity, which enhanced the lipid-system for antibody conjugation and drug encapsulation. The LB findings were used as a reference to carry out liposomes work as case studies.

Unsaturated C18 fatty acids liposomes, and their stealth and nonstealth antibody-targeted liposomes were prepared and characterized by monitoring their particle size and zeta potential for 28 days and 14 days respectively. L1/DP/AS25 can be considered as the most stable stealth antibody-targeted liposome system as their particle size remained in between 90 to 125 nm in 28 days for the entire investigated ranges. DPPC is a commonly used phospholipid in preparing liposomal drug delivery systems; hence, it was selected to illustrate phospholipid liposome systems as a comparison to fatty-acid liposomes. DPPC/DP/AS25 liposome system is more stable than L1/DP/AS25 liposome system. The particle size and zeta potential measurements of DPPC/DP/AS25 liposomes remained nearly constant for 28 days and 14 days

respectively. This stability showed agreement with the LB findings as large negative values of  $G_{mix}$  were obtained for DPPC/DP/AS25 mixed monolayer.

### 5.1 Future works

This study showed that LB is a versatile instrument to perform lipid-lipid and lipid-protein interactions. The exploration of the hydrophilic and hydrophobic of lipids bilayer membrane will allow self-assembly of therapeutic proteins in lipid membrane for fundamental knowledge and the development of novel nanocarrier. Intermolecular interactions play important roles in stability and function of liposomes. The embedded therapeutic proteins are dependent on lipid membrane composition and their physical properties.

Unsaturated C18 fatty acids are more cost effective than phospholipids. However, more work is required to be performed to stabilize fatty acid liposomes by mixing different types of fatty acids and phospholipids or therapeutic proteins in the liposomes.

## REFERENCES

- Adler-Moore, J., & Proffitt, R. T. (2002). AmBisome: liposomal formulation, structure, mechanism of action and pre-clinical experience. *Journal of Antimicrobial Chemotherapy*, 49(suppl 1), 21-30.
- Akbarzadeh, A., Rezaei-Sadabady, R., Davaran, S., Joo, S. W., Zarghami, N., Hanifehpour, Y., Samiei, M., Kouhi, M., & Nejati-Koshki, K. (2013). Liposome: Classification, preparation, and applications. *Nanoscale Research Letters*, 8(1), 1.
- Aliabadi, H. M., & Uludağ, H. (2016). Nanoparticle carriers to overcome biological barriers to siRNA delivery In M. Braddock (Ed), *Nanomedicines: Design, Delivery and Detection* (pp. 46-105). Royal Society of Chemistry.
- Allen, T. M., & Cullis, P. R. (2013). Liposomal drug delivery systems: From concept to clinical applications. *Advanced Drug Delivery Reviews*, 65(1), 36-48.
- Ambrosch, F., Wiedermann, G., Jonas, S., Althaus, B., Finkel, B., Glück, R., & Herzog, C. (1997). Immunogenicity and protectivity of a new liposomal Hepatitis A vaccine. *Vaccine*, 15(11), 1209-1213.
- Andrews, P. A., & Howell, S. B. (1990). Cellular pharmacology of cisplatin: perspectives on mechanisms of acquired resistance. *Cancer Cells (Cold Spring Harbor, NY: 1989)*, 2(2), 35-43.
- Anselmo, A. C., & Mitragotri, S. (2014). An overview of clinical and commercial impact of drug delivery systems. *Journal of Controlled Release*, 190, 15-28.
- Antonio, P. D., Lasalvia, M., Perna, G., & Capozzi, V. (2012). Scale-independent roughness value of cell membranes studied by means of AFM technique. *Biochimica et Biophysica Acta (BBA): Biomembranes*, 1818(12), 3141-3148.
- Baek, S., Dinh Phan, M., Lee, J., & Shin, K. (2016). Packing effects on polymerization of diacetylene lipids in liposomes and monolayers matrices. *Polymer Journal*, 48(4), 457-463.
- Barenholz, Y. C. (2012). Doxil® – the first FDA-approved nano-drug: Lessons learned. *Journal of Controlled Release*, 160(2), 117-134.
- Batist, G., Barton, J., Chaikin, P., Swenson, C., & Welles, L. (2002). Myocet (liposome-encapsulated doxorubicin citrate): a new approach in breast cancer therapy. *Expert Opinion on Pharmacotherapy*, 3(12), 1739-1751.
- Bayrak, Y. (2006). Application of Langmuir isotherm to saturated fatty acid adsorption. *Microporous and Mesoporous Materials*, 87(3), 203-206.
- Blanchard, C. R. (1996). Atomic force microscopy. *The Chemical Educator*, 1(5), 1-8.
- Boroujerdi, M. (2015). *Pharmacokinetics and toxicokinetics*: CRC Press.

- Bos, M. A., & Nylander, T. (1996). Interaction between  $\beta$ -lactoglobulin and phospholipids at the air/water interface. *Langmuir*, 12(11), 2791-2797.
- Bovier, P. A. (2008). Epaxal: A virosomal vaccine to prevent hepatitis A infection. *Expert Review of Vaccines*, 7(8), 1141-1150.
- Bressler, N. M., & Bressler, S. B. (2000). Photodynamic therapy with verteporfin (Visudyne): impact on ophthalmology and visual sciences. *Investigative Ophthalmology & Visual Science*, 41(3), 624-628.
- Brezesinski, G., & Möhwald, H. (2003). Langmuir monolayers to study interactions at model membrane surfaces. *Advances in Colloid and Interface Science*, 100-102, 563-584.
- Burnett, J. C., Rossi, J. J., & Tiemann, K. (2011). Current progress of siRNA/shRNA therapeutics in clinical trials. *Biotechnology Journal*, 6(9), 1130-1146.
- Camejo, G., Colacicco, G., & Rapport, M. M. (1968). Lipid monolayers: Interactions with the apoprotein of high density plasma lipoprotein. *Journal of Lipid Research*, 9, 562-569.
- Carvalho, B., Roland, L. M., Chu, L. F., Campitelli Iii, V. A., & Riley, E. T. (2007). Single-dose, extended-release epidural morphine (DepoDur™) compared to conventional epidural morphine for post-cesarean pain. *Anesthesia & Analgesia*, 105(1), 176-183.
- Cattel, L., Ceruti, M., & Dosio, F. (2002). From conventional to stealth liposomes: A new frontier in cancer chemotherapy. *Tumori*, 89(3), 237-249.
- Cevc, G., & Richardsen, H. (1999). Lipid vesicles and membrane fusion. *Advanced Drug Delivery Reviews*, 38(3), 207-232.
- Chang, H. I., & Yeh, M. K. (2012). Clinical development of liposome-based drugs: Formulation, characterization, and therapeutic efficacy. *International Journal of Nanomedicine*, 7, 49-60.
- Charbonneau, D. M., & Tajmir-Riahi, H.-A. (2009). Study on the interaction of cationic lipids with bovine serum albumin. *Journal of Physical Chemistry B*, 114(2), 1148-1155.
- Chen, J., Lu, W. L., Gu, W., Lu, S. S., Chen, Z. P., Cai, B. C., & Yang, X. X. (2014). Drug-in-cyclodextrin-in-liposomes: A promising delivery system for hydrophobic drugs. *Expert Opinion on Drug Delivery*, 11(4), 565-577.
- Chen, K. J., Liang, H. F., Chen, H. L., Wang, Y., Cheng, P. Y., Liu, H. L., Xia Y., & Sung, H. W. (2012). A thermoresponsive bubble-generating liposomal system for triggering localized extracellular drug delivery. *ACS Nano*, 7(1), 438-446.
- Chen, Q., Kang, X., Li, R., Du, X., Shang, Y., Liu, H., & Hu, Y. (2012). Structure of the complex monolayer of Gemini surfactant and DNA at the air/water interface. *Langmuir*, 28(7), 3429-3438.

- Cheung, Y. T., Lau, W. K. W., Yu, M. S., Lai, C. S. W., Yeung, S. C., So, K. F., & Chang, R. C. C. (2009). Effects of all-trans-retinoic acid on human SH-SY5Y neuroblastoma as in vitro model in neurotoxicity research. *NeuroToxicology*, *30*, 127-135.
- Chonn, A., & Cullis, P. R. (1998). Recent advances in liposome technologies and their applications for systemic gene delivery. *Advanced Drug Delivery Reviews*, *30*, 73-83.
- Chou, T. H., & Chang, C. H. (2000). Thermodynamic behavior and relaxation processes of mixed DPPC/cholesterol monolayers at the air/water interface. *Colloids and Surfaces B: Biointerfaces*, *17*(2), 71-79.
- Chou, H., Lin, H., & Liu, J. M. (2015). A tale of the two PEGylated liposomal doxorubicins. *OncoTargets and Therapy*, *8*, 1719.
- Cohen, S. R., & Bitler, A. (2008). Use of AFM in bio-related systems. *Current Opinion in Colloid & Interface Science*, *13*(5), 316-325.
- Colqui Quiroga, M. V., Monzón, L. M. A., & Yudi, L. M. (2010). Interaction of triflupromazine with distearoylphosphatidylglycerol films studied by surface pressure isotherms and cyclic voltammetry at a 1,2-dichloroethane/water interface. *Electrochimica Acta*, *55*(20), 5840-5846.
- Constantinescu, R., Constantinescu, A. T., Reichmann, H., & Janetzky, B. (2007). Neuronal differentiation and long-term culture of the human neuroblastoma line SH-SY5Y. *Journal of Neural Transmission*, *72*, 17-28.
- Cortesi, R., Esposito, E., Gambarin, S., Tello, P., Menegatti, E., & Nastruzzi, C. (1999). Preparation of liposomes by reverse-phase evaporation using alternative organic solvents. *Journal of Microencapsulation*, *16*(2), 251-256.
- Cullis, P. ., Kantarjian, H., Appelbaum, F., O'Brien, S., Wong, M., Choy, G. S., & Deitcher, S. R. (2007). Marqibo (vincristine sulfate liposomes injection, OPTISOME™) concentrates vincristine in tumor tissue and lymphoid malignancy oriented tissues in tumor-bearing mice. *Blood*, *110*(11), 1403.
- Davies, J. T., & Rideal, E. K. (1963). *Interfacial phenomena*. New York: Academic Press.
- De Oliveira, R., Albuquerque, D., Leite, F., Yamaji, F., & Cruz, T. (2012). *Measurement of the nanoscale roughness by atomic force microscopy: Basic principles and applications*. Croatia: INTECH Open Access Publisher.
- Debottona, N., Parnesa, M., Kadoucheb, J., & Benita, S. (2005). Overcoming the formulation obstacles towards targeted chemotherapy: In vitro, in vivo evaluation of cytotoxic drug loaded immunonanoparticles. *Journal of Controlled Release*, *127*, 219-230.
- Desai, N. (2016). Nanoparticle albumin-bound paclitaxel (Abraxane®). In M. Otagiri & V. T. G. Chuang (Eds.), *Albumin in medicine: Pathological and clinical applications* (pp. 101-119). Singapore: Springer.

- Du, X., Wang, Y., Ding, Y., & Guo, R. (2007). Protein-directed assembly of binary monolayers at the interface and surface patterns of protein on the monolayers. *Langmuir*, 23(15), 8142-8149.
- Dynarowicz-Łątka, P., Dhanabalan, A., & Oliveira Jr, O. N. (2001). Modern physicochemical research on Langmuir monolayers. *Advances in Colloid and Interface Science*, 91(2), 221-293.
- Efremov, R. G., Chugunov, A. O., Pyrkov, T. V., Priestle, J. P., Arseniev, A. S., & Jacoby, E. (2007). Molecular lipophilicity in protein modeling and drug design. *Current Medicinal Chemistry*, 14(4), 393-415.
- Ehsan, Z., Wetzel, J. D., & Clancy, J. P. (2014). Nebulized liposomal amikacin for the treatment of *Pseudomonas aeruginosa* infection in cystic fibrosis patients. *Expert Opinion on Investigational Drugs*, 23(5), 743-749.
- Elsadek, B., & Kratz, F. (2012). Impact of albumin on drug delivery – New applications on the horizon. *Journal of Controlled Release*, 157(1), 4-28.
- Escribá, P. V., González-Ros, J. M., Goñi, F. M., Kinnunen, P. K., Vigh, L., Sánchez-Magraner, L., Fernández A. M., Busquets X. Horváth I., & Barceló-Coblijn, G. (2008). Membranes: A meeting point for lipids, proteins and therapies. *Journal of Cellular and Molecular Medicine*, 12(3), 829-875.
- Ermacora, A., Michieli, M., Pea, F., Visani, G., Bucalossi, A., & Russo, D. (2000). Liposome encapsulated daunorubicin (daunoxome) for acute leukemia. *Haematologica*, 85(3), 324-325.
- Fanali, G., di Masi, A., Trezza, V., Marino, M., Fasano, M., & Ascenzi, P. (2012). Human serum albumin: From bench to bedside. *Molecular Aspects of Medicine*, 33(3), 209-290.
- Fassas, A., & Anagnostopoulos, A. (2005). The use of liposomal daunorubicin (DaunoXome) in acute myeloid leukemia. *Leukemia & Lymphoma*, 46(6), 795-802.
- Fleming, R. V., Kantarjian, H. M., Husni, R., Rolston, K., Lim, J., Raad, I., Pierce, S., Cortes, J., & Estey, E. (2001). Comparison of amphotericin B lipid complex (ABLCL) vs. ambisome in the treatment of suspected or documented fungal infections in patients with leukemia. *Leukemia & Lymphoma*, 40(5-6), 511-520.
- Frenkel, V., Etherington, A., Greene, M., Quijano, J., Xie, J., Hunter, F., Dromi, S., & Li, K. C. (2006). Delivery of liposomal doxorubicin (Doxil) in a breast cancer tumor model: investigation of potential enhancement by pulsed-high intensity focused ultrasound exposure. *Academic Radiology*, 13(4), 469-479.
- Funk, M., Michels, S., Wagner, J., Kiss, C., Sacu, S., & Schmidt-Erfurth, U. (2006). Vascular Effects of combined ranibizumab (Lucentis®) and verteporfin (Visudyne®) therapy in patients with neovascular age-related macular degeneration. *Investigative Ophthalmology & Visual Science*, 47(13), 353-353.

- Fujisawa, S., Kadoma, Y., Ishihara, M., Atsumi, T., & Yokoe, I. (2004). Dipalmitoylphosphatidylcholine (DPPC) and DPPC/cholesterol liposomes as predictors of the cytotoxicity of *bis*-GMA related compounds. *Journal of Liposome Research*, 14(1-2), 39-49.
- Gaines, G. L. (1966). *Insoluble monolayers at liquid-gas interfaces*. New York: Interscience.
- Gally, H. U., Niederberger, W., & Seelig, J. (1975). Conformation and motion of the choline head group in bilayers of dipalmitoyl-3-*sn*-phosphatidylcholine. *Biochemistry*, 14(16), 3647-3652.
- Gambling, D., Hughes, T., Martin, G., Horton, W., Manvelian, G., & Single-Dose, E. S. G. (2005). A comparison of Depodur™, a novel, single-dose extended-release epidural morphine, with standard epidural morphine for pain relief after lower abdominal surgery. *Anesthesia & Analgesia*, 100(4), 1065-1074.
- García-Sáez, A. J., & Schwille, P. (2010). Surface analysis of membrane dynamics. *Biochimica et Biophysica Acta (BBA): Biomembranes*, 1798(4), 766-776.
- Garofalakis, G., & Murray, B. S. (2002). Surface pressure isotherms, dilatational rheology, and brewster angle microscopy of insoluble monolayers of sugar monoesters. *Langmuir*, 18(12), 4765-4774.
- Gentine, P., Bourel-Bonnet, L., & Frisch, B. (2013). Modified and derived ethanol injection toward liposomes: development of the process. *Journal of Liposome Research*, 23(1), 11-19.
- Gew, L. T., & Misran, M. (2014). Albumin-fatty acid interactions at monolayer interface. *Nanoscale Research Letters*, 9(1), 218.
- Gew, L. T., & Misran, M. (2016). Energetic mixing of anti-SNAP25 on lipid monolayers: degree of saturation of C18 fatty acids. *Surface and Interface Analysis*, 49(5), 388-397.
- Gil, T., Ipsen, J. H., Mouritsen, O. G., Sabra, M. C., Sperotto, M. M., & Zuckermann, M. J. (1998). Theoretical analysis of protein organization in lipid membranes. *Biochimica et Biophysica Acta (BBA): Biomembranes*, 1376(3), 245-266.
- Girard-Egrot, A. P., Godoy, S., & Blum, L. J. (2005). Enzyme association with lipidic Langmuir-Blodgett films: Interests and applications in nanobioscience. *Advances in Colloid and Interface Science*, 116, 205-225.
- Glassa, T. L., aabeb, T. D., Garc aa, D. M., & Kokea, J. R. (2002). Phosphorylated neurofilaments and SNAP-25 in cultured SH-SY5Y neuroblastoma cells. *Brain Research*, 934, 43-48.
- Goksu, E. I., Vanegas, J. M., Blanchette, C. D., Lin, W. C., & Longo, M. L. (2009). AFM for structure and dynamics of biomembranes. *Biochimica et Biophysica Acta (BBA): Biomembranes*, 1788(1), 254-266.

- Gregoriadis, G. (1978). Liposomes in the therapy of lysosomal storage diseases. *Nature*, 275(5682), 695-696.
- Gregory, A. E., Williamson, D., & Titball, R. (2013). Vaccine delivery using nanoparticles. *Frontiers in Cellular and Infection Microbiology*, 3, 13.
- Gradishar, W. J., Tjulandin, S., Davidson, N., Shaw, H., Desai, N., Bhar, P., Hawkins M., & O'Shaughnessy, J. (2005). Phase III trial of nanoparticle albumin-bound paclitaxel compared with polyethylated castor oil-based paclitaxel in women with breast cancer. *Journal of Clinical Oncology*, 23(31), 7794-7803.
- Hąc-Wydro, K., Dynarowicz-Lątka, P., Grzybowska, J., & Borowski, E. (2005). Interactions of amphotericin B derivative of low toxicity with biological membrane components – The Langmuir monolayer approach. *Biophysical Chemistry*, 116(1), 77-88.
- Hąc-Wydro, K., & Dynarowicz-Lątka, P. (2006a). Interaction between nystatin and natural membrane lipids in Langmuir monolayers – The role of a phospholipid in the mechanism of polyenes mode of action. *Biophysical Chemistry*, 123(2), 154-161.
- Hąc-Wydro, K., & Dynarowicz-Lątka, P. (2006b). Nystatin in Langmuir monolayers at the air/water interface. *Colloids and Surfaces B: Biointerfaces*, 53(1), 64-71.
- Hąc-Wydro, K., & Wydro, P. (2007a). The influence of fatty acids on model cholesterol/phospholipid membranes. *Chemistry and Physics of Lipids*, 150(1), 66-81.
- Hąc-Wydro, K., Kapusta, J., Jagoda, A., Wydro, P., & Dynarowicz-Lątka, P. (2007b). The influence of phospholipid structure on the interactions with nystatin, a polyene antifungal antibiotic A Langmuir monolayer study. *Chemistry and Physics of Lipids*, 150(2), 125-135.
- Hąc-Wydro, K., & Dynarowicz-Lątka, P. (2008). Biomedical applications of the Langmuir monolayer technique *Annales UMCS, Chemistry* (Vol. 63, pp. 47).
- Hąc-Wydro, K., Jędrzejek, K., & Dynarowicz-Lątka, P. (2009). Effect of saturation degree on the interactions between fatty acids and phosphatidylcholines in binary and ternary Langmuir monolayers. *Colloids and Surfaces B: Biointerfaces*, 72(1), 101-111.
- Hamada, A., Kawaguchi, T., & Nakano, M. (2002). Clinical pharmacokinetics of cytarabine formulations. *Clinical Pharmacokinetics*, 41(10), 705-718.
- Hamrock, D. J. (2006). Adverse events associated with intravenous immunoglobulin therapy. *International Immunopharmacology*, 6(4), 535–542.
- Han, S. Y., Qiao, J. Q., Zhang, Y. Y., Yang, L. L., Lian, H. Z., Ge, X., & Chen, H. Y. (2011). Determination of *n*-octanol/water partition coefficient for DDT-related compounds by RP-HPLC with a novel dual-point retention time correction. *Chemosphere*, 83(2), 131-136.

- Hansel, T. T., Kropshofer, H., Singer, T., Mitchell, J. A., & George, A. J. T. (2010). The safety and side effects of monoclonal antibodies. *Nature Reviews Drug Discovery* 9, 325-338.
- Harris, M. (2004). Monoclonal antibodies as therapeutic agents for cancer. *Lancet Oncology*, 5(5), 292–302.
- Hay, R. J. (1994). Liposomal amphotericin B, AmBisome. *Journal of Infection*, 28, 35-43.
- Hao, C., Sun, R., & Zhang, J. (2013). Mixed monolayers of DOPC and palmitic acid at the liquid-air interface. *Colloids and Surface B: Biointerfaces*, 112, 441-445.
- Hasegawa, T., Matsuzaki, M., Takeda, A., Kikuchi, A., Furukawa, K., Shibahara, S., & Itoyama, Y. (2003). Increased dopamine and its metabolites in SH-SY5Y neuroblastoma cells that express tyrosinase. *Journal of Neurochemistry*, 87(2), 470-475.
- Herzog, C., Hartmann, K., Künzi, V., Kürsteiner, O., Mischler, R., Lazar, H., & Glück, R. (2009). Eleven years of Inflexal® V – A virosomal adjuvanted influenza vaccine. *Vaccine*, 27(33), 4381-4387.
- Hodel, A. (1998). Molecules in focus: SNAP-25. *International Journal of Biochemistry & Cell Biology*, 30, 1069-1073.
- Hsu, W. H., Liu, S. Y., Chang, Y. J., Chang, C. H., Ting, G., & Lee, T. W. (2014). The PEGylated liposomal doxorubicin improves the delivery and therapeutic efficiency of 188 Re-Liposome by modulating phagocytosis in C26 murine colon carcinoma tumor model. *Nuclear Medicine and Biology*, 41(9), 765-771.
- Hunte, C., & Richers, S. (2008). Lipids and membrane protein structures. *Current Opinion in Structural Biology*, 18(4), 406-411.
- Immordino, M. L., Dosio, F., & Cattel, L. (2006). Stealth liposomes: Review of the basic science, rationale, and clinical applications, existing and potential. *International Journal of Nanomedicine*, 1(3), 297-315.
- Isailović, B. D., Kostić, I. T., Zvonar, A., Đorđević, V. B., Gašperlin, M., Nedović, V. A., & Bugarski, B. M. (2013). Resveratrol loaded liposomes produced by different techniques. *Innovative Food Science & Emerging Technologies*, 19, 181-189.
- Jaafar-Maalej, C., Diab, R., Andrieu, V., Elaissari, A., & Fessi, H. (2010). Ethanol injection method for hydrophilic and lipophilic drug-loaded liposome preparation. *Journal of Liposome Research*, 20(3), 228-243.
- Jain, A., Jain, A., Gulbake, A., Shilpi, S., Hurkat, P., & Jain, S. K. (2013). Peptide and protein delivery using new drug delivery systems. *Critical Reviews™ in Therapeutic Drug Carrier Systems*, 30(4).

- Jing, Y., Shishkov, A., & Ponnappa, B. C. (2008). Inhibition of tumor necrosis factor alpha secretion in rat Kupffer cells by siRNA: In vivo efficacy of siRNA-liposomes. *Biochimica et Biophysica Acta (BBA): General Subjects*, 1780(1), 34-40.
- Joshua, Z., & Chernomordik, L. V. (1999). Membrane fusion. *Advanced Drug Delivery Reviews*, 38(3), 197-205.
- Jurak, M. (2013). Thermodynamic aspects of cholesterol effect on properties of phospholipid monolayers: Langmuir and Langmuir-Blodgett monolayer study. *Journal of Physical Chemistry B*, 117(13), 3496-3502.
- Kamilya, T., Pal, P., & Talapatra, G. B. (2007). Interaction and incorporation of ovalbumin with stearic acid monolayer: Langmuir-Blodgett film formation and deposition. *Colloids and Surface B: Biointerfaces*, 58(2), 137-144.
- Kamilya, T., Pal, P., & Talapatra, G. B. (2007). Interaction of ovalbumin with phospholipids Langmuir-Blodgett film. *Journal of Physical Chemistry B*, 111(5), 1199-1205.
- Kanicky, J. R., & Shah, D. O. (2002). Effect of degree, type, and position of unsaturation on the pKa of long-chain fatty acids. *Journal of Colloid and Interface Science* 256, 201-207.
- Khurana, M., Collins, H. A., Karotki, A., Anderson, H. L., Cramb, D. T., & Wilson, B. C. (2007). Quantitative in vitro demonstration of two-photon photodynamic therapy using Photofrin® and Visudyne®. *Photochemistry and Photobiology*, 83(6), 1441-1448.
- Kim, H. J., Kim, A., Miyata, K., & Kataoka, K. (2016). Recent progress in development of siRNA delivery vehicles for cancer therapy. *Advanced Drug Delivery Reviews*, 104, 61-77.
- Kim, K., Kim, C., & Byun, Y. (2001). Preparation of a dipalmitoylphosphatidylcholine/cholesterol Langmuir-Blodgett monolayer that suppresses protein adsorption. *Langmuir*, 17(16), 5066-5070.
- Komano, Y., Yagi, N., & Nanki, T. (2015). Joint-targeting drug delivery system for rheumatoid arthritis: siRNA encapsulated liposome. *Pharmaceutica Analytica Acta*, 6. doi:10.4172/2153-2435.1000352
- Korablyov, V., Zimran, A., & Barenholz, Y. (1999). Cerebroside- $\beta$ -glucosidase encapsulation in liposomes for Gaucher's disease treatment Revisited. *Pharmaceutical Research*, 16(3), 466-469.
- Korchowiec, B., Paluch, M., Corvis, Y., & Rogalska, E. (2006). A Langmuir film approach to elucidating interactions in lipid membranes: 1,2-dipalmitoyl-*sn*-glycero-3-phosphoethanolamine/cholesterol/metal cation systems. *Chemistry and Physics of Lipids*, 144(2), 127-136.
- Kratz, F. (2008). Albumin as a drug carrier: Design of prodrugs, drug conjugates and nanoparticles. *Journal of Controlled Release*, 132(3), 171-183.

- Kratz, F. (2014). A clinical update of using albumin as a drug vehicle – A commentary. *Journal of Controlled Release*, 190, 331-336.
- Kroon, J., Metselaar, J. M., Storm, G., & Pluijm, G. v. d. (2014). Liposomal nanomedicines in the treatment of prostate cancer. *Cancer Treatment Reviews*, 40(4), 578-584.
- Kundu, S., & Langevin, D. (2008). Fatty acid monolayer dissociation and collapse: Effect of pH and cations. *Colloids and Surfaces A: Physicochemical and Engineering Aspects*, 325(1-2), 81-85.
- Kürsteiner, O., Moser, C., Lazar, H., & Durrer, P. (2006). Inflflexal® V – The influenza vaccine with the lowest ovalbumin content. *Vaccine*, 24(44), 6632-6635.
- L. Armstrong, C., Sandqvist, E., & C. Rheinstadter, M. (2011). Protein-protein interactions in membranes. *Protein and Peptide Letters*, 18(4), 344-353.
- Laganowsky, A., Reading, E., Allison, T. M., Ulmschneider, M. B., Degiacomi, M. T., Baldwin, A. J., & Robinson, C. V. (2014). Membrane proteins bind lipids selectively to modulate their structure and function. *Nature*, 510(7503), 172-175.
- Laginha, K., Mumbengegwi, D., & Allen, T. (2005). Liposomes targeted via two different antibodies: Assay, B-cell binding and cytotoxicity. *Biochimica et Biophysica Acta (BBA): Biomembrane*, 1711, 25-32.
- Laouini, A., Charcosset, C., Fessi, H., Holdich, ., & Vladislavljević, G. (2013). Preparation of liposomes: A novel application of microengineered membranes – From laboratory scale to large scale. *Colloids and Surfaces B: Biointerfaces*, 112, 272-278.
- Lee, A. G. (2003). Lipid–protein interactions in biological membranes: A structural perspective. *Biochimica et Biophysica Acta (BBA): Biomembrane* 1612, 1-40.
- Lee, A. G. (2011). Lipid-protein interactions. *Biochemistry Society Transactions*, 39(3), 761-766.
- Lehtinen, J., Raki, M., Bergström, K. A., Uutela, P., Lehtinen, K., Hiltunen, A., Pikkarainen, J., Liang, H., Pitkänen, S., Määttä, M. A., Ketola, R. A., Yiperttula, M., Wirth, T., & Urtti, A. (2012). Pre-targeting and direct immunotargeting of liposomal drug carriers to ovarian carcinoma. *PLOS ONE*, 7(7), 1-10.
- Leo, A., Hansch, C., & Elkins, D. (1971). Partition coefficients and their uses. *Chemical Reviews*, 71(6), 525-616. Pons, M., Foradada, M., & Estelrich, J. (1993). Liposomes obtained by the ethanol injection method. *International Journal of Pharmaceutics*, 95(1), 51-56.
- Liau, J. J., Hook, S., Prestidge, C. A., & Barnes, T. J. (2015). A lipid based multi-compartmental system: Liposomes-in-double emulsion for oral vaccine delivery. *European Journal of Pharmaceutics and Biopharmaceutics*, 97, 15-21.
- Lingwood, D., & Simons, K. (2010). Lipid rafts as a membrane-organizing principle. *Science*, 327(5961), 46-50.

- Loeste, E., Díaz-Martí, E., Zorbakhsh, A., & Meldrum, F. C. (2003). Study of calcium Carbonate precipitation under a series of fatty acid Langmuir monolayers using brewster angle microscopy. *Langmuir*, *19*(7), 2830-2837.
- Lundberga, B. B., Griffithsb, G., & Hansen, H. J. (2004). Cellular association and cytotoxicity of anti-74-targeted lipid drug carriers in B lymphoma cells. *Journal of Controlled Release*, *94*, 155-161.
- Ma, M., & Bong, D. (2013). Controlled fusion of synthetic lipid membrane vesicles. *Accounts of Chemical Research*, *46*(12), 2988-2997.
- Maitani, Y., Soeda, H., Junping, W., & Takayama, K. (2001). Modified ethanol injection method for liposomes containing  $\beta$ -sitosterol  $\beta$ -D-glucoside. *Journal of Liposome Research*, *11*(1), 115-125.
- Makyla, K., & Paluch, M. (2009). The linoleic acid influence on molecular interactions in the model of biological membrane. *Colloids and Surface B: Biointerfaces*, *71*(1), 59-66.
- Manjappa, A. S., Chaudhari, K. R., Venkatarajua, M. P., Dantuluri, P., Nanda, B., Sidda, C., Sawant, K. K., & Murthy, R. S. R. (2011). Antibody derivatization and conjugation strategies: Application in preparation of stealth immunoliposome to target chemotherapeutics to tumor. *Journal of Controlled Release*, *150*, 2-22.
- Markman, M., Bundy, B. N., Alberts, D. S., Fowler, J. M., Clark-Pearson, D. L., Carson, L. F., Wadler, S., & Sichel, J. (2001). Phase III trial of standard-dose intravenous cisplatin plus paclitaxel versus moderately high-dose carboplatin followed by intravenous paclitaxel and intraperitoneal cisplatin in small-volume stage III ovarian carcinoma: an intergroup study of the Gynecologic Oncology Group, Southwestern Oncology Group, and Eastern Cooperative Oncology Group. *Journal of Clinical Oncology*, *19*(4), 1001-1007.
- Marsden, H. R., Tomatsu, I., & Kros, A. (2011). Model systems for membrane fusion. *Chemistry Society Reviews*, *40*(3), 1572-1585.
- Martín-Banderas, L., Holgado, M. A., Durán-Lobato, M., Infante, J. J., Álvarez-Fuentes, J., & Fernández-Arévalo, M. (2016). Role of nanotechnology for enzyme replacement therapy in lysosomal diseases. A focus on Gaucher's disease. *Current Medicinal Chemistry*, *23*(9), 929-952.
- Martins, S., Sarmiento, B., Ferreira, D. C., & Souto, E. B. (2007). Lipid-based colloidal carriers for peptide and protein delivery-liposomes versus lipid nanoparticles. *International Journal of Nanomedicine*, *2*(4), 595.
- Mastrobattista, E., Koning, G. A., & Storm, G. (1999). Immunoliposomes for the targeted delivery of antitumor drugs. *Advanced Drug Delivery Reviews*, *40*, 103-127.
- McManus, J. J., Charbonneau, P., Zaccarelli, E., & Asherie, N. (2016). The physics of protein self-assembly. *Current Opinion in Colloid & Interface Science*, *22*, 73-79.

- Miele, E., Spinelli, G. P., Miele, E., Tomao, F., & Tomao, S. (2009). Albumin-bound formulation of paclitaxel (Abraxane® ABI-007) in the treatment of breast cancer. *International Journal of Nanomedicine*, 4, 99-105.
- Mischler, R., & Metcalfe, I. C. (2002). Inflexal® V a trivalent virosome subunit influenza vaccine: production. *Vaccine*, 20, B17-B23.
- Mishra, B., Patel, B. B., & Tiwari, S. (2010). Colloidal nanocarriers: a review on formulation technology, types and applications toward targeted drug delivery. *Nanomedicine: Nanotechnology, Biology, and Medicine*, 6, 9-24.
- Mita, T. (1989). Lipid-protein interaction in mixed monolayers from phospholipids and proteins. *Bulletin Chemical Society of Japan*, 62, 3114-3121.
- Moghaddam, B., Ali, M. H., Wilkhu, J., Kirby, D. J., Mohammed, A. R., Zheng, Q., & Perrie, Y. (2011). The application of monolayer studies in the understanding of liposomal formulations. *International Journal of Pharmaceutics*, 417(1-2), 235-244.
- Moghimia, S. M., & Szebenib, J. (2003). Stealth liposomes and long circulating nanoparticles: critical issues in pharmacokinetics, opsonization and protein-binding properties. *Progress in Lipid Research*, 42, 463-478.
- Morigaki, K., & Walde, P. (2007). Fatty acid vesicles. *Current Opinion in Colloid & Interface Science*, 12(2), 75-80.
- Mrozek, E., Rhoades, C., Allen, J., Hade, E., & Shapiro, C. (2005). Phase I trial of liposomal encapsulated doxorubicin (Myocet™; D-99) and weekly docetaxel in advanced breast cancer patients. *Annals of Oncology*, 16(7), 1087-1093.
- Nag, O. K., & Awasthi, V. (2013). Surface engineering of liposomes for stealth behavior. *Pharmaceutics*, 5, 542-569.
- Nagle, P. C., & Gerancher, J. C. (2007). DepoDur®(extended-release epidural morphine): a review of an old drug in a new vehicle. *Techniques in Regional Anesthesia and Pain Management*, 11(1), 9-18.
- Nakamura, T., Peng, K. W., Vongpunsawad, S., Harvey, M., Mizuguchi, H., Hayakawa, T., Cattaneo R., & Russell, S. J. (2004). Antibody-targeted cell fusion. *Nature Biotechnology*, 22(3), 331-336.
- Niu, N. K., Yin, J. J., Yang, Y. X., Wang, Z. L., Zhou, Z. W., He, Z. X., Chen, X. W., Zhang, X., Duan, W., Yang, T. & Zhou, S. F. (2015). Novel targeting of PEGylated liposomes for codelivery of TGF-β1 si NA and four antitubercular drugs to human macrophages for the treatment of mycobacterial infection: A quantitative proteomic study. *Drug Design, Development and Therapy*, 9, 4441.
- Ng, K. Y., Zhao, L., Liu, Y., & Mahapatro, M. (2000). The effects of polyethyleneglycol (PEG)-derived lipid on the activity of target-sensitive immunoliposome. *International Journal of Pharmaceutics*, 193, 157-166.

- Nydegger, U. E., & Sturzenegger, M. (1999). Adverse effects of intravenous immunoglobulin therapy. *Drug Safety*, 21, 171-185.
- O'Brien, S., Thomas, D. A., Heffner, L. T., Stock, W., Messerschmidt, G. L., Hagey, A., Deither S. R., & Kantarjian, H. (2010). Marqibo®(vincristine sulfate liposomes injection; VSLI) in the treatment of adult patients with advanced, relapsed/refractory acute lymphoblastic leukemia (ALL): A combined analysis of the VSLI-06 and RALLY studies. *Blood*, 116(21), 2143-2143.
- O'Shaughnessy, J. A. (2003). Pegylated liposomal doxorubicin in the treatment of breast cancer. *Clinical Breast Cancer*, 4(5), 318-328.
- Ott, J. J., Irving, G., & Wiersma, S. T. (2012). Long-term protective effects of hepatitis A vaccines. A systematic review. *Vaccine*, 31(1), 3-11.
- Palsdottir, H., & Hunte, C. (2004). Lipids in membrane protein structures. *Biochimica et Biophysica Acta (BBA): Biomembrane*, 1666(1-2), 2-18.
- Park, J. W., Kirpotin, D. B., Hong, K., Shalaby, R., Shao, Y., Nielsen, U. B., Mark, J., D., Papahadjopoulos, D., & Benz, C. C. (2001). Tumor targeting using anti-her2 immunoliposomes. *Journal of Controlled Release*, 74(1-3), 95-113.
- Patil, Y. P., & Jadhav, S. (2014). Novel methods for liposome preparation. *Chemistry and Physics of Lipids*, 177, 8-18.
- Pattni, B. S., Chupin, V. V., & Torchilin, V. P. (2015). New developments in liposomal drug delivery. *Chemical Reviews*, 115(19), 10938-10966.
- Peters, T. (1995). *All About Albumin: Biochemistry, Genetics, and Medical Applications*. USA: Academic Press Elsevier Science.
- Phan, M. D., & Shin, K. (2015). Effects of cardiolipin on membrane morphology: A Langmuir monolayer study. *Biophysical Journal*, 108(8), 1977-1986.
- Phuphanich, S., Maria, B., Braeckman, R., & Chamberlain, M. (2007). A pharmacokinetic study of intra-CSF administered encapsulated cytarabine (DepoCyt®) for the treatment of neoplastic meningitis in patients with leukemia, lymphoma, or solid tumors as part of a phase III study. *Journal of Neuro-oncology*, 81(2), 201-208.
- Piccaluga, P. P., Visani, G., Martinelli, G., Isidori, A., Malagola, M., Rondoni, M., Baccarani, M., & Tura, S. (2002). Liposomal daunorubicin (DaunoXome) for treatment of relapsed meningeal acute myeloid leukemia. *Leukemia*, 16(9), 1880-1881.
- Pisal, D. S., Kosloski, M. P., & Balu-Iyer, S. V. (2010). Delivery of therapeutic proteins. *Journal of Pharmaceutical Sciences*, 99(6), 2557-2575.
- Pons, M., Foradada, M., & Estelrich, J. (1993). Liposomes obtained by the ethanol injection method. *International Journal of Pharmaceutics*, 95(1), 51-56.

- Qiu, Y., Guo, L., Zhang, S., Xu, B., Gao, Y., Hu, Y., Hou, J., Bai, B., Shen, H., & Mao, P. (2015). DNA-based vaccination against hepatitis B virus using dissolving microneedle arrays adjuvanted by cationic liposomes and CpG ODN. *Drug Delivery*, 1-8.
- Rawat, M., Singh, D., Saraf, S., & Saraf, S. (2008). Lipid carriers: a versatile delivery vehicle for proteins and peptides. *Yakugaku Zasshi*, 128(2), 269-280.
- Reddy, L. H., & Couvreur, P. (2011). Nanotechnology for therapy and imaging of liver diseases. *Journal of Hepatology*, 55(6), 1461-1466.
- Résibois-Grégoire, A. (1967). Electron microscopic studies of metachromatic leucodystrophy. *Acta Neuropathologica*, 9(3), 244-253.
- Rothman, J. E. (1994). Mechanisms of intracellular protein transport. *Nature*, 372, 55.
- Rothman, J. E. (2014). The principle of membrane fusion in the cell (Nobel Lecture). *Angewandte Chemie International Edition*, 53(47), 12676-12694.
- Sakurai, Y., Hatakeyama, H., Sato, Y., Hyodo, M., Akita, H., & Harashima, H. (2013). Gene silencing via RNAi and siRNA Quantification in tumor tissue using MEND, a liposomal siRNA delivery system. *Molecular Therapy*, 21(6), 1195-1203.
- Sangster, J. (1989). Octanol-Water Partition coefficients of simple organic compounds. *Journal of Physical and Chemical Reference Data*, 18(3), 1111-1229.
- Sarisozen, C., Salzano, G., & Torchilin, V. P. (2015). Recent advances in siRNA delivery. *Biomolecular Concepts*, 6(5-6), 321-341.
- Sarisozen, C., Salzano, G., & P Torchilin, V. (2016). Lipid-based siRNA delivery systems: challenges, promises and solutions along the long journey. *Current Pharmaceutical Biotechnology*, 17(8), 728-740.
- Samad, A., Sultana, Y., & Aqil, M. (2007). Liposomal drug delivery systems: An update review. *Current Drug Delivery*, 4(4), 297-305.
- Seelig, J., Gally, G. U., & Wohlgemuth, R. (1977). Orientation and flexibility of the choline head group in phosphatidylcholine bilayers. *Biochimica et Biophysica Acta (BBA): Biomembranes*, 467(2), 109-119.
- Seoane, R., Miñones, J., Conde, O., Miñones, J., Casas, M., & Iribarnegaray, E. (2000). Thermodynamic and Brewster angle microscopy studies of fatty acid/cholesterol mixtures at the air/water interface. *Journal of Physical Chemistry B*, 104(32), 7735-7744.
- Silverman, J. A., & Deitcher, S. R. (2013). Marqibo®(vincristine sulfate liposome injection) improves the pharmacokinetics and pharmacodynamics of vincristine. *Cancer Chemotherapy and Pharmacology*, 71(3), 555-564.
- Simone, E. A., Dziubla, T. D., & Muzykantov, V. R. (2008). Polymeric carriers: Role of geometry in drug delivery. *Expert Opinion Drug Delivery*, 5(12), 1283-1300.

- Singer, S. J., & Nicolson, G. L. (1972). The fluid mosaic model of the structure of cell membranes. *Science*, *175*(4023), 720-731.
- Singh, B. N., Prateeksha, C. V. R., Rawat, A. K. S., Upreti, D. K., & Singh, B. R. (2015). Antimicrobial nanotechnologies: What are the current possibilities? *Current Science*, *108*(7), 1210.
- Sperotto, M. M., May, S., & Baumgaertner, A. (2006). Modelling of proteins in membranes. *Chemistry and Physics of Lipids*, *141*(1-2), 2-29
- Stefaniu, C., Brezesinski, G., & Möhwald, H. (2014). Langmuir monolayers as models to study processes at membrane surfaces. *Advances in Colloid and Interface Science*, *208*, 197-213.
- Stockmann, C., Roberts, J. K., Yellepeddi, V. K., & Sherwin, C. M. T. (2015). Clinical pharmacokinetics of inhaled antimicrobials. *Clinical Pharmacokinetics*, *54*(5), 473-492.
- Sułkowska, A. (2002). Interaction of drugs with bovine and human serum albumin. *Journal of Molecular Structure*, *614*(1), 227-232.
- Suzuki, Y. (2013). Chaperone therapy update: Fabry disease, GM1-gangliosidosis and Gaucher disease. *Brain and Development*, *35*(6), 515-523.
- Tan, H. W., & Misran, M. (2012). Characterization of fatty acid liposome coated with low-molecular-weight chitosan. *Journal of Liposome Research*, *22*(4), 329-335.
- Teixeira, A. C., Fernandes, A. C., Garcia, A. R., Ilharco, L. M., Brogueira, P., & Goncalves da Silva, A. M. (2007). Microdomains in mixed monolayers of oleanolic and stearic acids: thermodynamic study and BAM observation at the air-water interface and AFM and FTIR analysis of LB monolayers. *Chemistry and Physics of Lipids*, *149*(1-2), 1-13.
- Teo, Y. Y., Misran, M., Low, K. H., & Zain, S. M. (2011). Effect of unsaturation on the stability of C18 oolyunsaturated fatty acids vesicles suspension in aqueous solution. *Bulletin of the Korean Chemical Society*, *32*(1), 59-64.
- Teo, Y. Y., Misran, M., & Low, K. H. (2012). Effect of pH on physicochemical properties and encapsulation efficiency of PEGylated linolenic acid vesicles. *Journal of Chemistry*, *9*(2), 729-738.
- Teo, Y. Y., Misran, M., & Low, K. H. (2014a). Effect of PEGylated lipid and Lecinol S-10 on physico-chemical properties and encapsulation efficiency of palmitoleate-palmitoleic acid vesicles. *Journal of Liposome Research*, *24*(3), 241-248.
- Teo, Y. Y., Misran, M., & Low, K. H. (2014b). Studies of lateral interactions between C18 unsaturated fatty acid with polyethoxylated phospholipid mixed Langmuir monolayer at air-aqueous interface for liposome formulation. *Asian Journal of Chemistry*, *26*(14), 4149.

- Thekkedath, R., Koshkaryev, A., & Torchilin, V. P. (2013). Lysosome-targeted octadecyl-rhodamine B-liposomes enhance lysosomal accumulation of glucocerebrosidase in Gaucher's cells in vitro. *Nanomedicine (London, England)*, *8*(7), 1055-1065.
- Thomas, D. A., Jabbour, E., Kantarjian, H., & O'Brien, S. (2007). Neurologic toxicity of intrathecal liposomal cytarabine when used for CNS prophylaxis in conjunction with the hyper-CVAD regimen. *Blood*, *110*(5), 1698-1699.
- Tokatlian, T., & Segura, T. (2010). siRNA applications in nanomedicine. *Wiley Interdisciplinary Reviews: Nanomedicine and Nanobiotechnology*, *2*(3), 305-315.
- Torchilin, V., & Weissig, V. (2003). *Liposomes: A practical approach*. Oxford University Press.
- Torchilin, V. P. (2005). Recent advances with liposomes as pharmaceutical carriers. *Nature Reviews Drug Discovery*, *4*, 145-160.
- Uludağ, H., Landry, B., Valencia-Serna, J., Remant-Bahadur, K., & Meneksedağ-Erol, D. (2016). Current attempts to implement siRNA-based RNAi in leukemia models. *Drug Discovery Today*, *21*(9), 1412-1420.
- Vollhardt, D. (2007). Effect of unsaturation in fatty acids on the main characteristics of Langmuir monolayers. *Journal of Physical Chemistry C*, *111*(18), 6805-6812.
- Wang, C., Liu, P., Zhuang, Y., Li, P., Jiang, B., Pan, H., Liu, L., Cai, L., & Ma, Y. (2014). Lymphatic-targeted cationic liposomes: A robust vaccine adjuvant for promoting long-term immunological memory. *Vaccine*, *32*(42), 5475-5483.
- Weiss, A., Neuberg, P., Philippot, S., Erbacher, P., & Weill, C. O. (2011). Intracellular peptide delivery using amphiphilic lipid-based formulations. *Biotechnology Bioengineering*, *108*(10), 2477-2487.
- Wibroe, P. P., Ahmadvand, D., Oghabian, M. A., Yaghmur, A., & Moghimi, S. M. (2016). An integrated assessment of morphology, size, and complement activation of the PEGylated liposomal doxorubicin products Doxil®, Caelyx®, DOXOrubicin, and SinaDoxosome. *Journal of Controlled Release*, *221*, 1-8.
- Working, P. K., Newman, M. S., Huang, S. K., Mayhew, E., Vaage, J., & Lasic, D. D. (1994). Pharmacokinetics, biodistribution and therapeutic efficacy of Doxorubicin encapsulated in Stealth® Liposomes (Doxil®). *Journal of Liposome Research*, *4*, 667-687.
- Wydro, P., Krajewska, B., & Hac-Wydro, K. (2007). Chitosan as a lipid binder: A Langmuir monolayer study of chitosan-lipid interactions. *Biomacromolecules*, *8*(8), 2611-2617.
- Xia, Y., Tian, J., & Chen, X. (2016). Effect of surface properties on liposomal siRNA delivery. *Biomaterials*, *79*, 56-68.

- Xu, C. F., & Wang, J. (2015). Delivery systems for siRNA drug development in cancer therapy. *Asian Journal of Pharmaceutical Sciences*, 10(1), 1-12.
- Yan, F., Li, L., Deng, Z., Jin, Q., Chen, J., Yang, W., Yeh, C., K., Wu, J., Shandas, R., Liu, X., & Zheng, H. (2013). Paclitaxel-liposome-microbubble complexes as ultrasound-triggered therapeutic drug delivery carriers. *Journal of Controlled Release*, 166(3), 246-255.
- Yanga, T., Choi, M. K., Cuia, F. D., Kim, J. S., Chung, S. J., Shimb, C. K., & Kim, D. D. (2007). Preparation and evaluation of paclitaxel-loaded PEGylated immunoliposome. *Journal of Controlled Release*, 120, 169-177.
- Yeagle, P. L. (2014). Non-covalent binding of membrane lipids to membrane proteins. *Biochimica et Biophysica Acta (BBA): Biomembranes*, 1838(6), 1548-1559.
- Yong-Hoon, K., Ryugo, T., Morio, T., & Tsuneo, U. (2004). Characterization of dipalmitoylphosphatidylcholine/cholesterol Langmuir-Blodgett monolayers Investigated by Atomic Force Microscopy and fourier transform infrared spectroscopy. *Japanese Journal of Applied Physics*, 43(6S), 3860.
- Yoshizawa, Y., Kono, Y., Ogawara, K. I., Kimura, T., & Higaki, K. (2011). PEG liposomalization of paclitaxel improved its in vivo disposition and anti-tumor efficacy. *International Journal of Pharmaceutics*, 412, 132-141.
- Zamble, D. B., & Lippard, S. J. (1995). Cisplatin and DNA repair in cancer chemotherapy. *Trends in Biochemical Sciences*, 20(10), 435-439.
- Zimmerberg, J., Vogel, S. S., & Chernomordik, L. V. (1993). Mechanisms of membrane fusion. *Annual Review of Biophysics and Biomolecular Structure*, 22(1), 433-466.

## LIST OF PUBLICATIONS

1. Gew, L. T., & Misran, M. (2014). Albumin-fatty acid interactions at monolayer interface. *Nanoscale research Letters*, 9(1), 218.
2. Gew, L. T., & Misran, M. (2016). Energetic mixing of anti-SNAP25 on lipid monolayers: degree of saturation of C18 fatty acids. *Surface and Interface Analysis*, 49(5), 388-397.
3. Gew, L. T., & Misran, M. (2017). Interaction between C18 fatty acids and DOPE PEG2000 in Langmuir monolayers: effect of degree of unsaturation. *Journal of Biological Physics*. doi: 10.1007/s10867-017-9459-2. (In print)

University of Malaya